



UNIVERSIDADE FEDERAL DE PERNAMBUCO

CENTRO DE CIÊNCIAS BIOLÓGICAS

**PROGRAMA DE PÓS-GRADUAÇÃO EM
CIÊNCIAS BIOLÓGICAS**

**AVALIAÇÃO DA EFICÁCIA DE DERIVADOS FENOTIAZÍNICOS COMO CANDIDATOS
A FOTOSSENSIBILIZADORES EM FOTOQUIMIOTERAPIA ANTIPARASITÁRIA
CONTRA *Trypanosoma cruzi* E *Leishmania braziliensis***

Aluno: Artur Felipe Santos Barbosa

Orientadora: Profa. Dra. Suely Lins Galdino (*In memoriam*)

Prof. Dr. Ivan da Rocha Pitta

Co-orientador: Prof. Dr. Antônio Luiz Barbosa Pinheiro

Recife-PE
2013

ARTUR FELIPE SANTOS BARBOSA

**AVALIAÇÃO DA EFICÁCIA DE DERIVADOS FENOTIAZÍNICOS COMO CANDIDATOS
A FOTOSSENSIBILIZADORES EM FOTOQUIMIOTERAPIA ANTIPARASITÁRIA
CONTRA *Trypanosoma cruzi* E *Leishmania braziliensis***

Tese apresentada ao Programa de Pós-Graduação em Ciências Biológicas da Universidade Federal de Pernambuco, como requisito para obtenção do título de **Doutor em Ciências Biológicas**

Área de Concentração: Química Medicinal

Aluno: Artur Felipe Santos Barbosa

Orientadora: Profa. Dra. Suely Lins Galdino (*In memoriam*)

Prof. Dr. Ivan da Rocha Pitta

Co-orientador: Prof. Dr. Antônio Luiz Barbosa Pinheiro

Recife-PE
2013

Catálogo na fonte

Elaine Barroso

CRB 1728

Barbosa, Artur Felipe Santos

Avaliação da eficácia de derivados fenotiazínicos como candidatos a fotossensibilizadores em fotoquimioterapia antiparasitária contra *Trypanosoma cruzi* e *Leishmania braziliensis*/ Recife: O Autor, 2013.

144 folhas : il., fig., tab.

Orientadores: Suely Lins Galdino e Ivan da Rocha Pitta

Coorientador: Antonio Luiz Barbosa Pinheiro

**Mestrado (dissertação) – Universidade Federal de Pernambuco,
Centro de Ciências Biológicas, Ciências Biológicas, 2013.**

Inclui bibliografia e anexos

- 1. Terapêutica I. Galdino, Suely Lins (orientadora) II. Pitta, Ivan da Rocha (orientador) III. Pinheiro, Antonio Luiz Barbosa (coorientador) IV. Título**

FOLHA DE APROVAÇÃO**DESCOBERTA DE UMA NOVA ABORDAGEM PARA FOTOQUIMIOTERAPIA
ANTIPARASITÁRIA COMO UMA FORMA DE TRATAMENTO CONTRA *Trypanosoma*
cruzi E *Leishmania braziliensis***

Tese apresentada a Universidade Federal de Pernambuco (UFPE), como parte das exigências do Programa de Pós-Graduação em Ciências Biológicas – Área de concentração: Química Medicinal, para obtenção do título de Doutor em Ciências Biológicas.

TESE APRESENTADA: 28/11/2013

DECISÃO: APROVADA

Banca Examinadora

Prof. Dr. Ivan da Rocha Pitta (Orientador)

Prof. Dr. Antônio Luiz Barbosa Pinheiro (Co-orientador)

Profa. Dra. Adriana Fontes (Membro Interno)

Profa. Dra. Maira Galdino da Rocha Pitta (Membro Externo)

Prof. Dr. Moacyr Jesus Barreto de Melo Rêgo (Membro Externo)

***Recife-PE
2013***

DEDICATÓRIA

*Ao único que é Digno de receber, a Honra e a Glória, ao Deus eterno imortal, invisível mas
real; a Ele eu dedico!*

AGRADECIMENTOS

Primeiramente a Deus por ser meu Guia em minha jornada, e auxiliar pelos caminhos nos quais devo seguir;

A minha esposa porque somente ela, além de Deus, sabe o que passei por este objetivo, não existe outra mulher no mundo capaz de realizar o que você, Ivana, fez por mim!

Ao meu filho amado Asaph (porque o SENHOR foi benevolente comigo), presente que Deus nos deu para encher a nossa família e ser uma inspiração a prosseguir!

Aos meus pais, que durante toda a minha vida, se empenharam de todas as formas possíveis para que este dia chegasse! Agora chegou minha vez de retribuir!

Ao meu irmão, que vem sendo um belo exemplo de homem para mim, meu amigo para todas as horas, à Hericássia que entrou em nossa família pondo juízo em meu irmão, e ao meu sobrinho Pedrinho, que fez a nossa família se unir ainda mais quando voltamos para Recife.

Ao Professor Pitta, homem fundamental na idealização e realização desta obra, seus olhos viram um juvenzinho sem perspectivas e o lapidaram gerando algo com valor e resultados!

A Profa. Maíra pelo acolhimento, aceitação, estímulo e ensinamentos assemelhando-se demais em todas as virtudes da Profa. Suely Galdino!

Ao Professor Pinheiro, responsável por grandes experiências em minha vida e um relevante transformação em nós!

Ao Centro de Laser da UFBA, onde foram alguns anos inesquecíveis com grandes pesquisadores (Guilherme, Joubert, João, Cristiane, Isabele, Fabiola e Cida).

As “PANTERAS” do Laser (Nicole, Priscila, Suzana, Juliana e Ana Paula) meu muito obrigado!

Ao Prof. Manoel Barral, foi um prazer e honra desfrutar dos seus ensinamentos e de seus alunos (Bruno Sangiorgi e Kiyoshi Fukutani).

A Profa. Milena Botelho, obrigado em acreditar no projeto e ajudá-lo a realizar este sonho!

Aos Alunos do LETI, em especial a Tanira Matutino, Cassio Santana, Tais Soares, Nanashara Carvalho e Marlene Cerqueira, vocês são demais!

Aos novos amigos do LINAT, pois é bom estar de volta a casa e reviver as amizades pernambucanas!

A minha família da Fé, que sempre esteve junto nos fortalecendo e encorajando a nunca tirarmos o foco do nosso Senhor Jesus Cristo (Ap. Doriel, Pra Liane, Dorinho, Lilian, Maca, Messias, Lu, Margo, Mana, Marinho);

RESUMO

A doença de Chagas e a Leishmaniose cutânea são duas doenças de grande relevância a saúde pública mundial. Acredita-se que as duas doenças juntas infectam aproximadamente 20 milhões de pessoas atualmente, em mais de 80 países. *Trypanosoma cruzi* e *Leishmania braziliensis* são os agentes etiológicos da doença de Chagas e Leishmaniose cutânea, respectivamente, e fazem parte da família dos Tripanossomatídeos. De acordo com a Organização Mundial de Saúde, são classificadas como Doenças Tropicais Negligenciadas pela carência de tratamentos disponíveis, sendo os disponíveis repletos de efeitos colaterais, pelos poucos financiamentos de pesquisas para diagnóstico e tratamento das mesmas. Atualmente, estas doenças contam com medicamentos comercializados a mais de 40 anos, os quais já não são tão eficazes em várias situações, além de serem tóxicos e alguns necessitarem de uma intervenção hospitalar. A pesquisa por novos tratamentos e terapias são incentivados pela Organização Mundial de Saúde. A fotoquimioterapia antiparasitária é uma técnica que baseia-se na administração de uma substância sensível a luz (fotossensibilizador) e em seguida, a irradiação desta substância por uma fonte de luz (Laser ou LED), para que haja excitação da molécula fotossensibilizadora e esta reaja com o parasito a ser eliminado através da formação de Espécies Reativas de Oxigênio (EROs). Os derivados fenotiazínicos (azul de metileno e azul de toluidina) apresentaram-se como ótimos candidatos a moléculas fotossensibilizantes. O objetivo deste trabalho foi avaliar a capacidade tripanocida e leishmanicida da Fotoquimioterapia Antiparasitária, utilizando os derivados fenotiazínicos azul de metileno e azul de toluidina, como moléculas fotossensibilizantes, identificando as suas máximas concentrações atóxicas e a melhor configuração do laser excitante destas moléculas. Para avaliar a citotoxicidade dos compostos foram realizados três experimentos distintos (incorporação de timidina tritiada, ensaio com o cristal violeta e através do Alamarblue). Posteriormente foi realizado teste de atividade tripanocida e leishmanicida destes compostos. Testou-se a ação isolada dos compostos (fase escura) contra as diversas formas evolutivas do *T. cruzi* e do *L. braziliensis* bem como com os compostos sendo excitados pelo laser (fase clara). Após estes experimentos constatou-se uma boa ação da Fotoquimioterapia Antiparasitária utilizando os derivados fenotiazínicos como fotossensibilizadores. Os resultados de citotoxicidade pelos três métodos testados, indicaram que a máxima concentração atóxica dos compostos foi equivalente a 20 µg/ml ou 25 µM. O laser em sua melhor configuração ($\lambda = 660$ nm, 40 mW, 4.2 J/cm², CW) ocasionou modificações morfo-estruturais nas formas epimastigotas de *T. cruzi*, porém não apresentou estimulação ou inibição na proliferação parasitária. Foi constatado apenas uma espécie de resistência dos macrófagos irradiados à infecção por amastigotas de *T. cruzi*. Para os *T. cruzi* o composto Azul de Metileno apresentou os melhores resultados como fotossensibilizador associado ao laser, com um IC₅₀ (0,4607 µM) bem menor que o do fármaco padrão de tratamentos que é o benzonidazol (IC₅₀ = 3,8 µM) e contra o *L. braziliensis* o composto Azul de Toluidina apresentou os melhores resultados (10 µg/ml) associado ao laser. Desta forma conclui-se que a Fotoquimioterapia Antiparasitária utilizando os derivados fenotiazínicos Azul de Metileno e Azul de Toluidina como fotossensibilizadores foi eficaz nos ensaios *in vitro* e revela-se promissora para ensaios clínicos contra a doença de Chagas e a Leishmaniose cutânea.

Palavras-Chave: Azul de Metileno, Azul de Toluidina, Fenotiazinas, Laser, Leishmaniose, Doença de Chagas

ABSTRACT

Chagas disease and cutaneous leishmaniasis are two diseases of great importance to public health worldwide. It is believed that the two diseases together infect about 20 million people currently in more than 80 countries. *Trypanosoma cruzi* and *Leishmania braziliensis* are the etiological agents of Chagas disease and cutaneous leishmaniasis, respectively, and are part of the family of trypanosomatids. According to the World Health Organization, are classified as Neglected Tropical Diseases by the lack of treatments available, and the available full of side effects, the few funding research for diagnosis and treatment of the same. Currently, these diseases have marketed drugs for more than 40 years, which are not as effective in many situations, besides being toxic and some requiring hospital intervention. The search for new treatments and therapies are encouraged by the World Health Organization. Antiparasitic Photochemotherapy is a technique that is based on the administration of a substance sensitive to light (photosensitizer), and then irradiation of the substance by a light source (laser or LED), so that there excitation photosensitizer and the molecule that react with the parasite to be eliminated. Phenothiazine derivatives (methylene blue and toluidine blue) were as great candidates photosensitizing molecules. The aim of this study was to evaluate the ability trypanocidal and leishmanicidal of the Antiparasitic Photochemotherapy, using phenothiazine derivatives as methylene blue and toluidine blue as photosensitizing molecules, identifying their maximum non-toxic concentrations and the best configuration of the laser that exciting these molecules. To evaluate the cytotoxicity of the compounds were performed three separate experiments (tritiated thymidine incorporation, crystal violet assay and AlamarBlue). Later tests were trypanocidal and leishmanicidal activity of these compounds. We tested whether the isolated action of the compounds (dark phase) against the various evolutives forms of *T. cruzi* and *L. braziliensis* as well as the compounds being excited by the laser (light phase). After these experiments it was found a good action Antiparasitic Photochemotherapy using phenothiazine derivatives as photosensitizers. The results of cytotoxicity by three methods indicated that the highest non-toxic concentration of the compounds was equivalent to 20 mg / ml or 25 μ M. The laser in its best configuration ($\lambda = 660$ nm, 40 mW, 4.2 J/cm², CW) caused morpho-structural changes in epimastigotes of *T. cruzi*, but no showed stimulation or inhibition of parasite proliferation. It featured in only one species of resistance to infection by macrophage irradiated amastigotes of *T. cruzi*. For the *T. cruzi*, the compound Methylene Blue showed the best results as a photosensitizer associated with the laser, with an IC₅₀ (0.4607 μ M) much smaller than the standard drug treatments is benznidazole (IC₅₀ = 3.8 μ M) and against the *L. braziliensis* compound toluidine blue showed the best results (10 μ g/ml) associated with the laser. Thus it is concluded that the Antiparasitic Photochemotherapy using phenothiazine derivatives as methylene blue and toluidine blue as photosensitizer was effective in *in vitro* and shows promise for clinical trials against Chagas disease and cutaneous leishmaniasis.

Key Words: Methylene blue, toluidine blue, Phenothiazines, Laser, leishmaniasis, Chagas disease

LISTA DE FIGURAS DA REVISÃO BIBLIOGRÁFICA

Figura 1: A – Amastigotas <i>Leishmania sp</i> ; B – Promastigotas de <i>Leishmania sp</i> . Obtidos: http://dpd.cdc.gov/dpdx/HTML/ImageLibrary/Leishmaniasis_il.htm	22
Figura 2: Ciclo de vida <i>Leishmania sp</i> . Obtido: http://www.cdc.gov/parasites/leishmaniasis/biology.html	22
Figura 3: Carlos Chagas no dia de sua posse como professor catedrático de Medicina Tropical da Faculdade de Medicina do Rio de Janeiro. Rio de Janeiro, 23 maio 1925. Departamento de Arquivo e Documentação da Casa de Oswaldo Cruz /Fiocruz. Obtido em: http://www.fiocruz.br/chagas/cgi/cgilua.exe/sys/start.htm?sid=33	24
Figura 4: Ciclo de vida do <i>Trypanosoma cruzi</i> . Obtido em: http://www.google.com.br/imgres?rlz=1C1NNVC_enBR492BR497&biw=1600&bih=799&tbm=isch&tbnid=FvYxNJA2kRsgM:&imgrefurl=http://pt.wikipedia.org/wiki/Doen%25C3%25A7a_de_Chagas&docid=3eY4sPHnMFQ15M&imgurl=http://upload.wikimedia.org/wikipedia/commons/a/a9/Chagas_ciclo_de_doen%2525C3%2525A7a.JPG&w=700&h=533&ei=paKkUcjCMZDo8QSsmICIAQ&zoom=1&ved=1t:3588,r:0,s:0,i:92&iact=rc&dur=802&page=1&tbnh=176&tbnw=231&start=0&ndsp=20&tx=147&ty=100	26
Figura 5: Formas evolutivas do <i>T. cruzi</i> . A – tripomastigotas sanguíneas; B – Epimastigotas; C – tripomastigotas metacíclicas; D- Amastigota intracelular. Obtidas em: http://www.fiocruz.br/chagas/cgi/cgilua.exe/sys/start.htm?sid=69	27
Figura 6: Benzonidazol: <i>N</i> -benzyl-2-(2-nitro-1 <i>H</i> -imidazol-1-yl)acetamide (COURA, 2002)....	28
Figura 7: Nifurtimox: 3-methyl- <i>N</i> -[(1 <i>E</i>)-(5-nitro-2-furyl)methylene] thiomorpholin-4-amine 1,1-dioxide (COURA, 2002).....	28
Figura 8: Diagrama de Jablonski, demonstrando como um fotossensibilizador (FS), quando excita por uma Energia (E), sai do seu estado fundamental para um estado mais excitado chamado singleto. Em seu estado singleto a molécula poderá voltar ao seu estado fundamental (Fluorescência) ou passar para uma estágio intermediário denominado tripleto e deste retornar ao seu estado fundamental (Fosforecência). Em seu estado tripleto, o fotossensibilizador poderá reagir com as moléculas de O ₂ presentes na vizinhança e desencadear as reações do tipo I e II, gerando produtos tóxicos e aumentando a citotoxicidade no interior das células tratadas.....	31
Figura 9 – Artigo 2 (A,B) Control group; (C,D,E) Laser treated.....	52
Figura 10 – Artigo 3 Cytotoxicity Assay – Methylene Blue values.....	57
Figura 11 – Artigo 3 Percentage of lysis of the parasites.....	61

LISTA DE TABELAS DA REVISÃO BIBLIOGRÁFICA

<i>Tabela 1.</i> Derivados fenotiazínicos avaliados como potenciais fotossensibilizadores contra Tripanossomatídeos.....	<i>34</i>
<i>Tabela 2.</i> Artigo 1 - Percentage Lethality for Each Parameter Tested (Photosensitizer, Photosensitizer Concentration, Incubation Time, and Energy Density).....	<i>45</i>
<i>Tabela 3.</i> Artigo 5: Percentage of lethality.....	<i>71</i>

LISTA DE SIGLAS E ABREVIACES

AT - Azul de Toluidina

DNA – Ácido Desoxirribonucleico

DNDi - (*Iniciativa* Medicamentos para Doenas Negligenciadas

EROs – Esp cies Reativas de Oxig nio

FBML - Fotobiomodula  o a Laser

FQTAp - Fotoquimioterapia Antiparasit ria

H₂O₂ – Per xido de Hidrog nio

HeNe - h lio-ne nio

L. donovani - *Leishmania donovani*

LAFEPE - Laborat rio Farmac utico do Estado de Pernambuco

Laser – Light Amplification by Stimulated Emission Radiation

MB – Methylene Blue (Azul de Metileno)

nm - nan metro

O₂⁻ - Oxig nio

OMS - Organiza  o Mundial de Sa de

ROS - do ingl s esp cies reativas de oxig nio

SMF - Sistema Mononuclear fagocit rio

SOD - Super xido Dismutase

TBO – Toluidine blue (Azul de Toluidina)

T. brucei brucei – *Trypanosoma brucei brucei*

T. brucei gambiensi – *Trypanosoma brucei gambiensi*

T. brucei rhodensiense - *Trypanosoma brucei rhodensiense*

T. cruzi – *Trypanosoma cruzi*

T. evansi - *Trypanosoma evansi*

SUMÁRIO

1.1.INTRODUÇÃO.....	14
1.2. OBJETIVOS.....	16
1.2.1. Geral.....	16
1.2.2. Específicos.....	16
2.REVISÃO LITERATURA.....	17
2.1.Tripanosomatídeos:.....	17
2.2. Leishmaniose	18
2.3. Leishmaniose - Tratamento:	20
2.4. Doenças de Chagas	21
2.5. Doença de Chagas – Tratamento:	24
2.6. Fotoquimioterapia Antiparasitária - FQTAp	26
2.7. Fontes de Luz	28
2.8. Fotossensibilizadores	30
3. RESULTADOS: Artigos Publicados em Periódicos ou Proceedings.....	32
3.1. Photodynamic Antimicrobial Chemotherapy (PACT) Using Phenothiazine Derivatives as Photosensitizers Against <i>Leishmania braziliensis</i> / Fotoquimioterapia Antiparasitária (FQTAp) utilizando derivados fenotiazínicos como fotossensibilizadores contra <i>Leishmania braziliensis</i>	33
3.2.Morpho-Structural Effects Caused by 660nm Laser Diode in Epimastigotes Forms of <i>Trypanosoma cruzi</i> : In Vitro Study / Efeitos morfo-estruturais causados por diodo laser 660nm em formas epimastigotas de <i>Trypanosoma cruzi</i> : estudo <i>in vitro</i>	52
3.3. Evaluation of Photodynamic Antimicrobial Therapy (PACT) against Trypomastigotes of <i>Trypanosoma cruzi</i> : In Vitro Study / Avaliação da Fotoquimioterapia Antiparasitária (FQTAp) contra tripomastigotas de <i>Trypanosoma cruzi</i> : Estudo <i>in vitro</i>	57
3.4.Evaluation of Photodynamic Antimicrobial Therapy (PACT) against promastigotes Form of the <i>Leishmania (Viannia) braziliensis</i> : In Vitro Study / Avaliação de Fotoquimioterapia Antiparasitária (FQTAp) contra formas promastigotas de <i>Leishmania (Viannia) braziliensis</i> : Estudo <i>in vitro</i>	63
3.5. In vitro study of the Photodynamic Antimicrobial Therapy (PACT) against promastigotes form of the <i>Leishmania (Viannia) braziliensis</i> : In Vitro Study /	

Estudo <i>in vitro</i> da Fotoquimioterapia Antiparasitária (FTQAp) contra formas promastigotas de <i>Leishmania (Viannia) braziliensis</i> : Estudo <i>in vitro</i>	70
4. DISCUSSÃO.....	79
5. CONCLUSÕES.....	83
6. PERSPECTIVAS.....	85
7. REFERÊNCIAS.....	86
8. ANEXOS.....	93
8.1. Resultados Complementares para <i>T. cruzi</i>.....	94
8.2. Anexos: Artigos.....	97
8.2.1. Light microscopic description of the effects of laser phototherapy on bone defects grafted with mineral trioxide aggregate, bone morphogenetic proteins, and guided bone regeneration in a rodent model	98
8.2.2. Bone Repair on Fractures Treated with Osteosynthesis, ir Laser, Bone Graft and Guided Bone Regeneration: Histomorfometric Study.....	109
8.2.3. Effects of LED phototherapy on bone defects grafted with MTA, bone morphogenetic proteins and guided bone regeneration: a Raman spectroscopic study.....	116
8.2.4. Does LED phototherapy influence the repair of bone defects grafted with MTA, bone morphogenetic proteins, and guided bone regeneration? A description of the repair process on rodents	131
8.2.5. The efficacy of the use of IR laser phototherapy associated to biphasic ceramic graft and guided bone regeneration on surgical fractures treated with miniplates: a Raman spectral study on rabbits.....	144
8.2.6. The efficacy of the use of IR laser phototherapy associated to biphasic ceramic graft and guided bone regeneration on surgical fractures treated with wire osteosynthesis: a comparative laser fluorescence and Raman spectral study on rabbits.....	151
8.2.7. Effect of the laser and light-emitting diode (LED) phototherapy on midpalatal suture bone formation after rapid maxilla expansion: a Raman spectroscopy analysis	160
8.2.8. Raman Study of the Effect of LED Light on Grafted Bone Defects.....	170
8.2.9. Raman study of the repair of surgical bone defects grafted with biphasic synthetic microgranular HA+ β -calcium triphosphate and irradiated or not with λ 780 nm laser	178

8.2.10. Use of Laser Fluorescence in Dental Caries Diagnosis: a Fluorescence x Biomolecular Vibrational Spectroscopic Comparative Study	191
9. PREMIAÇÕES.....	197

1. INTRODUÇÃO

A família Trypanosomatidae é composta por um grande grupo de protozoários parasitas flagelados que causam infecções em humanos e animais. As doenças infecciosas mais importantes para o homem são causadas por espécies de *Trypanosoma* (doença do sono e doença de Chagas) e *Leishmania* (leishmaniose). A maioria dos afetados por estas doenças parasitárias são as populações de baixa renda dos países em desenvolvimento em áreas tropicais e subtropicais do mundo. Estas doenças são transmitidas ao humanos (ou para outros hospedeiros mamíferos) por um inseto vetor, e afetam mais que 500 mil pessoas pelo mundo. Devido ao fato destas doenças terem poucos tratamentos disponíveis e as pesquisas se limitarem pelos financiamentos, estas têm sido consideradas como Doenças Tropicais Negligenciadas (CAFFREY, 2008).

O tratamento clínico das doenças causadas por tripanossomatídeos continua sendo basicamente através de quimioterápicos. No entanto, as drogas convencionais estão longe de satisfazer a demandas atuais das populações endêmicas, devido ao seu custo, problemas de toxicidade e de resistência, resultando em uma urgente necessidade de identificar e desenvolver novas alternativas terapêuticas (FIDALGO, 2011). De acordo com o DNDi (*Iniciativa Medicamentos para Doenças Negligenciadas*) são necessárias melhores opções de tratamento para todas as infecções tropicais.

Em sua essência, a Fotoquimioterapia Antiparasitária significa destruição de células ou tecidos-alvo induzida por uma reação fotoquímica onde uma luz em comprimento de onda específico excita uma substância fotossensível (fotossensibilizador). O fotossensibilizador ativado e na presença do oxigênio da célula, pode reagir com moléculas na sua vizinhança por transferência de elétrons ou hidrogênio, levando a produção de radicais livres (reação tipo I) ou por transferência de energia ao oxigênio molecular distribuído pelo sistema vascular (reação tipo II), levando a produção de oxigênio singlete, altamente oxidante. Ambos os caminhos podem levar a morte celular e a destruição de tecido doente (BARBOSA, 2012).

O objetivo deste trabalho foi avaliar a possibilidade e os melhores parâmetros da Fotoquimioterapia Antiparasitária - FQTAp contra parasitas da família dos Tripanossomatídeos (*Trypanosoma cruzi* e *Leishmania braziliensis*). Para isto, buscou-se avaliar a citotoxicidade dos derivados fenotiazínicos utilizados como fotossensibilizadores, avaliou-se a atividade fotossensibilizante dos derivados fenotiazínicos contra os parasitos e analisou-se todos os dados obtidos para se determinar o melhor ajuste de Dose, Potência e comprimento de onda do Laser

em combinação com diferentes concentrações dos fotossensibilizadores e seus respectivos tempos de pré-incubação.

Um dos principais problemas com os medicamentos convencionais é seu único sítio e modo de ação. Após determinada exposição, a maioria dos microrganismos são capazes de desenvolver mecanismos resistentes para um único ponto de ataque. (CORREA et al, 2001, PARVEEN, 2005; LIMA e BARREIRO, 2005) Ao contrário dos medicamentos convencionais, os fotossensibilizadores agem via produção de oxigênio singlete e ROS (do inglês espécies reativas de oxigênio), os quais não apresentam uma especificidade com relação ao alvo biomolecular, reagindo rapidamente com uma variedade de substratos incluindo o colesterol, acilas insaturadas das camadas lipídicas das membranas, resíduos de aminoácidos tais como cisteína, histidina e triptofano das proteínas, bem como bases de ácidos nucleicos do DNA, particularmente a guanina e timina. Desta forma, a fotodinamização poderá induzir danos nas biomoléculas que conduzirão à perda da funcionalidade biológica apropriada, levando a inativação da célula. (CAMINOS, 2006)

As fenotiazinas tem demonstrado grande afinidade pelos Tripanossomatídeos (T'UNG, 1938, FERREIRA, 2006; BUCHHOLZ, 2008) Possuem ação contra duas enzimas importantes, a Trypanothiona redutase e a Superóxido Desmutase. Todos estes tripanossomatídeos possuem em comum uma única via de metabolismo de thiol no qual o sistema ubíquo glutathione / glutathione redutase é substituído por trypanothione e trypanothione redutase (metabolismo antioxidante). Uma outra enzima encontrada nos tripanossomatídeos, a Superóxido Dismutase (SOD) (TEMPERTON, 1998), tem seu mecanismo de ação envolvidos com enzimas antioxidantes as quais catalizam a dismutação do O_2^- a H_2O_2 e O_2 protegendo a catalase e a peroxidase contra a inibição pelo O_2^- , que pode ser proveniente dos derivados fenotiazínicos como demonstrado por Kim et al (2001).

Baseado nas informações existentes sobre a eficácia da FQTAp contra vírus, fungos e bactérias, agindo principalmente sobre suas membranas ou estruturas internas, associado a afinidade e atuação química que os derivados fenotiazínicos possuem pelos tripanossomatídeos, acreditamos que esta nova abordagem para uma Fotoquimioterapia Antiparasitária, utilizando derivados fenotiazínicos como fotossensibilizadores, também será eficaz contra o *Trypanosoma cruzi* e *Leishmania braziliensis*.

1.2. OBJETIVOS

1.2.1. Geral

- Verificar a melhor condição de Fotoquimioterapia Antiparasitária sobre parasitos de *Trypanosoma cruzi* e *Leishmania braziliensis*

1.2.2. Específicos

- Avaliar citotoxicidade dos novos compostos candidatos a fotossensibilizantes;
- Avaliar a atividade fotossensibilizante dos novos compostos contra o parasito do *Trypanosoma cruzi* e *Leishmania braziliensis*
- Analisar o melhor ajuste de Dose e potência do Laser, a serem empregados na Fotoquimioterapia Antiparasitária associados as melhores concentrações dos fotossensibilizadores;

2. REVISÃO BIBLIOGRÁFICA

2.1. Tripanosomatídeos:

Trypanosoma cruzi e *Leishmania sp.* são protozoários parasitas unicelular e uniflagelados, pertencentes ao filo *Euglenozoa*, classe *Mastigophora*, ordem *Kinetoplastida* e família *Trypanosomatidae*, que é uma das linhagens mais antigas da evolução dos *Eucariotas*, responsáveis pela Doença de Chagas e a Leishmaniose, respectivamente. Estas doenças são transmitidas ao humanos (ou para outros hospedeiros mamíferos) por um inseto vetor, e afetam mais que 500 mil pessoas pelo mundo. Durante a infecção, estes parasitas migram através da circulação do hospedeiro, onde eles tem que evitar a resposta imune inata do hospedeiro, e infectar as células (SIQUEIRA-BATISTA, 2007, CESTARI, 2013).

Assim, as características típicas dos tripanosomatídeos extracelulares são: (a): corpo em geral alongado contendo um único flagelo, que emerge na extremidade anterior da célula (o protozoário nada com o flagelo à frente, isto é, o batimento flagelar puxa o corpo); (b) o cinetoplasto, um local da mitocôndria (um túbulo alongado e único) onde DNA mitocondrial (próximo ao flagelo) está acumulado. Um conjunto de microtúbulos subpeliculares regularmente espaçados está presente abaixo da membrana plasmática (ICC/FIOCRUZ, 2013).

O ciclo de vida das espécies patogênicas aos humanos envolve a adaptação do parasita a viver dentro do inseto vetor ou o hospedeiro mamífero. Para lidar com diferentes ambientes do hospedeiro, esses organismos têm desenvolvido mecanismos adaptativo baseados em recursos bioquímicos e ultra estruturais excepcionais (MANTA, 2013).

O primeiro tripanosoma foi descoberto, evidentemente, sem qualquer relação a essas doenças devastadoras, como um aparentemente e inofensivo parasita no sangue dos símios em meados do século 19. Em geral, porém, as pesquisas relacionadas foram impulsionadas por pressão econômica, seja por problemas na pecuária devido à doenças no gado na faixa endêmica, pela mosca tsé-tsé, ou as perdas no comércio de escravos, devido à doença do sono Africana, ou a preocupação dos governos coloniais com a saúde de seus soldados e oficiais na África. Não surpreendentemente, o primeiro tripanosoma patogênico a ser identificado foi aquele que afeta o gado, tais como *T. evansi* causando surra em cavalos e *T. brucei brucei* causando nagana ao gado. Os mais importantes parasitos que infectam humanos foram aqueles identificados na primeira década do Século 20: *T. brucei gambiensi* em 1902 por Joseph Everett Dutton, *L. donovani* por William Leishman e Charles Donovan em 1903, *L. braziliensis* por Gaspar Viana em 1906, *T. cruzi*, por Carlos Chagas em 1909 e o *T. brucei rhodensiense* em 1910 por John William Watson Stephens e Harold Benjamin Fantham (FLOHÉ, 2012).

2.2. Leishmaniose

Leishmaniose é uma infecção ocasionada por protozoários parasitas transmitidos para os mamíferos, incluindo os seres humanos, pela picada de um minúsculo inseto vetor, apenas 2-3 mm de comprimento, o flebotomíneo, e clinicamente classificadas em três formas: visceral, cutânea e mucocutânea (DE MUYLDER, 2011; TAVARES, 2011). A Leishmaniose ameaça cerca de 350 milhões de pessoas em 88 países pelo o mundo e estima-se que cerca de 12 milhões de pessoas atualmente estejam infectadas, com cerca de 1-2 milhões de novos casos estimados que ocorrem a cada ano (MONTE-NETO, 2011).

Os parasitas residem intracelularmente causando a doença. Os hospedeiros primários são vertebrados, entre eles os humanos, cães e ratos. Depois da Malária e da Doença do Sono, a Leishmaniose é a terceira mais importante doença transmitida por insetos e em nono lugar no ranking global de todas as doenças infecciosas e parasitárias. Aproximadamente 90% da Leishmaniose cutânea ocorre no Afeganistão, Paquistão, Síria, Arábia Saudita, Argélia, Irã, Brasil e Perú (STOCKDALE, 2013).

Os protozoários do gênero *Leishmania* são os agentes etiológicos da doença tegumentar ou visceral em humanos. As diferenças entre as espécies de *Leishmania* resultam na diversidade de manifestações clínicas na leishmaniose. *Leishmania braziliensis* é o agente etiológico da Leishmaniose Cutânea Americana, a qual a caracterizada por sua cronicidade e a possibilidade de uma metástase levando a forma clínica denominada mucocutânea. (TAVARES, 2011).

No momento em que um a fêmea de um flebotomíneo infectado realiza o repasto sanguíneo, injeta parasitos em seu estágio infectivo (promastigota) (Figura 1b) no hospedeiro vertebrado, através da probóscide do inseto. Os promastigotas que chegam até o local da picada são fagocitados pelos macrófagos e outros tipos de células mononucleares fagocitárias. No interior destas células, os promastigotas transformam-se na forma intracelular deste parasita, amastigota (Figura 1a). Estes amastigotas continuam a se multiplicar por divisão simples e procedem a infecção de outras células mononucleares fagocitárias. Alguns fatores que interagem entre os parasitas e o hospedeiro afetam e/ou determinam o curso da infecção,

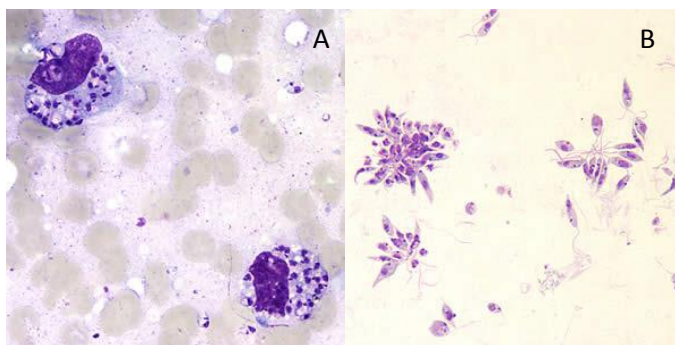


Fig. 1: A – Amastigotas *Leishmania* sp; B – Promastigotas de *Leishmania* sp. Obtidos: http://dpd.cdc.gov/dpdx/HTML/ImageLibrary/Leishmaniasis_il.htm

resultando nas formas de Leishmaniose visceral ou cutânea. Posteriormente, um novo inseto, ao picar este hospedeiro infectado, ingerirá sangue com macrófagos infectados com amastigotas, e no intestino do inseto, estes amastigotas transformam-se em promastigotas e em seguida migram para a probóscide do inseto conforme figura (Figura 2) (CDC, 2013).

As apresentações clínicas da Leishmaniose cutânea variam desde ulcerações na pele a vários graus de envolvimento das mucosas (cutânea difusa ou muco cutânea). A mortalidade associada à Leishmaniose cutânea não é significativa, no entanto, a morbidade, sob a forma de deformação, com a subsequente estigma social, que surge a pessoas têm a crença de que partir

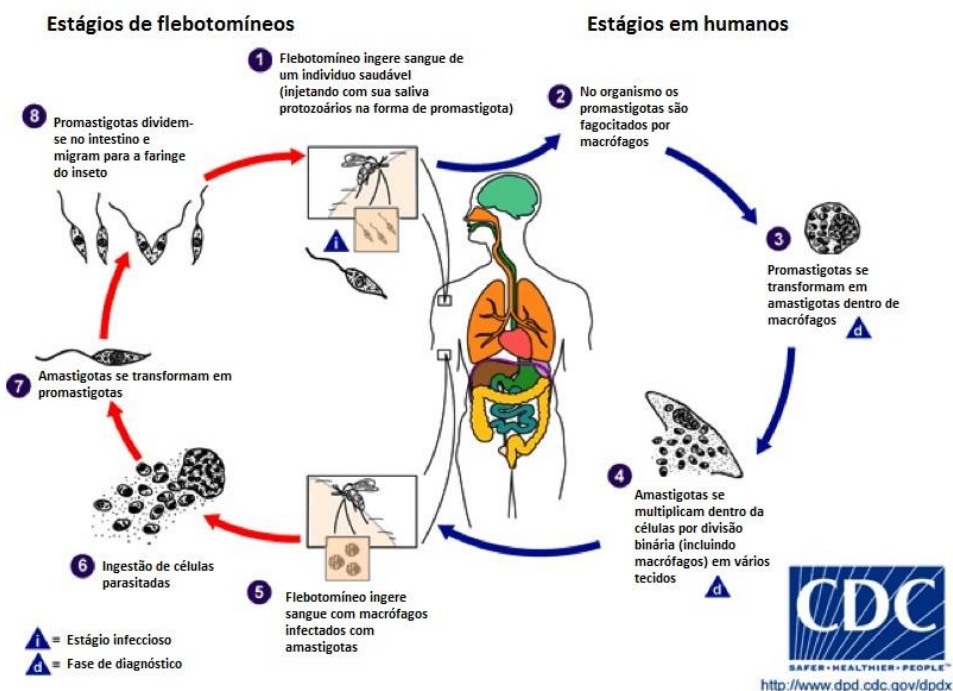


Fig. 2 - Ciclo de vida *Leishmania* sp. Obtido em <http://www.cdc.gov/parasites/leishmaniasis/biology.html>

de lesões cutâneas e as cicatrizes resultantes são muito importante. Em áreas endêmicas, muitas a doença pode ser transferido através do contato físico, resultando em restrição de participação social. Indiscutivelmente, os efeitos econômicos e na saúde ocasionados pela doença causam um impacto na qualidade de vida e na saúde mental dos pacientes resultante de estigma social (STOCKDALE, 2013).

2.3. Leishmaniose - Tratamento:

Devido à falta de uma vacina segura e eficaz, a quimioterapia tem sido uma alternativa preferida no controle desta doença, e em particular os antimoniais pentavalentes que têm sido utilizados no tratamento das lesões cutâneas. No entanto, os efeitos adversos foram notificados desde os primeiros testes em populações afetadas, incluindo outros vertebrados, tais como caninos, sendo esta toxicidade principalmente relacionada com danos no fígado e pâncreas. Tendo em conta estes efeitos adversos, a segurança das formulações de antimoniais pentavalentes está sendo objeto de intenso debate, sugerindo que estas formulações também são potencialmente imunotóxicas. Outro aspecto importante relacionado com esta doença são seus altos encargos econômicos impostos pelo seu tratamento no Sistema de Saúde (DELGADO, 2011).

Vários medicamentos disponibilizados para o tratamento da leishmaniose já possuem mais de 50 anos. O desenvolvimento de novos procedimentos terapêuticos tem sido um dos setores mais interessantes da medicina humana e veterinária. O principal alvo de novas drogas é o combate contra o parasita em seus diferentes aspectos: fisiológicos e bioquímicos, e para promover a resposta imune do hospedeiro. Até agora, não tem-se visto medicamentos que pareçam ser eficaz, de baixo custo financeiro, fácil de manipular, e sem quaisquer efeitos secundários, ao mesmo tempo (MASMOUDI, 2013).

Alguns tratamentos sistêmicos tem sido utilizados para o tratamento da leishmaniose cutânea. Derivados de Antimoniais Pentavalentes como o Glucantime (antimoniato de meglumine) (Figura 3A) tem sido utilizado atualmente e preferencialmente ao francofone e o stibogluconato, como medicamentos de primeira opção para o tratamento da leishmaniose cutânea (MASMOUDI, 2013).

A anfotericina B (Figura 3B) é o segundo fármaco de escolha, quando não há nenhuma resposta ao tratamento com antimoniais ou quando não é possível utilizá-lo. O Isotionato de Pentamidina (Figura 3C), o terceiro fármaco de escolha, é utilizado já há alguns anos contra a

leishmaniose visceral e tem sido usado atualmente em diferentes protocolos para o tratamento de leishmaniose cutânea (BARBOSA, 2012).

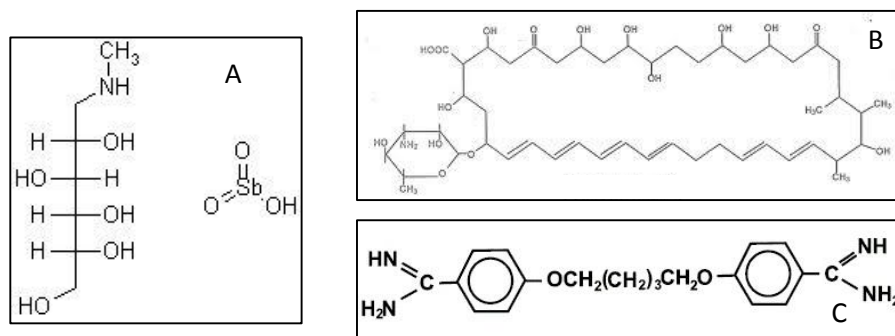


Fig. 3- Estrutura química dos compostos utilizados para o tratamento da Leishmaniose: A- Glucantime; B- Anfotericina B; C- Isotionato de Pentamidina.

Vários efeitos colaterais tem sido atribuídos a estes compostos e podem ser observados na literatura (BARBOSA, 2012; MASMOUDI, 2013).

Outros tipos de tratamentos também veem sendo empregados no tratamento da leishmaniose cutânea como: injeções intralesional com derivados antimoniais pentavalentes, a crioterapia (baseado na sensibilidade do parasito a baixas temperaturas ocasionada pela aplicação do Nitrogênio líquido através de um criospray), antibióticos (Paromomicina), Termoterapia (realizando um aquecimento controlado que é doloroso e requer anestesia), além de técnicas promissoras *in vivo* como a eletroterapia e a fitoterapia (MASMOUDI, 2013)

2.4. Doenças de Chagas

A doença de Chagas (Tripanossomíase Americana), descoberta por Carlos Chagas (Figura 4) em 1909 através de um grande feito na medicina onde identificou a doença, o agente vetor e o parasito, é causado por um protozoário intracelular obrigatório chamado *Trypanosoma cruzi* (Bilate, 2008). É endêmica entre as Américas do Sul e Central, onde estima-se que cerca de 8 a 11 milhões de pessoas estão infectadas com o parasito e a cada ano que de 10 a 14 mil pessoas morram por conta da doença. É reconhecida pela Organização Mundial de Saúde (OMS) como uma das 13 doenças tropicais mais negligenciadas no mundo (COURA, 2010; RASSI, 2012; NAKAJIMA-SHIMADA, 2013).



Fig. 4: Carlos Chagas no dia de sua posse como professor catedrático de Medicina Tropical da Faculdade de Medicina do Rio de Janeiro. Rio de Janeiro, 23 maio 1925. Departamento de Arquivo e Documentação da Casa de Oswaldo Cruz /Fiocruz. Obtido em: <http://www.fiocruz.br/chagas/cgi/cgilua.exe/sys/start.htm?sid=33>

A doença de Chagas afeta principalmente as populações pobres, rurais e apresenta duas fases clínicas: a fase aguda, que aparece logo após a infecção, e a fase crônica, a qual desenvolve-se em cerca de um terço das pessoas infectadas após um período assintomático (fase indeterminada) que pode durar anos ou décadas (BILATE, 2008; CLAYTON, 2010; DE CASTRO 2011).

O *T. cruzi*, pode ser transmitido para humanos através dos seguintes mecanismos divididos em dois grupos: (i) de insetos triatomíneos sugadores de sangue, por via oral ou contato com o sangue contaminado, e (ii) por acidentes de laboratórios, manejo de animais infectados, transplantes de órgãos, transmissão sexual, ferimentos, contato com esperma ou fluido menstrual contaminado e, hipoteticamente, inoculação criminal proposital ou contaminação de comida com o parasita (CHAGAS, 1909; MONCAYO, 2009; DIAS, 1997; COURA, 2007, DE CASTRO, 2011). Recentemente, a doença de Chagas vem gerando uma nova preocupação devido a globalização mundial, onde a imigração de indivíduos infectados para regiões não-endêmica, tem espalhado a doença (DE CASTRO, 2011).

O ciclo de vida (Figura 5) deste parasita envolve um inseto vetor triatomíneo hematófago, e diversos hospedeiros animais (mamíferos). Inicialmente, os tripomastigotas sanguíneos (Figura 6a) são ingeridos pelos insetos no momento que picam e sugam o sangue de um animal infectado. Em seguida, estes tripomastigotas são convertidos em epimastigotas (Figura 6b) no intestino deste inseto, e em sua porção posterior, se proliferam e diferenciam em

formas tripomastigotas metacíclicos (Figura 6c), por um processo denominado metaciclogênese (BONALDO, 1991; DE CASTRO, 2011). Estas formas evolutivas, misturam-se em meio as fezes e urina do inseto a serem excretadas pelo inseto. Ao realizar o hematofagismo, o inseto infectado alimenta-se do sangue do hospedeiro invertebrado o que o força a eliminar sua massa de excreta depositada em seu sistema digestivo, sendo geralmente depositada na superfície da pele. Nestas fezes encontra-se a forma infectante tripomastigota metacíclico. Devido à movimentação dos parasitos e a presença de enzimas histolíticas, o indivíduo picado causa escoriações ou feridas na pele facilitando a entrada dos protozoários para a circulação e para outras regiões do corpo como a mucosa ocular, formando o conhecido **Sinal de Romana**. Os tripomastigotas metacíclicos são extremamente infectantes, podendo invadir os primeiros tipos celulares que encontram – fibroblastos, macrófagos ou células epiteliais, que geralmente os fagocitam. No interior destes elementos do Sistema Mononuclear fagocitário (SMF), ocorre à proliferação e liberação de formas tripomastigotas e estas formas por sua vez podem atingir a corrente circulatória e atingir todos os tecidos do hospedeiro, onde sofreram por grandes transformações estruturais tornando-se amastigotas (Figura 6d) multiplicativos. Tais formas sofrerão uma série de divisões binárias sucessivas no interior das células infectadas. Aproximadamente 12 horas antes da ruptura da célula, as formas amastigotas transformam-se em tripomastigotas sanguíneas, os quais após a lise das células, poderão invadir novas células, viabilizando a permanência no hospedeiro. (SIQUEIRA-BATISTA, 2007; FIOCRUZ-DE SOUZA, 2009).

As manifestações clínicas apresentadas na fase aguda podem variar entre febre, taquicardia não relacionada com o grau de hipertermia, linfadenopatia, esplenomegalia leve e edemas. As células brancas apresentam-se em linfocitose e o envolvimento do coração é semelhante aqueles que ocorrem com outros tipos de miocardites. Já na fase crônica, 2 a 4 meses após as manifestações agudas desaparecerem e os parasitas serem raramente identificados no sangue periférico, a doença entra em sua fase crônica. Em geral, inicia-se com um longo período de latência, denominado forma indeterminada o qual poderá durar vários anos. Após este período vários pacientes relatam o comprometimento de alguns órgãos como o coração, esôfago, cólon e o sistema nervoso, caracterizando a segunda forma clínica (PRATA, 2001).

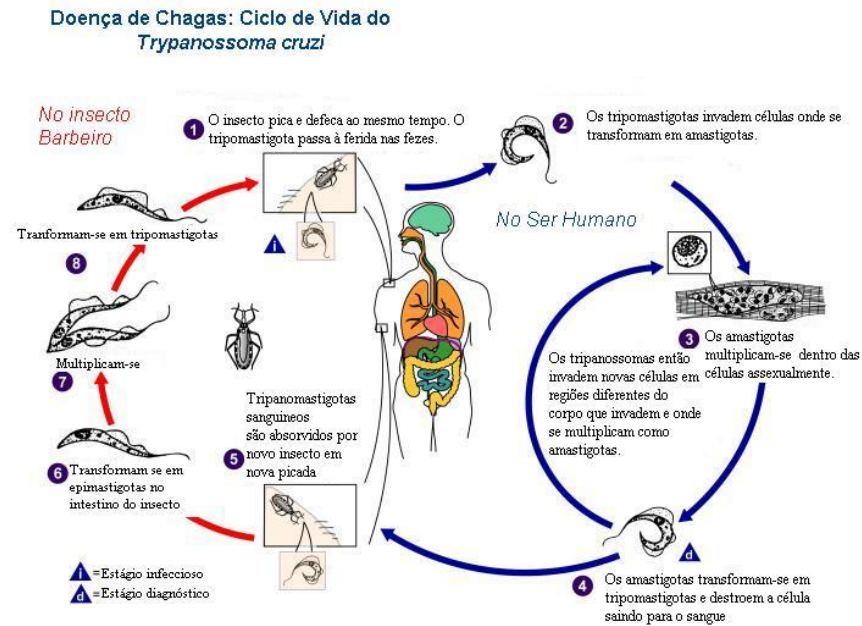


Fig. 5: Ciclo de vida do *Trypanosoma cruzi*. Obtido em:

http://www.google.com.br/imgres?rlz=1C1NNVC_enBR492BR497&biw=1600&bih=799&tbm=isch&tbnid=FvYxNJA2kRsgM:&imgrefurl=http://pt.wikipedia.org/wiki/Doen%25C3%25A7a_de_Chagas&docid=3eY4sPHnMFQ15M&imgurl=http://upload.wikimedia.org/wikipedia/commons/a/a9/Chagas_ciclo_de_doen%2525C3%2525A7a.JPG&w=700&h=533&ei=paKkUcjCMZDo8QSsmICIAQ&zoom=1&ved=1t:3588,r:0,s:0,i:92&iact=rc&dur=802&page=1&tbnh=176&tbnw=231&start=0&ndsp=20&tx=147&ty=100

A prevenção e o controle da Doença de Chagas podem ser feitos através de várias estratégias: tratamento das residências com inseticidas, triagem sanguínea nas transfusões, tratamento com medicamentos em determinados casos, melhoria da estrutura das casas (substituindo paredes e telhados), entre outros (COURA, 2007).

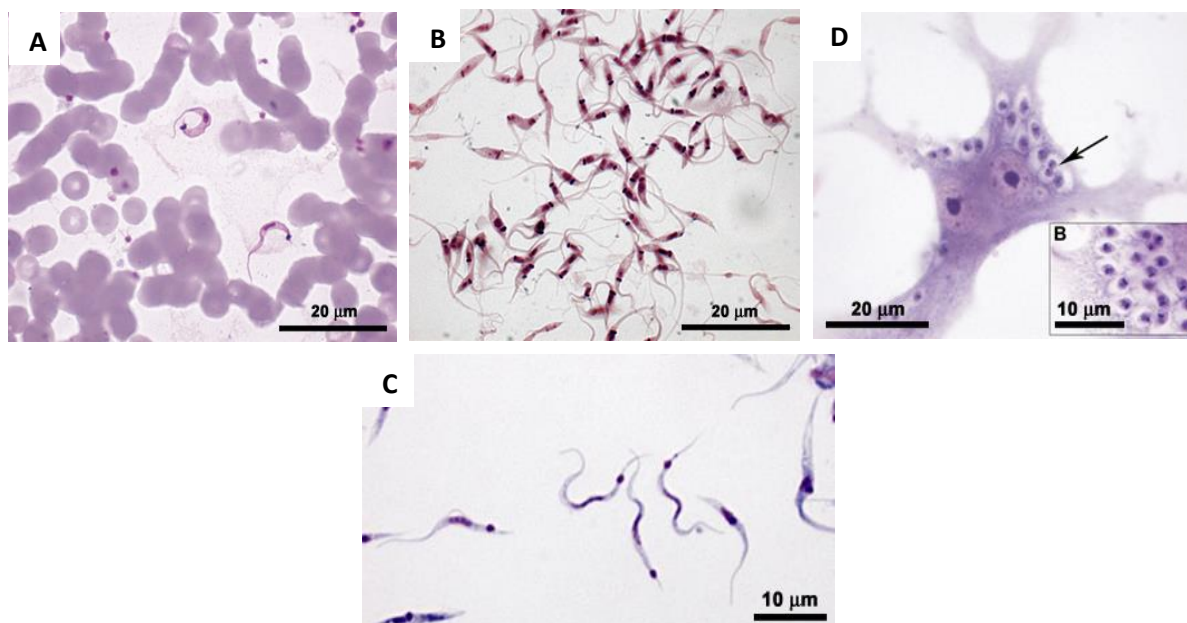


Fig. 6: Formas evolutivas do *T. cruzi*. A – tripomastigotas sanguíneas; B – Epimastigotas; C – tripomastigotas metacíclicas; D- Amastigota intracelular. Obtidos em: <http://www.fiocruz.br/chagas/cgi/cgilua.exe/sys/start.htm?sid=69>

2.5. Doença de Chagas – Tratamento:

Poucos investimentos tem sido alocados para o desenvolvimento de novos agentes anti-*T. cruzi*. Passados mais de 100 anos após o seu descobrimento por Carlos Chagas, a Doença de Chagas, atualmente, só possui dois fármacos com eficácia comprovada para o seu tratamento, o Benzonidazol e o Nifurtimox. Desenvolvidos em meados dos anos 60, são utilizados principalmente para tratar a fase aguda e a etapa inicial da fase crônica da doença. Frequentemente ambas substâncias apresentam efeitos adversos (possuem similaridade química e vias metabólicas comuns possibilitando que haja reações cruzadas entre eles). Apresentam uma relação desfavorável entre suas doses seguras e eficácia de cura na fase crônica tardia. Esta real eficácia do tratamento é desconhecida em virtude da paralisação do tratamento a longo prazo. Desta forma, prefere-se o benzonidazol ao nifurtimox pois este primeiro é mais tolerável, possui uma melhor penetração tecidual e uma melhor eficácia (BERN, 2007; COURA, 2011; PEREZ-MOLINA, 2012; PÉREZ-MOLINA, 2013)

Benzonidazol (Figura 7), um derivado nitroimidazol com atividade contra as formas tripomastigota e epimastigota, é localmente produzido pelo Laboratório Farmacêutico do Estado de Pernambuco (LAFEPE), antes foi produzido pela Roche com o nome Radanil® ou Rochagan®. Ele foi introduzido no mercado, em 1971, e tem sido largamente utilizado como

um agente efetivo para terapia antiparasitária nos casos agudos ou subagudos da doença de Chagas, incluindo transfusões e doenças adquiridas em laboratório e reativação da infecção em transplantados e outros pacientes imunossuprimidos (MARIN-NETO, 2009). Nifurtimox (Figura 8), um derivado nitrofurano, de nome comercial Lampit® (Bayer 2503, Leverkusen, Alemanha) tem sido extensivamente utilizado por mais de três décadas, mas atualmente não é mais recomendado em vários países, incluindo o Brasil (URBINA, 2003; MARIN-NETO, 2009).

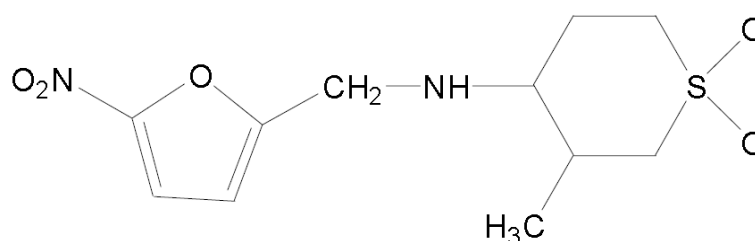


Fig. 7: Benzonidazol: (N-benzyl-2-nitroimidazol acetamida (COURA, 2002)

Benzonidazol e o Nifurtimox são pró-fármacos e precisam submeter-se a uma ativação mediada por enzimas dentro do patógeno para gerar efeitos citotóxicos; reações que são catalisadas pela nitrorredutase tipo II. Estes compostos induzem a formação de espécies reativas de oxigênio (ERO) que em humanos são eliminados pela Superóxido Dismutase I (SOD 1). Os parasitos que tiveram o gene de SOD 1 danificados ficam mais sensíveis a estes compostos (NAKAJIMA-SHIMADA, 2013).

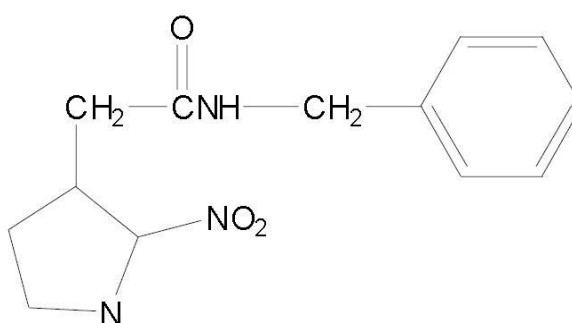


Fig. 8: Nifurtimox: 3-metil-4-(5'-nitrofurfurilidenoamino)tetrahydro-4H-1, 4-tiazina-1,1-dióxido (COURA, 2002)

Diversos efeitos colaterais são descritos na literatura pelo uso destas medicações. Efeitos colaterais cutâneos, gastrointestinais e neurológicos são mais comumente observados na terapia com o benzonidazol. Já com o nifurtimox, as manifestações gastrointestinais, perda de peso, fadiga, dor de cabeça, mudança de humor, artralgia, mialgia, erupções na pele e neuropatia periférica (PÉREZ-MOLINA, 2013). Por estas restrições, destaca-se a necessidade

de desenvolvimento de novos compostos, sintéticos ou naturais, ou novas terapias mais efetivas para o tratamento da doença de chagas (ADADE, 2013)

Desde a introdução da Benzonidazol e Nifurtimox, apenas o alopurinol e algumas azóis, tais como o itraconazol, fluconazol e cetoconazol, passaram para ensaios clínicos. Na verdade, esforços para o desenvolvimento de drogas para a doença de Chagas são quase exclusivamente em pesquisa pré-clínica, embora estudos de fase II para o fármaco antifúngico posaconazol e de um pró-fármaco de ravuconazol estão sendo planejadas (DE CASTRO, 2011).

2.6. Fotoquimioterapia Antiparasitária - FQTAp

A Fotoquimioterapia Antiparasitária tem sido considerada uma terapia relativamente nova uma vez que começou a ser empregada com uma sistemática científica recentemente (SIMPLICIO, 2002). Baseia-se numa derivação da Terapia Fotodinâmica antitumoral, que é uma forma de tratamento cuja eficácia depende da produção e liberação de altas quantidades de Espécies Reativas de Oxigênio (ERO), após a administração tópica ou sistêmica de uma substância fotossensibilizadora, em concentrações não tóxicas e sensível a luz, seguida pela irradiação com uma luz visível em um comprimento de onda apropriado ao fotossensibilizador, e na presença de oxigênio (GAD, 2004; COUPIENE, 2011). Porém há mais de 3400 anos, os indianos deram início a esta terapia, visando o tratamento do vitiligo, ao empregar um fotossensibilizador exógeno obtido de plantas (*Psoralenos*), usado sob a forma de uma loção aplicada sobre a pele e que era capaz de absorver a luz solar (PINHEIRO, 2010).

No início do século XX, Raab e Von Tappeiner, constataram acidentalmente que um meio de cultura contendo Acridina diluída, quando exposto a uma luz intensa, apresentava, como consequência, a morte dos microrganismos cultivados. Estes pesquisadores, em experimentos subseqüentes, observaram que quando da associação do corante e da exposição à luz sobre os meios contendo os microrganismos, apresentava como resultado maior toxicidade, em relação àquela observada com o uso isolado de luz ou Acridina. Postulou-se, portanto, que algum produto da fluorescência e não a luz por si só, seria responsável pela elevada toxicidade observada (PINHEIRO, 2010).

Em 1913, Mayer-Betz fez uma auto injeção de 200mg do que ele pensava ser hematoporfirina pura e não sentiu nenhum efeito, porém ao se expor à luz apresentou fotossensibilidade na pele por vários meses. Em 1924, ocorreu o primeiro relato de fluorescência espontânea de tumores induzidos experimentalmente com o auxílio de uma lâmpada de Wood. Neste mesmo ano, Policard, postulou ser este fenômeno ocasionado pela

Porfirina (PINHEIRO, 2010).

Com o atual fenômeno da resistência aos antibióticos em diversas doenças infecciosas pelo mundo, o interesse por novas alternativas de tratamento vem se multiplicando. A QTFAp volta ao cenário de pesquisas como uma nova alternativa de tratamento a estes patógenos resistentes a fármacos, pois não existe relatos na literatura de microrganismos resistentes a técnica, mesmo aqueles submetidos a vários ciclos de tratamento (KHARKWAL, 2012).

Na presença de oxigênio encontrado nas células, os fotossensibilizadores excitados podem reagir com moléculas de sua vizinhança através da transferência de elétrons ou hidrogênio, levando a produção de radicais livres (reação Tipo I) ou pela transferência de energia para o oxigênio, levando a produção de oxigênio singleto (reação Tipo II). Ambas as vias levam a morte das células ou tecido alvo (DEMIDOVA, 2005; LAMBRECHTS, 2005; BARBOSA, 2011). As espécies reativas de oxigênio (EROs) atacam múltiplas moléculas responsáveis pelas mais variadas propriedades, FQTAp não deve causar resistência às drogas utilizadas e merece atenção especial como uma nova estratégia para contornar este problema tão comum encontrado no tratamento convencional de certas doenças (Figura 9) (DUTTA, 2011).

A FQTAp é potencialmente segura, aplicável e oferecem opções de tratamento para pacientes que sofrem de muitos problemas (gestantes, imunocomprometidos, idosos, crianças) se tornando uma outra opção de tratamento as quimioterapias tradicionais. Também não induz resistência aos microrganismos e não necessita de inúmeras sessões de tratamento (BARBOSA, 2012). Segundo a Sociedade Americana de Câncer, vários fatores são favoráveis ao tratamento a Fotoquimioterapia, quando realizada corretamente, não apresenta efeitos colaterais a longo prazo; é menos invasiva que uma cirurgia; normalmente é um procedimento muito rápido e pode ser realizado em ambulatorios; caso seja necessário, o procedimento pode ser repetido diversas vezes, ao contrário da radiação; pouca ou nenhuma cicatrização local. Sua desvantagem consiste basicamente no alcance da luz, ou seja, a técnica só funciona onde a luz possa chegar (em decorrência da absorção tecidual) e/ou a sensibilidade do organismo aos fotossensibilizadores.

A utilização da QTFAp para o tratamento de algumas infecções ainda apresenta certas limitações que precisam ser superadas para aplicações terapêuticas futuras significantes para o tratamento de doenças infecciosas, e a questão-chave consiste na melhor forma de entrega da luz e do fotossensibilizador às células alvo. Além disso, é preciso determinar dosimetria

precisas, usando dispositivos de iluminação adequada com parâmetros bem definidos (KHARKWAL,2012).

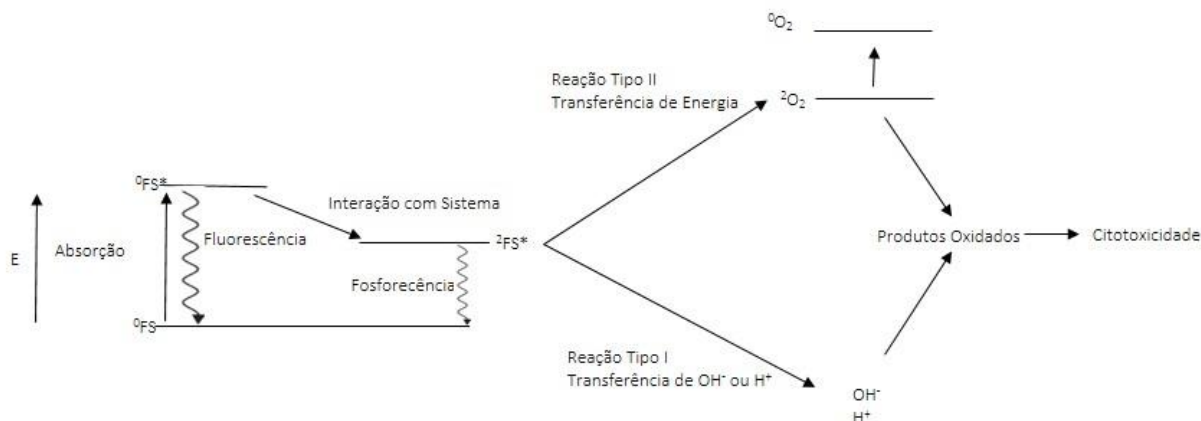


Fig. 9 – Diagrama de Jablonski, demonstrando como um fotossensibilizador (FS), quando excita por uma Energia (E), sai do seu estado fundamental para um estado mais excitado chamado singlete. Em seu estado singlete a molécula poderá voltar ao seu estado fundamental (Fluorescência) ou passar para uma estágio intermediário denominado tripleto e deste retornar ao seu estado fundamental (Fosforecência). Em seu estado tripleto, o fotossensibilizador poderá reagir com as moléculas de O_2 presentes na vizinhança e desencadear as reações do tipo I e II, gerando produtos tóxicos e aumentando a citotoxicidade no interior das células tratadas.

2.7. Fontes de Luz

Em termos de óptica, pode-se dizer que a primeira revolução marcante veio com o advento da luz elétrica. A capacidade do homem em produzir de forma controlada radiação luminosa, mudou seu próprio uso e permitiu que ela se tornasse um excelente elemento para diversas aplicações. Com o advento da luz elétrica, os aparelhos ópticos ganharam um grande impulso. Depois veio o LASER (abreviação para Light Amplified by Stimulated Emission of Radiation) e com ele uma nova revolução. Poucos feitos científicos modernos tiveram a abrangência conquistada pelo laser. O laser tem encontrado, desde a sua descoberta, uma vasta aplicabilidade cobrindo desde as pesquisas científicas mais fundamentais até aplicativos na área médica. Num futuro não muito distante é possível que se tenha lasers implantados dentro de nosso corpo para realizarem diagnósticos de distúrbios ou doenças e que também poderão promover o tratamento adequado. (BAGNATO, 2008)

O laser, cuja teoria é creditada ao físico Albert Einstein, que em seu artigo “*Zur Quantum Theories der Strahlung*”, publicado em 1916, utilizou o nome de emissão estimulada pela primeira vez, sendo um termo bastante peculiar para a época. O trabalho de Einstein discutiu a interação de átomos, íons e moléculas com a radiação eletromagnética em termos da

absorção e emissão espontânea de radiação. Com a aplicação de princípios termodinâmicos, Einstein concluiu que o terceiro processo de interação, a emissão estimulada, deveria existir, e nela a radiação eletromagnética deveria ser produzida por um processo atômico. (VEÇOSO, 1993; PINHEIRO, 2010).

A luz é uma energia radiante produzida por todos os estados físicos da matéria (sólido, líquido e gasoso). Esta energia contida em todas as estruturas atômicas forma um espectro eletromagnético que por sua vez é metodicamente organizado, sendo denominado de comprimento de onda. Dessa forma, a energia radiante possui um espectro de comprimento de onda, visível ao olho humano, entre $\lambda 385$ nm e $\lambda 760$ nm. Abaixo de $\lambda 385$ nm, a luz é denominada de ultravioleta e acima de $\lambda 760$ nm de infravermelha, ambas não visíveis pelo homem (ATKINSON, 1997; PINHEIRO, 2010).

As características especiais da luz laser, tais como: coerência, monocromaticidade, unidirecionalidade, a diferencia totalmente da luz natural. A luz coerente: todas as ondas são do mesmo comprimento, isto é, a uniformidade da luz; monocromática, a luz laser é pura e composta de uma única cor, e o efeito colimado apresenta todas as ondas sempre paralelas entre si, não havendo dispersão, ou seja, não aumentam seu diâmetro (PINHEIRO, 1992; PINHEIRO, 2010;).

Essa laserterapia foi utilizada primeiramente por Mester e colaboradores, que usaram o laser de argônio de $\lambda 488$ nm e $\lambda 515$ nm. Subsequentemente foi introduzido o laser de hélio-neônio (HeNe) que emite luz vermelha com comprimento de onda de $\lambda 632,8$ nm. Atualmente estes aparelhos foram substituído por outros de preços mais reduzido e mais potente; o laser de diodo, com comprimentos de onda entre $\lambda 660$ - 950 nm. Os tratamentos experimentais em pacientes iniciaram-se na década de 1970 após relatos de resultados positivos da irradiação com a Fotobiomodulação a Laser (FBML) em culturas de células e em experimentos animais. Estudos realizados foram insuficientes para confirmar os efeitos benéficos da FBML. Efeitos positivos surgiram, mas falharam devido ao grande número de intervenções e à insatisfatória qualidade da metodologia (ROCHA-JUNIOR, 2006; PINHEIRO, 2010).

2.8.Fotossensibilizadores

Um fotossensibilizador é uma molécula que age como um pró-fármaco, que pode ser natural ou sintética, inerte (não-tóxica), e que na presença da luz, em um comprimento de onda específico, pode absorver essa energia luminosa e ser fotoativada. Este precursor chamado de

fotossensibilizador, sofre excitação enquanto está sendo irradiado, passando a ser uma molécula farmacologicamente ativa. Após sua ativação pela luz, os fotossensibilizadores desencadeiam reações químicas que produzem diretamente ou indiretamente espécies citotóxicas, como radicais livres e oxigênio singleto (figura 9) (NAGY, 2010).

A maioria dos fotossensibilizadores que estão sendo avaliados e testados em terapia fotodinâmica seja contra o câncer ou outros microrganismos são baseados em diversos compostos entre eles destacam-se: porfirinas, hematoporfirinas, protoporfirina, clorinas, ftalocianinas, acridinas, fenotiazinas entre outros. (PERUSSI, 2007)

Os fenotiazínicos são moléculas com potencial fotossensibilizante e com grande propensão à formação de espécies reativas de oxigênio (EROs). São considerados hidrofílicos, tricíclicos contendo Nitrogênio e Enxofre, e, conhecidas a mais de 100 anos. Até agora mais de 5 mil derivados fenotiazínicos já foram obtidos e esta classe vem se destacando por sua variedade de propriedades químicas e biológicas. As fenotiazinas possuem um custo relativamente baixo, são facilmente encontradas, bem toleradas. Exibem atividade promissoras contra bactérias, fungos, câncer, vírus, inflamação, protozoários além de suas propriedades anticonvulsivante, analgésica e imunossupressora (WAINWRIGHT, 1998; BARBOSA, 2012)

O Azul de Metileno (MB) e Azul de Toluidina (TBO) (tabela 1) são fotossensibilizantes fenotiazínicos aceitos na prática médica e demonstrados em estudos na literatura. Possuem capacidade fotoantimicrobiana contra diferentes organismos incluindo vírus, bactérias e fungos. Apresentam estrutura química e propriedades físico-químicas semelhantes. Embora suas propriedades sejam semelhantes, a eficiência fotodinâmica destes compostos, varia entre os diversos microrganismos (DEMIDOVA, 2005).

A banda de absorção do MB varia entre 620 nm e 700 nm, com ótima penetração nos tecidos e absorção máxima em 665 nm em solução aquosa (FERNANDEZ, 1997). Para o TBO, a banda máxima de absorção é de 636 nm (GARCEZ, 2003). O uso desses fotossensibilizantes pode ser tópico ou sistêmico e não apresenta toxicidade. Teichert *et al.* (2002) relataram que o MB possui baixa toxicidade, com grande aceitação no campo médico devido à sua potencial ação antimicrobiana fotoativa.

Durante o período inicial de pesquisas na Terapia Fotodinâmica moderna, tem sido um padrão de fotossensibilizador bioativo, dando um rendimento razoável de oxigênio singleto (forma do oxigênio mais reativo e oxidante que o oxigênio molecular) e absorvendo luz na janela terapêutica (definida pela faixa de frequência onde a laser terapia é mais efetiva) para

terapia fotodinâmica (600 – 900 nm), sendo assim um ponto inicial de síntese de novas moléculas. (WAINWRIGHT, 2005; RONSEIN, 2006)

O corante fenotiazínico azul de metileno é um corante aromático heterocíclico solúvel em água ou em álcool, que absorve intensamente na região espectroscópica do ultravioleta-visível. É um agente fotossensibilizante muito eficaz na inativação de microrganismos como bactérias e vírus (WAINWRIGHT, 1998). O Azul de Toluidina é uma fenotiazina análoga ao azul de metileno, com mínimas divergências estruturais, que seria a presença de dois metilaminas no azul de metileno. Tem sido amplamente empregado na coloração biológica, especialmente na hematologia. (WAINWRIGHT, 2005)

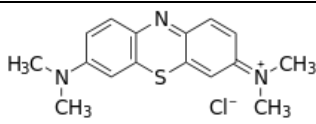
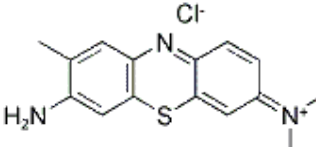
SIGLA	NOME QUÍMICO	PM (g/mol)	FORMULA MOLECULAR	ESTRUTURA QUÍMICA
MB	3,7-bis(Dimethylamino)-phenothiazin-5-ium chloride	319,85	C ₁₆ H ₁₈ N ₃ SCl	
TBO	(7-amino-8-methylphenothiazin-3-ylidene)-dimethylazanium chloride	305,83	C ₁₅ H ₁₆ ClN ₃ S	

Tabela 1. Derivados fenotiazínicos avaliados como potenciais fotossensibilizadores contra *Tripanosomatídeos*

3. RESULTADOS

Artigos Publicados em Periódicos ou Proceedings

3.1. Lasers Surg Med. 2012 Dec;44(10):850-5. doi: 10.1002/lsm.22099. Epub 2012 Nov 26

Photodynamic Antimicrobial Chemotherapy (PACT) Using Phenothiazine Derivatives as Photosensitizers Against *Leishmania braziliensis*

Leishmaniose cutânea e mucocutânea são doenças caracterizadas por manifestações na pele ou nas mucosas. No Novo Mundo, *Leishmania braziliensis* é o principal agente etiológico da leishmaniose cutânea, numa condição que pode evoluir para uma forma mucocutânea. O arsenal terapêutico empregado rotineiramente para tratar pacientes infectados é insatisfatório, especialmente os antimonial pentavalentes, que são recomendados pela Organização Mundial de Saúde, mas são altamente tóxicos, pouco tolerados e vários efeitos colaterais. Neste trabalho buscou-se avaliar, de forma *in vitro*, a eficácia da Fotoquimioterapia Antiparasitária como uma nova abordagem para o tratamento da leishmaniose. Para isto foi utilizado um laser ($\lambda 660$ nm, 40 mW, 4,2 J/cm² 8,4 J/cm², CW) associado a derivados fenotiazínicos em concentrações de 5 e 10 µg/ml do azul de metileno, azul de toluidina, e de uma mistura de 1:1 de ambos os compostos contra a forma promastigota de *L. braziliensis*. Após uma incubação de 72h depois do tratamento pela Fotoquimioterapia Antiparasitária, as amostras foram contadas através de um hematocítômetro para determinar a viabilidade dos parasitas. Uma importante diminuição no número de parasitas viáveis em todos os grupos tratados com a FTQAp, em comparação aos grupos controles foi observado em todos os grupos testados, demonstrando uma significativa letalidade para a dose com 10 µg/ml do azul de toluidina.

Photodynamic Antimicrobial Chemotherapy (PACT) using phenothiazine derivatives as photosensitizers against *Leishmania braziliensis*

Artur Felipe S. Barbosa, M.Sci.^{a, b, c, e}, Bruno Sangiorgi, Biol^b, Suely L. Galdino, PhD^c,
Manoel Barral-Netto, MD, PhD^b, Ivan R. Pitta, PhD^c, Antônio Luiz B. Pinheiro, PhD^{a, d}

^aCenter of Biophotonics, School of Dentistry, Federal University of Bahia (UFBA), 62 Araujo Pinho Ave, Canela, Salvador, BA, Brazil, 40110-150. [AFSB, ALBP]

^bCentro de Pesquisas Goncalo Moniz (FIOCRUZ), Rua Waldemar Falcão 121, Candeal, Salvador, BA, Brazil, 40296-710 [BS, MBN]

^cLaboratory Planning and Synthesis of Drugs, Federal University of Pernambuco, 1235 Prof. Moraes Rego Ave, Cidade Universitária, Recife, PE, Brazil, 50670-901 [SLG,IRP]

^dNational Institute of Optics and Photonics, University of São Paulo, 400 Trabalhador Sancarlense Ave, São Carlos, SP, Brazil, 13560-970 [ALBP]

^eSão Camilo School, 102 Visconde de Itaborai Street, Amaralina, Salvador, BA, Brazil, 41900-000 [AFSB]

Corresponding Author

Antônio Luiz Barbosa Pinheiro: Center of Biophotonics, School of Dentistry, Federal University of Bahia, 62 Araujo Pinho Ave, Canela, Salvador, BA, Brazil, 40110-150.
Phone/fax: +55 71 3283 9010. Email: albp@ufba.br

Disclosure statement: We certify that we have no affiliation with or financial involvement in any organization or entity with a direct financial interest in the subject matter or materials discussed in the manuscript.

ABSTRACT:

Background and Objective: Cutaneous and mucocutaneous leishmaniasis are diseases characterized by skin or mucosal manifestations. In the new world, *Leishmania braziliensis* is the main etiological agent of cutaneous leishmaniasis, condition that may evolve to the mucocutaneous form. The therapeutic arsenal routinely employed to treat infected patients is unsatisfactory, especially for pentavalent antimonials, treatment recommended by the WHO, as they are often highly toxic, poorly tolerated and of variable effectiveness. This work aimed to evaluate in vitro the effectiveness of Photodynamic Antimicrobial Chemotherapy as a new approach for the treatment of Leishmaniasis. **Materials and Methods:** A Laser ($\lambda 660\text{nm}$, 40mW, $4.2\text{J}/\text{cm}^2$ and $8.4\text{J}/\text{cm}^2$, CW) associated to phenothiazine's derivatives (5 and 10 $\mu\text{g}/\text{ml}$, Toluidine Blue O, Methylene Blue or Phenothiazine) on the promastigote forms of *L. braziliensis* in a single session. Samples were removed and analyzed in a hemocytometer 72h after PACT and viability of the parasites was assessed in quadruplicates. **Results:** An important decrease in the number of viable parasites on all treated groups in comparison to their controls was observed as all tested compounds lead to significant parasite lethality being the highest lethality achieved with 10 $\mu\text{g}/\text{ml}$ of TBO. No lethality was observed on groups treated with laser or with any of the compounds separately. **Conclusions:** TBO presented higher parasite lethality in comparison to MB with impressive reduction from 1 h to 5 minutes of pre-incubation time.

Keywords: Laser-therapy, Leishmaniasis, Methylene Blue, Toluidine Blue O, Treatment

INTRODUCTION

Leishmaniasis are protozoan parasitic infections transmitted to mammals, including humans, by phlebotomine sandflies and clinically classified in three forms: visceral, cutaneous, and mucocutaneous [1]. Leishmaniasis threatens about 350 million people in 88 countries worldwide and 12 million people are believed to be currently infected, with about 1–2 million estimated new cases occurring every year [2].

Cutaneous leishmaniasis is mainly caused by *Leishmania major* in the old world and by *Leishmania amazonensis* or *Leishmania braziliensis* in the Americas, in particular in Brazil [2–4]. *Leishmania braziliensis* is the etiologic agent of American cutaneous leishmaniasis (ACL), which is characterized by its chronicity and the possibility to metastasize leading to the mucocutaneous clinical form [5].

Current treatment for leishmaniasis relies mainly on chemotherapy, as no efficient vaccine is available. Pentavalent antimonials meglumine antimoniate and sodium stibogluconate have been considered the first option of treatment of leishmaniasis since the 1940s [1,6]. Amphotericin B is the second drug of choice when there is no response to treatment with antimonials or when it is not possible to use it. The efficacy of pentamidine, the third drug of choice, is less well known. Pentavalent antimonials are expensive, toxic many organs. Furthermore, the administration of antimonials is forbidden in many situations such as during both pregnancy and lactation, in very small children, in case of hypersensitivity to the drugs, and in people suffering from certain chronic diseases [7,8]. Several side effects from use of these compounds may be found elsewhere in the literature [2].

Recently, photodynamic antimicrobial chemotherapy (PACT) has been studied for the treatment of leishmaniasis [9–11]. PACT is a potentially applicable, safe and affordable option for treating patients suffering from many conditions being an attractive option to the use of

conventional antimicrobial chemotherapy [12]. PACT neither induces resistant strains nor demands multiple sessions of treatment [13,14].

Phenothiazines, nitrogen- and sulfur-containing tricyclic compounds, are known for over a hundred years. Up to now over 5000 phenothiazine's derivatives have been obtained and this class of organic compounds became extremely important due to their varied biological and chemical properties. Recent reports dealt with promising anticancer, antibacterial, antiplasmodium, multidrug resistance (MDR) reversal activities and potential treatment in Alzheimer's and Creutzfeldt–Jakob diseases of classical phenothiazines [15]. Phenothiazines are relatively inexpensive, widely available, well-tolerated and nontoxic compounds. New phenothiazines exhibit promising antibacterial, antifungal, anticancer, antiviral, anti-inflammatory, antimalarial, antifilarial, trypanocidal, anticonvulsant, analgesic, immunosuppressive and multidrug resistance reversal properties [15].

The present investigation aimed to evaluate the effectiveness of PACT against the promastigote form of *Leishmania braziliensis*, as a new approach to therapy against human cutaneous leishmaniasis.

MATERIALS AND METHODS

Chemicals

MB and TBO were purchased from Sigma-Aldrich Corporation (Milwaukee, WI, USA). Three compounds were used: MB, TBO and a 1:1 mixture of MB + TBO, here named as phenothiazine - MB-TBO. The stock solutions were diluted in distilled water (10 or 20 µg /ml).

Culture Promastigote Forms

L. braziliensis promastigotes (strain MHOM/BR/01/BA788 - cultivated and maintained by the Integrated Laboratory of Microbiology and immunoregulation) were cultivated in Schneider's Insect Medium (Sigma Chemical Co., St Louis, Mo, USA) supplemented with 20% heat-inactivated fetal bovine serum (Gibco, Carlsbad, CA, USA), L-glutamine (2 mM),

penicillin (100 U/ml), streptomycin (100 µg/ml) at 26 °C (Thermostat cabinets – LS Scientific, Ikeja, Lagos, Nigeria) for 5–7 days when the parasites reached the stationary-phase. After reaching the stationary-phase, the culture was sedimented by centrifugation (5810 R, Eppendorf, Hamburg, Germany, 10 min, 4°C, 4000 rpm), suspended in 1 mL of the same medium and quantified in a Neubauer chamber (LO - Laboroptik GmbH, Friedrichsdorf, Germany) with the aid of a microscope (Nikon Eclipse E200, Melville, NY, USA). Enough medium was added in order to adjust the parasitic concentration to 2×10^6 promastigotes/mL [4].

Leishmanicidal Activity against Promastigotes Forms

The determination of the leishmanicidal activity was performed in 96-well plates (Tesplate 96F - TPP, Zollstrasse, Trasadingen, Switzerland). The compounds were tested in quadruplicate in two concentration 5 or 10 µg/mL. The parasitic concentration in the wells was that of 2×10^6 promastigotes/mL. A negative control was performed with four wells containing only parasites and the incubation medium. After 72 h of incubation at 26°C, 10 µL of each well was diluted in 90 µL of the PBS and the parasites were quantified in a Neubauer chamber. The data obtained from this quantification were plotted in a graph using Microsoft Excel and the values of the lethality of the treated groups were obtained through the difference in percentage of viable parasites in the groups treated with the amount of viable parasites in the control group.

Photodynamic Antimicrobial Chemotherapy (PACT)

Metacyclic promastigotes were pre-incubated during either 5 or 60 minutes, in darkness, with the different concentrations of the photosensitizers in Schneider's Drosophila medium (pH 7.2) with 10% FBS in 96-well plates. After pre-incubation each well was irradiated with a diode laser which has a semiconductor active medium InGaAlP ($\lambda = 660\text{nm}$, 40mW, $4.2\text{J}/\text{cm}^2$, CW, TwinFlex[®], MMOptics, São Carlos, São Paulo, Brazil). After 72 h of incubation at 26°C, 10 µL of each well was diluted in 90 µL of the formaline 10% and the parasites were quantified in a

Neubauer chamber. The data obtained from this quantification were plotted in a graph using Microsoft Excel and the values of the lethality of the treated groups were obtained through the difference in percentage of viable parasites in the groups treated with the amount of viable parasites in the control group. Four protocols were carried out: I: Pre-incubation of 5 minutes and 2 minutes of irradiation (4.2 J/cm^2); II: Pre-incubation of 5 minutes and 4 minutes of irradiation (8.4 J/cm^2); III: Pre-incubation of 60 minutes and 2 minutes of irradiation (4.2 J/cm^2); and IV: Pre-incubation of 60 minutes and 4 minutes of irradiation (8.4 J/cm^2).

Crystal Violet Toxicity Assay

In order to assess the toxicity of certain phenothiazines concentrations to human cells, we made a Crystal Violet Toxicity assay from macrophages derived from peripheral blood mononuclear cells (PBMC). PBMC were obtained from blood bags processed with buffy coat, donated from the local hemocenter (Fundação de Hematologia e Hemoterapia da Bahia), by a gradient centrifugation on Ficoll-Hypaque (GE Healthcare, Uppsala, Sweden) at 1500 RPM with room temperature. The PBMC collected were then washed with PBS following centrifugations at 1400, 1300 and 1200 RPM. For macrophage differentiation, the PBMC remaining were disposed in a 96 well dish with 200 μL of RPMI (LGCBIO, Cotia, SP, Brazil) with 10% inactivated AB human serum (Sigma Chemical Co., St Louis, Mo, USA), at concentration of 10^5 PBMC/ml, remaining for 7 days with exchanging half of the media at every 2 days. One day after photochemotherapy, the culture media was removed from the wells (Tesplate 96F - TPP, Zollstrasse, Trasadingen, Switzerland) and 100 μL of methanol was added and the plate, and incubated for 20 minutes at room temperature (25°C). Methanol was then removed from the wells, being added 50 μL of Cristal Violet Dye (0.5% Crystal Violet, 20% Methanol, 80% dH_2O , Sigma-Aldrich Corporation, Milwaukee, WI, USA) followed by incubation for 10 minutes at room temperature. After that period, the dye was removed and the

wells washed twice with tap water, followed by 2 immersions of the plate in a beaker filled with tap water. To extract the dye from the cells, 100 μ L of Sorenson's buffer (SDS) was added in the wells and the plate was incubated in a rotate shaker for 30 minutes. An ELISA - SpectraMax 190 Microplate Reader[®] (Sunnyvale, CA, USA) plate reader was used for the absorbance measurement at wavelength of 540nm.

Statistical Analysis

The data was analyzed using the Minitab15 software (Minitab, Belo Horizonte – MG, Brazil). Significance level was fixed in 5%.

RESULTS

From Crystal Violet toxicity assay, we observed that MB and TBO presented a very similar pattern of toxicity. When compared to control group, both have a trend to decrease the cells viability along with concentration increasing, although this effect was showed to be significant only at 20 μ g/ml. Thus, concentrations below these levels were chosen from both phenothiazines for PACT assays.

The overall analysis showed that, the use of energy density of 4.2 J/cm² achieved the best results of lethality when using incubation time of 5 minutes and using either 10 μ g/ml of TBO or MB-TBO. When the incubation time was increased to 60 minutes, all compounds are similarly effective, independent of the energy density used. So the use of either 10 μ g/ml of TBO or MB-TBO during 5 minutes prior irradiation with 4.2J/cm² λ 660nm laser light was the most efficient protocol (Table 1).

DISCUSSION

According to the WHO, leishmaniasis is among the six most important tropical diseases, affecting around 12 million people in 88 countries [16]. Chemotherapy remains the most

effective control measure for this disease. The therapeutic arsenal routinely employed to treat patients with leishmaniasis is limited and unsatisfactory. For cutaneous leishmaniasis, pentavalent antimonials (sodium stibogluconate or meglumine antimoniate) are the first line therapeutic scheme recommended by the WHO, the second drug of choice (amphotericin B) and the third drug of choice is pentamidine. All of these medications are parenterally administered and may result in mild to severe side effects. These compounds are highly toxic, poorly tolerated, require long-term treatment and their effectiveness highly variable [17-19].

Pentavalent antimonials may cause hyperamylasemia, ECG abnormalities, bone marrow suppression and hepatotoxicity, as well as constitutional symptoms, such as myalgia, arthralgia, headache, fever, nausea, vomiting, and pain at the site of drug application, when administered intramuscularly. Amphotericin B may result in anemia, cardiac and nephrotoxic effects, hypokalemia, and constitutional side effects, such as nausea, vomiting, phlebitis, shivering and fever, which sometimes require the interruption of treatment. Pentamidine is known for its cardiac toxicity, nephrotoxicity, hypotension, hypoglycemia, but the major concern is the possibility of development of diabetes mellitus [19].

Antimicrobial Chemotherapy (PACT) which may also be called Photosensitization lethal laser (PLL), based on topical or systemic non-toxic dye sensitive to light irradiation followed by at low doses with visible light of appropriate wavelength [20]. The photodynamic inactivation can be performed in a localized way, different from photodynamic therapy against cancer, where the compound photosensitizer is usually injected into the bloodstream and accumulates in the tumor, photodynamic inactivation may be made by local employment in the area of the photosensitizer infected by topical application, instillation, or interstitial injection [21].

In the presence of oxygen found in the cells, photosensitizer (FS) enabled can react with molecules in their neighborhood by electron transfer or hydrogen, leading to production of free

radicals (type I reaction) or by energy transfer to oxygen, leading to production of singlet oxygen (type II reaction). Both paths may lead to cell death and the destruction of diseased tissue [22, 23, 24].

Reagent Oxygen Species (ROS) simultaneously attack multiple molecules of varied properties. PACT is considered to have the potential to circumvent drug-resistance that is common to both infectious and non-infectious diseases. PACT should not cause resistance to the drugs used and deserves special attention as a new strategy to circumvent this so common problem encountered in the chemotherapy of some diseases [25].

The light sources can be used to bring the excitement of photosensitizing molecules, such as pulsed light, lights incoherent, xenon lamp, among others, all with specific filters that let you select the wavelength with greater penetration in tissues and of maximum absorption of the drug [26,27]. The radiation used often is provided by a laser system, which are preferably employed because they have specific characteristics that differ from the light as being monochromatic, coherent and collimated [28].

MB and TBO are photosensitizing phenothiazine accepted at the practice medical and demonstrated in studies in literature. Exhibit intense absorption of 600-660nm, region of the spectrum useful in PACT to be in the "therapeutic window" required for efficient penetration of light in tissues [29,30]. Although its properties physical and chemical are similar the efficiency photodynamic of compounds, varies between the several microorganisms [23]. The use of staining agents such as MB and TBO in the analysis of the pathology of the microbial diseased state is well established, as mentioned above [31].

The phenothiazine dye Toluidine blue O (TBO) is a heterocyclic aromatic colorant soluble in water or alcohol, which absorbs strongly in the region of the ultraviolet-visible. A photosensitizing agent that is very effective in inactivating pathogenic organisms. TBO is a phenothiazine analogous to MB with minimal structural differences. It has been widely used in

biological staining, especially in hematology [31]. TBO is a phenothiazine dye that interacts with biological molecules and mediators. Previous studies have demonstrated the high ability of TBO molecules to bind to DNA. DNA is an important target in the phenothiazinium dye photosensitized biological damage, and guanine residues. Resonance light scattering spectra of TBO in the presence of DNA indicated that TBO could aggregate along DNA surface [23].

TBO in solution is playing a highly active role in the light-mediated killing of the cells. There are two possible explanations for this observation. First, it may be due to the light-mediated extracellular generation of ROS (particularly singlet oxygen) that may diffuse itself into the cell producing damage cell death. The second explanation is that the first part of the Photodynamic Inactivation - PDI process produces some damage at the cell surface that allows more TBO molecules present in solution to bind and/or penetrate the cell and therefore increasing the potency of the PDI process. The finding that there was a significant dependence of killing on cell density also implies that there is binding or interaction of the cells with a limited concentration of some species and that this occurs whether or not the PS is washed out from the cell suspension [23].

The methylene blue (MB) has shown to be an effective broad-spectrum photoantimicrobial agent [32]. Due to the hydrophilic nature of the outer cell membrane, MB acts leading both to a lack of activity against intracellular targets as membrane photodamage, hemolysis, etc. MB is a long established biological dye and has been known as a photoantimicrobial since 1928. The antiprotozoal activity of MB includes both African and American trypanosomiasis and leishmaniasis. The continuing use of MB as a lead compound for antimalarial research underlines its activity against *Plasmodium spp* [33].

The electronically excited MB molecule is relatively stable and can undergo an electronic rearrangement. The excited form is known as an excited triplet state and it is this that facilitates photodynamic action. A relatively long-lived excited triplet state allows the excited

MB molecule to pass on the excitational energy to other molecules. Direct interaction with adjacent molecules leads to electron transfer or hydrogen abstraction and the formation of radical species. This is known as Type I photosensitization, and with membrane-related molecules leads to the formation of lipid hydroperoxides and thus to membrane damage [22]. If the excited triplet state molecule interacts directly with oxygen, the excitational energy is transferred causing the formation of a highly reactive species, singlet oxygen. Formed in situ within a cellular environment, singlet oxygen is highly toxic on account of its oxidizing activity, although it has a very short lifetime and will decay to the ground state (non-toxic triplet oxygen) within microseconds. Singlet oxygen-mediated photosensitization is known as the Type II pathway [34].

Phenothiazines possess great affinity by Trypanosomatides [35-37]. Trypanothione and trypanothione reductase (TryR)-based redox metabolism found in *Leishmania sp.* and other trypanosomatides exemplify the unique features of this group of organisms. Its absence in mammalian hosts, together with the sensitivity of trypanosomes against oxidative stress, makes this enzyme a unique target for exploitation for potential antileishmanial chemotherapeutics [34, 38-40]. Trypanothione reductase (TR) was irreversibly inhibited phenothiazine derivatives. The inactivation of TR depends on (a) of incubation with the phenothiazine derivatives (b) the free radicals formed (c) and the concentration and structure of phenothiazine derivatives [38].

Another enzyme found in *Leishmania sp.* is the Superoxide Dismutase (SOD) SOD has its mechanism of action involved in anti-oxidant enzymes which catalyze the dismutation of O_2^- to H_2O_2 and O_2 protecting catalase and peroxidase against inhibition by O_2^- , which can be derived from the phenothiazine [41, 42].

Based on this knowledge about the actions of phenothiazine derivatives on structures and enzymes of *Leishmania*, we can better understand why the choice of some works of PACT with MB [43,44].

Other advantages of PACT are: The procedure can be repeated several times if necessary, since no toxic effects and is usually non-invasive. In addition, due to its low risk, can be used in people who are elderly or frail to undergo other surgery. The main side effect is sensitization to light, which is circumvented by avoiding exposure to sunlight and interior light too intense for a period of up to 6 weeks depending on the photosensitizer [45].

Because of its ability to interact at a more internal MB, we decided to evaluate the TBO, individually and combined with MB for comparison with results previously available in the literature with MB. Our results showed that TBO really stands out when compared to MB. The contribution that this work can also provide for new research PACT with *Leishmania*, especially *L. braziliensis*, which is in respect to the parameters used in the irradiation for stimulation of the compounds used together with the low concentration of photosensitizers.

The concentrations used were well below those considered toxic based on toxicity test with crystal violet, giving us greater security to work and to modify the concentrations without causing problems cytotoxicity. Another point worth highlighting in this work is the total time for which the technique is carried out. We conducted four experimental periods, one where the child understands the pre-incubation of 5 minutes with 2 minutes of irradiation, a total of 7 minutes of dealing with a dose of 4.2 J/cm^2 . Already the longest period includes a pre-incubation of 60 minutes with 4 minutes of irradiation, totaling 64 minutes of procedure and a dose of 8.4 J/cm^2 . As there was no statistical difference of the best concentration, $10 \text{ }\mu\text{g/ml}$ of TBO compared the times of pre-incubation of 5 or 60 minutes, we suggest that among these possibilities tested at work, the best procedure would be to use $10 \text{ }\mu\text{g/ml}$ of TBO irradiated by a laser device with a dose of 4.2 J/cm^2 . In this procedure, we have less time with greater lethality.

REFERENCES

1. De Muylder G, Ang KKH, Chen S, Arkin MR, Engel JC, McKerrow JH. A Screen against *Leishmania* Intracellular Amastigotes: Comparison to a Promastigote Screen and Identification of a Host Cell-Specific Hit. *PLoS Negl Trop Dis* 2011; 5: e1253.
2. do Monte-Neto RL, Coelho AC, Raymond F, Légaré D, Corbeil J, Melo MN, Frézard F, Ouellette M. Gene Expression Profiling and Molecular Characterization of Antimony Resistance in *Leishmania amazonensis*. *PLoS Negl Trop Dis* 2011; 5: e1167.
3. Santos DO, Coutinho MFM, Bottino CG, Vieira RT, Nascimento SB, Bernardino A, Bourguignon SC, Corte-Real S, Pinho RT, Rodrigues CR, Castro HC. Leishmaniasis treatment – a challenge that remains: a review. *Parasitol Res* 2008; 103: 1–10.
4. Machado PR, Ampuero J, Guimarães LH, Villasboas L, Rocha AT, Schrieffer A, Sousa RS, Talhari A, Penna G, Carvalho EM. Miltefosine in the Treatment of Cutaneous Leishmaniasis Caused by *Leishmania braziliensis* in Brazil: A Randomized and Controlled Trial. *PLoS Negl Trop Dis* 2010; 4: (12), e912
5. Tavares NM, Silva RA, Costa DJ, Pitombo MA, Fukutani KF, Miranda JC, Valenzuela JG, Barral A, de Oliveira CI, Barral-Netto M, Brodskyn C. *Lutzomyia longipalpis* Saliva or Salivary Protein LJM19 Protects against *Leishmania braziliensis* and the Saliva of Its Vector, *Lutzomyia intermedia*. *PLoS Negl Trop Dis* 2011; 5:(5): e1169.
6. Soto J, Soto P. Current situation and future of anti-leishmanial therapy in Colombia. *Biomedica* 2006; 26: 194 – 206.
7. Machado-Pinto J, Pinto J, da Costa CA, Genaro O, Marques MJ, Modabber F, Mayrink W. Immunochemotherapy for cutaneous leishmaniasis: a controlled trial using killed *Leishmania* (*Leishmania*) *amazonensis* vaccine plus antimonial. *Int J Dermatol* 2002; 41: 73-78.
8. Vélez I, López L, Sánchez X, Mestra L, Rojas C, Rodríguez E. Efficacy of Miltefosine for the Treatment of American Cutaneous Leishmaniasis. *Am J Trop Med. Hyg* 2010; 83: 351–356.

9. Enk CD, Fritsch C, Jonas F, Nasereddin A, Ingber A, Jaffe CL, Ruzicka T. Treatment of cutaneous leishmaniasis with photodynamic therapy. *Arch Dermatol* 2003; 139: 432–434.
10. Gardlo K, Horska Z, Enk CD, Rauch L, Megahed M, Ruzicka T, Fritsch C. Treatment of cutaneous leishmaniasis by photodynamic therapy. *J Am Acad Dermatol* 2003; 48: 893–896.
11. Dutta S, Ray D, Kolli BK, Chang KP. Photodynamic Sensitization of *Leishmania amazonensis* in both Extracellular and Intracellular Stages with Aluminum Phthalocyanine Chloride for Photolysis In Vitro. *Antimicrob Agents Chemotherap* 2005; 49: 4474–4484.
12. Montanari J, Maidana C, Esteva MI, Salomon C, Morilla MJ, Romero EL. Sunlight triggered photodynamic ultradeformable liposomes against *Leishmania braziliensis* are also leishmanicidal in the dark. *J. Control Release* 2010; 147: 368–376.
13. Nitzan Y, Wexler HM, Finegold SM. Inactivation of anaerobic bacteria by various photosensitized porphyrins or by hemin. *Curr Microbiol* 1994; 29: 125–131.
14. Calzavara-Pinton PG, Venturini M, Sala R. A comprehensive overview of photodynamic therapy in the treatment of superficial fungal infections of the skin. *J Photochem Photobiol B* 2005; 78: 1-6.
15. Pluta K, Mlodawska BM, Jelen M. Recent progress in biological activities of synthesized phenothiazines. *Eur J Med Chem* 2011; 46: 3179-3189.
16. Bailey MS, Lockwood DN. Cutaneous leishmaniasis. *Clin Dermatol* 2007; 25: 203–211.
17. Foroumadi A, Pournourmohammadi S, Soltani F, Asgharian-Rezaee M, Dabiri S, Kharazmi A, Shafiee A. Synthesis and in vitro leishmanicidal activity of 2-(5-nitro-2-furyl) and 2-(5-nitro-2-thienyl)-5-substituted- 1,3,4-thiadiazoles. *Bioorg Med Chem Letters* 2005; 15: 1983–1985.

18. Zauli-Nascimento RC, Miguel DC, Yokoyama-Yasunaka JKU, Pereira LIA, Oliveira MAP, Ribeiro-Dias F, Dorta ML, Uliana SR. In vitro sensitivity of *Leishmania (Viannia) braziliensis* and *Leishmania (Leishmania) amazonensis* Brazilian isolates to meglumine antimoniate and amphotericin B. *Trop Med Int Health* 2010; 15: 68–76.
19. Pimentel MIF, Baptista C, Rubin EF, Vasconcellos ECF, Lyra MR, Salgueiro Mde M, Saheki MN, Rosalino CM, Madeira de F, Silva AF, Confort EM, Schubach Ade O. American cutaneous leishmaniasis caused by *Leishmania (Viannia) braziliensis* resistant to meglumine antimoniate, but with good response to pentamidine: a case report. *Rev Soc Bras Med Trop* 2011; 44: 254-256.
20. Gad F, Zahra T, Hasan T, Hamblin MR. Photodynamic inactivation of Gram-positive pathogenic bacteria: effect of growth phase and extracellular slime. *Antimicrob Agents Chemother* 2004; 48: 2173-2178.
21. Hamblin MR, Hasan T. Photodynamic therapy: a new antimicrobial approach to infectious disease? *Photochem Photobiol Sci* 2004; 3: 436-450.
22. Barbosa AFS, Soares LGP, Aciole JMS, Aciole GTS, Pitta IR, Galdino SL, Pinheiro ALB. Evaluation of Photodynamic Antimicrobial Therapy (PACT) against Trypomastigotes of *Trypanosoma cruzi*: In Vitro Study. *AIP Conf Proc* 2011; 1364: 55-59.
23. Demidova TN, Hamblin MR. Effect of Cell-Photosensitizer Binding and Cell Density on Microbial Photoinactivation. *Antimicrob Agents Chemother* 2005; 49: 2329-2335.
24. Lambrechts SAG, Aalders MCG, Marle JV. Mechanistic study of the photodynamic inactivation of *Candida albicans* by a cationic porphyrin. *Antimicrob Agents Chemother* 2005; 49: 2026-2034.
25. Dutta S, Ongarora BG, Li H, Vicente MGH, Kolli BK, Chang KP. Intracellular Targeting Specificity of Novel Phthalocyanines Assessed in a Host Parasite Model for Developing Potential Photodynamic Medicine. *PLoS ONE* 2011; 6: e20786.

26. Machado AEH. Photodynamic Therapy: principles, potential of application and perspectives. *Quím Nova* 2000; 23: 237-243.
27. Mang TS. Lasers and light sources for PDT: past, present and future. *Photodiag Photodyn Therapy* 2004; 1: 43-48.
28. Pierce LA. Laser Physics and Physiology. *Plast Surg Nurs* 1997; 17:123-128.
29. Wainwright M, Grice NJ, Pye LEC. Phenothiazine Photosensitisers. Part II. 3,7-Bis(aryl amino)phenothiazines. *Dyes Pigments* 1999; 42: 45-51.
30. Sommer AP, Pinheiro AL, Mester AR, Franke RP, Whelan HT. Biostimulatory windows in low-intensity laser activation: lasers, scanners, and NASA's light-emitting diode array system. *J Clin Med Laser Surg* 2001; 19: 29-33.
31. Wainwright M. The development of phenothiazinium photosensitisers. *Photodiagnosis Photodyn Ther* 2005; 2: 263-272.
32. Wainwright M, Mohr H, Walker W. Phenothiazinium derivatives for pathogen inactivation in blood products. *J Photochem Photobiol B* 2007; 86: 45-58.
33. Wainwright M, Baptista MS. The application of photosensitisers to tropical pathogens in the blood supply. *Photodiagnosis Photodyn Ther* 2011; 8: 240-248.
34. Ilanchelian M, Ramaraj R. Binding Interactions of Toluidine Blue O with Escherichia coli DNA: Formation of Bridged Structure. *J Fluoresc* 2011; 21: 1439-1453.
35. T'ung T. In vitro photodynamic action of methylene blue on Trypanosoma brucei. *Proc Soc Exp Biol Med* 1938; 38: 29–31.
36. Ferreira CS, Bezerra RC, Pinheiro AA. Methylene Blue Vital Staining for Trypanosoma cruzi trypomastigotes and Epimastigotes. *Rev Inst Med Trop* 2006; 48: 347 – 349.

37. Buchholz K, Comini MA, Wissenbach D, Schirmer RH, Krauth-Siegel RL, Gromer S. Cytotoxic interactions of methylene blue with trypanosomatid-specific disulfide reductases and their dithiol products. *Mol Biochem Parasitol* 2008; 160: 65–69.
38. Correa JG, Fairlamb AH, Stoppani AOM. Trypanosoma cruzi Trypanothione Reductase is Inactivated by Peroxidase-Generate Phenothiazine Cationic Radicals. *Free Rad Res* 2001; 34: 363 – 368.
39. Parveen S, Kahn MOF, Austin SE, Croft SL, Yardley V, Rock P, Douglas KT. Antitrypanosomal, antileishmanial, and antimalarial activities of quaternary arylalkylammonium 2-amino-4-chlorophenyl phenyl sulfides, a new class of trypanothione reductase inhibitor, and of N-acyl derivatives of 2-amino-4-chlorophenyl phenyl sulfide. *J Med Chem* 2005; 48: 8087 – 8097.
40. Lima LM, Barreiro EJ. Bioisosterism: a useful strategy for molecular modification and drug design. *Curr Med Chem* 2005; 12: 23 – 49.
41. Kim SY, Kwon OJ, Park JW. Inactivation of catalase and superoxide dismutase by singlet oxygen derived from photoactivated dye. *Biochemie* 2001; 83 : 437 – 444.
42. Khouri R, Bafica A, Silva Mda P, Noronha A, Kolb JP, Wietzerbin J, Barral A, Barral-Netto M, Van Weyenbergh J. IFN- β Impairs Superoxide-Dependent Parasite Killing in Human Macrophages: Evidence for a Deleterious Role of SOD1 in Cutaneous Leishmaniasis. *J Immunol* 2009; 182: 2525-2531.
43. Peloi LS, Biondo CE, Kimura E, Politi MJ, Lonardon MV, Aristides SM, Dorea RC, Hioka N, Silveira TG. Photodynamic therapy for American cutaneous leishmaniasis: The efficacy of methylene blue in hamsters experimentally infected with Leishmania (Leishmania) amazonensis. *Exp Parasitol* 2011; 128: 353–356.
44. Song D, Lindoso JA, Oyafuso LK, Kanashiro EH, Cardoso JL, Uchoa AF, Tardivo JP, Baptista MS. Photodynamic Therapy Using Methylene Blue to Treat Cutaneous Leishmaniasis.

Photomed Laser Surg 2011; 29: 711-715.

45. Capella MAM, Capella LS. A Light in Multidrug Resistance: Photodynamic Treatment of Multidrug-Resistant Tumors. J Biomed Sci 2003: 10

3.2. AIP Conference Proceedings;, Vol. 1364 Issue 1, p51

Morpho-Structural Effects Caused by 660nm Laser Diode in Epimastigotes Forms of *Trypanosoma cruzi*: In Vitro Study

As doenças parasitárias representam um dos principais problemas de saúde pública na América Latina, em particular, a doença de Chagas ou Tripanossomíase americana, causada pelo protozoário *Trypanosoma cruzi*, infecta mais de 18 milhões de pessoas em todos os países da América Latina. A luz visível induz a uma reação fotoquímica, que induz a ativação de enzimas utilizadas principalmente na cadeia respiratória e, esta luz tem como alvos primários os lisossomos e mitocôndrias no interior das células, aumentando a produção de ATP mitochondrial. O objetivo deste estudo foi avaliar as modificações morfo-estruturais geradas nas formas epimastigotas de *Trypanosoma cruzi*, após a irradiação com um laser semicondutor AlGaInP, a um comprimento de onda (λ) igual a 660 nm \pm 10 nm, 40 mW de potência óptica, emitindo luz vermelha no espectro visível, com uma dose de 6J/cm² em modo contínuo. Em seguida, os parasitas que foram submetidos a irradiação foram analisadas ao microscópio óptico e comparadas com outros não tratados. Constatou-se o aumento do tamanho do cinetoplástico (estrutura com elevada concentração de DNA extracelular - kDNA, cuja principal função é a codificar as enzimas da cadeia respiratória tais como ATPase e citocromoxidase), do núcleo da célula e do volume da célula parasita, deixando-o mais arredondado.

Morpho-Structural Effects Caused by 660nm Laser Diode in Epimastigotes Forms of *Trypanosoma cruzi*: *In Vitro* Study

Artur F. S. Barbosa^{a,b}, Luiz G. P. Soares^b, Joubert M. S. Aciole^b, Gilberth T. S. Aciole^b, Ivan R. Pitta^a, Suely L. Galdino^a, Antonio L. B. Pinheiro^b

^aLaboratório de Planejamento e Síntese de Fármacos, Federal University of Pernambuco, 1235 Prof. Moraes Rego Ave, Cidade Universitária, Recife, PE, Brazil, 50670-901

^bCenter of Biophotonics, School of Dentistry, Federal University of Bahia, 62 Araujo Pinho Ave, Canela, Salvador, BA, Brazil, 40110-150.

Abstract: Parasitic diseases represent a major public health problems in Latin America, in particular, Chagas disease or American trypanosomiasis, caused by the protozoan parasite *Trypanosoma cruzi*, infects more than 18 million people in all countries of Latin America. Visible light induces a photochemical reaction, that induces the activation of enzymes used mainly in the respiratory chain, and that light has the primary targets lysosomes and mitochondria of cells, increasing, the mitochondrial ATP production. The purpose of this study was to assess the morpho-structural generated in the epimastigote form of *Trypanosoma cruzi*, after irradiation with a semiconductor laser InGaAlP, at a wavelength (λ) equal to 660nm \pm 10nm, 40 mW optical Power, emitting red light in the visible spectrum, with a dose of 6J/cm² in continuous mode. Then the parasites that have undergone irradiation were analyzed by optical microscopy and compared to untreated. It found the increase in size of the kinetoplast (structure with high concentration of extracellular DNA - kDNA, whose main function is to encode the respiratory chain enzymes such as ATPase and citocromoxidase), the cell nucleus and the cell volume of the parasite, leaving the more rounded.

Keywords: laser Effects, *Trypanosoma cruzi*, photo-biological mechanism

PACS: 42.62.-b.

INTRODUCTION

In 1909, Carlos Chagas realised a unique medical finding describing a new disease known as American trypanosomiasis, as well as its vector and causative agent, the haemoflagellate protozoan *Trypanosoma cruzi* [1].

One hundred years after its discovery, Chagas disease is still epidemiologically relevant, afflicting 16-18 million people in 18 endemic countries in Latin America [2,3]. Several hundred thousand *T. cruzi*-infected individuals may also be living in North America, Europe and other countries as a result of immigration to these areas in search of a better life [4], demonstrating that Chagas disease is a far-reaching public health issue.

The first records of human infection with *Trypanosoma cruzi* date back nine thousand years, to a time when the first humans peopled the Andean coast. Molecular analyses of tissues extracted from human mummies of the Northern Chile and Southern Peru regions showed the presence of the parasite's kinetoplast DNA in 41% of the samples taken [5].

Two types of DNA rings are present in the kinetoplast, the minicircles and the maxicircles. There are several thousand minicircles, which range in size from about 0.5-2.5 kb (depending on the species) and a few dozen maxicircles, usually varying from 20-40 kb [6, 7]. They encode guide RNAs that modify maxicircle transcripts by extensive uridylation insertion or deletion, a process known as RNA editing. Maxicircles are structurally and functionally analogous to the mitochondrial DNA in higher eukaryotes that encodes rRNAs and the subunits of respiratory complexes [8].

Exists in the animal organism a photo-regulator function, based on certain photoreceptor capable of absorbing photons of a certain length where, arriving to cause a change in functional and metabolic activity of the cell. The energy of the photons forming a laser radiation absorbed by a cell will be transformed into biochemical energy and used in its chain [9].

In 1988, Karu found the mechanism of action of different lasers. The lasers used in laser therapy emitting both wavelengths in the visible range and near infrared. The visible laser light induces a photo-chemical reaction, that is, there is a direct activation of synthesis of enzymes [10, 11, 12] and this light has the primary targets lysosomes and mitochondria of cells [9]. The increase in mitochondrial ATP that is produced after laser irradiation, favors a large number of reactions involved in cellular metabolism. The laser accelerates the increase of ATP [13, 14, 15, 16].

MATERIALS AND METHODS

Parasites

Epimastigote forms of Y-strain *T. cruzi* were axenically grown and maintained in complex medium containing 37 g L⁻¹ brain heart infusion (BHI; Difco®, MA, USA), 10 µg L⁻¹ hemin (Sigma®, MO, USA), 20 µg L⁻¹ folic acid (Sigma), and 10% (v/v) fetal bovine serum (FBS; Gibco, BRL®) for 7 days at 28°C.

Laser Therapy

Each well of the culture plate will receive, individual form, irradiation with the laser connected to an optical fiber, with optical power of 30 mW, emitting light in the red visible specter, with a dose of 4J/cm² in continuous mode. After the plate was then incubated at 28°C for 3 hours. After this period a sample was taken from each well and then viewed in the light microscope.

Light microscopy

Epimastigote measurement. The control group and irradiated with the laser were observed in Microscopy Carls-Zeiss Axiostar Plus equipped with a Canon PowerShot A640. Contrasting images of epimastigotes were acquired, both the control and the irradiated with the laser. The images were treated in the Axionvision and analyzed by the researchers who conducted the test.

RESULTS AND DISCUSSION

Throughout the 80s, the researcher Tiina I. Karu, showed the groundwork for understanding the molecular mechanisms underlying the effects of low power light on biological systems [17, 18, 19]. We know the existence of the action of a photo-biological mechanism that regulates the light energy on the respiratory chain of eukaryotic and prokaryotic enzymes with terminal respiratory chain, cytochrome c oxidase in mitochondria, acting as photoreceptor [20]. Cellular responses occur in primary reaction in the respiratory chain reaction and secondary in the cytoplasm and the nucleus of cells [21]. Some of the effects of photostimulation on biological systems are: increased rate of cell proliferation [22], increasing the production rate of fibroblasts and collagen synthesis [23, 24], increased rate of synthesis of RNA and DNA [20,22], ATP synthesis [25], increased vascularity [26], changes in nerve conduction [27], etc.

The mechanisms of action of light after absorption are characterized in primary and secondary. According to Karu (2003) the different mechanisms may lead to similar results by stimulating the mitochondrial redox state toward greater oxidation. Is discussed, however, what mechanisms are critical in a given situation, since factors such as light dose and intensity of use may favor the dominance of either [28]. The primary mechanisms have not been well established with a number of assumptions associated with the generation of singlet oxygen $^1\text{O}_2$ [29]. The secondary mechanisms are responsible for the connection between the response to the action of light by photoreceptor located in the mitochondria and the mechanisms of synthesis of DNA and RNA localized in the nucleus or other phenomena in other components of the cell. There are different regulatory processes associated with control of photo-acceptors on the level of intracellular ATP, transcription factors sensitive to cellular redox state or homeostatic cell signaling cascades in the cytoplasm through the cell membrane to the nucleus [28].

In this study, we observed the morphological and structural changes caused by 660nm laser diode on protozoan *Trypanosoma cruzi*. A larger volume of the nucleus and the mitochondrion-kinetoplast can be observed when comparing the irradiated with the parasite without treatment. The body of the organism treated with the laser also has a change of form, from a more elongated form to a rounder. Mobility was also affected, with the parasites treated a movement noticeably smaller than the control group (Figure 1).

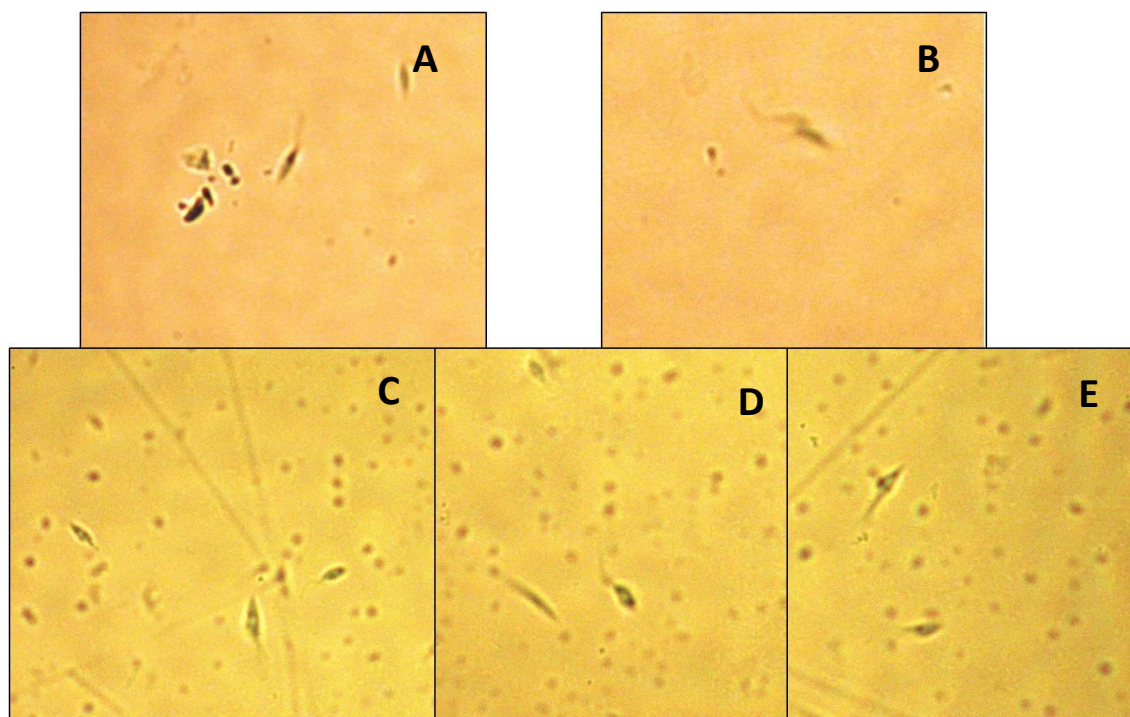


FIGURE 1 – (A,B) Control group; (C,D,E) Laser treated

CONCLUSION

In conclusion, we verified the viability of using laser therapy, so *in vitro* on *Trypanosoma cruzi* parasites. It can be concluded that the laser cause morphological and structural changes in the parasites. These new results leads us, rationally, for the use of photodynamic therapy or lethal photosensitization as a means to combat Chagas disease.

ACKNOWLEDGMENTS

The authors would like to thanks the Coordenação de Aperfeiçoamento de Pessoal de Nível Superior - CAPES for the Grant that allowed the realization of this work

REFERENCES

1. C. Chagas, *Mem Inst Oswaldo Cruz* **1**, 159-218 (1909).
2. J. R. Coura, *Mem Inst Oswaldo Cruz* **102**, 113-122 (2007).
3. J. C. Dias, *Mem Inst Oswaldo Cruz* **102**, 11-18 (2007).
4. G. A. Schmunis, *Mem Inst Oswaldo Cruz* **102**, 75-85 (2007).
5. A. C. Aufderheide, W. Salo, M. Madden, J. Streitz, J. Buikstra, F. Guhl, B. Arriaza, C. Renier, L. E. Wittmers Jr, G. Fornaciari, M. Allison, *Proc Natl Acad Sci USA* **17**, 2034-2039 (2004).
6. T. A. Shapiro, P. T. Englund, *Ann Rev Microbiol* **4**, 117-143 (1995).
7. W. De Souza, D. P. Cavalcanti, *Trends Cell Mol Biol* **2**, 89-104 (2008).
8. W. De Souza, *Mem Inst Oswaldo Cruz* **104**, 89-100 (2009).
9. A. Almeida-Lopes, In: http://www.nupen.com.br/Revista_port/referencias.php, (2009).
10. L. Bolognani, G. Majni, M. Costato, M. Milani, *Bioelectrochem Bioenergetics* **32**, 155 -164 (1993).
11. A. Ostuni, S. Passarella, E. Quaglianillo, *Laser Technol* **4**, 13-16 (1994).
12. P. Bolton, S. Young, M. Dyson, *Laser Therapy* **7**, 55-60 (1995).
13. T. I. Karu, N. K. Smolyaninova, A. V. Zelenin, *Lasers Life Sci* **4**, 167 (1991).
14. H. Loevschall, D. Arenholt-Bindslev, *Lasers Surg Med* **14**, 347-354 (1994).
15. R. Lubart, H. Friedmann, N. Grossmann, M. Adamer, A. Shainberg, *Laser Technol* **6**, 79-84 (1996).
16. R. Lubart, H. Friedmann, M. Sinyakov, A. Shiman, N. Grossman, M. Adamek, A. Shainberg, *Laser Therapy* **9**, 115-120 (1997).
17. T. I. Karu, G. S. Kalendo, V. S. Letokhov, V. V. Lobko, *Nuovo Cimento D* **6**, 828-840 (1982a).
18. T. I. Karu, O. A. Tiphlova, V. S. Letokhov, V. V. Lobko, *Nuovo Cimento D* **4**, 1138-1144 (1983c).
19. T. I. Karu, G. S. Kalendo, V. S. Letokhov, V. V. Lobko, *Soviet Journal of Quantum Electronics* **13**, 1169-1172 (1983a).

20. T. I. Karu, S. F. Kolyakov, *Photomedicine and Laser Surgery* **23**, 355-361 (2005).
21. J. C. P. Dias. 2010.
22. T. I. Karu, *IEEE Journal of Quantum Electronics* **23**, 1703-1717 (1987).
23. Y. Takahashi, S. Hitomi, T. Hirata, T. Fukuse, F. Yamazaki, K. Cho, H. Wada, *The Journal of Thoracic Cardiovascular Surgery* **40**, 288-291 (1992).
24. E. Vinck, B. J. Cagnie, M. J. Cornelissen, H. Declercq, D. C. Cambier, *Lasers in Medical Science* **18**, 95-99 (2003).
25. W. Yu, J. A. Naim, R. J. Lanzaflame, *Laser in Surgery and Medicine* **29**, 105-106 (1997).
26. M. J. Conlan, J. W. Rapley, C. M. Cobb, *Journal of Clinical Periodontology* **23**, 492-496 (1996).
27. E. Vinck, P. Coorevits, B. J. Cagnie, M. Martine, G. Vanderstraeten, D. C. Cambier, *Lasers in Medical Science* **20**, 35-40 (2005).
28. T. I. Karu, *Boca Raton: CRC Press*, 2003.
29. T. I. Karu, *Photobiology of Lower-Power Laser Therapy*. London: Harwood Academic, 1989.
30. T. I. Karu, *Lasers Life Sci* **2**, 53-74 (1988).

3.3. AIP Conference Proceedings;8/24/2011, Vol. 1364 Issue 1, p55

Evaluation of Photodynamic Antimicrobial Therapy (PACT) against Trypomastigotes of *Trypanosoma cruzi*: In Vitro Study

Políticas públicas para o combate da doença de Chagas apresentam-se com um considerável grau de negligência e são classificadas pelo TDR (Programa Especial para Treinamento e Pesquisas em Doenças Tropicais) como nível III, onde o foco das pesquisas deve ser baseado na melhoria e disseminação mundial das ferramentas existentes e das estratégias para o combate destas doenças. Uma nova terapia é proposta para o tratamento da doença de Chagas. A Fotoquimioterapia Antiparasitária é baseada na administração tópica ou sistêmica de um corante não-tóxico e sensível a luz, seguido da irradiação por uma baixa dose de luz visível em um comprimento de onda apropriado ao fotossensibilizador. Na presença do oxigênio encontrado nas células, esta molécula fotossensibilizadora é ativada e pode reagir com moléculas em sua vizinhança através da transferência de elétrons ou hidrogênio, levando a formação de radicais livres (reação tipo I) ou pela transferência de energia ao oxigênio (reação tipo II). Ambos os caminhos podem levar as células a morte e/ou destruição do tecido tratado. Neste trabalho, foi verificada a eficácia da fotoquimioterapia antiparasitária associada a um laser semiconductor de InGaAlP ($\lambda 660\text{nm}$, 30mW , 4J/cm^2 , CW) utilizando o azul de metileno como fotossensibilizador diluído em 6 diferentes concentrações contra as formas tripomastigotas de *T. cruzi*. Para determinar-se a viabilidade dos parasitas, uma amostra de cada grupo tratado em cada concentração foi removido e analisado em um hemocítômetro, observando a diminuição do número de parasitas vivos e sendo comparado com o grupo controle sem tratamento. Os resultados demonstraram um significativo percentual de lises parasitária, o que não pode ser observado nos grupos tratados apenas com o laser ou com os compostos sem a irradiação com o laser.

Evaluation of Photodynamic Antimicrobial Therapy (PACT) against Trypomastigotes of *Trypanosoma cruzi*: In Vitro Study

Artur F. S. Barbosa^{a,b}, Luiz G. P. Soares^b, Joubert M. S. Aciole^b, Gilberth T. S. Aciole^b, Ivan R. Pitta^a, Suely L. Galdino^a, Antonio L. B. Pinheiro^b

^aLaboratório de Planejamento e Síntese de Fármacos, Federal University of Pernambuco, 1235 Prof. Moraes Rego Ave, Cidade Universitária, Recife, PE, Brazil, 50670-901

^bCenter of Biophotonics, School of Dentistry, Federal University of Bahia, 62 Araujo Pinho Ave, Canela, Salvador, BA, Brazil, 40110-150.

Abstract: Policies to combat Chagas disease presents a considerable degree of negligence and is classified at level III by TDR, where the focus of research is based on the improvement and wider dissemination of existing tools and strategies for combating them. The PACT is based on topical or systemic administration of a nontoxic dye sensitive to light, followed by low dose irradiation with visible light of wavelength appropriate. In the presence of oxygen found in the cells, the photosensitizer (FS) enabled may react with molecules in its vicinity by electron transfer or hydrogen, leading to production of free radicals (type I reaction) or by energy transfer to oxygen (type II reaction), leading to production of singlet oxygen. Both paths can lead to cell death and the destruction of diseased tissue. In this work, we verify the effectiveness of PACT associated with a semiconductor laser InGaAlP, a wavelength (λ) equal to $660\text{nm} \pm 10\text{nm}$, 30 mW optical power, emitting red light in the visible spectrum, with a dose of $4\text{J}/\text{cm}^2$ in continuous mode, using methylene blue in five different concentrations on the infective trypomastigote forms of *Trypanosoma cruzi*. To determine the viability of the parasites, one sample from each treatment group at each concentration was removed and analyzed in a hemocytometer, observing the decrease in the number of live parasites for the solution without treatment. The results demonstrated significant percentage of parasite lysis (up to 86% lethality), what can not be observed in the groups treated with laser or with the FS.

Keywords: Photodynamic Antimicrobial Therapy, PACT, *Trypanosoma cruzi*, Chagas Disease

PACS: 42.62.-b.

INTRODUCTION

The protozoan parasite *Trypanosoma cruzi* is the causative agent of American trypanosomiasis or Chagas disease, a human harmful disease affecting 16 to 18 million people in South and Central America [1]. The treatment of Chagas disease, which is endemic in Latin America and caused by the protozoan *Trypanosoma cruzi*, is based on two nitroheterocycles (nifurtimox and benznidazole) that present severe side effects, and their efficacy during the chronic phase is still controversial with poor indices of apparent cure [2].

This parasite has a single mitochondrion, which contains a branched electron transport chain, cyanide-resistant respiration mediated by an alternative oxidase [3], and a specialized region rich in DNA named a kinetoplast, which is a hallmark of Kinetoplastida protozoa [4], making this organelle an extraordinary drug target [5] and for a new technique, the photodynamic antimicrobial therapy (PACT).

PACT is based on topical or systemic administration of a nontoxic dye sensitive light followed by low dose irradiation with visible light of appropriate wavelength [6]. In the presence oxygen found in the cells, the photosensitizer (FS) system can react with molecules in its neighborhood by electron transfer or hydrogen, leading to production of free radicals (reaction type I) or by energy transfer to oxygen (type II reaction), leading to production of singlet oxygen. Both paths can lead to cell death and the destruction of diseased tissue [7,8].

Compared with other cytotoxic therapy, PACT has advantage of dual selectivity: not only the FS can be directed to the cells or diseased tissue, but also the light can be precisely focused at the lesion site. [9, 10]. The procedure can be repeated several times, if necessary, since no toxic effects and is usually not invasive. Also, because of their low risk, can be used in elderly or who are too weak to be undergo surgery [11].

Methylene blue (MB) is a well known blue dye. The blue colour of an aqueous solution of MB is due to the fact that the phenothiazinium molecule absorbs visible light strongly in the region 600–700 nm, thus allowing the remainder of the visible spectrum (350–600 nm) to be transmitted. Where the MB molecule differs from other

blue dye types (e.g. blue azoic or anthraquinone dyes) is that the absorbed light energy can be passed on efficiently to other molecules in the vicinity [12].

The electronically excited MB molecule is relatively stable and can undergo an electronic rearrangement. The rearranged form is known as an excited triplet state and it is this that facilitates photodynamic action. A relatively long-lived excited triplet state allows the excited MB molecule to pass on the excitational energy to other molecules. Direct interaction with adjacent molecules leads to electron transfer or hydrogen abstraction and the formation of radical species. This is known as Type I photosensitization, and with membrane-related molecules leads to the formation of lipid hydroperoxides and thus to membrane damage.

If the excited triplet state molecule interacts directly with oxygen, the excitational energy is transferred causing the formation of a highly reactive species, singlet oxygen. Formed in situ within a cellular environment, singlet oxygen is highly toxic on account of its oxidising activity, although it has a very short lifetime and will decay to the ground state (non-toxic triplet oxygen) within microseconds. Singlet oxygen-mediated photosensitization is known as the Type II pathway [12]. The study of the parasite-specific trypanothione-based thiol metabolism as a target of methylene blue (MB, MB⁺) or of MB-containing drug combinations is recommended for Boda et al. Other papers had previously shown effects of MB on *T. cruzi* [13,14] and several leishmania species [15,16].

MATERIALS AND METHODS

Cytotoxicity Assay

The cytotoxicity of the compounds was determined using BALB/c mice splenocytes (5×10^6 cells/well), obtained by Pereira et al 2004 [17], cultured in 96-well plates in RPMI 164 (Sigma Chemical Co) supplemented with 10% of fetal calf serum (Cultilab, Campinas, SP) and 50 µg/mL of gentamycin (Novafarma, Anápolis, GO). Each compound was dissolved in NaCl 0,9 and was evaluated for their ability to inhibit splenocytes proliferation at concentration in six concentrations (0,78 – 0,39 – 0,19 – 0,1 – 0,05 e 0,025 µg/mL), in duplicate. Cell proliferation was determined by adding 1 µCi of [³H] – thymidine per well for 24 h at 37°C and 5% CO₂. After this period, the content of the plate was harvested to determine the ³H-thymidine incorporation using a beta-radiation counter (β-matrix 9600, Packard). The toxicity of the compounds was determined comparing the percentage of ³H-thymidine incorporation of drug-treated wells in relation to untreated wells. Non-toxic concentrations were defined as those causing a reduction of ³H-thymidine incorporation below 30% in relation to untreated controls.

Parasites

Trypanosoma cruzi Y strains were used. *T. cruzi* tissue culture trypomastigotes were obtained from the supernatant of 5–6 day-old infected Vero cells. Infected cells were maintained in RPMI-1640 medium supplemented with 2% fetal calf serum (FCS) for 5–6 days at 37 °C in a 5% humidified CO₂ atmosphere. After this time, supernatant was collected, centrifuged at 500×g for 5 min and allowed to remain at 37 °C for 30 min. During this period, trypomastigotes in the pellet moved into the supernatant medium which was collected and centrifuged at 1000×g for 10 min. Trypomastigotes concentrated in the pellet were counted in a Neubauer chamber, and used in a concentration of 5×10^6 cells to infect a monolayer of host cells cultivated in 25 cm² culture flasks. After a 24 h infection, culture medium was changed to remove free parasites, being the host cells then incubated again at 37 °C in a 5% humidified CO₂ atmosphere. Culture medium was changed every 48 h.

Phototherapy

To determine the effect of irradiation with the laser diode on trypomastigotes of *Trypanosoma cruzi*, 2×10^5 parasites were placed in triplicate in wells of culture plates of 96 wells in 200 µl volume. Each well of the culture will receive, individual form, irradiation with the laser connected to an optical fiber, with optical power of 30 mW, emitting light in the red visible specter, with a dose of 4J/cm² in continuous mode. After the plate was then incubated again at 37 °C in a 5% humidified CO₂ atmosphere for 24 hours and after this period was performed to count the parasites. The equipment used for photosensitization will be the Laser[®] Hand (MM Optics, São Carlos, SP), class 3R ANVISA. The Laser Hand[®] has a semiconductor diode InGaAlP, it emits radiation of continuous form (CW), in a wave length (λ) equal 660nm ± 10nm, optic power of 40 mW, frequency of 50-60Hz and diameter of spot (Φ) of 0,4mm². Fiber optics are provided by the manufacturer and are made of flexible material e promotes a loss of up to 30% of the energy. The tests will be conducted to a control culture of parasites without treatment. The percentage of activity against the parasite is determined by comparing the values of viable parasites counted by the hemocytometer, wells irradiated with the laser and the values of the untreated control. All the procedures that to involve the laser use will be executed with eyeglasses supplied for the manufacturer.

Anti-proliferative Effect For *Trypanosoma cruzi*

To determine the anti-proliferative effect for *Trypanosoma cruzi*, trypomastigotes ($4 \times 10^6/\text{ml}$) grown as Bisaggio (2006) [18], will be placed in 96-well plates in 100 μl volume. The growth of trypomastigote forms will be held in the absence and presence of different concentrations of photosensitizer for 24 hours under appropriate conditions (37°C and 5% CO_2). The tests will be conducted as control cultures of parasites without treatment. The percentage of activity against the parasite is determined by comparing the values of viable parasites counted by the hemocytometer, the wells incubated with the photosensitizer and the values of untreated control. Next will be evaluated in terms of percentage of mortality of the parasites.

Photodynamic Antimicrobial Chemistry Therapy

The samples then will be increased of the photosensitizer of form that reaches the desired concentration. The culture plate is then closed and stored in the dark for a period of five minutes, that is the pre-irradiation period (PIP). After this time, each well of the culture will receive, individual form, irradiation with the laser connected to an optical fiber, with optical power of 30 mW, emitting light in the red visible specter, with a dose of $4\text{J}/\text{cm}^2$ in continuous mode. After the plate was then incubated again at 37°C in a 5% humidified CO_2 atmosphere for 24 hours and after this period was performed to count the parasites. The equipment used for photosensitization will be the Laser® Hand (MM Optics, São Carlos, SP), class 3R ANVISA. The Laser Hand® has a semiconductor diode InGaAlP, it emits radiation of continuous form (CW), in a wave length (λ) equal $660\text{nm} \pm 10\text{nm}$, optic power of 40 mW, frequency of 50-60Hz and diameter of spot (ϕ) of $0,4\text{mm}^2$. Fiber optics are provided by the manufacturer and are made of flexible material e promotes a loss of up to 30% of the energy. All the procedures that to involve the laser use will be executed with eyeglasses supplied for the manufacturer.

RESULTS AND DISCUSSION

Cytotoxicity Assay

Methylene blue was shown to be atoxic at concentrations below $1\mu\text{g}/\text{ml}$ (Figure 1). At concentrations below this, methylene blue did not affect the cell viability to undermine their development.

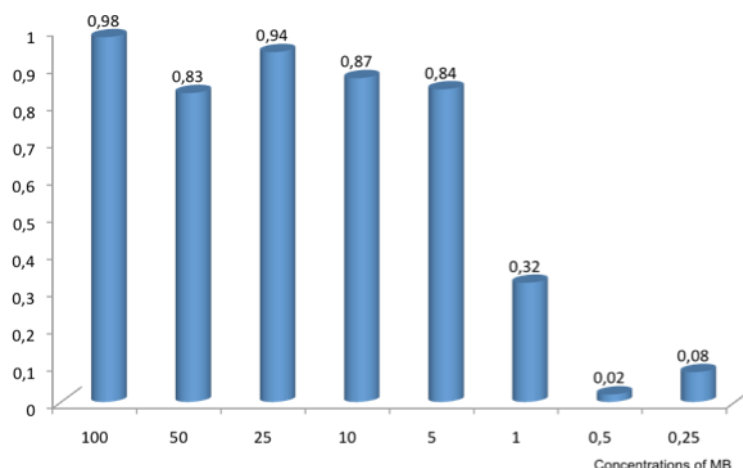


FIGURE 1: Cytotoxicity Assay – Methylene Blue values

After 24 hours the day of PACT, the parasites were counted using a Neubauer chamber to determine the percentage of lysis caused by the technique. Most non-toxic concentration ($0,78\mu\text{g}/\text{ml}$) the percentage of lysis was 86% as the chart (Figure 2). Since this is a work job, some parameters used were based on existing information on Photodynamic antimicrobial Therapy and previous data acquired by our research group.

The compound phenothiazine methylene blue proved to be toxic to animal cells at concentrations above $1\mu\text{g}/\text{ml}$. Nontoxic concentrations were those that showed a reduction below 30% in the 3H-thymidine incorporation compared to untreated controls. Based on these data, the concentrations used and employed in testing anti-proliferative effect against *T. cruzi* and the test for Photodynamic Antimicrobial Therapy was always below $1\mu\text{g}/\text{ml}$. Another important feature of these concentrations on the work, is the fact that they are much smaller when

compared to concentrations of methylene blue used in the literature, with other microorganisms such as bacteria for example.

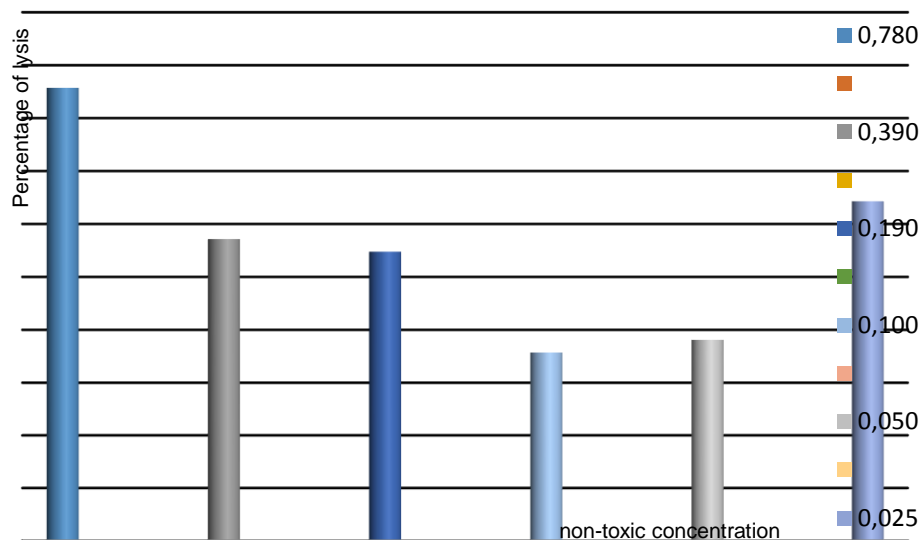


FIGURE 2: Percentage of lysis of the parasites

Phototherapy with laser diode was analyzed by comparing the laser group with the control group. After 24 hours of irradiation with the laser, in this experiment were not found significant differences in mortality between groups of parasites tested. Also not proliferative effect was observed in the parasites after laser application, as statistical analysis.

Several authors have published on the inactivation of *Trypanosoma cruzi* by phenothiazine derivatives [13, 19, 20, 21]. Some enzymes has been demonstrated to be targets of methylene blue as trypanothione reductase inhibitors and other (di) thiols were oxidized to disulfides by the dye. The superoxide dismutase also demonstrated suffer inactivation by methylene blue [22]. But this behavior of the parasites was not observed at the concentrations tested, because we did not identify statistical variations in mortality of the parasites causes by methylene blue compared to the control group.

All parameters used for Photodynamic Antimicrobial Therapy were based on prior information acquired by the group in working with other microorganisms. As initial work, we opted to use the best values of the dose and potency of the laser and the incubation time observed in bacteria. Parallel studies, evaluating the best values on dose and laser power, and the incubation period of more effective are being conducted in our laboratory.

With this dose we used to demonstrate the effectiveness of photosensitization in killing the parasite *Trypanosoma cruzi* trypomastigotes. As the Photodynamic Antimicrobial Therapy against *Trypanosoma cruzi* was first employed by us, some points that cause the lethality of the parasite are not explained, creating a new strand of research for our group to analyze.

The mechanism by which death occurs, the parasite could perhaps be explained by photodynamic reaction type II, when the molecule of the photosensitizer in its excited triplet state with one molecule of oxygen, which also has its triplet ground state, it transfers its energy to this molecule forming the excited state singlet oxygen. This state of oxygen is chemically very active and can induce various chain reactions with cell components such as DNA, proteins, cell membrane phospholipids, resulting in cell death.

Other experiments employing Photodynamic Antimicrobial Therapy with the protozoan *Trypanosoma brucei*, *Leishmania brasiliensis*, *Leishmania chagasi*, *Plasmodium falciparum* and *Plasmodium vivax* parasites causing the sleeping sickness (African trypanosomiasis), cutaneous leishmaniasis visceral leishmaniasis and malaria, respectively, are also being conducted by our research group for upcoming publications.

CONCLUSION

In conclusion, we studied the use of laser with a new approach, activity anti-*Trypanosoma cruzi*. The lethal photosensitization can serve as a new tool in the fight against Chagas disease. The promising results in vitro study lead you to further studies to better use of therapy.

ACKNOWLEDGMENTS

The authors would like to thanks the Coordenação de Aperfeiçoamento de Pessoal de Nível Superior - CAPES for the Grant that allowed the realization of this work.

REFERENCES

1. World Health Organization, 2002 World Health Organization (2002). Chagas Disease. Tropical Disease Research, 18th Program Report, UNDP/WB/TDR, Geneva
2. J. Jannin, L. Villa, Mem. Inst. Oswaldo Cruz **102**, 95–97 (2007).
3. J. Fang, D. S. Beattie, Arch. Biochem. Biophys. **414**, 294–302 (2003).
4. T. A. Shapiro, P. T. Englund, Annu. Rev. Microbiol **49**, 117–143 (1995).
5. M. N. Soeiro, S. L. De Castro, Expert Opin. Ther. Targets **13**, 105–121 (2009).
6. F. Gad, T. Zahra, T. Hasan, M.R. Hamblin, Antimicrob. Agents Chemother **48**, 2173 (2004).
7. S. A. G. Lambrechts, M. C. G. Aalders, J. V. Marle, Antimicrob. Agents Chemother **49**, 2026 (2005).
8. T. N. Demidova, M. R. Hamblin, Antimicrob. Agents Chemother **49**, 2329 (2005).
9. T. N. Demidova, M. R. Hamblin, Int. J. Immunopathol. Pharmacol **17**, 245 (2004).
10. M. R. Hamblin, T. Hasan, Photochem. Photobiol. Sci **3**, 436 (2004).
11. J. R. Perussi, Quím. Nova, **30** (2007).
12. M. Wainwright, International Journal of Antimicrobial Agents **16**, 381-394 (2000).
13. C. S. Ferreira, R.C. Bezerra, A. A. Pinheiro, Rev Inst Med Trop **48**, 347–349 (2006).
14. N. Girones, J. .L Bueno, J. Carrion, M. Fresno, E. Castro, Vox Sang **91**, 285–291 (2006).
15. J. Mauel, Mol Biochem Parasitol **13**, 83–96 (1984).
16. D. A. Maugeri, J. J. Cazzulo, R. J. Burchmore, M. P. Barrett, P. O. Ogbunode, Mol Biochem Parasitol **130**, 117–25 (2003).
17. V. R. A. Pereira, V. M. B. Lorena, A. P. Galvão da Silva, E. M. Coutinho, P. Miranda, E. D. Silva, A. G. P. Ferreira, M. A. Krieger, S. Goldenberg, R. Correa-Oliveira, Y. M. Gomes, Parasitology **129**, 563-570 (2004).
18. D. F. R. Bisaggio, L. Companati, R. C. V. Pinto, T. S. Padrón, Acta Tropica **98**, 162 - 175 (2006).
19. M. J. M. Alves, M. Rabinovitch, Infection and Immunity **39**, 435-438 (1983).
20. K. Buchholz, M. A. Comini, D. Wissenbach, R. H. Schirmer, R. L. Krauth-Siegel, S. Gromer, Molecular & Biochemical Parasitology **160**, 65–69 (2008).
21. M. Wainwright, H. Mohr, W. H. Walker, Journal of Photochemistry and Photobiology B: Biology **86**, 45–58 (2007).
22. S. Y. Kim, O. K. Kwon, J. W. Park, Biochimie **83**, 437-444 (2001).

3.4. Proc. SPIE, 8211, 82110N, doi: 10.1117/12.909409

Evaluation of Photodynamic Antimicrobial Therapy (PACT) against Promastigotes Form of the *Leishmania (Viannia) braziliensis*: In Vitro Study

Leishmaniose é uma doença complexa que afeta cerca de 12 milhões de pessoas em 88 países ao redor do mundo. *Leishmania braziliensis* é a espécie mais comum nas Américas e a principal espécie causadora de leishmaniose cutânea e mucocutânea no Brasil. As opções terapêuticas disponibilizadas para o tratamento dos pacientes são muito limitados ou insatisfatórios. Para a leishmaniose cutânea, os antimoniais pentavalentes são a primeira opção de indicação preconizado pela Organização Mundial de Saúde, porém não são muito bem aceitos e apresentam uma série de efeitos adversos. Neste trabalho, neste trabalho buscou avaliar a eficácia da Fotoquimioterapia Antiparasitária de forma *in vitro*, como uma nova opção para o tratamento da leishmaniose cutânea. Para isto um semiconductor laser ($\lambda 660\text{nm}$, 40mW, 4,2 e 8,4 J/cm², CW) associado a derivados fenotiazínicos em duas concentrações, 5 e 10 µg/ml, contra as formas promastigotas de *L. braziliensis* com um período de pré-irradiação de 5 minutos. Após 72h de incubados após a fotoquimioterapia antiparasitária, a viabilidade destes parasitas foi analisada e a contagem dos parasitas viáveis foi realizada para se identificar o percentual de letalidade da FQTAp. Não foi identificada letalidade dos compostos nas doses testadas, assim como, da ação isolada do laser, porém o composto azul de toluidina na concentração de 10 µg/ml apresentou o melhor resultado.

Evaluation of Photodynamic Antimicrobial Therapy (PACT) against Promastigotes Form of the *Leishmania (Viannia)* *braziliensis*: In Vitro Study

Artur F. S. Barbosa^{a,b,c}, Bruno B. Sangiorgi^b, Suely L. Galdino^a, Ivan R. Pitta^a, Manoel Barral-Netto^b, Neandder A. Correia^c, Antônio L. B. Pinheiro^{c,d}

^aLaboratory of Planning and Synthesis of Drugs, Federal University of Pernambuco, 1235 Prof. Moraes Rego Ave, Cidade Universitária, Recife, PE, Brazil, 50670-901

^bLaboratory Integrated of Microbiology and Immunoregulation, Research Center Gonçalves Moniz, 121 Waldemar Falcão Street, Candeal, Salvador, BA, Brazil, 40296-710

^cCenter of Biophotonics, School of Dentistry, Federal University of Bahia, 62 Araujo Pinho Ave, Canela, Salvador, BA, Brazil, 40110-150.

^dNational Institute of Optics and Photonics, University of São Paulo, 400 Trabalhador Sancarlense Ave, São Carlos, SP, Brazil, 13560-970

ABSTRACT

Leishmaniasis is a complex disease that affects more than 12 million people in 88 countries worldwide. *Leishmania (Viannia) braziliensis* is the most common species in the Americas and the most important causative agent of cutaneous and mucocutaneous leishmaniasis in Brazil. The therapeutic arsenal routinely employed to treat patients with leishmaniasis is limited and unsatisfactory. For cutaneous leishmaniasis, pentavalent antimonials are the first line therapeutic scheme recommended by the WHO. These compounds are highly toxic, poorly tolerated and their effectiveness highly variable. In this work, a technique with, so far, an unknown disadvantage is discussed. The aim of this study was to verify the effectiveness of PACT in vitro, as a new technique for the treatment of Leishmaniasis. For this, semiconductor laser ($\lambda = 660\text{nm}$, 40mW, 4.2J/cm², CW) associated to phenothiazine's derivatives (5 and 10 $\mu\text{g/ml}$, TBO, Methylene Blue or Phenothiazine) on the promastigotes form of *Leishmania braziliensis* in a single session was used. Viability of the parasites was assessed in quadruplicates of each group. The samples were removed and analyzed in a hemocytometer 72h after PACT. We found an important decrease in the number of viable parasites on all treated groups in comparison to their controls. The results of present study showed significant percentage of lethality (above 95%) of the protocol. The 99.23% of lethality was achieved with 10 $\mu\text{g/ml}$ of TBO. No lethality was seen on groups treated neither with laser nor with each compounds separately. The results are promising and indicative that the use of PACT may be a powerful treatment of leishmaniasis when compared to already available ones.

Key words: New Therapy- Leishmaniasis- Toluidine Blue O - Methylene Blue - Phenothiazine.

1. INTRODUCTION

Antimicrobial Photodynamic Therapy (PACT) is a new technique-based on topical or systemic administration of a nontoxic dye sensitive light followed by low dose irradiation with visible light of appropriate wavelength. In the presence oxygen found in the cells, the photosensitizer (PS) system may react with molecules in its neighborhood by electron transfer or hydrogen, leading to production of free radicals (reaction type I) or by energy transfer to oxygen (type II reaction), leading to production of singlet oxygen. Both paths may lead to cell death and the destruction of diseased tissue ¹. Compared with other cytotoxic therapy, PACT has advantage of dual selectivity: not only the PS may be directed to the cells or diseased tissue, but also the light may be precisely focused at the lesion site^{2,3}. The procedure may be repeated several times, if necessary, since no toxic effects and is usually not invasive. Also, because of their low risk, may be used in elderly or who are too weak for undergoing surgery ⁴.

Photosensitizers are drugs that when combined with light in specific wavelength, produces reactive oxygen species (ROS) and reactive nitrogen species (RNS), leading to cell death^{5,6}. When the aromatic molecules that are stimulated by light energy, they suffer an electronic transition to the singlet excited state. Depending on the molecular structure and environment, this molecule may lose its energy by physical or electronic, returning to its

ground state, or may undergo a transition to its excited triplet state. At this stage the molecule may again suffer a decay back to the ground state, and may suffer redox reactions with the environment, or your excitational energy may be transferred to other molecules of oxygen (also in triplet state) leading to the formation of labile singlet oxygen⁵. Various photosensitizers (PSs) have demonstrated light-induced killing activities toward different cell types; however, in dermatologic settings. Porphyrin, chlorin, and phenothiazine molecules demonstrated significant antimicrobial PDT activity in vitro, some of which have been used in clinical practice in the treatment of malignancies⁷.

Phenothiaziniuns are blue dyes (max 600–660 nm) such as Methylene Blue (MB) and Toluidine Blue O (TBO). The first report of its photodynamic action (against bacteriophages and viruses) appeared as early as 1930. Both MB and TBO are used in surgical identification of abnormal cells at reasonably high concentrations (normally 1% w/v) without causing human toxicity. TBO is known to be membrane active, since it causes increased permeability, whereas MB causes strand breaks in this nucleic acid⁵. Phenothiazine derivatives exhibit promising biological activities such as anticancer, antiviral, anti-inflammatory, anticonvulsant, analgesic, immunosuppressive, multidrug resistance reversal properties, antifungal, antimalarial, antifilarial, trypanocidal and leishmanicidal⁸.

Leishmaniasis is a disease caused by protozoan parasites belonging to the genus *Leishmania*. The parasites are transmitted by the bite of a tiny – only 2–3 mm long – insect vector, the phlebotomine sandfly. Leishmaniasis threatens about 350 million men, women and children in 88 countries around the world. As many as 12 million people are believed to be currently infected, with about 1–2 million estimated new cases occurring every year. The disease may have a wide range of clinical symptoms, which may be cutaneous, mucocutaneous or visceral. Cutaneous leishmaniasis is the most common form. Visceral leishmaniasis is the most severe form, in which vital organs of the body are affected⁹.

Among several drugs used in the treatment of leishmaniasis, pentavalent antimonials, considered a gold standard in the treatment, are known to be very toxic to humans. Pentavalent antimonials meglumine antimoniate and sodium stibogluconate have been considered the first option of treatment of leishmaniasis and Amphotericin B is the second drug of choice when there is no response to treatment with antimonials or when it is not possible to use it. The efficacy of pentamidine, the third drug of choice, is less well known¹⁰. Furthermore, as the drugs used in treatment are expensive and their use is mostly limited in undeveloped and developing countries. Ineffectiveness of drugs against several species of *Leishmania* is another disadvantage. For these reasons, new approaches in the treatment of leishmaniasis are urgently needed¹¹.

The aim of this study was to investigate, *in vitro*, the possible antileishmanial effects of the use of Photodynamic Antimicrobial Chemotherapy in *Leishmania brasiliensis* in culture

2. MATERIALS AND METHODS

2.1. Chemicals

Methylene Blue (MB) and Toluidine Blue O (TBO) were purchased from Sigma-Aldrich Corporation (Milwaukee, WI, USA). Three compounds were used: MB, TBO and a 1:1 mixture of MB + TBO, here named as phenothiazine - FTZ. The stock solutions were diluted in distilled water (10 or 20 µg / ml).

2.2. Culture Promastigotes forms

L. braziliensis (strain MHOM/BR/01/BA788 - cultivated and maintained by the Laboratorio Integrado de Microbiologia e Imunoregulação) promastigotes were cultivated in Schneider's Insect Medium (Sigma Chemical Co., St Louis, Mo, USA) supplemented with 20% heat-inactivated fetal bovine serum (Gibco, Carlsbad, CA, USA), L-glutamine (2 mM), penicillin (100 U/ml), streptomycin (100 µg/ml) at 26 °C (Thermostat cabinets – LS Scientific, Ikeja, Lagos, Nigeria) for 5–7 days when the parasites reached the stationary-phase. After reaching the stationary-phase, the culture was sedimented by centrifugation (5810 R, Eppendorf, Hamburg, Germany, 10 min, 4°C, 4000 rpm), suspended in 1 mL of the same medium and quantified in a Neubauer chamber (LO - Laboroptik GmbH, Friedrichsdorf, Germany) with the aid of a microscope (Nikon Eclipse E200, Melville, NY, USA). Enough medium was added in order to adjust the parasitic concentration to 2×10^6 promastigotes/mL¹².

2.3. Leishmanicidal activity against Promastigotes

The determination of the leishmanicidal activity was performed in 96-well plates (Tesplate 96F - TPP, Zollstrasse, Trasadingen, Switzerland). The compounds were tested in quadruplicate in two concentration 5 or 10 $\mu\text{g/mL}$. The parasitic concentration in the wells was that of 2×10^6 promastigotes/mL. A negative control was performed with four wells containing only parasites and the incubation medium. After 72 h of incubation at 26°C , 10 μL of each well was diluted in 90 μL of the PBS and the parasites were quantified in a Neubauer chamber. The data obtained from this quantification were plotted in a graph using Microsoft Excel and the values of the lethality of the treated groups were obtained through the difference in percentage of viable parasites in the groups treated with the amount of viable parasites in the control group.

2.4. Photodynamic Therapy

Metacyclic promastigotes were pre-incubated during 5 or 60 minutes, in darkness, with the different concentrations of the photosensitizers in Schneider's Drosophila medium (pH 7.2) with 10% FBS in 96-well plates. After this pre-incubation, each well was irradiated by a Laser device ($\lambda = 660\text{nm}$, 40mW, $4.2\text{J}/\text{cm}^2$, CW, TwinFlex, MMOptics, São Carlos, São Paulo, Brazil). After 72 h of incubation at 26°C , 10 μL of each well was diluted in 90 μL of of the PBS and the parasites were quantified in a Neubauer chamber. The data obtained from this quantification were plotted in a graph using Microsoft Excel and the values of the lethality of the treated groups were obtained through the difference in percentage of viable parasites in the groups treated with the amount of viable parasites in the control group.

2.5. Crystal Violet Toxicity Assay

One day after photochemotherapy, the culture media was removed from the wells (Tesplate 96F - TPP, Zollstrasse, Trasadingen, Switzerland) and 100 μL of methanol was added and the plate, and incubated for 20 minutes at room temperature (25°C). Methanol was then removed from the wells, being added 50 μL of Cristal Violet Dye (0.5% Crystal Violet, 20% Methanol, 80% dH_2O , Sigma-Aldrich Corporation (Milwaukee, WI, USA) followed by incubation for 10 minutes at room temperature. After that period, the dye was removed and the wells washed twice with tap water, followed by two immersions of the plate in a becker filled with tap water. To extract de dye from the cells, 100 μL of Sorenson's buffer (SDS) was added in the wells and the plate was incubated in a rotate shaker for 30 minutes. An ELISA - SpectraMax 190 Microplate Reader (Sunnyvale, CA, USA) plate reader was used for the absorbance measurement at wavelength of 540nm

2.6. Statistical analysis

Statistical analysis was performed using the software Minitab14 (Minitab, Belo Horizonte, MG, Brazil) where the ANOVA was used to test intergroup and for intragroup, we used the t-student test. The level of significance was set at 95%.

3. RESULTS

On regarding the type of photosensitizer used we found that protocols using MB at 5 $\mu\text{g/mL}$ showed significant differences were observed between groups $4.2\text{J}/\text{cm}^2/5\text{min}$ and $4.2\text{J}/\text{cm}^2/60\text{min}$ ($p < 0.001$). When increasing the concentration to 10 $\mu\text{g/mL}$, no significant differences were seen between group $4.2\text{J}/\text{cm}^2/5\text{min}$ and $4.2\text{J}/\text{cm}^2/60\text{min}$ ($p > 0.05$).

When using TBO at 5 $\mu\text{g/mL}$, no significant differences were seen between groups $4.2\text{J}/\text{cm}^2/5\text{min}$ and $4.2\text{J}/\text{cm}^2/60\text{min}$ ($p > 0.05$). Increasing the concentration to 10 $\mu\text{g/mL}$, no significant differences were observed between groups $4.2\text{J}/\text{cm}^2/5\text{min}$ and $4.2\text{J}/\text{cm}^2/60\text{min}$ ($p > 0.05$).

Using the FTZ at 5 $\mu\text{g/mL}$, no significant differences were observed between groups $4.2\text{J}/\text{cm}^2/5\text{min}$ and $4.2\text{J}/\text{cm}^2/60\text{min}$ ($p > 0.05$). Increasing the concentration to 10 $\mu\text{g/mL}$, no significant differences were observed between groups $4.2\text{J}/\text{cm}^2/5\text{min}$ and $4.2\text{J}/\text{cm}^2/60\text{min}$ ($p > 0.05$).

Analyzing the energy density, we found that, using an energy density of $4.2\text{J}/\text{cm}^2$ and incubation time of 5 minutes, was found significant differences between groups MB $5\mu\text{g}/\text{ml}$ and $10\mu\text{g}/\text{ml}$ ($p < 0.001$), TBO $5\mu\text{g}/\text{ml}$ and $10\mu\text{g}/\text{ml}$ ($p < 0.001$). Significant differences were also found between groups MB $5\mu\text{g}/\text{ml}$ and TB $10\mu\text{g}/\text{ml}$ ($p < 0.001$), MB $5\mu\text{g}/\text{ml}$ and FTZ $10\mu\text{g}/\text{ml}$ ($p < 0.001$), TB $5\mu\text{g}/\text{ml}$ and MB $10\mu\text{g}/\text{ml}$ ($p < 0.001$), TB $5\mu\text{g}/\text{ml}$ and FTZ $10\mu\text{g}/\text{ml}$ ($p < 0.001$), and between groups FTZ $5\mu\text{g}/\text{ml}$ and TB $10\mu\text{g}/\text{ml}$ ($p < 0.001$), and FTZ $5\mu\text{g}/\text{ml}$ and FTZ $10\mu\text{g}/\text{ml}$ ($p = 0.02$).

So the use of either $10\mu\text{g}/\text{ml}$ of TBO or FTZ during 5 minutes prior irradiation with $4.2\text{J}/\text{cm}^2$ 660nm laser light was the best protocol used to kill *Leishmania brasiliensis*. When the incubation time was increased to 60 minutes, all compounds were similarly effective.

4. DISCUSSION

Leishmaniasis are protozoan parasitic infections transmitted to humans as well as several vertebrate species, by phlebotomine sandflies and they are associated with three main types of disease manifestations: visceral, cutaneous, and mucocutaneous, causing a broad spectrum of clinical conditions with different degrees of severity depending on the tissue they invade (superficial [skin and mucous membranes] or deep [hematopoietic tissues such as spleen, bone marrow, etc])^{13,14}. The principal species causing cutaneous leishmaniasis (CL) in Brazil is *Leishmania brasiliensis* which most often leads to a cutaneous form of the disease characterized by one or more ulcers with raised borders, most frequently located on the upper and lower extremities, but also found on the head, face, and trunk^{15,16}.

The drugs for the treatment of CL nevertheless, adverse effects have been reported since the first trials in affected populations, including other vertebrates such as canines, being this toxicity mostly related to pancreatic and liver damage¹⁷⁻¹⁹. Toxicity is due to an osmolarity increase in batches or emergence of free trivalent metabolites whose presence should only be detected after the pentavalent fraction is processed by the effect of pH in the parasitophorous vacuole within macrophages where it should arrive to exert its leishmanicidal function. Given these adverse effects, the safety of pentavalent antimonial formulations is currently being subject of intense debate, especially as the residual effects of these metabolites on other target organs are still ignored and previous reports pointing out to a reduction in cellular populations such as polymorphonuclear cells; suggest that these formulations are also potentially immunotoxic¹⁴.

The present study investigated the antileishmanial effects of PACT, using phenothiazines derivatives as photosensitizer, against *L. brasiliensis* parasites using two different incubation times (5 and 60 minutes). It was found that both 5 and 60 minutes of pre-irradiation resulted in antileishmanial effects by inhibiting growth, metabolic activity, and infectivity of promastigotes in culture. It was also demonstrated that the antileishmanial effect of both phenothiazines derivatives and the Laser in ($4.2\text{J}/\text{cm}^2$) used isolated did not present inhibition. Inhibition was achieved when association of the Laser and the photosensitizer was used. Despite several previous studies on the its antibacterial, antiviral, and antifungal activities, with phenothiazines⁸ we were not able to find any study on regards the antileishmanial effect of TBO on *L. brasiliensis* parasites.

The phenothiazines have established great affinity by the Trypanosomatídeos²⁰⁻²². Trypanothione and trypanothione reductase (TryR)-based redox metabolism found in *Leishmania sp.* and other trypanosomatids exemplify the unique features of this group of organisms. Its absence in mammalian hosts, together with the sensitivity of trypanosomes against oxidative stress, makes this enzyme a unique target for exploitation for potential antileishmanial chemotherapeutics²³⁻²⁶. Trypanothione reductase (TR) was irreversibly inhibited phenothiazine derivatives. The inactivation of TR depends on (a) of incubation with the phenothiazine derivatives (b) the free radicals formed (c) and the concentration and structure of phenothiazine derivatives²⁴.

The main reason for using phenothiazine derivatives in this study was their capacity to produce ROS and RNS, when excited by laser, which *Leishmania* parasites are known to be susceptible to¹¹. In PACT, a light-activated molecule known as photosensitizer (PS) is used to generate cytotoxic reactive chemical species with spatial specificity governed by both the localization of the PS itself and the delivery of light of a specific wavelength required for therapeutic excitation of the PS²⁷. The Ps produce highly reactive hydroxyl radical species from Type I PACT reactions and singlet oxygen species from Type II PACT reactions. Both pathways may induce cell death. Singlet oxygen is the predominant cytotoxic agent with a very short lifetime for highly localized tissue damage restricted to the small region around photosensitizers²⁸. Hydroxyl radical species from Type I PDT reactions may become more dominant when the photosensitizers are highly concentrated in a region, especially under hypoxic conditions¹⁹. Cytotoxic photochemical and photobiological responses resulting from the interaction of these

reactive species with tissues cause irreversible damage through direct cytotoxicity (necrosis and apoptosis), vascular damage, inflammation, and immune host response³⁰.

The final cellular localization of photosensitizers is crucial to photodynamic efficacy. Due to the high activity and short lifetime of the singlet oxygen, the damage induced by PACT is restricted to the area where photosensitizers localize, usually the cellular membrane or subcellular membrane²⁸. The mitochondria, lysosomes, Golgi apparatus, nucleus, and plasma membrane of tumor cells, as well as tumor vasculature have been evaluated and considered as potential PACT and PDT targets³¹. Photosensitizers localized at mitochondria or endoplasmic reticulum induces apoptosis, while photosensitizers in the plasma membrane or in lysosomes tend to trigger necrosis³¹. The localization of photosensitizers depends on multiple factors, including the structure and properties of photosensitizers, the passive or active targeting strategy, whether a triggered release method is applied, and the cell type^{28,32}.

Important advantages of PACT over other therapies are that: (1) it is precisely targeted by selective illumination, (2) it may be repeated at the same site if needed, (3) it has low morbidity, and (4) it is much less invasive than surgery³³. Other evident advantage of PACT over other conventional treatments such as chemotherapy and radiotherapy is its selective targeting and reduced toxicity³⁴.

Our results strongly suggest that phenothiazine derivatives have activity against *Leishmania brasiliensis*^{35,36}. In this study, it was observed, that using a reduced pre-irradiation (5 minutes) and low energy density 4.2 J/cm² of laser light, improved results were observed when compared to previously published PACT reports on *Leishmania*³⁵⁻³⁸. The novelty and relevance of this study is the fact that there is no significant difference between a long period of pre-irradiation of parasites with a short time. In this case, the use shorter time, 5 minutes, instead of 60 minutes suggested in the literature³⁵⁻³⁸. Another advantage presented here is to use an energy density of 4.2 J/cm², well below the average reported 10J/cm²³⁵⁻³⁸.

5. CONCLUSION

The results of the present investigation indicates that the use of the present protocol using a single application of 10 ug / ml of TBO, incubation time of 5 minutes and 4.2 J/cm² was efficient on killing of *Leishmania brasiliensis*.

6. REFERENCES

- [1]Barbosa, A.F.S., Soares, L.G.P., Aciole, J.M.S., Aciole, G.T.S., Pitta, I.R., Galdino, S.L. and Pinheiro, A.L.B., "Evaluation of Photodynamic Antimicrobial Therapy (PACT) against Trypomastigotes of Trypanosoma cruzi: In Vitro Study." AIP Conf Proc 1364, 55-59 (2011).
- [2]Demidova, T. N. and Hamblin, M. R., "Photodynamic therapy targeted to pathogens." Int. J. Immunopathol. Pharmacol 17, 245-254 (2004).
- [3]Hamblin, M. R. and Hasan, T., "Photodynamic Therapy: a new antimicrobial approach to infectious diseases?" Photochem. Photobiol. Sci 3, 436-450 (2004).
- [4]Perussi, J.R., "Photodynamic inactivation of microorganisms" Quím. Nova, 30, 988-994 (2007).
- [5]Wainwright, M., "Photodynamic antimicrobial chemotherapy (PACT)" J Antimicrob Chemother 42, 13-28 (1998).
- [6]Huang L., Mackenzie, G.G., Sun, Y., Ouyang, N., Xie, G., Vrankova, K., Komninou, D. and Rigas, B., "Chemotherapeutic properties of phospho-nonsteroidal anti-inflammatory drugs, a new class of anticancer compounds." Cancer Res Epub ahead of print (2011).
- [7]Akilov, O.E., Kosaka, K., O'Riordan, K., Song, X., Sherwood, M., Flotte, T.J., Foley, J.W., and Hasan, T., "The Role of Photosensitizer Molecular Charge and Structure on the Efficacy of Photodynamic Therapy against Leishmania Parasites." Chemistry Biology 13, 839-847 (2008).
- [8]Pluta, K., Morak-Młodawska, B. and Jeleń, M., "Recent progress in biological activities of synthesized phenothiazines." Eur J Med Chem 46, 3179-3189 (2011).
- [9]WHO, World Health Organization, "Report of the Consultative Meeting on Cutaneous Leishmaniasis." Geneva (2007).
- [10]Vélez, I., López, L., Sánchez, X., Mestra, L., Rojas, C. and Rodríguez, E., "Efficacy of Miltefosine for the Treatment of American Cutaneous Leishmaniasis." Am J Trop Med Hyg 83, 351-356 (2010).
- [11]Allahverdiyev, A.M., Abamor, E.S., Ustundag, M.B.C.B., Kaya, C., Kaya, F. and Rafailovich, M., "Antileishmanial effect of silver nanoparticles and their enhanced antiparasitic activity under ultraviolet light." Int J Nanomed 6, 2705-2714 (2011).
- [12]Machado, P.R., Ampuero, J., Guimarães, L.H., Villasboas, L., Rocha, A.T., et al., "Miltefosine in the Treatment of Cutaneous Leishmaniasis Caused by Leishmania braziliensis in Brazil: A Randomized and Controlled Trial." PLoS Negl Trop Dis doi:10.1371/journal.pntd.0000912 (2010).

- [13]Antinori, S., Schifanella, L. and Corbellino M., "Leishmaniasis: new insights from an old and neglected disease" *Eur J Clin Microbiol Infect Dis* DOI 10.1007/s10096-011-1276-0 (2011).
- [14]Delgado, G., Sanches, Y., Plaza, D. and Granados D., "An experimental approach to studying the effectiveness and safety of meglumine antimoniate formulations" *Biomed Pharmacother* 65, 565-577 (2011).
- [15]Barral-Netto, M., Machado, P., Bittencourt, A. and Barral, A., "Recent Advances in the Pathophysiology and Treatment of Human Cutaneous Leishmaniasis" *Curr Op Dermatol* 4, 51-58 (1997).
- [16]Jones, T.C., Johnson, W.D.J., Barretto, A.C., Lago, E. and Marsden, P.D., "Epidemiology of American cutaneous leishmaniasis due to *Leishmania braziliensis*" *J Infect Dis* 156, 73-83 (1987).
- [17]Hepburn, N.C., "Cutaneous leishmaniasis: an overview" *J Postgraduate Med* 49, 50-54 (2003).
- [18]Aste, G., Di Tommaso, M., Steiner, J.M., Williams, D.A. and Boari, A., "Pancreatitis associated with N-methyl-glucamine therapy in a dog with leishmaniasis" *Vet Res Commun* 29, 269-72 (2005).
- [19]Ikeda-Garcia, F.A., Lopes, R.S., Ciarlini, P.C., Marques, F.J., Lima, V.M., Perri, S.H. and Feitosa, M.M., "Evaluation of renal and hepatic functions in dogs naturally infected by visceral leishmaniasis submitted to treatment with meglumine antimoniate" *Res Vet Sci* 83, 105-108 (2007).
- [20]T'ung, T., "In vitro photodynamic action of methylene blue on *Trypanosoma brucei*." *Proc Soc Exp Biol Med* 38, 29-31 (1938).
- [21]Ferreira, C.S., Bezerra, R.C. and Pinheiro, A.A., "Methylene Blue Vital Staining for *Trypanosoma cruzi* trypomastigotes and Epimastigotes." *Rev Inst Med Trop* 48, 347-349 (2006).
- [22]Buchholz, K., Comini, M.A., Wissenbach, D., Schirmer, R.H., Krauth-Siegel, R.L. and Gromer, S., "Cytotoxic interactions of methylene blue with trypanosomatid-specific disulfide reductases and their dithiol products." *Mol Biochem Parasitol* 160, 65-69 (2008).
- [23]Ilanchelian, M. and Ramaraj, R., "Binding Interactions of Toluidine Blue O with *Escherichia coli* DNA: Formation of Bridged Structure." *J Fluoresc* 21, 1439-1453 (2011).
- [24]Correa, J.G., Fairlamb, A.H. and Stoppani, A.O.M., "Trypanosoma cruzi Trypanothione Reductase is Inactivated by Peroxidase-Generate Phenothiazine Cationic Radicals." *Free Rad Res* 34, 363-368 (2001).
- [25]Parveen, S., Kahn, M.O.F., Austin, S.E., Croft, S.L., Yardley, V., Rock, P. and Douglas, K.T., "Antitrypanosomal, antileishmanial, and antimalarial activities of quaternary arylalkylammonium 2-amino-4-chlorophenyl phenyl sulfides, a new class of trypanothione reductase inhibitor, and of N-acyl derivatives of 2-amino-4-chlorophenyl phenyl sulfide." *J Med Chem* 48, 8087 - 8097 (2005).
- [26]Lima, L.M. and Barreiro, E.J., "Bioisosterism: a useful strategy for molecular modification and drug design." *Curr Med Chem* 12, 23 - 49 (2005).
- [27]Celli, J.P., Solban, N., Liang, A., Pereira, S.P. and Hasan, T., "Verteoporphin-Based Photodynamic Therapy Overcomes Gemcitabine Insensitivity in a Panel of Pancreatic Cancer Cell Lines." *Lasers Surg Med* 43, 565-574 (2011).
- [28]MacDonald, I.J. and Dougherty, D.J., "Basic principles of photodynamic therapy." *J Porphyr Phthalocyanines* 5(2), 105- 129 (2001).
- [29]Foote, C.S., "Mechanisms of photooxygenation." *Prog Clin Biol Res* 170, 3-18 (1984).
- [30]Jin, C.S. and Zheng, G., "Liposomal Nanostructures for Photosensitizer Delivery." *Lasers Surg Med* 43, 734-748 (2011).
- [31]Dougherty, T.J., Gomer, C.J., Henderson, B.W., Jori, G., Kessel, D., Korbek, M., Moan, J. and Peng, Q., "Photodynamic therapy." *J Natl Cancer Inst* 90, 889-905 (1998).
- [32]Takeuchi, Y., Ichikawa, K., Yonezawa, S., Kurohane, K., Koishi, T., Nango, M., Namba, Y. and Oku, N., "Intracellular target for photosensitization in cancer antiangiogenic photodynamic therapy mediated by polycation liposome." *J Control Release* 97, 231-240 (2004).
- [33]O'Connor, A.E., Gallagher, W.M. and Byrne, A.T., "Porphyrin and nonporphyrin in oncology: Preclinical and clinical advances in photodynamic therapy." *Photochem Photobiol* 85, 1053-1074 (2009).
- [34]Bhuvaneshwari, R., Yuen, G.Y., Chee, S.K. and Olivo, M., "Antiangiogenesis Agents Avastin and Erbitux Enhance the Efficacy of Photodynamic Therapy in a Murine Bladder Tumor Model." *Lasers Surg Med* 43, 651-662 (2011).
- [35]Song, D., Lindoso, J.A., Oyafuso, L.K., Kanashiro, E.H., Cardoso, J.L., Uchoa, A.F., Tardivo, J.P. and Baptista, M.S., "Photodynamic Therapy Using Methylene Blue to Treat Cutaneous Leishmaniasis" *Photomed Laser Surg* 29, 711-715 (2011).
- [36]Peloi, L.S., Biondo, C.E., Kimura, E., Politi, M.J., Lonardoni, M.V., Aristides, S.M., Dorea, R.C. and Silveira, T.G., "Photodynamic therapy for American cutaneous leishmaniasis: The efficacy of methylene blue in hamsters experimentally infected with *Leishmania (Leishmania) amazonensis*." *Exp Parasitol* 128, 353-356 (2011).
- [37]Dutta, S., Ray, D., Kolli, B.K. and Chang, K.P., "Photodynamic Sensitization of *Leishmania amazonensis* in both Extracellular and Intracellular Stages with Aluminum Phthalocyanine Chloride for Photolysis In Vitro." *Antimicrob Agents Chemother* 49, 4474-4484 (2005).
- [38]Kosaka, S., Akilov, O.E., O'Riordan, K. and Hasan, T., "A Mechanistic Study of d-Aminolevulinic Acid-Based Photodynamic Therapy for Cutaneous Leishmaniasis." *J Invest Dermatol* 127, 1546-1549 (2007).

3.5. Mechanisms for Low-Light Therapy VIII, Proc. of SPIE Vol. 8569, doi: 10.1117/12.2005157

In vitro study of the Photodynamic Antimicrobial Therapy (PACT) against promastigotes form of the *Leishmania (Viannia) braziliensis*: In Vitro Study

A leishmaniose é uma doença parasitária de importância a saúde pública mundial pois é endêmica em vários países. O tratamento da leishmaniose é difícil devido ao seu alto custo financeiro, sua toxicidade sistêmica e ao desenvolvimento do fenômeno de resistência dos parasitas aos medicamentos. Por isto, o desenvolvimento de novas terapias para o tratamento é muito importante. Neste trabalho, neste trabalho buscou avaliar a eficácia da Fotoquimioterapia Antiparasitária de forma *in vitro*, como uma nova opção para o tratamento da leishmaniose cutânea. Para isto um semiconductor laser ($\lambda 660\text{nm}$, 40mW, 4,2 e 8,4 J/cm², CW) associado a derivados fenotiazínicos em duas concentrações, 5 e 10 µg/ml, contra as formas promastigotas de *L. braziliensis* com um período de pré-irradiação de 60 minutos. Após 72h de incubados após a fotoquimioterapia antiparasitária, a viabilidade destes parasitas foi analisada e a contagem dos parasitas viáveis foi realizada para se identificar o percentual de letalidade da FQTAp. Não foi identificada letalidade dos compostos nas doses testadas, assim como, da ação isolada do laser, porém a mistura de 1:1 do azul de metileno com o azul de toluidina na concentração de 10 µg/ml apresentou o melhor resultado.

In vitro study of the Photodynamic Antimicrobial Therapy (PACT) against promastigotes form of the *Leishmania (Viannia) braziliensis*:

Artur F. S. Barbosa^{a,b,c}, Bruno B. Sangiorgi^b, Suely L. Galdino^a, Ivan R. Pitta^a, Manoel Barral-Netto^b, Antônio L. B. Pinheiro^{c,d}

^aLaboratory of Planning and Synthesis of Drugs, Federal University of Pernambuco, 1235 Prof. Moraes Rego Ave, Cidade Universitária, Recife, PE, Brazil, 50670-901

^bLaboratory Integrated of Microbiology and Immunoregulation, Research Center Gonçalo Moniz, 121 Waldemar Falcão Street, Candeal, Salvador, BA, Brazil, 40296-710

^cCenter of Biophotonics, School of Dentistry, Federal University of Bahia, 62 Araujo Pinho Ave, Canela, Salvador, BA, Brazil, 40110-150.

^dNational Institute of Optics and Photonics, University of São Paulo, 400 Trabalhador Sancarlene Ave, São Carlos, SP, Brazil, 13560-970

ABSTRACT

Leishmaniasis, a protozoan parasitic disease that remains a major worldwide health problem with high endemicity in developing countries. Treatment of Cutaneous Leishmaniasis (CL) should be decided by the clinical lesions, etiological species and its potential to develop into mucosal leishmaniasis. High cost, systemic toxicity, and diminished efficacy due to development of parasite resistance are the serious drawbacks of current treatment options. Thus, identifying new, effective, and safer anti-leishmanial drug(s) is of paramount importance. The aim of this study was to verify the effectiveness of PACT in vitro, as a new technique for the treatment of Leishmaniasis. For this, semiconductor laser ($\lambda = 660\text{nm}$, 40mW, 8.4J/cm², CW) associated to phenothiazine's derivatives (5 and 10 $\mu\text{g/ml}$, TBO, Methylene Blue or Phenothiazine) on the promastigotes form of *Leishmania braziliensis* in a single session was used. Viability of the parasites was assessed in quadruplicates of each group. The samples were removed and analyzed in a hemocytometer 72h after PACT. We found an important decrease in the number of viable parasites on all treated groups in comparison to their controls. The results of present study showed significant percentage of lethality (above 92%) of the protocol. The 98.33% of lethality was achieved with 10 $\mu\text{g/ml}$ of FTZ. No lethality was seen on groups treated neither with laser nor with each compounds separately. The results are promising and indicative that the use of PACT may be a powerful treatment of leishmaniasis when compared to already available ones.

Key words: New Therapy- Leishmaniasis - Toluidine Blue O - Methylene Blue - Phenothiazine.

1. INTRODUCTION

Leishmaniasis threatens about 350 million people in 88 countries worldwide and 12 million people are believed to be currently infected, with about 1–2 million estimated new cases occurring every year ¹. Leishmaniasis is a disease caused by protozoan parasites belonging to the genus *Leishmania*. The parasites are transmitted by the bite of a tiny – only 2–3 mm long – insect vector, the phlebotomine sandfly. *Leishmania braziliensis* is the etiologic agent of American Cutaneous Leishmaniasis (ACL), which is characterized by its chronicity and the possibility to metastasize leading to the muco-cutaneous clinical form ².

Due to the lack of a safe and effective vaccine, chemotherapy has been the preferred alternative in the control of this disease, particularly pentavalent antimonials, which have been used successfully in the treatment of cutaneous lesions. Nevertheless, adverse effects have been reported since the first trials in affected populations, including other vertebrates such as canines, being this toxicity mostly related to pancreatic and liver damage. Given these adverse effects, the safety of pentavalent antimonial formulations is currently being subject of intense debate,

suggest that these formulations are also potentially immunotoxic. Another important aspect associated to this disease is the high economic burden imposed by its treatment on health systems ³.

PACT is a procedure characterized by the use of a photosensitizer (PS) and a light source of specific wavelength. Photosensitizers are drugs that when combined with light in specific wavelength, produces reactive oxygen species (ROS) and reactive nitrogen species (RNS), leading to cell death ^{4,5}. In the presence oxygen found in the tissues, the PS is excited by either Laser or LED light causing, by either by electron or hydrogen transfer, the production and release of free radicals (reaction type I) or by energy transfer to oxygen (type II reaction), leading to production of singlet oxygen. Both pathways may lead to cell death and consequent destruction of diseased tissue ⁶.

Phenothiaziniuns are blue dyes (max 600–660 nm) such as Methylene Blue (MB) and Toluidine Blue O (TBO). The first report of its photodynamic action (against bacteriophages and viruses) appeared as early as 1930. Both MB and TBO are used in surgical identification of abnormal cells at reasonably high concentrations (normally 1% w/v) without causing human toxicity. TBO is known to be membrane active, since it causes increased permeability, whereas MB causes strand breaks in this nucleic acid ⁴. Phenothiazine derivatives exhibit promising biological activities such as anticancer, antiviral, anti-inflammatory, anticonvulsant, analgesic, immunosuppressive, multidrug resistance reversal properties, antifungal, antimalarial, antifilarial, trypanocidal and leishmanicidal ⁷.

The aim of this study was to investigate, *in vitro*, the increasing effects of the use of Photodynamic Antimicrobial Chemotherapy in *Leishmania brasiliensis* in culture.

2. MATERIALS AND METHODS

2.1. Chemicals

Methylene Blue (MB) and Toluidine Blue O (TBO) were purchased from Sigma-Aldrich Corporation (Milwaukee, WI, USA). Three compounds were used: MB, TBO and a 1:1 mixture of MB + TBO, here named as phenothiazine - FTZ. The stock solutions were diluted in distilled water (10 or 20 µg / ml).

2.2. Culture Promastigotes forms

L. braziliensis (strain MHOM/BR/01/BA788 - cultivated and maintained by the Laboratorio Integrado de Microbiologia e Imunoregulação) promastigotes were cultivated in Schneider's Insect Medium (Sigma Chemical Co., St Louis, Mo, USA) supplemented with 20% heat-inactivated fetal bovine serum (Gibco, Carlsbad, CA, USA), L-glutamine (2 mM), penicillin (100 U/ml), streptomycin (100 µg/ml) at 26 °C (Thermostat cabinets – LS Scientific, Ikeja, Lagos, Nigeria) for 5–7 days when the parasites reached the stationary-phase. After reaching the stationary-phase, the culture was sedimented by centrifugation (5810 R, Eppendorf, Hamburg, Germany, 10 min, 4°C, 4000 rpm), suspended in 1 mL of the same medium and quantified in a Neubauer chamber (LO - Laboroptik GmbH, Friedrichsdorf, Germany) with the aid of a microscope (Nikon Eclipse E200, Melville, NY, USA). Enough medium was added in order to adjust the parasitic concentration to 2×10^6 promastigotes/mL ⁸.

2.3. Leishmanicidal activity against Promastigotes

The determination of the leishmanicidal activity was performed in 96-well plates (Tesplate 96F - TPP, Zollstrasse, Trasadingen, Switzerland). The compounds were tested in quadruplicate in two concentration 5 or 10 $\mu\text{g/mL}$. The parasitic concentration in the wells was that of 2×10^6 promastigotes/mL. A negative control was performed with four wells containing only parasites and the incubation medium. After 72 h of incubation at 26°C , 10 μL of each well was diluted in 90 μL of the PBS and the parasites were quantified in a Neubauer chamber. The data obtained from this quantification were plotted in a graph using Microsoft Excel and the values of the lethality of the treated groups were obtained through the difference in percentage of viable parasites in the groups treated with the amount of viable parasites in the control group.

2.4. Photodynamic Therapy

Metacyclic promastigotes were pre-incubated during 5 or 60 minutes, in darkness, with the different concentrations of the photosensitizers in Schneider's *Drosophila* medium (pH 7.2) with 10% FBS in 96-well plates. After this pre-incubation, each well was irradiated by a Laser device ($\lambda = 660\text{nm}$, 40mW, 8.4J/cm^2 , CW, TwinFlex, MMOptics, São Carlos, São Paulo, Brazil). After 72 h of incubation at 26°C , 10 μL of each well was diluted in 90 μL of the PBS and the parasites were quantified in a Neubauer chamber. The data obtained from this quantification were plotted in a graph using Microsoft Excel and the values of the lethality of the treated groups were obtained through the difference in percentage of viable parasites in the groups treated with the amount of viable parasites in the control group.

2.5. Crystal Violet Toxicity Assay

One day after photochemotherapy, the culture media was removed from the wells (Tesplate 96F - TPP, Zollstrasse, Trasadingen, Switzerland) and 100 μL of methanol was added and the plate, and incubated for 20 minutes at room temperature (25°C). Methanol was then removed from the wells, being added 50 μL of Cristal Violet Dye (0.5% Crystal Violet, 20% Methanol, 80% dH_2O , Sigma-Aldrich Corporation (Milwaukee, WI, USA) followed by incubation for 10 minutes at room temperature. After that period, the dye was removed and the wells washed twice with tap water, followed by two immersions of the plate in a becker filled with tap water. To extract de dye from the cells, 100 μL of Sorenson's buffer (SDS) was added in the wells and the plate was incubated in a rotate shaker for 30 minutes. An ELISA - SpectraMax 190 Microplate Reader (Sunnyvale, CA, USA) plate reader was used for the absorbance measurement at wavelength of 540nm

2.6. Statistical analysis

Statistical analysis was performed using the software Minitab14 (Minitab, Belo Horizonte, MG, Brazil) where the ANOVA was used to test intergroup and for intragroup, we used the t-student test. The level of significance was set at 95%.

3. RESULTS

From Crystal Violet toxicity assay, we observed that MB and TBO presented a very similar pattern of toxicity. When compared to control group, both have a trend to decrease the cells viability along with concentration increasing, although this effect was showed to be significant only at 20µg/ml. Thus, concentrations below these level were chosen from both phenothiazines for PACT assays.

On regarding the type of photosensitizer used we found that protocols using MB at 5 µg/ml showed significant differences were observed between groups 8.4J/cm²/5min and 8.4J/cm²/60min (**p < 0.001**). When increasing the concentration to 10 µg/ml, significant differences were seen between group 8.4J/cm²/5min and 8.4J/cm²/60min (**p < 0.001**) (TABLE 1).

Photosensitizer(ug/ml)	Incubation Time (min) / Energy Density (J/cm2)	
	5/8.4	60/8.4
MB – 5	93.89%	95.59%
TBO – 5	92.59%	97.11%
FTZ – 5	93.89%	96.67%
MB – 10	92.59%	96.67%
TBO – 10	93.15%	97.11%
FTZ – 10	93.33%	98.33%

TABLE 1: Percentage of lethality

When using TBO at 5 µg/ml, significant differences were seen between groups 8.4J/cm²/5min and 8.4J/cm²/60min (**p < 0.001**). Increasing the concentration to 10 µg/ml, no significant differences were observed between groups 8.4J/cm²/5min and 8.4J/cm²/60min (**p < 0.001**).

Using the FTZ at 5 µg/ml, significant differences were observed between groups 8.4J/cm²/5min and 8.4J/cm²/60min (**p < 0.001**). Increasing the concentration to 10 µg/ml, significant differences were observed between groups 8.4J/cm²/5min and 8.4J/cm²/60min (**p < 0.001**).

Analyzing the energy density, we found that, using an energy density of 8.4J/cm² and incubation time of 10 minutes, was found significant differences between groups MB 5µg/ml and 10µg/ml (**p < 0.001**), TBO 5 µg/ml and 10 µg/ml (**p < 0.001**). Significant differences were also found between groups MB 5 µg/ml and TB 10 µg/ml (**p < 0.001**), MB 5µg/ml and FTZ 10µg/ml (**p < 0.001**), TB 5 µg/ml and MB 10 µg/ml (**p < 0.001**), TB 5 µg/ml and FTZ 10 µg/ml (**p < 0.001**), and between groups FTZ 5µg/ml and TB 10 µg/ml (**p < 0.001**), and FTZ 5 µg/ml and FTZ 10 µg/ml (**p < 0.001**).

So the use of either 10 µg/ml of FTZ during 60 minutes prior irradiation with 8.4J/cm² λ660nm laser light was the best protocol used to kill *Leishmania brasiliensis* in the study.

4. DISCUSSION

Leishmaniasis is caused by parasitic protozoa of the genus *Leishmania*. Humans are infected via the bite of phlebotomine sandflies, which breed in forest areas, caves and adobe brick houses where most of the transmission to humans takes place. There are four main types of the disease: Cutaneous, Diffuse Cutaneous, Mucocutaneous and Visceral (kala azar). In cutaneous forms, skin ulcers usually form on exposed areas, such as the face, arms and legs. These usually heal within a few months, leaving scars ⁹.

There is currently no satisfactory treatment for any form of CL. Many treatment regimens are associated with significant failure rates and considerable toxicity. Relapses are common and there are increasing reports of drug resistance emergence. Pentavalent antimonials (*i.e.* Sodium stibogluconate or meglumine antimonite) are given as first-line drugs through a series of intramuscular, intravenous, or intralesional injections. These drugs have serious side effects, require long treatment, are not affordable for most patients and are difficult to administer in poor rural areas. Alternative treatments as Liposomal amphotericin-B, which is efficacious in VL, has not been fully tested on CL caused by the target parasites described above. Even if efficacious, it cannot be deployed widely because of cost and delivery requirements. Miltefosine, developed for VL, is potentially teratogenic and has side effects that make it unsuitable to treat CL. Other treatments, such as thermotherapy and cryotherapy are being used in certain clinics, but these treatments are expensive ¹⁰.

Recently, a new technique has been studied for the treatment of leishmaniasis ^{11,12,13}, which we will call this paper Photodynamic Antimicrobial Chemotherapy (PACT). PACT is a potentially applicable, safe and affordable option for treating patients suffering from many conditions being an attractive option to the use of conventional antimicrobial chemotherapy ¹⁴. PACT neither induces resistant strains nor demands multiple sessions of treatment ^{15, 16}.

PACT is a procedure characterized by the use of a photosensitizer (PS) and a light source of specific wavelength. In the presence oxygen found in the tissues, the PS is excited by either Laser or LED light causing, by either by electron or hydrogen transfer, the production and release of free radicals (reaction type I) or by energy transfer to oxygen (type II reaction), leading to production of singlet oxygen. Both pathways may lead to cell death and consequent destruction of diseased tissue ¹⁷.

The methylene blue (MB) and toluidine blue (TBO) are photosensitizing phenothiazine accepted at the practice medical and demonstrated in studies in literature. Exhibit intense absorption of 600-660nm, region of the spectrum useful in PACT to be in the "therapeutic window" required for efficient penetration of light in tissues ^{18,19}. Although its properties physycal and chemical are similar the efficiency photodynamic of compounds, varies between the several microorganisms ²⁰. The use of staining agents such as MB and TBO in the analysis of the pathology of the microbially diseased state is well established, as mentioned above ²¹.

The present study investigated the antileishmanial effects of PACT, using phenothiazines derivates as photosensitizer, against *L. brasiliensis* parasites using two different incubation times (5 and 60 minutes). It was found that both 5 and 60 minutes of pre-irradiation resulted in antileishmanial effects by inhibiting growth, metabolic activity, and infectivity of promastigotes in culture. It was also demonstrated that the antileishmanial effect of both phenothiazines derivates and the Laser in (8.4J/cm²) used isolated did not present inhibition. Inhibition was achieved when association of the Laser and the photosensitizer was used. Despite several previous studies on the its antibacterial, antiviral, and antifungal activities, with phenothiazines ²² we were not able to find

any study on regards the antileishmanial effect of TBO on *L. brasiliensis* parasites.

The final cellular localization of photosensitizers is crucial to photodynamic efficacy. Due to the high activity and short lifetime of the singlet oxygen, the damage induced by PACT is restricted to the area where photosensitizers localize, usually the cellular membrane or subcellular membrane²³. The mitochondria, lysosomes, Golgi apparatus, nucleus, and plasma membrane of tumor cells, as well as tumor vasculature have been evaluated and considered as potential PACT and PDT targets²⁴. Photosensitizers localized at mitochondria or endoplasmic reticulum induces apoptosis, while photosensitizers in the plasma membrane or in lysosomes tend to trigger necrosis²⁴. The localization of photosensitizers depends on multiple factors, including the structure and properties of photosensitizers, the passive or active targeting strategy, whether a triggered release method is applied, and the cell type^{23,35}.

Our results strongly suggest that phenothiazine derivatives have activity against *Leishmania brasiliensis*^{26,27}. In this study, it was observed, that using a reduced pre-irradiation (60 minutes) and low energy density 8.4 J/cm² of laser light, improved results were observed when compared to previously published PACT reports on *Leishmania*²⁶⁻²⁹.

5. CONCLUSION

The results of the present investigation indicates that the use of the present protocol using a single application of 10 ug / ml of FTZ, incubation time of 60 minutes and 8.4 J/cm² was efficient on killing of *Leishmania brasiliensis*.

REFERENCES

- [1] do Monte-Neto, R.L., Coelho, A.C., Raymond, F., Légaré, D., Corbeil, J., Melo, M.N., Frézard, F., Ouellette, M. "Gene Expression Profiling and Molecular Characterization of Antimony Resistance in *Leishmania amazonensis*." PLoS Negl. Trop. Dis. 5,(5): e1167 (2011).
- [2] Tavares, N.M., Silva, R.A., Costa, D.J., Pitombo, M.A., Fukutani, K.F., Miranda, J.C., Valenzuela, J.G., Barral, A., de Oliveira, C.I., Barral-Netto, M., Brodskyn, C. "*Lutzomyia longipalpis* Saliva or Salivary Protein LJM19 Protects against *Leishmania brasiliensis* and the Saliva of Its Vector, *Lutzomyia intermedia*." PLoS Negl. Trop. Dis 5,(5): e1169 (2011).
- [3] Delgado, G., Sanches, Y., Plaza, D. and Granados D., "An experimental approach to studying the effectiveness and safety of meglumine antimoniate formulations" Biomed Pharmacother 65, 565-577 (2011).
- [4] Wainwright, M., "Photodynamic antimicrobial chemotherapy (PACT)" J Antimicrob Chemother 42, 13-28 (1998).
- [5] Huang, L., Mackenzie, G.G., Sun, Y., Ouyang, N., Xie, G., Vrankova, K., Komninou, D. and Rigas, B., "Chemotherapeutic properties of phospho-nonsteroidal anti-inflammatory drugs, a new class of anticancer compounds." Cancer. Res. Epub ahead of print (2011).
- [6] Barbosa, A.F., Sangiorgi, B.B., Galdino, S.L., Barral-Netto, M., Ivan, R.P., Pinheiro, A.L. "Photodynamic Antimicrobial Chemotherapy (PACT) Using Phenothiazine Derivatives as Photosensitizers Against *Leishmania brasiliensis*." Lasers Surg. Med. 44(10):850-855 (2012)
- [7] Pluta, K., Morak-Młodawska, B. and Jeleń, M., "Recent progress in biological activities of synthesized

phenothiazines.” Eur. J. Med. Chem. 46, 3179-3189 (2011).

[8] Machado, P.R., Ampuero, J., Guimarães, L.H., Villasboas, L., Rocha, A.T., et al., “Miltefosine in the Treatment of Cutaneous Leishmaniasis Caused by *Leishmania braziliensis* in Brazil: A Randomized and Controlled Trial.” PLoS Negl. Trop Dis doi:10.1371/journal.pntd.0000912 (2010).

[9] WHO, 2007. Report of the Consultative Meeting on Cutaneous Leishmaniasis. Geneva.

[10] Modabber, F., Buffet, P.A., Torreele, E., Milon, G. and Croft, S.L. “Consultative meeting to develop a strategy for treatment of cutaneous leishmaniasis. Institute Pasteur, Paris. 13–15 June, 2006.” *Kinetoplastid Biology and Disease* (6):3-27 (2007).

[11] Enk, C.D., Fritsch, C., Jonas, F., Nasereddin, A., Ingber, A., Jaffe, C.L., Ruzicka, T. “Treatment of cutaneous leishmaniasis with photodynamic therapy.” Arch. Dermatol. 139, 432–434 (2003).

[12] Gardlo, K., Horska, Z., Enk, C.D., Rauch, L., Megahed, M., Ruzicka, T., Fritsch, C. “Treatment of cutaneous leishmaniasis by photodynamic therapy.” J. Am. Acad. Dermatol. 48, 893–896 (2003).

[13] Dutta, S., Ray, D., Kolli, B.K., Chang, K.P. “Photodynamic Sensitization of *Leishmania amazonensis* in both Extracellular and Intracellular Stages with Aluminum Phthalocyanine Chloride for Photolysis In Vitro.” Antimicrob. Agents Chemotherap. 49, 4474–4484 (2005).

[14] Montanari, J., Maidana, C., Esteva, M.I., Salomon, C., Morilla, M.J., Romero, E.L. “Sunlight triggered photodynamic ultradeformable liposomes against *Leishmania braziliensis* are also leishmanicidal in the dark.” J. Control Release 147, 368–376 (2010).

[15] Nitzan, Y., Wexler, H.M., Finegold, S.M. “Inactivation of anaerobic bacteria by various photosensitized porphyrins or by hemin.” Curr. Microbiol. 29, 125–131 (1994).

[16] Calzavara-Pinton, P.G., Venturini, M., Sala, R. “A comprehensive overview of photodynamic therapy in the treatment of superficial fungal infections of the skin.” J. Photochem. Photobiol. B 78, 1-6 (2005).

[17] Barbosa, A.F.S., Soares, L.G.P., Aciole, J.M.S., Aciole, G.T.S., Pitta, I.R., Galdino, S.L., Pinheiro, A.L.B. “Evaluation of Photodynamic Antimicrobial Therapy (PACT) against Trypomastigotes of *Trypanosoma cruzi*: In Vitro Study.” AIP Conf. Proc. 1364, 55-59 (2011).

[18] Wainwright, M., Grice, N.J., Pye, L.E.C. “Phenothiazine Photosensitisers. Part II. 3,7-Bis(aryl amino)phenothiazines.” Dyes Pigments 42, 45-51 (1999).

[19] Sommer, A.P., Pinheiro, A.L., Mester, A.R., Franke, R.P., Whelan, H.T. “Biostimulatory windows in low-intensity laser activation: lasers, scanners, and NASA's light-emitting diode array system.” J. Clin. Med. Laser Surg. 19, 29-33 (2001).

[20] Demidova, T.N., Hamblin, M.R. “Effect of Cell-Photosensitizer Binding and Cell Density on Microbial Photoinactivation.” Antimicrob. Agents. Chemother. 49, 2329-2335 (2005).

[21] Wainwright, M. “The development of phenothiazinium photosensitisers.” Photodiagnosis Photodyn. Ther. 2, 263-272 (2005).

[22] Pluta, K., Morak-Młodawska, B. and Jeleń, M., “Recent progress in biological activities of synthesized phenothiazines.” Eur J Med Chem 46, 3179-3189 (2011).

[23] MacDonald, I.J. and Dougherty, D.J., “Basic principles of photodynamic therapy.” J Porphyr Phthalocyanines 5(2), 105– 129 (2001).

[24] Dougherty, T.J., Gomer, C.J., Henderson, B.W., Jori, G., Kessel, D., Korbek, M., Moan, J. and Peng, Q., “Photodynamic therapy.” J Natl Cancer Inst 90, 889–905 (1998).

[25] Takeuchi, Y., Ichikawa, K., Yonezawa, S., Kurohane, K., Koishi, T., Nango, M., Namba, Y. and Oku, N., “Intracellular target for photosensitization in cancer antiangiogenic photodynamic therapy mediated by polycation

liposome.” J Control Release 97, 231–240 (2004).

[26] Song, D., Lindoso, J.A., Oyafuso, L.K., Kanashiro, E.H., Cardoso, J.L., Uchoa, A.F., Tardivo, J.P. and Baptista, M.S., “Photodynamic Therapy Using Methylene Blue to Treat Cutaneous Leishmaniasis” Photomed Laser Surg 29, 711-715 (2011).

[27] Peloi, L.S., Biondo, C.E., Kimura, E., Politi, M.J., Lonardoni, M.V., Aristides, S.M., Dorea, R.C. and Silveira, T.G., “Photodynamic therapy for American cutaneous leishmaniasis: The efficacy of methylene blue in hamsters experimentally infected with *Leishmania (Leishmania) amazonensis*.” Exp Parasitol 128, 353–356 (2011).

[28] [37] Dutta, S., Ray, D., Kolli, B.K. and Chang, K.P., “Photodynamic Sensitization of *Leishmania amazonensis* in both Extracellular and Intracellular Stages with Aluminum Phthalocyanine Chloride for Photolysis In Vitro.” Antimicrob Agents Chemotherap 49, 4474–4484 (2005).

[29] Kosaka, S., Akilov, O.E., O’Riordan, K. and Hasan, T., “A Mechanistic Study of d-Aminolevulinic Acid-Based Photodynamic Therapy for Cutaneous Leishmaniasis.” J Invest Dermatol 127, 1546–1549 (2007).

4. DISCUSSÃO

No início deste trabalho, não se tinha conhecimento da ação do laser vermelho ($\lambda 660\text{nm}$) sobre as espécies *T. cruzi* e *L. braziliensis*. Inicialmente buscou-se observar quais os efeitos que os parasitos apresentariam após a irradiação com um laser de baixa potência. Com base nos parâmetros de laser que o nosso grupo utilizava contra bactérias, iniciou-se as pesquisas com a forma epimastigota de *T. cruzi*, utilizando um laser semiconductor InGaAlP ($\lambda 660\text{nm}$, 30mW, 6 J/cm², CW).

Após a irradiação de uma cultura de epimastigotas de *T. cruzi*, foi observado alterações na morfologia dos parasitos. O grupo irradiado perderam sua forma alongada e de cinetoplasto típico além de um movimento flagelar característico, passando a apresentar-se mais arredondado, com um complexo cinetoplasto-mitocôndria bem mais denso e desenvolvido em relação ao controle e com uma movimentação flagelar mais agitada.

Ao longo da década de 80, a pesquisadora Tiina I. Karu, mostrou as bases para a compreensão dos mecanismos moleculares subjacentes aos efeitos da luz de baixa intensidade em sistemas biológicos (KARU, 1982; KARU, 1983a; KARU, 1983b). Sabe-se da existência da ação de um mecanismo foto-biológico que regula a energia luminosa na cadeia respiratória de enzimas eucariotas e procariotas, como a citocromo c oxidase localizada na mitocôndria, com a cadeia respiratória terminal, atuando como fotorreceptores. A resposta celular ocorre primariamente nas reações da cadeia respiratória e em seguida, no citoplasma e/ou núcleo da célula (KARU, 2005). Alguns dos efeitos de fotoestimulação em sistemas biológicos são: o aumento da taxa de proliferação celular, o aumento da taxa de síntese de fibroblastos e produção de colagênio, o aumento da taxa de síntese de RNA e DNA, aumento da síntese de ATP, entre outras (KARU, 1987; TAKAHASHI, 1992; CONLAN, 1996; YU, 1997; VINCK, 2003; KARU, 2005).

Estes diferentes mecanismos de interação da luz com os sistemas biológicos podem levar a resultados similares a toda estimulação do estado redox mitocondrial direcionando a uma maior oxidação. É discutido ainda, qual dos mecanismos é realmente ativado, pois, dependendo da situação, a dose de luz ou a intensidade, por exemplo, podem favorecer um ou o outro mecanismo (KARU, 2003). No mecanismo primário não se está bem estabelecido a rota para a geração do oxigênio singlete. O mecanismo secundário é responsável pela ligação entre a resposta à ação da luz pelos fotorreceptores, localizados nas mitocôndrias, e os mecanismos de síntese de DNA e RNA, localizada no núcleo, ou outros fenômenos de outros componentes da

célula. Existem diferentes processos regulatórios associados ao controle dos níveis de fotoreceptores de ATP intracelular, fatores de transcrição sensíveis ao estado redox celular, ou cascatas de sinalização da homeostase celular no citoplasma através da membrana celular para o núcleo (KARU, 2003).

Foram observadas alterações morfológicas e estruturais causadas por diodo laser 660nm nas formas evolutivas epimastigotas de *Trypanosoma cruzi*. Um maior volume do núcleo e do complexo mitocôndria-cinetoplástico pode ser observado quando comparado os parasitas irradiados com os parasitas sem tratamento luminoso. O corpo dos parasitas tratados com o laser também apresentaram alterações em sua forma típica, passando de uma forma mais alongada a uma mais arredondada. A mobilidade também foi afetada, com os parasitas tratados movimentando-se sensivelmente menos do que o grupo de controle.

Em seguida, buscamos verificar se a Fotoquimioterapia Antiparasitária também funcionaria contra parasitos. Para isso, utilizou-se de um laser semiconductor de InGaAlP ($\lambda 660\text{nm} \pm 10\text{nm}$; 30mW; 4 J/cm²; CW) associado ao azul de metileno, em diferentes concentrações, como fotossensibilizador contra a forma infectante do *T. cruzi*.

Primeiro, testou-se a citotoxicidade do composto azul de metileno contra células esplênicas de camundongo do tipo BALB/c através da técnica de incorporação da Timidina tritiada usando um contador de radiação β . Foi realizada uma diluição de oito concentrações (100 – 0,025 $\mu\text{g/ml}$). A toxicidade dos composto foi determinada comparando o percentual de incorporação da timidina das células presentes nos poços tratados com o percentual de incorporação da timidina das células dos poços não tratados com o azul de metileno. Foram consideradas concentrações atóxicas, aquelas que apresentaram uma redução de incorporação inferior a 30%. Neste ensaio, foi verificado que a toxicidade do azul de metileno seria de 1 $\mu\text{g/ml}$.

Vários autores têm publicado sobre a capacidade de derivados fenotiazínicos inativarem algumas enzimas de tripanossomatídeos, como por exemplo a tripanotiona redutase e a Superóxido desmutase (ALVES, 1983; FERREIRA, 2006; WAINWRIGHT, 2007; BUCHHOLZ, 2008)

Em seguida, realizou-se a Fotoquimioterapia Antiparasitária diluindo-se o azul de metileno em seis concentrações a partir de 0,78 $\mu\text{g/ml}$ (concentração atóxica) até 0,025 $\mu\text{g/ml}$, associado ao laser ($\lambda 660\text{nm} \pm 10\text{nm}$; 30mW; 4 J/cm²; CW). Para se determinar a atividade anti-proliferativa da técnica, avaliou-se a ação de forma isolada do laser, dos compostos sem irradiação nas doses supracitadas, e com a fotoquimioterapia contra cultura de tripomastigota

de *T. cruzi*. Os resultados demonstraram que tanto o laser como os compostos sem serem irradiados não apresentaram efeito significativo contra tripomastigotas de *T. cruzi*. Porém ao se realizar a FQTAp, houve uma redução da quantidades de parasitos na cultura tratada quando comparado ao grupo controle sem tratamento, demonstrando a ação da FQTAp contra tripomastigotas de *T. cruzi*.

Posteriormente realizou-se novos experimentos com uma outra espécie de tripanossomatídeos, a *L. braziliensis*. Neste próximo passo do trabalho, buscou-se avaliar a ação da FQTAp contra os parasitos causadores da leishmaniose cutânea. Para isto, utilizou-se de um semiconductor laser ($\lambda = 660\text{nm}$, 40mW, 4,2 e 8,4 J/cm², CW) associado a duas concentrações de derivados fenotiazínicos (azul de metileno e azul de toluidina) contra a forma promastigota de *L. braziliensis*.

Inicialmente, realizou-se mais dois diferentes ensaios de citotoxicidade dos compostos. No primeiro ensaio, determinou-se a toxicidade do azul de metileno e do azul de toluidina, através da coloração por cristal violeta incorporados aos parasitas viáveis após os tratamentos, e o segundo experimento, através da degradação do Alamarblue, onde os parasitas viáveis, em através de seu metabolismo, realizam reações de REDOX com o Alamarblue, gerando alterações de cor e fluorescência nos poços testados. Para a citotoxicidade, os experimentos demonstraram que ambos os compostos são atóxicos em concentrações inferiores a 20 µg/ml ou 25 µM.

Por fim, avaliou-se o efeito da anti-proliferativo da FQTAp contra os parasitos de *L. braziliensis*. Foram utilizadas apenas duas concentrações dos compostos azul de metileno e azul de toluidina, 5 µg/ml e 10 µg/ml de cada. Estas concentrações foram testadas sem a irradiação (fase escura), e não demonstrou nenhuma redução da quantidade de promastigotas de *L. braziliensis*. Em seguida, uma luz laser de forma isolada foi aplicada sobre a cultura dos parasitas para avaliar o a energia entregue alteraria a quantidade de parasitas, porém nenhuma alteração de contagem foi observada quando utilizou-se um laser ($\lambda 660\text{nm}$, 40mW, 4,2 ou 8,4 J/cm², CW) em relação ao grupo controle. O próximo passo foi realizar a FQTAp. Incubou-se os parasitos com as concentrações de 5 µg/ml e 10 µg/ml de ambos os fotossensibilizadores,

seguido de um tempo de pré-irradiação de 5 ou 60 minutos para em seguida realizar a irradiação com o laser variando a dose de energia entregue entre 4,2 e 8,4 J/cm².

Ao se analisar os resultados, em um tempo de pré-irradiação de 5 minutos, os tratamentos com uma energia de 4,2 J/cm² apresentaram-se melhores que quando tratados com 8,4 J/cm², tendo a concentração 10 µg/ml do azul de toluidina demonstrado o melhor resultado. Ao se analisar os resultados dos experimentos com um período de pré-irradiação de 60 minutos, os percentuais de letalidade foram um pouco maiores que os tratados com um período de pré-irradiação de 5 minutos, porém não se encontrou diferença estatística significativa entre estes valores. Desta forma, como não existe uma diferença estatística significativa para se justificar a utilização de um período de pré-irradiação de 60 minutos, optamos por um período menor de pré-irradiação para que o tratamento seja mais rápido. Já quando a energia do laser foi avaliada, também não foi observado um aumento significativo da letalidade com uma dose de 8,4 J/cm².

Em suma, o melhor parâmetro encontrado para o tratamento das formas promastigotas de *L. braziliensis* seria a incubação dos parasitas com 10 µg/ml de azul de toluidina seguido por um período de pré-irradiação de 5 minutos e a irradiação com uma dose de 4,2 J/cm² com uma laser (λ660nm, 40mW, 4,2 ou 8,4 J/cm², CW).

5. CONCLUSÕES

- Após os experimentos apresentados, os compostos MB e TBO apresentaram atividades fotossensibilizante contra os parasitos de *T. cruzi* e *L. braziliensis* nas concentrações atóxicas testadas;
- A melhor condição de energia a ser entregue configurou-se em:
 - ✓ Laser Vermelho: 660nm
 - ✓ Potência de Saída: 40 mW
 - ✓ Frequência: 50-60Hz
 - ✓ Modo Contínuo (CW)
 - ✓ Fluência: 4J/cm²
 - ✓ Tempo: 120 segundos
- A fototerapia empregada ocasionou alterações morfo-estruturais em *Trypanosoma cruzi*.
- A energia empregada não ocasionou inibição ou estimulação na proliferação parasitária de *T. cruzi* e *L. braziliensis*.
- Os compostos apresentam-se atóxicos em concentrações inferiores a 20 µg/mL ou 25 µM.
- Em situação *in vitro*, para *L. braziliensis* o composto TBO em sua concentração de 10µg/mL associado a configuração do laser previamente descrita apresentou o melhor percentual de letalidade nos experimentos testados.
- Em situação *in vitro*, para *T. cruzi* o composto MB apresentou um IC₅₀ de 0,4607 µM associado a configuração do laser previamente descrita, sendo desta forma bem menor que o IC₅₀ da fármaco padrão de tratamento Benzonidazol (3,8 µM).
- Em infecções intracelulares, a Fotoquimioterapia Antiparasitária apresentou efetividade contra as formas amastigotas de *T. cruzi*, quando comparado a quimioterapia tradicional com os candidatos a fotossensibilizadores.

Com base em todos os resultados sob os mais diversos parâmetros avaliados pode-se demonstrar a eficácia dos derivados fenotiazínicos como excelentes fotossensibilizadores a serem utilizados na Fotoquimioterapia Antiparasitária contra os parasitos de *Trypanosoma cruzi* e *Leishmania braziliensis*. Os compostos apresentaram Índices de seletividade satisfatórios, isto é, as concentrações utilizadas na técnica possuíam valores muito abaixo das maiores concentrações atóxicas testadas. A potencialização da letalidade pela FQTAp também pode ser demonstrada contra as várias formas evolutivas dos parasitos. Com todos esses

resultados positivos, a FQTAp revela-se promissora para ensaios clínicos contra a doença de Chagas e a Leishmaniose cutânea.

6. PERSPECTIVAS

Como perspectivas, nós temos:

- Análises *in vivo* contra *Leishmania braziliensis* – Leishmaniose cutânea;
- Análises Clínicas contra *Leishmania braziliensis*;
- Avaliação *in vitro* contra *Trypanosoma cruzi*;
- Desenvolvimento de dispositivo para irradiação clínica.

7. REFERÊNCIAS

- ADADE, C.M., OLIVEIRA, I.R.S., PAIS, J.A.R., SOUTO-PADRÓN, T.. Melittin peptide kills *Trypanosoma cruzi* parasites by inducing different cell death pathways. *Toxicon*, v. 69, p. 227-239, 2013.
- ALVES, M. J. M., RABINOVITCH, M. Destruction of Intracellular *Trypanosoma cruzi* After Treatment of Infected Macrophages with Cationic Electron Carriers. *Infection and Immunity* v. 39, n. 1, p. 435-438, 1983.
- ATKINSON, R.J. Gas-Phase Tropospheric Chemistry of Volatile Organic Compounds: 1. Alkanes and Alkenes. *Phys. Chem. Ref. Data*, v. 26, n. 215, 1997.
- BAGNATO VS, 2008. Novas Técnicas Ópticas para as áreas da saúde. Ed. Livraria da Física – São Paulo.
- BARBOSA, A.F.S., SOARES, L.G.P., ACIOLE, J.M.S., ACIOLE, G.T.S., PITTA, I.R., GALDINO, S.L., PINHEIRO, A.L.B. Evaluation of photodynamic antimicrobial therapy (PACT) against trypomastigotes of *Trypanosoma cruzi*: In vitro study. *AIP Conf Proc*, v. 1364, p.55–59, 2010.
- BARBOSA, A.F.S., SANGIORGI, B.B., GALDINO, S.L., BARRAL-NETTO, M., PITTA, I.R., PINHEIRO, A.L.B. Photodynamic Antimicrobial Chemotherapy (PACT) Using Phenothiazine Derivatives as Photosensitizers Against *Leishmania braziliensis*. *Lasers Surg* v. 44, n. 10, p. 850-855, 2012.
- BERN, C., MONTGOMERY, S.P., HERWALDT, B.L., RASSI JR., A., MARIN-NETO, J.A., DANTAS, R.O., MAGUIRE, J.H., ACQUATELLA, H., MORILLO, C., KIRCHHOFF, L.V., GILMAN, R.H., REYES, P.A., SALVATELLA, R., MOORE, A.C. Evaluation and treatment of Chagas disease in the United States: a systematic review. *JAMA*, v. 298, n. 18, p. 2171–2181, 2007.
- BILATE, A.M.B., CUNHA-NETO, E. Chagas disease cardiomyopathy: current concepts of an old disease. *Rev Inst Med Trop São Paulo*, v. 50, n. 2, p. 67–74, 2008.
- BOLOGNANI, L., MAJNI, G., COSTATO, M., MILANI, M. ATPase and ATPsynthetase activity in myosin exposed to low power laser and pulsed electromagnetic fields. *Bioelectrochem Bioenergetics*, v.32, p. 155-164, 1993.
- BOLTON, P., YOUNG, S., DYSON, M. The direct effect of 860nm light on cell proliferation and on succinic deshydrogenate activity of human fibroblasts in vitro. *Laser Therapy*, v. 7, p. 55-60, 1995.
- BONALDO, M.C., D'ESCOFFIER, L.N., SALLES, J.M., GOLDENBERG, S. Characterization and expression of proteases during *Trypanosoma cruzi* metacyclogenesis. *Exp Parasitol*, v. 73, n. 1, p. 44–51, 1991.
- BUCHHOLZ, K., COMINI, M.A., WISSENBAACH, D., SCHIRMER, R.H., KRAUTH-SIEGEL, R.L., GROMER, S. Cytotoxic interactions of methylene blue with trypanosomatid-

specific disulfide reductases and their dithiol products. *Mol Biochem Parasitol*, v. 160, n. 1, p. 65–69, 2008.

CAFFREY, C.R., STEVERDING, D. Recent initiatives and strategies to developing new drugs for tropical parasitic diseases. *Expert Opin Drug Discov.* v. 3, p.173–86, 2008

CAMINOS, D.A., SPESIA, M.B., DURANTINI, E.P. Photodynamic inactivation of *Escherichia coli* by novel meso-substituted porphyrins by 4-3-N,N,N-trimethylammoniumpropoxyphenyl and 4-trifluoromethylphenyl groups. *Photochem Photobiol Sci*, v. 5, p.56 – 65, 2006.

CASTRO, S.L., BATISTA, D.G.J., BATISTA, M.M., BATISTA, W., DALIRY, A., SOUZA, E.M., MENNA-BARRETO, R.F.S., OLIVEIRA, G.M., SALOMÃO, K., SILVA, C.F., SILVA, P.B., SOEIRO, M.N.C. Experimental Chemotherapy for Chagas Disease: A Morphological, Biochemical, and Proteomic Overview of Potential *Trypanosoma cruzi* Targets of Amidines Derivatives and Naphthoquinones. *Molecular Biology International*, v. 2011, doi:10.4061/2011/306928, 2011.

CDC – Centro para Prevenção e Controle de Doenças – Leishmaniose, 2013. Acessado em 17/07/2013; <http://www.cdc.gov/parasites/leishmaniasis/biology.html>

CESTARI, I., EVANS-OSSES, I., SCHLAPBACH, L.C., MESSIAS-REASON, I., RAMIREZ, M.I. Mechanisms of complement lectin pathway activation and resistance by trypanosomatid parasites. *Mol Immunol*, v. 53, n. 4, p. 328– 334, 2013.

CHAGAS, C. Nova Tripanosomíase humana. Estudos sobre a morfologia e o ciclo evolutivo do *Schizotrypanum cruzi* n.g., n.sp., agente etiológico de nova entidade mórbida do homem. *Mem Inst Oswaldo Cruz*, v. 1, n. 2, p. 159-218, 1909.

CLAYTON, J. Chagas disease: pushing through the pipeline. *Nature*, v. 465, n. 7301, p. S12–S15, 2010.

CONLAN, M. J.; RAPLEY, J. W.; COBB, C. M. Biostimulation of wound healing by low-energy irradiation: A review. *Journal of Clinical Periodontology*, Copenhagen, v. 23, n. 5, p. 492-496, 1996.

CORREA, J.G., FAIRLAMB, A.H., STOPPANI, A.O.M. *Trypanosoma cruzi* Trypanothione Reductase is Inactivated by Peroxidase-Generate Phenothiazine Cationic Radicals. *Free Rad Res*, v. 34, n. 4, p. 363 – 368, 2001.

COURA, JR. Chagas Disease: what is known and what is needed – a background article. *Mem Inst Oswaldo Cruz*, v. 102, n. 1, p. 113 – 122, 2007.

COURA, J.R., VIÑAS, P.A. Chagas disease: a new worldwide challenge. *Nature*, 465, S6–S7, 2010.

COURA, J.R., BORGES-PEREIRA, J. Chronic phase of Chagas disease: why should it be treated? A comprehensive review. *Mem Inst Oswaldo Cruz*, v. 106, n. 641–645, 2011.

CROFT, S.L., OLLIARO, P. Leishmaniasis chemotherapy—challenges and opportunities. *Clin Microbiol Infect.* v. 17, n. 10, p. 1478–1483, 2011.

DELGADO, G., SANCHES, Y., PLAZA, D. AND GRANADOS D. An experimental approach to studying the effectiveness and safety of meglumine antimoniate formulations. *Biomed Pharmacother.* v. 65, n. 8, p. 565-577, 2011.

DEMIDOVA, T.N., HAMBLIN, M.R. Effect of cell-photosensitizer binding and cell density on microbial photoinactivation. *Antimicrob Agents Chemother.* v.49, n. 6, p.2329–2335, 2005

DE MUYLDER, G., ANG, K.K.H., CHEN, S., ARKIN, M.R., ENGEL, J.C., MCKERROW, J.H. A screen against Leishmania intracellular amastigotes: Comparison to a promastigote screen and identification of a host cell-specific hit. *PLoS Negl Trop Dis.* v. 5:e1253, 2011.

DIAS, J.C.P.; COURA, JR, 1997. Epidemiologia. In JCP Dias, JR Coura (Eds), Clínica e terapêutica da Doença de Chagas, Ed. Fiocruz, Rio de Janeiro.

DUTTA, S., ONGARORA, B.G., LI, H., VICENTE, M.G.H., KOLLI, B.K., CHANG, K.P. Intracellular targeting specificity of novel phthalocyanines assessed in a host parasite model for developing potential photodynamic medicine. *PLoS ONE*, v. 6, n.6, e20786, 2011.

FERNANDEZ, J. M., BILGIN, M. D., GROSSWEINER, L. I. Singlet oxygen generation by photodynamic agents. *J Photochem Photobiol B*, v. 37, p. 131-140, 1997.

FERREIRA, C.S., BEZERRA, R.C., PINHEIRO, A.A. Methylene Blue Vital Staining for *Trypanosoma cruzi* trypomastigotes and Epimastigotes. *Rev Inst. Med. Trop S. Paulo*, v. 48, n. 6, p. 347 – 349, 2006.

FIDALGO, L.M., GILLE, L. Mitochondria and Trypanosomatids: Targets and Drugs. *Pharm Res.* v. 28, p. 2758-2770, 2011.

FIOCRUZ-AZAMBUJA – Portal da Doença de Chagas [capturado em 07/05/13] <<http://www.fiocruz.br/chagas/cgi/cgilua.exe/sys/start.htm?sid=11>>

ICC/FIOCRUZ – Instituto Carlos Chagas [capturado em 07/05/2013] disponível em: <<http://www.fiocruz.br/icc/cgi/cgilua.exe/sys/start.htm?sid=37>>

FLOHÉ, L. The trypanothione system and its implications in the therapy of trypanosomatid diseases. *Int J Med Microbiol*, v. 302, n. 4-5, p. 216– 220, 2012.

GAD, F., ZAHRA, T., HASAN, T., HAMBLIN, M.R. Photodynamic inactivation of Gram-positive pathogenic bacteria: Effect of growth phase and extracellular slime. *Antimicrob Agents Chemother*, v. 48, n.6, p. 2173–2178, 2004.

GARCEZ, A.S., SOUZA, F.R., NÚÑES, S.C., KATHER, J.M., RIBEIRO, M.S. Terapia Fotodinâmica em Odontologia – Laser de baixa potência para redução microbiana. *Rev APCD*, n. 57, p. 223-226, 2003.

KARU, T.I., KALENDU, G.S., LETOKHOV, V.S., LOBKO, V.V. Biostimulation of HeLa cells by low intensity visible light. *Il Nuovo Cimento D*. v. 1, n. 6, p. 828-840, 1982.

KARU, T.I., TIPHLOVA, O.A., LETOKHOV, V.S., LOBKO, V.V. Stimulation of E.coli growth by laser and incoherent red light". *Il Nuovo Cimento D*. v. 2, n. 4, p. 1138-1144, 1983a.

KARU, T.I., KALENDU, G.S., LETOKHOV, V.S., LOBKO, V.V. Biological action of low-intensity visible light on HeLa cells as a function of the coherence, dose, wavelength, and irradiation regime II. *Sov.J. Quantum Electronics*. v. 13, n. 9, p. 1169-1172, 1983b.

KARU, T.I., KOLYAKOV, S.F. Exact Action Spectra for Cellular Responses Relevant to Phototherapy. *Photomedicine and Laser Surgery*. v. 23, n. 4, p. 355–361, 2005.

KARU, T.I. Photobiological fundamentals of low-power laser therapy. *IEEE J.Quantum Electronics*. v. QE-23, n. 1, p. 1703-1717, 1987.

KARU, T.I. Low-power laser therapy In: Biomedical Photonics Handbook. Ch. 48, Editor-in-chief Tuan Va-Dinh, Boca Raton: CRC Press, 2003.

KARU, T.I. Photobiology of Low-Power Laser Therapy. Chur, London, Paris, New York: Harwood Academic Publishers, 1989.

KARU, T.I. Molecular mechanism of the therapeutic effect of low-intensity laser radiation. *Lasers Life Sci*. v. 2, n. 1, p. 53-74, 1988.

KHARKWAL, G.B., SHARMA, S.K., HUANG, Y., DAI, T., HAMBLIN, M.R. Photodynamic Therapy for Infections: Clinical Applications. *Lasers Surg Med*, v. 43, n. 7, p. 755–767, 2011.

KIM, S.Y., KWON, O.J., PARK, J.W. Inactivation of catalase and superoxide dismutase by singlet oxygen derived from photoactivated dye. *Biochemie*, v. 83, n. 5, p. 437 – 444, 2001.

LAMBRECHTS, S.A.G., AALDERS, M.C.G., MARLE, J.V. Mechanistic study of the photodynamic inactivation of *Candida albicans* by a cationic porphyrin. *Antimicrob Agents Chemother*, v. 49, n. 5, p. 2026–2034, 2005.

LIMA, L.M., BARREIRO, E.J. Bioisosterism: A Useful Strategy for Molecular Modification and Drug Design. *Curr Med Chem*, v. 12, n. 1, p. 23 – 59, 2005.

MANTA, B., COMINI, M., MEDEIROS, A., HUGO, M., TRUJILLO, N., RADI, R. Trypanothione: A unique bis-glutathionyl derivative in trypanosomatids. *Biochim Biophys Acta*, v.1830, n. 5, p. 3199–3216, 2013.

MARIN-NETO, J.A. et al. The BENEFIT Trial: testing the hypothesis that trypanocidal therapy is beneficial for patients with chronic Chagas heart disease. *Memórias do Instituto Oswaldo Cruz*. v. 104, n. 3, p. 319 – 324, 2009.

MASMOUDI, A., MAALEJ, N., MSEDDEI, M., SOUISSI, A., TURKI, H., BOUDAYA, S., BOUASSIDA, S., ZAHAF, A. Glucantime injection: benefit versus toxicity. *Med Mal Infect.* v. 35, n. 1, p.42–45, 2005.

MASMOUDI, A., HARIZ, W., MARREKCHI, S., AMOURI, M., TURKI, H. Old World cutaneous leishmaniasis: diagnosis and treatment. *J Dermatol Case Rep.* v. 7, n. 2, p. 31–41, 2013

MISERENDINO LJ; PICK RM, 1995. Lasers in Dentistry. Quintessence Books. Chicago.

MONCAYO, A., SILVEIRA, A.C. Current epidemiological trends for Chagas disease in Latin America and future challenges in epidemiology, surveillance and health policy. *Mem Inst Oswaldo Cruz*, v. 104, n. 1, p. 17–30, 2009.

MONTE-NETO, R.L., COELHO, A.C., RAYMOND, F., LÉGARÉ, D., CORBEIL, J., MELO, M.N., FRÉZARD, F., OUELLETTE, M. Gene expression profiling and molecular characterization of antimony resistance in *Leishmania amazonensis*. *PLoS Negl Trop Dis.* :e1167. doi: 10.1371/journal.pntd.0001167, 2011.

NAGY, E.M., VIA, L.D., RONCONI, L., FREGONA, D. Recent Advances in PUVA Photochemotherapy and PDT for the Treatment of Cancer. *Curr Pharma Des*, v. 16, n. 16, p. 1863-1876, 2010.

NAKAJIMA-SHIMADA, J., HATABU, T., HOSOI, Y., ONIZUKA, Y., KIKUCHI, H., OSHIMA, Y., KUBOHARA, Y. Derivatives of *Dictyostelium discoideum* differentiation-inducing factor-3 suppress the activities of *Trypanosoma cruzi* in vitro and in vivo. *Biochem Pharmacol*, v. 85, n. 11, p. 1603-1610, 2013.

NOODT, B.B., RODAL, G.H., WAINWRIGHT, M., PENG, Q., HOROBIN, R., NESLAND, J.M., BERG, K. Apoptosis induction by different pathways with methylene blue derivative and light from mitochondrial sites in V79 cells. *Int J Cancer*, v.75, n.6, p.941-948, 1998.

OSTUNI, A., PASSARELA, S., QUAGLIANIELLO, E. The energy dose dependence of the activity of glutamate de hydrogenase irradiated with helium neon laser. *Laser Technol*, v. 4, p.13-16, 1994.

PARVEEN, S., KAHN, M.O.F., AUSTIN, S.E., CROFT, S.L., YARDLEY, V., ROCK, P., DOUGLAS, K.T. Antitrypanosomal, antileishmanial, and antimalarial activities of quaternary arylalkylammonium 2-amino-4-chlorophenyl phenyl sulfides, a new class of trypanothione reductase inhibitor, and of N-acyl derivatives of 2-amino-4-chlorophenyl phenyl sulfide. *J Med Chem*, v. 48, n. 25, p. 8087 – 8097, 2005.

PASSARELLA, S., CASAMASSIMA, E., MOLINARI, S., PASTORE, D., QUAGLIARIELLO, E., CATALANO I.M. CINGOLANI, A. Increase of proton electrochemical and ATP synthesis in rat liver mitochondria irradiated in vitro by Helium-Neon laser. *Febs Letters* , v.175, n. 1, p. 95-99, 1984.

PEREZ-MOLINA, J.A., NORMAN, F., LOPEZ-VELEZ, R. Chagas disease in non-endemic countries: epidemiology, clinical presentation and treatment. *Curr Infect Dis Rep*, v. 14, p. 263–274, 2012.

PÉREZ-MOLINA, J.A.; SOJO-DORADO, J.; NORMAN, F.; MONGE-MAILLO, B.; DÍAZ-MENÉNDEZ, M.; ALBAJAR-VIÑAS, P.; LÓPEZ-VÉLEZ, R. Nifurtimox therapy for Chagas disease does not cause hypersensitivity reactions in patients with such previous adverse reactions during benznidazole treatment. *Acta Tropica*, v.127, n.2, p. 101-104, 2013.

PERUSSI, J.R. inativação Fotodinâmica de Microrganismos. *Química Nova*, v. 30, n. 4, p. 988-994, 2007.

PINHEIRO, A.L.B.; FRAME, J.W. Laser em Odontologia. Seu uso atual e perspectivas futuras. *RGO*, Porto Alegre, v.40, n.5, p.327-332, 1992.

PINHEIRO, ANTÔNIO LUIZ B. Aplicação do laser na odontologia – Editora Santos: São Paulo, 2010.

PRATA, A. Clinical and epidemiological aspects of Chagas disease. *The Lancet Infectious Diseases*, v. 1, n. 2, p.92–100, 2001.

RASSI-JR, A., RASSI, A., MARCONDES DE REZENDE, J. American trypanosomiasis (Chagas disease). *Infect Dis Clin North Am*, v. 26, n. 2, p. 275–291, 2012.

ROCHA JÚNIOR, A.M., ANDRADE, L.C.F., OLIVEIRA, R.G., AERESTRUP, F.M., FARIAS, R.E. Modulação da proliferação fibroblástica e da resposta inflamatória pela terapia a laser de baixa intensidade no processo de reparo tecidual. *An Bras Dermatol*, v. 81, n. 2, p. 150-156, 2006.

SIMPLICIO, F.I., MAIONCHI, F., HIOKA, N. Terapia Fotodinâmica: Aspectos Farmacológicos, Aplicações e Avanços Recentes no Desenvolvimento de Medicamentos. *Quim. Nova*, v.25, n.5, p.801-807, 2002.

SIQUEIRA-BATISTA, R. Moléstia de Chagas 2 ed. *Editora Rubio*: Rio de Janeiro, 2007.

STOCKDALE, L., NEWTON, R. A Review of Preventative Methods against Human Leishmaniasis Infection. *PLoS Negl Trop Dis*. v. 7, n. 6: e2278, 2013.

TAKAHASHI, Y.; HITOMI, S.; HIRATA, T.; FUKUSE, T.; YAMAZAKI, F.; CHO, K.; WADA, H. Neovascularization effect with He-Ne laser in the rat trachea. *The Journal of Thoracic and Cardiovascular Surgery*, Saint Louis, v. 40, n. 5, p. 288-291, 1992.

TAVARES, N.M., SILVA, R.A., COSTA, D.J., PITOMBO, M.A., FUKUTANI, K.F., MIRANDA, J.C., VALENZUELA, J.G., BARRAL, A., DE OLIVEIRA, C.I., BARRAL-NETTO, M., BRODSKYN, C. *Lutzomyia longipalpis* Saliva or Salivary Protein LJM19 Protects against *Leishmania braziliensis* and the Saliva of Its Vector, *Lutzomyia intermedia*. *PLoS Negl. Trop. Dis*. v. 5, e1169, 2011.

T'UNG, T. *In vitro* photodynamic action of methylene blue on *Trypanosoma brucei*. *Proc Soc Exp Biol Med*, v. 38, p. 29–31, 1938.

TEICHERT, M.C., JONES, J.W., USACHEVA, M.N., BIEL, M.A. Treatment of oral candidiasis with methylene blue-mediated photodynamic therapy in an immunodeficient murine model. *Oral Surg Oral Med Oral Pathol Oral Radiol Endod*, v. 93, n. 2, p.155-60, 2002.

TEMPERTON, N.J., WILKINSON, S.R., MEYER, D.J., KELLY, J.M. Overexpression of superoxide dismutase in *Trypanosoma cruzi* results in increased sensitivity to the trypanocidal agents gentian violet and benznidazole. *Mol Biochem Parasitol*, v. 96, n. 1-2, p.167 – 176, 1998.

URBINA, J. A.; DOCAMPO, R. Specific chemotherapy of Chagas disease: controversies and advances. *Trends Parasitol*, v. 19, n. 11, p. 495-501, 2003.

USACHEVA; M.N., TEICHERT, M.C., SIEVERT, C.E., BIEL, M.A. Effect of Ca⁺ on the photobactericidal efficacy of methylene blue and toluidine blue against gram-negative bacteria and the dye affinity for lipopolysaccharides. *Lasers Surg Med*, v. 38, n. 10, p. 946-954, 2006.

VEÇOSO, M C. Laser em Fisioterapia. Ed. Lovise: São Paulo, 1993.

VINCK, E. M.; CAGNIE, B. J.; CORNELISSEN, M. J.; DECLERCQ, H. A.; CAMBIER, D. C. Increased fibroblast proliferation induced by light emitting diode and low power laser irradiations. *Lasers in Medical Science*, London, v. 18, n. 2, p. 95-99, 2003.

VINCK, E.; COOREVITS, P.; CAGNIE, B.; DE MUYNCK, M.; VANDERSTRAETEN, G.; CAMBIER, D. Evidence of changes in sural nerve conduction mediated by light emitting diode irradiation. *Lasers in Medical Science*, London, v. 20, n. 1, p. 35-40, 2005.

WAGNER, S.J., SKRIPCHENKO, A., ROBINETTE, D., MALLORY, D.A., CINCOTTA, L. Preservation of red cell properties after virucidal phototreatment with dimethylmethylene blue. *Transfusion*, v. 36, n. 8, p. 729-737, 1998.

WAINWRIGHT, M. Photodynamic antimicrobial chemotherapy (PACT). *J Antimicrob Chemother*, v. 42, n. 1, p. 13-28, 1998.

WAINWRIGHT, M. Methylene Blue Derivatives – suitable photoantimicrobials for blood product disinfection? *Int J Antimicro Agents*, v. 16, n. 4, p. 381 – 394, 2000.

WAINWRIGHT, M. The development of phenothiazinium photosensitisers. *Photodiag Photodyn Ther*, v. 2, n. 4, p. 263 – 272, 2005.

WHO/TDR, 2011. For Research on Diseases of Poverty. Disponível em:
<<http://www.who.int/tdr/diseases-topics/african-trypanosomiasis/en/index.html>>, acessado em: 17/07/2013

YU, W.; NAIM, J. O.; MCGOWAN, M.; IPPOLITO, K.; LANZAFAME, R. J. a) Photomodulation of oxidative metabolism and electron chain enzymes in rat liver mitochondria. *Photochemistry and Photobiology*, Oxford, v. 66, n. 6, 866-871, 1997.

8. ANEXOS

8.1. RESULTADOS COMPLEMENTARES PARA *TRYPANOSOMA CRUZI*

Os critérios utilizados para a escolha das formas amastigotas intracelulares e tripomastigotas deveu-se a sua importância na infecção de humanos. Seguiu-se uma ordem para os experimentos, dividindo-se os estudos *in vitro* em duas etapas.

A primeira etapa consistiu em avaliar o efeito dos compostos contra as formas tripomastigota e amastigota intracelulares. Nesta etapa, foi feita a administração dos compostos, de forma isolada, sobre os parasitas, monitorando-se os efeitos sobre as formas tripomastigota e amastigota. Os valores médios das concentrações utilizadas foram de, no máximo, $10\ \mu\text{M}$. Foi realizada uma diluição seriada até a obtenção de concentrações inferiores até $0,002\ \mu\text{M}$, buscando determinar se a redução dos parasitas seria superior a aquela obtida com o uso do Benzonidazol, droga padrão usada atualmente no tratamento da patologia.

A segunda etapa consistiu na determinação do *Índice de Seletividade* – *SI*, o qual é determinado com base na relação do valor de IC_{50} na célula hospedeira, dividido pelo valor de IC_{50} do parasita. A determinação do *índice de seletividade* (*SI*) foi realizada através do cálculo da relação do valor de IC_{50} das células hospedeiras dividido pelo valor de IC_{50} do parasita, testada através do protocolo *AlamarBlueTM*, utilizado para avaliar a toxicidade para as células hospedeira. Os compostos que causaram morte celular $\leq 50\%$ foram utilizados na etapa seguinte.

Os testes de *atividade anti-Trypanosoma cruzi* contra a forma tripomastigota, em sua fase escura, isto é, sem a utilização da fonte de luz, avaliou a ação isolada dos compostos. Os resultados demonstraram eficácia contra os parasitas e apresentaram valores de IC_{50} inferiores ao IC_{50} do Benzonidazol (BZ), droga padrão no tratamento da doença de Chagas (aproximadamente $3,8\ \mu\text{M}$). Os compostos testados MB e TBO apresentaram, respectivamente, IC_{50} de $2,59$ e $1,21\ \mu\text{M}$, respectivamente.

Quando foi realizada a **FQTAp** proposta, foram encontrados valores ainda menores de IC_{50} . Utilizando-se de uma densidade de energia fixa (J/cm^2) para excitar os compostos, foi possível reduzir os valores de IC_{50} encontrados na fase escura do experimento. Foi verificado que esta densidade de energia usada de forma isolada sobre os parasitas, não alterou a população de parasitas, não interferindo de forma inibitória ou estimulatória na cultura durante o tempo experimental. Os novos valores de IC_{50} após a **FQTAp** foram respectivamente para os compostos MB e TBO de $0,4607$ e $1,148\ \mu\text{M}$. Estes valores demonstram um percentual de

redução da ordem de **82,21 e 5,78**. A redução ocorreu devido ao efeito que a luz utilizada produziu nos compostos, demonstrando assim a eficácia da **FQTA_p** sobre os parasitas.

Outro importante critério na busca por compostos ativos, contra os parasitas de *T. cruzi*, com potencial terapêutico é sua baixa toxicidade para células de mamíferos. Os compostos *MB* e *TBO* foram testados na fase escura e não demonstraram nenhum efeito citotóxico as células testadas (esplenócitos) em concentrações até 25 μM , através do método do AlamarBlue, (Romanha e colaboradores, 2010). Ao se realizar a **FQTA_p**, os compostos *MB* e *TBO* continuaram exibindo um IC_{50} , para células de mamíferos, superior a 25 μM (Tab.1). O efeito citotóxico da fonte de luz também foi avaliado, e na densidade de energia utilizada, não foi identificado nenhum efeito citotóxico sobre as células de mamíferos.

	MB	TBO
LC ₅₀ escuro	>25 μM	>25 μM
IC ₅₀ tripo escuro	2,59 μM	1,21 μM
Índice de seletividade	>9.65	>20.66
FQTA _p		
LC ₅₀ FQTA _p	>25 μM	>25 μM
IC ₅₀ tripo FQTA _p	0.4607 μM	1.148 μM
Índice de seletividade	>54.34	>21.77

Tabela 1: índice de Seletividade dos compostos em sua fase clara e escura

No ensaio utilizando a forma amastigota intracelular, macrófagos foram infectados com tripomastigotas para a transformação em amastigotas. Dois experimentos foram realizados para avaliar a atividade potencial dos compostos contra amastigotas intracelulares. O primeiro se baseou na administração isolada dos compostos sem a excitação com a fonte de luz. Foram escolhidas concentrações que não apresentaram nenhuma atividade contra esta forma específica. Ao avaliar-se o efeito dos compostos sobre os parasitos intracelulares, verificou-se um percentual de redução inferior a 10% para os compostos *MB* e *TBO*. Os dados demonstram também que os compostos apresentam certa capacidade em reduzir a quantidade de células infectadas.

Verificou-se que após o tratamento, houve um percentual de redução de infecção de macrófagos de 35,96 e 44,94 para os compostos *MB* e *TBO* respectivamente. Assim, os compostos nas concentrações testadas não reduziram, de forma acentuada, a quantidade de amastigotas, porém foram capazes de reduzir a quantidade de células infectadas. Isto pode ser indicativo de alterações morfofisiológicas que podem ter reduzido o potencial infectante dos parasitos.

Quando foi realizada a **FQTAp** proposta contra amastigotas intracelulares, as concentrações testadas na fase escura foram também utilizadas para avaliar o seu possível efeito tripanocida. As concentrações testadas foram de 0,04 e 0,078 μM para os compostos *MB* e *TBO*, respectivamente. Os percentuais de redução da quantidade de amastigotas foram superiores a 73% para estas concentrações, o que demonstram um efeito importante da **FQTAp** sobre os amastigotas.

Ao se avaliar o *percentual de redução de células infectadas*, os resultados mostraram uma redução superior a 52%. Neste experimento, um fato inesperado foi o feito da luz utilizada sobre os macrófagos. Foi evidenciado que a luz sozinha apresentou tanto uma redução na quantidade de amastigotas intracelulares, quanto na quantidade de macrófagos infectados. Foram observadas alterações morfológicas, não demonstradas em imagem, nos macrófagos irradiados. Possivelmente, existe uma estimulação dos macrófagos pela luz, que de alguma forma aumenta sua atividade contra os parasitas.

Quando se comparou a infecção de amastigotas intracelulares tratados com a **FQTAp** com os tratados apenas com os compostos, verificou-se uma melhora da atividade quando comparados todos os compostos. A **FQTAp** utilizando o composto *MB* apresentou um aumento de aproximadamente 75% na redução da quantidade de amastigotas. O composto *TBO* apresentou um aumento de aproximadamente 65% quando comparado a sua ação isolada na fase escura.

Ao se analisar o percentual de redução da quantidade de células infectadas, a **FQTAp** também apresentou valores melhores do que os obtidos na fase escura. A **FQTAp** utilizando o composto *MB* apresentou um aumento de aproximadamente 16% e o *TBO* apresentou uma redução de aproximadamente 20% quando comparados as suas ações isoladas na fase escura.

8.2.Anexos: Demais Artigos Publicados

J Biomed Mater Res A. 2011 Aug;98(2):212-21. doi: 10.1002/jbm.a.33107. Epub 2011 May 4.

Light microscopic description of the effects of laser phototherapy on bone defects grafted with mineral trioxide aggregate, bone morphogenetic proteins, and guided bone regeneration in a rodent model

Light microscopic description of the effects of laser phototherapy on bone defects grafted with mineral trioxide aggregate, bone morphogenetic proteins, and guided bone regeneration in a rodent model

Antonio L. B. Pinheiro,^{1,2,3} Luiz G. P. Soares,¹ Gilberth T. S. Aciole,¹ Neandder A. Correia,¹ Artur F. S. Barbosa,¹ Luciana M. P. Ramalho,^{1,3} Jean N. dos Santos^{3,4}

¹Center of Biophotonics, School of Dentistry, Federal University of Bahia, Salvador, BA 40110-150, Brazil

²Institute of Biomedical Engineering, Camilo Castelo Branco University, São José dos Campos, SP 12245-230, Brazil

³National Institute of Optics and Photonics, Physics Institute, University of São Carlos, São Carlos, SP 13560-970, Brazil

⁴Laboratory of Surgical Pathology, School of Dentistry, Federal University of Bahia, Salvador, BA 40110-150, Brazil

Received 25 November 2010; accepted 21 February 2011

Published online 4 May 2011 in Wiley Online Library (wileyonlinelibrary.com). DOI: 10.1002/jbm.b.33107

Abstract: We carried out a histological analysis on bone defects grafted with mineral trioxide aggregate (MTA) treated or not with laser, bone morphogenetic protein (BMP), and guided bone regeneration (GBR). Benefits of the use of MTA, laser, BMPs, and GBR on bone repair are well known, but there is no report on their association with laser light. Ninety rats were divided into 10 groups each subdivided into 3. Defects on G II and I were filled with the blood clot. G II was further irradiated with LED. G III and IV were filled with MTA; G IV was further irradiated with laser. G V and VI, the defects filled with MTA and covered with a membrane (GBR). G VI was further irradiated with laser. G VII and VIII, BMPs were added to the MTA and group VIII further irradiated with laser. G IX and X, the MTA + BMP graft was covered with a mem-

brane (GBR). G X was further irradiated with laser. Laser light ($\lambda = 850$ nm, 150 mW, 4 J/cm²) was applied over the defect at 48-h intervals and repeated for 15 days. Specimens were processed, cut and stained with H&E and Sirius red and underwent histological analysis. Subjects on group X were irradiated. The results showed different tissue response on all groups during the experimental time. Major changes were seen on irradiated subjects and included marked deposition of new bone in advanced maturation. It is concluded that near infrared laser phototherapy improved the results of the use of the MTA on bone defects. © 2011 Wiley Periodicals, Inc. *J Biomed Mater Res Part A: JBM* 98A: 212–221, 2011.

Key Words: biomaterial, LLLT, mineral trioxide aggregate

INTRODUCTION

The treatment of bone defects using biomaterials has been extensively studied in the dental field.^{1–7} Since the pioneer work by Urist, who demonstrated heterotrophic formation of bone induced by devitalized demineralized bone matrix, a new possibility of treating bone defects was established. Demineralized bone matrix has osteoinductive properties due to the presence of soluble growth factors on its composition.⁸ Bone loss may be a result of several pathologies, trauma, or a consequence of surgical procedures. This aspect led to extensive studies on the process of bone repair worldwide. Several techniques for the treatment of bone defects have been proposed, including the use of several types of grafts, membranes, and the association of both techniques.⁹

Mineral trioxide aggregate (MTA) is a powder aggregate, containing mineral oxides that have no cytotoxicity and good biological response. It stimulates tissue repair by increasing cellular adhesion, growth, and proliferation at its surface. The use of MTA has been shown to cause an

overgrowth of cementum and on facilitating the regeneration of the periodontal ligament as well as the deposition of new bone.^{9–20}

Previous histological reports have indicated that new bone or cementum is formed adjacent to MTA when it is placed in contact with the periodontal tissue or in artificial bone defects.^{9–14,21,22} It has antibacterial properties,²³ enhances tissue dissolution, and induces bone formation.²⁴

Previous studies suggested that the rise of pH induced by calcium hydroxide combined with the availability of Ca²⁺ and OH⁻ ions has a stimulating effect on bone mineralization.^{25–28}

Guided bone regeneration (GBR) is a procedure based upon the guided tissue regeneration technique, which is a periodontal surgical procedure, which has been used in the dental clinical practice for more than a decade.^{29,30} This procedure is used as a way to stimulate wound healing and to favor the regeneration of tooth supporting structures.³¹ Its principles were based upon the selective permeability

Correspondence to: A. L. B. Pinheiro; e-mail: albp@ufba.br

Contract grant sponsor: Conselho Nacional de Desenvolvimento Científico e Tecnológico (CNPq)

provided by the use of membranes on the isolation of tissues, essential for bone repair. Previous studies have demonstrated that such regeneration may occur following this procedure.^{29–32} The use GBR associated to the use of biomaterials has been considered to be beneficial for the healing of bones.⁸

Our previous results indicate that near infrared laser phototherapy (NIR LPT) is effective to improve bone repair mainly due to its good penetration on tissues when compared to visible laser light. The use of laser phototherapy (LPT) on studies involving bone healing has been a hot topic lately and many of them have demonstrated positive results, including its association to biomaterials.^{33–46}

We have shown that the improvement of bone neoformation and maturation, on irradiated subjects, is associated to the increased deposition of calcium hydroxyapatite (CHA) during early stages of healing. The maturation of the newly formed bone probably represents an increased capacity of secretion by osteoblasts on irradiated subjects. It is well accepted that the deposition of CHA represents bone maturation. Large amounts of CHA on bone are indicative of a more resistant and calcified bone.^{33–46}

It is known that LPT has the ability to stimulate cell proliferation, including fibroblasts, which have the capacity to secrete collagen, the main organic component observed during bone repair.^{33–46}

Despite the growing successful application of the LPT on bone repair, there are a few studies assessing the association of the laser light with biomaterials.^{8,34,36–38,43}

Although several reports have suggested benefits of the isolated or combined use of MTA, BMPs, GBR, and LPT on the repair of bone defects, the associated use of all of these techniques were not studied yet. It might be possible that the observed benefits of the isolated use of each one could be improved with their association.^{33–46}

As suggested by previous reports on the current literature, laser light is capable of improving bone healing and may be possible that the use of laser light associated with the MTA may also improve the outcome of the treatment of bone defects.^{33–46}

The aim of the present study was to study, histologically, the effect of NIR LPT on the healing of surgical bone defects grafted or not with MTA and associated or not to the use of bone morphogenetic proteins (BMPs) and GBR on a rodent model.

MATERIALS AND METHODS

This study was approved by the Animal Ethics Committee of the Vale do Paraíba University and obeyed national and international guidelines for animal experimentation. Ninety healthy adult male Wistar rats (~2-months-old, average weight 295 ± 25 g) were housed under natural conditions of light, humidity, and temperature at the Animal House of the Research and Development Institute of the Vale do Paraíba University during all experimental period. The sample size was relatively small due to ethical constraints and recommendations of the Ethics Committee. The animals were fed with standard laboratory pelleted diet and had water

ad libitum. The animals were kept in groups of five on individual metallic cages and kept at a day/night light cycle and controlled temperature (22°C) during the experimental period. The animals were randomly distributed into 10 groups and then subdivided into 3 subgroups according to the animal sacrifice timing. The number of experimental groups was determined to allow us to use the MTA under different clinical conditions, such as in association with the technique of GBR, as well as to allow the comparison of the results with similar model used by our team in which other types of biomaterials were used and were reported previously.⁸ The distribution of the animals may be seen in Table I.

Prior intramuscular general anesthesia, the animals received 0.04 mL/100 g of atropine subcutaneously. The anesthesia was carried out with 10% Ketamine (Syntec do Brasil, Cotia, SP, Brazil) (0.1 mL/100 g) + 2% Xylazine (Syntec do Brasil) (0.1 mL/100 g). The animals had the right leg shaved and a 3-cm-long incision was performed at the right tibia with a no. 15 scalpel blade. Skin and subcutaneous tissues were dissected down to the periosteum, which was gently sectioned exposing the bone and a 2-mm partial thickness round bone defect was surgically produced (low speed drill, 1200 rpm, under refrigeration) in each animal.

The bone defects on groups II and I were filled only with the blood clot. Bone defects on group II were further irradiated with laser light. The bone defects on the remaining groups were filled with MTA (Angelus[®]—Angelus Indústria de Produtos Odontológicos S/A, Londrina, PR, Brazil) (III); bone defects of group IV were further irradiated with laser light. On groups V and VI, the bone defects were filled with the MTA and covered with a resorbable membrane (Gendern[®], Baumer SA, Mogi das Cruzes, São Paulo, Brazil). Bone defects of group VI were further irradiated with laser light. On groups VII and VIII, a pool of BMPs (Genpro[®], Baumer SA, Mogi das Cruzes, São Paulo, Brazil) was added to the biomaterial (MTA); group VII was further irradiated with laser light. On groups IX and X, the MTA + BMP graft was covered with the membrane (GBR). Bone defects on group X were further irradiated with laser light. All wounds were routinely sutured and the animals received a single dose of Pentabiotin[®] (Penicillin, Streptomycin, 20,000 UI, Fort Dodge Ltda, Campinas, SP, Brazil) (0.02 mL/100 g) immediately after surgery. Animal death

TABLE I. Distribution of the Experimental Groups

Group	Subgroups	n	Protocol
I	I15/I21/I30	9	Control (Clot)
II	II15/II21/II30	9	NIR LPT
III	III15/III21/III30	9	MTA
IV	IV15/IV21/IV30	9	MTA + NIR LPT
V	V15/V21/V30	9	MTA + GBR
VI	VI15/VI21/VI30	9	MTA + GBR + NIR LPT
VII	VII15/VII21/VII30	9	MTA + BMP
VIII	VIII15/VIII21/VIII30	9	MTA + BMP + NIR LPT
IX	IX15/IX21/IX30	9	MTA + BMP + GBR
X	X15/X21/X30	9	MTA + BMP + GBR + NIR LPT

TABLE II. Semiquantitative Criteria Used for the Light Microscopy Analysis

Score Criterion	Discrete	Moderate	Intense
Bone reabsorption	Presence of <25% of the reabsorption of the graft remnants and/or the surgical bed.	Presence of 25–50% of the reabsorption of the graft remnants and/or the surgical bed.	Presence of >75% of the reabsorption of the graft remnants and/or the surgical bed.
Bone neoformation	Presence of <25% of newly formed bone similar to adjacent untreated bone tissue.	Presence of 25–50% of newly formed bone similar to adjacent untreated bone tissue.	Presence of >50% of newly formed bone similar to adjacent untreated bone tissue.
Inflammatory infiltrate	Presence of <25% of inflammatory cells in the area.	Presence of 25–50% of inflammatory cells in the area.	Presence of >50% of inflammatory cells in the area.
Collagen deposition	Presence of <25% of collagen deposition in the area.	Presence of 25–50% of collagen deposition in the area.	Presence of >50% of collagen deposition in the area.

occurred after 15, 21, and 30 days after the surgery with an overdose of general anesthetics.

NIR LPTP was carried out with the Twin Laser[®] device (MMOptics, São Carlos, São Paulo, Brazil; $\lambda = 850$ nm, 150 mW, $\phi = 0.5$ cm², 4 J/cm²) and was transcutaneously applied on four points around the bone defect at 48-h intervals (4 J/cm², per point) being the first session carried out immediately after surgery and repeated at every 48 h during 15 days (16 J/cm² per session) and a total treatment dose of 112 J/cm². Doses used in this study were based upon previous studies carried out by our group.⁸

Following animal death, the samples were longitudinally cut under refrigeration (Buehler[®], Isomet TM1000; Markham, Ontario, Canada) and the specimens kept in 10% formalin solution for 24 h. The specimens were routinely processed to wax, cut, and stained with Hematoxylin and Eosin and Sirius red and underwent histological analysis^{9,14,16–20,42} (Table II) at the Laboratory of Surgical Pathology of the School of Dentistry of the Federal University of Bahia by a experienced pathologist in a blind manner using a Light microscope (AxioStar[®], Zeiss, Germany).

RESULTS

Clot

On day 15, the bone defect was partially filled with newly formed bone displaying nonaligned osteocytes as well as the presence of thin and irregular trabeculi. Medullar tissue and chronic inflammation were seen and scored as discrete. Osteoblastic activity could be seen and there were no signs of bone reabsorption. On day 21, the bone defect was mostly filled with new bone that was more regular than that type of bone seen on the 15th day. Discrete chronic inflammation was observed at this stage. Some specimens of this group showed remnants of cartilaginous tissue, and no signs of bone reabsorption were seen [Fig. 1(A)]. At the end of the experimental period, the bone defect was completely filled by lamellar bone and few Haversian systems were seen. Bone trabeculi were present and were more regularly disposed. The trabeculi showed some osteocytes as well as remnants of cartilage surrounded by bone. Neither reabsorption nor inflammation was observed at this time.

MTA

On day 15, the bone defect was mostly filled by neoformed bone that was characterized by the presence of interconnecting trabeculi containing osteocytes on its matrix and osteoblasts at their surface. Remnants of cartilage and chronic inflammation were also seen dispersed within a fibrovascular tissue. A few points of surface necrosis and remnants of the biomaterial could be seen at this time [Fig. 1(B)]. Bone reabsorption was observed at this stage. On day 21, a regular neoformed bone dispersed in few medullar spaces covered the bone defect and discrete chronic inflammation was observed. The new bone showed osteocytes as well as basophilic reversal lines, and osteoblasts were seen at the osseous surface. At the end of the experimental time, the bone defect was filled by bone without signs of inflammation. Small bone trabeculi, medullar tissue, surface necrosis, and remnants of the biomaterial were also seen at this time.

MTA + GBR

On day 15, interconnecting bone trabeculi showing nonaligned osteocytes as well as active osteoblasts at the periphery of the trabeculi filled the bone defect. In a few cases, delicate bone fragments, usually immature, were seen within a highly vascularized medullar tissue. In some specimens, surface necrosis could be seen. Beneath the necrosis, a band of fibrous connective tissue was detected as well as chronic inflammatory infiltrate and remnants of the biomaterial. On day 21, the bone defect was filled by thick newly formed bone usually showing interconnecting bone trabeculi, nonaligned osteocytes, and basophilic reversal lines. Areas of superficial necrosis were also observed in some specimens as well as the presence of remnants of the biomaterial. At the end of the experimental time, the bone defect was filled by new bone that was characterized by few medullar spaces and irregular small bone fragments. In few specimens, remnants of cartilage could be seen as well as tissue necrosis extending down to the medulla. Remnants of the biomaterial were also seen at this stage [Fig. 1(C)].

MTA + BMP

On day 15, the bone defect was filled by interconnecting bone trabeculi, few medullar spaces, nonaligned osteocytes,

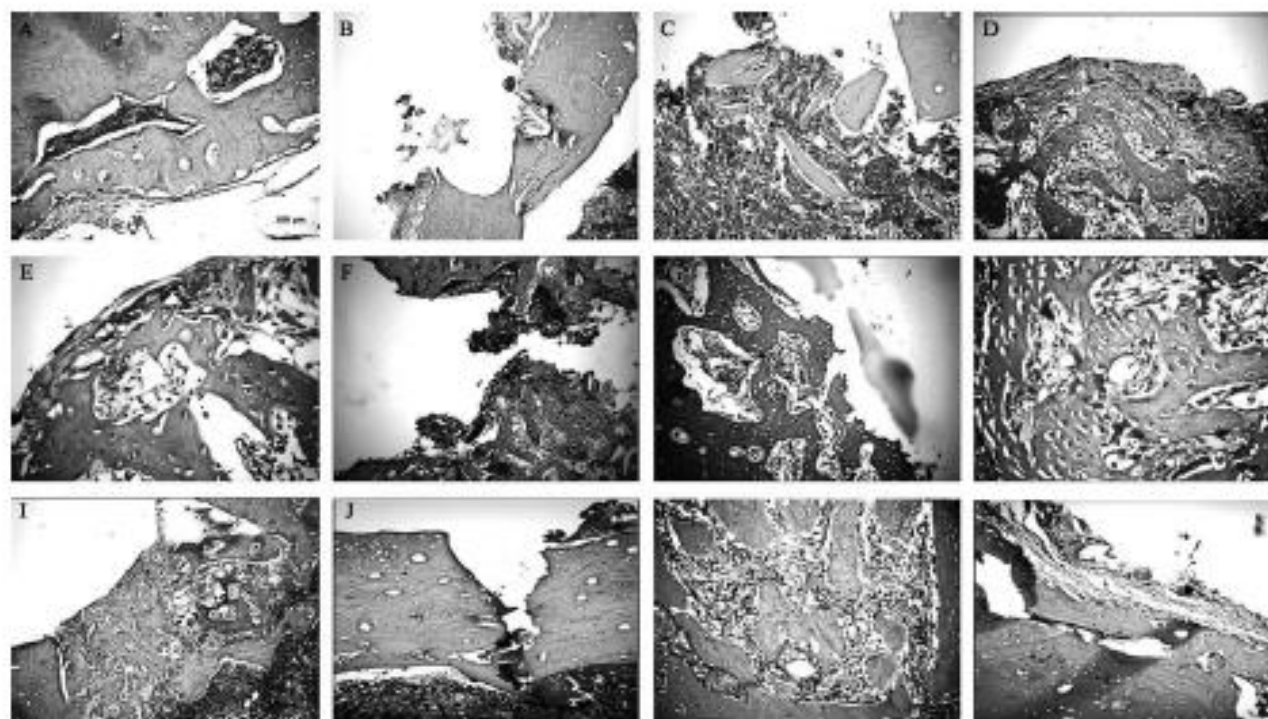


FIGURE 1. (A) Photomicrography of a control specimen on day 21 showing the bone defect completely filled with newly formed extending down to the medullar tissue and displaying osteocytes nonaligned and basophilic reversal lines. (B) Photomicrography of a specimen grafted with MTA on day 15 showing the bone spicules amidst bone defect whose superficial area shows bone necrosis. Note inferior margin with bone walls close to medullar tissue. (C) Photomicrography of a specimen of the MTA + GBR group on day 21 showing the bone defect filled by bone spicules of variable size amidst inflammation composed of lymphocytes and macrophages. Note necrosis due to the biomaterial on surface. (D) Photomicrography of specimen of the group MTA + BMP on day 15 showing the fibrous band with small areas of necrosis and remnant of the biomaterial (seen on top right), followed by the bone defect filled by newly formed bone in the form of interconnecting that displays osteocytes nonaligned. There were signs of reabsorption. (E) Photomicrography of a specimen of group MTA + BMP + GBR on day 15 showing the bone defect partially filled with bone spicules and trabeculi extending from one cortical side, and the other whose surface displays necrosis, cartilage remnants, and osteocytes nonaligned are also observed. (F) Photomicrography of group NIR LPT on day 15 showing the bone defect filled by interconnecting and newly formed bone with nonaligned osteocytes and discrete basophilic reversal lines, amidst medullar tissue. (G) Photomicrography MTA + NIR LPT on day 15 showing a fibrous band with remnants of the biomaterial and necrosis followed by irregular trabeculi displaying nonaligned osteocytes and some medullar tissue. (H) Photomicrography of a specimen of group MTA + NIR LPT on day 21 showing newly formed bone displaying numerous osteocytes and active multinucleated giant cells amidst fibrous tissue with chronic inflammation. (I) Photomicrography of a specimen of group MTA + GBR + NIR LPT on day 15 showing the bone defect filled by interconnecting and newly formed bone and displaying nonaligned osteocytes. No signs of reabsorption were seen, and inferior part showed extensive irregular bone close to medullar tissue. (J) Photomicrography of a specimen of group MTA + BMP + NIR LPT on day 15 showing the bone defect displaying small bone spicules and areas of necrosis. (K) Photomicrography of a specimen of group MTA + BMP + NIR LPT on day 15 showing the bone defect filled by interconnecting trabeculi displaying active osteoblasts, osteocytes nonaligned, and reversal basophilic lines amidst inflamed tissue. Note that neoformation progressed of bone cortical as seen on the bottom. (L) Photomicrography of a specimen of group MTA + GBR + BMP + NIR LPT on day 21 showing a fibrous band with remnants of the biomaterial and necrosis followed by extensive displaying osteocytes nonaligned and some medullar tissue.

and active osteoblasts at the periphery of bone trabeculi. At the surface, a band of fibrous connective tissue and small areas of necrosis could be seen as well as both remnants of the biomaterial and osteodasts [Fig. 1(D)]. On day 21, the newly formed bone was thick and irregular and showed irregular osteocytes and few medullar spaces. In a few cases, a band of fibrous connective tissue and remnants of the biomaterial covered the surface of the bone defect. These remnants were associated to foreign body reaction, and there were signs of bone reabsorption. At the end of the experimental period, necrotic debris was seen at the surface as well as macrophages and bony fragments were seen extending down to the center of the bone defect. The core of the bone defect showed irregular bone trabeculi and

the presence of osteocytes. Discrete chronic inflammation was seen during all experimental period.

MTA + BMP + GBR

On day 15, there was surface necrosis extending down to the core of the bone defect. Irregular bone fragments and few remnants of the biomaterial were seen associated to macrophages. In many cases, an area of necrosis was observed and, beneath it, a band of fibrous tissue was seen. Large number of bony fragments associated to basophilic reversal lines as well as a large amount of remnants of cartilage was noticed [Fig. 1(E)]. Irregular osteoid tissue was also seen at this stage. On day 21, the bone defect was filled by newly formed tissue showing either regular or irregular

deposition. Irregular osteocytes, basophilic reversal lines, and few medullary spaces were also seen. At the surface, besides the presence of remnants of the biomaterial, a band of fibrotic tissue was also seen as well as evidence of bone reabsorption, and moderate chronic inflammation. At the end of the experimental time, the bone defect was partially or completely filled by newly formed bone displaying nonaligned osteocytes and few medullary spaces. In some cases, at the surface, a band of fibrous tissue and remnants of the biomaterial were seen. No inflammation was observed at this stage.

NIR LPT

On day 15, the bone defect was partially filled by newly formed bone. Interconnecting delicate bone trabeculi, nonaligned osteocytes, and basophilic reversal lines were seen at this time. In some specimens, osteoblasts and remnants of cartilage were seen at the surface [Fig. 1(F)]. The newly formed bone was dispersed on medullar tissue and no signs of reabsorption could be seen. On day 21, the newly formed bone was regularly distributed and showed no signs of reabsorption. At the end of the experimental period, the bone defect was mostly filled by newly formed bone that was either regular or irregularly distributed and showed few medullar spaces. No signs of reabsorption were seen.

MTA + NIR LPT

On day 15, surface necrosis was observed as well as the presence of an irregularly distributed, either thin or thick newly formed interconnecting bone trabeculi, with nonaligned osteocytes and basophilic reversal lines [Fig. 1(G)]. The presence of remnants of the biomaterial was also seen at the surface. There was evidence of sites of reabsorption of the bone. On day 21, the bone filling the bone defect was either thick or thin and also showed nonaligned osteocytes, basophilic reversal lines, and few medullary spaces. No evidence of reabsorption was seen at this stage [Fig. 1(H)]. At the end of the experimental period, the bone defect was filled by newly formed bone and focal area displaying reabsorption was seen. Chronic inflammation was seen during all experimental time.

MTA + GBR + NIR LPT

On day 15, the bone defect was either partially or completely filled by irregular bone trabeculi dispersed on

medullar tissue. The bone showed nonaligned osteocytes and active osteoblasts at the periphery of bone trabeculi [Fig. 1(I)]. In a few cases, bony fragments were observed. Foci of necrosis could also be seen at the surface at this stage. Remnants of the biomaterial were also seen in all cases as well as a band of fibrotic tissue. These remnants were sometimes observed incorporated to the newly formed bone and they assumed a crystalloid aspect. Despite the presence of some foci of necrosis close to the bony fragments, deeper region (within the bone defect) showed newly formed bone. No evidence of bone reabsorption could be seen at this stage, but chronic inflammation was seen. On day 21, the bone defect was mostly filled with interconnecting bone trabeculi, displaying nonaligned osteocytes and basophilic reversal lines as well as discrete chronic inflammation. No signs of necrosis or reabsorption could be seen at this stage. A delicate mesh of newly formed bone and medullary tissue filled the bone defect. In some cases, a band of connective tissue was also seen at surface. No inflammation was found at this time.

MTA + BMP + NIR LPT

On day 15, the bone defect was partially covered by necrotic tissue and showed foci of remnants of the biomaterial [Fig. 1(J)]. Beneath it, bony fragments dispersed within necrotic tissue were seen. In some cases, the newly formed bone was thick and showed osteocytes and few medullary spaces. The inferior margin of the bone defect showed a thin bone wall [Fig. 1(L)]. On day 21 thick newly formed bone, containing remnants of the biomaterial filled the bone defect. In some specimens, a band of fibrosis was present and usually it projected itself within the medulla. At the end of the experimental period, the bone defect was completely filled by a dense newly formed bone sometimes irregular, osteocytes, and basophilic reversal lines. Discrete chronic inflammation was seen during all times.

MTA + GBR + BMP + NIR LPT

On day 15, the bone defect was filled by newly formed bone that was distributed in an irregular manner and showed both osteocytes and remnants of the biomaterial within it. Some specimens showed osteoblasts at the surface and signs of bone reabsorption at this time. On day 21, the histological aspect varied: one specimen showed remnants of the biomaterial dispersed on granulation tissue, lamellar

TABLE III. Summary of the Histological Analysis

Criterion/Group	Bone Reabsorption	Bone Neoformation	Inflammatory Infiltrate	Collagen Deposition
Clot	Absent	Intense	Discrete (chronic)	Moderate
MTA	Absent	Moderate	Discrete (chronic)	Moderate
MTA + GBR	Discrete	Moderate	Discrete (chronic)	Moderate
MTA + BMP	Moderate	Moderate	Absent	Moderate
MTA + BMP + GBR	Discrete	Intense	Moderate (chronic)	Moderate
NIR LPT	Absent	Intense	Absent	Intense
MTA + NIR LPT	Discrete	Intense	Absent	Intense
MTA + GBR + NIR LPT	Absent	Intense	Moderate (chronic)	Intense
MTA + GBR + BMP + NIR LPT	Discrete	Intense	Discrete	Intense

bone, and remnants of cartilage [Fig. 1(M)]; one specimen showed newly formed bone and osteocytes. Others showed newly formed bone, of variable thickness projecting from the borders of the bone defect, displaying osteocytes, basophilic reversal lines, and remnants of the biomaterial. The bone defect was filled by newly formed bone containing osteocytes, basophilic reversal lines, and remnants of both cartilage and the biomaterial. Discrete chronic inflammation was seen throughout the experimental time. A summary of the results may be seen in Table III.

DISCUSSION

Natural processes of healing should be allowed to take their usual course, and any interference on them should be attempted only when there is a demonstrable need or substantial advantage for the patient. Bone healing has been under extensive investigation for many years.

The Wistar rat experimental model used in this study possesses advantages such as allowing a rapid healing period, animals easily lodged and fed, resistance to climatic variations, low cost, besides being routinely used in other experimental conditions involving bone reconstruction.⁴⁷

Critical size defects (CSDs) do not repair well because it exceeds the body's ability to regenerate adequate amounts of bone fast enough. This lesion is defined as a defect that heals by less than 10% bony regeneration during the lifetime of the individual. The CSDs in the long bones of rats have not been as well studied as those in the calvaria. However, the creation of a CSD may still be used if long bones are needed to test.⁴⁸

The CSD, as an experimental model, was originally developed as a model of fibrous nonunion and was intended to standardize the testing of bone repair materials that could be used as alternatives to bone allografting or autografting, and was originally defined as "the smallest size intraosseous defect in a particular bone and species of animal that will not heal spontaneously during the lifetime of the animal" by Schmitz and Hollinger in 1986. The critical size tibia defect in rats was then defined as 1-mm round defect and, by definition, it is supposed to be unable to heal spontaneously.⁴⁹

In the present study, we opted to use a larger bone defect than a critical size one intending to increase the severity of the damage to the bone. It is important to note that similar model has been in use by our group for more than a decade, and its effectiveness well reported elsewhere in the literature.^{8,11-33,35,40-42,44,47} The development of non-unions occurs only in fractures. It is characterized by the deposition of fibrous tissue instead of bone. Despite bone formation may occur eventually, the restoration of the morphology and function are impaired. On the present study, we were unable to find any such phenomena as we created a partial thickness surgical defect and not a fracture.

Over the past years, our group has been working extensively on the study of the effects of the use of NIR LPT on bone using different animal models. In these studies, we have also used many assessment methods to determine the effects of the NIR LPT on bone including the use of

histology,^{33-37,40,42-44} computerized morphometry,⁴⁶ SEM,^{39,45} and Raman spectroscopy.^{30,39,41,47}

In all previously used protocols, models and parameters, we were able to demonstrate that NIR LPT caused important tissue responses during healing and these were responsible for a quicker repair process as well as on the improved quality of the newly formed bone.^{8,33-47}

We have found that the advanced bone maturation, as observed in irradiated subjects, shall be due to an increased deposition of CHA.^{30,39,41,47} The maturation represents the improved ability of more mature osteoblasts to secrete CHA in irradiated subjects. Deposition of CHA represents bone maturation, and increased amount of CHA on the bone is indicative of a more resistant and calcified bone.^{8,33-39,42-44,47}

It is known that LPT, at specific wavelengths, has the capability to stimulate cell proliferation, including fibroblasts, which are major secretors of collagen, an important organic component present during bone repair.⁸ It is important to consider that the presence of fibroblasts and increased secretion of collagen found in the present study mean that there was a ongoing bone repair and not the development of fibrous nonunion.

It is known that LPT stimulates cell proliferation, including fibroblasts; this cell has the capacity to secrete collagen. In the bone matrix, hydroxyapatite crystals have been observed, and they will grow in clusters, which later coalesce to completely calcify the matrix, filling the spaces between and within the collagen fibers. It is known that, during the many stages in bone healing, several cytokines and growth factors regulate matrix production. Various factors such as BMPs, TGF β and PDGF have been successfully used to augment healing in experimental models. LPT also has positive effects on the release of several such mediators.³³⁻⁴⁶

MTA is a white or gray powder containing calcium oxide 65%, calcium silicate 21%, ferric oxide 5%, calcium aluminate 4%, calcium sulfates 2.5%, magnesium oxide 2%, sodium, and potassium oxide 0.5%. Its pH (12.5), both biologically and histologically, makes it similar to calcium hydroxide. Hydration of the powder results in a colloidal gel that solidifies to a hard structure. Unlike other cements, which demand a completely dry field, MTA is indicated when moisture control is inadequate, without loss of its properties and it is not resorbable. MTA is less toxic and has a powerful bacteriostatic effect with lower marginal percolation. Because of its hydrophilic properties and setting in a moisture environment, perfect isolation is counter indicated. The setting time for the cement is nearly 4 h. Because of the slow setting time, the initial looseness of the MTA after mixing can make the material difficult to handle. In this study, the MTA was handled and inserted quickly into the bone defect. When the MTA mixture was dry, it became crumbly and unmanageable.⁴⁷

MTA is a powder aggregate containing mineral oxides. Besides its noncytotoxicity and good biological action, it stimulates tissue repair because of cellular adhesion, growth, and proliferation on its surface. MTA has been shown to result in the overgrowth of cementum and in

facilitating regeneration of the periodontal ligament and formation of bone.

As far as we are concerned this is the first histological report to describe, histologically, the mechanisms of the repair bone defects treated or not with laser light, MTA, BMPs, and GBR. The comparison of our results with other previous reports is difficult. This is the first report of the use of this model. Our previous experience using other types of biomaterials already reported in the literature is also suggestive that the association of NIR LPT with biomaterials causes improvement on the repair of bone defects.⁸

A previous report from our team evaluated the effect laser light associated to MTA on the alveolar bone repair process. We found that laser-irradiated sockets substantial formation of thick interwoven osteocyte-rich trabecular bone, with an evident osteoblastic rimming when compared to the use of MTA as well as to untreated controls showing that laser light was the most successful treatment to improve alveolar bone repair.⁴⁹

This study was designed to carry out a qualitative assessment of the repair process, as this is the first report of its kind and the description of the process considered an appropriated method of assessing the effects of different techniques used both isolated or in combination, allowing us to have a qualitative "picture" of the process.

The present study is the histological analysis of the study recently published by our team in which Raman spectroscopy was used as assessment method and showed results aligned with the histological findings of the present study.⁴⁷ This aspect is important, as the only use of histological findings could be considered inadequate by anyone and some authors suggested that this kind of data would be better utilized if correlated with other test such as radiological evaluation or with mechanical tests of the bone.⁵⁰⁻⁵²

In the Raman study we found that, laser-irradiated subjects, showed significant higher levels of CHA in the earlier period of healing. However, these levels were similar to the observed when the association of MTA + BMP + GBR + Laser was used. Lowest levels of deposition were observed when MTA + Laser and MTA + GBR were used. At the end of the experimental period, all defects were found to be similar. However, higher levels of CHA were seen in group MTA + GBR + Laser and lower in group MTA + Laser. As increased peaks of CHA are indicative of bone maturation, the association of MTA, GBR, and laser resulted in a more advanced repair.⁴⁷

We found differences among the groups during all experimental timing. It is important to keep in mind that the MTA probably acted as a local irritant even on being considered biocompatible. When the MTA was associated to GBR, no major morphological changes were seen. But, we observed crystalloid structures that may be attributable to the MTA as its anhydrous phases involve the formation of crystals, an important physiologic event in the formation of the bone.⁵³ Again, these changes might be attributed to the presence of the MTA. The addition of BMPs to the MTA did not improve the process significantly. When the MTA + BMP graft was associated to GBR, the major observed

change was of irregular osteoid tissue, whose appearance may be attributed to the GBR technique. The use of NIR LPT caused both early deposition of bone trabeculi and the cessation of the osteoclastic activity,⁵⁴ which plays a pivotal role on the remodeling of the bone.⁵⁵⁻⁵⁷ These lines were not seen on controls but were present on LPT and on MTA + BMP + GBR treated subjects. This may be indicative that the use alone of the LPT may cause similar results to the use of the association of conventional techniques alone.

Later on, untreated controls and MTA-grafted subjects showed similar healing pattern as seen at early stages. We also found remnants of cartilaginous tissue on the controls that may be indicative of evolution of the process. The MTA seemed to cause a small delay in the repair process. The use of the GBR caused the presence of thick newly formed bone. Increased thickness might have been caused by the GBR technique. Adding BMPs to the biomaterial also caused the appearance of thick and irregular newly formed bone. However, despite remnants of the graft causing foreign body reaction there was no bone resorption. The use of the BMPs might have caused more bone deposition during the repair due to its properties.

The use of the GBR to the association of MTA and BMPs caused no major improvement on the repair. The use of the LPT caused the deposition of a regularly distributed newly formed bone. On the other hand, MTA grafts irradiated caused irregular deposition of bone. The association of the LPT with GBR did not improve the repair significantly. The LPT associated to the MTA, BMPs, and GBR caused variable responses including the presence of newly formed bone, of variable thickness, projecting from the borders of the bone defect. This was not seen on other groups.

At the end of the experimental period, the controls showed the bone defect completely filled by lamellar trabecular bone and few Haversian systems. The use of GBR or not on MTA-grafted subjects caused a deposition of a less dense bone. The addition of BMPs caused the appearance necrotic debris and macrophages. The use of MTA, BMPs, and GBR caused the presence of newly formed bone either partially or completely filling the bone defects. LPT-treated subjects showed the bone defect mostly filled regular or irregular bone. The use of MTA caused the appearance of newly formed bone of varied thickness. Using NIR LPT on grafts subjected to GBR did not affect the overall repair much. NIR LPT associated to MTA and BMPs caused the complete filling of the bone defect by a dense newly formed bone. The laser light associated to MTA, BMPs, and GBR also resulted in the deposition of newly formed bone and remnants of cartilage. It is possible that the chondrogenic differentiation occurred due to mesenchymal stem cells present in the bone marrow, and represents the presence of progenitor cells capable of differentiating into osteoblasts. Thus, these cartilage remnants could play a key role as scaffold in the bone repair.

One may question that it is expected inflammatory response to develop against bone repair materials (i.e., scaffold) as these materials, no matter how biocompatible they are, they are foreign materials. In the present study we

found more inflammatory response in clot group, in which there is no scaffold applied at all, than the ones in MTA + BMP, NIR LPT, and MTA + NIR LPT groups. This may be explained by previous investigations that have indicated that, the persistence of the inflammatory response in the later phases of alveolar bone repair might be a result of a phlogistic activity of residual blood clots.^{49,50}

In terms of bone neoformation, we found more bone formation in clot group than on the ones in MTA (in which there is osteoconductive scaffold), MTA + GBR (in which there is osteoconductive scaffold and GBR was induced), and MTA + BMP (in which there is osteoconductive scaffold and osteoinductive cytokine). Despite the presence of MTA to be expected to facilitate the process of bone deposition, due to its biochemical properties, such as alkalinity and high content of calcium phosphate, calcium oxide and silica, which are important inorganic constituents widely required for bone mineralization, this material probably, due to some phlogistic activity promoted by its handling during the filling of the defect, delayed the process. It may be speculated that MTA handling within the alveolar wound caused a disarrangement of part of the blood clot and altered the bone regeneration process.⁴⁹

We were not able to find in the literature any previous reports on the association of MTA with BMPs. Despite we have shown that the use of BMPs may improve the outcome of bone healing when associated with LPT, in the present study it was not the case. This was probably due to the properties of the MTA.

It has also been demonstrated by our group that, the use of GBR, is helpful in the healing of bone defects and that the association with LPT improves the outcome of this therapeutic approach as demonstrated previously by our using different models.³³⁻⁴⁷

The results of our study indicate that irradiated bone showed increased osteoblastic proliferation, collagen deposition, and bone neoformation when compared to nonirradiated one. The results of our studies and others indicate that bone irradiated mostly with IR wavelengths shows increased osteoblastic proliferation, collagen deposition, and bone neoformation when compared to nonirradiated bone. The effects observed in irradiated subjects might be a result of positive effects of laser irradiation on the cell membrane and mitochondria. Laser light influences the production of ATP and it is more effective at when used at early stages and depends on the physiologic status of the cell.³³⁻⁴⁷

Vascularization is also an important and decisive factor for the healing of wounds and it is improved after the use of laser light as well as increased release of mediators such as PGE₂ that is also increased after irradiation. There is evidence that PGE₂ is also produced by osteoblasts and that its effects may be therapeutic or adverse.³³⁻⁴⁶

It is known that laser light stimulates cell proliferation, including fibroblasts; this cell has the capacity to secrete collagen. In the bone matrix, hydroxyapatite crystals have been observed, and they will grow in clusters, which later coalesce to completely calcify the matrix, filling the spaces between and within the collagen fibers. It is known that,

during the many stages in bone healing, several cytokines and growth factors regulate matrix production.³³⁻⁴⁶

Various factors such as BMPs, transforming growth factor- β , and platelet-derived growth factor have been successfully used to augment healing in experimental models. Laser light also has positive effects on the release of several such mediators.³³⁻⁴⁶

A parameter able to produce any photo biological response alone does not exist. The photoreponse depends on the conjugation of different parameters. It still remains uncertain if bone stimulation by laser light is a general effect or if the isolate stimulation of osteoblasts is possible. It is possible that laser's effect on bone regeneration depends not only on the total dose of irradiation, but also on the irradiation time and the irradiation mode. Most importantly, the threshold parameter energy density and intensity are biologically independent of one another. This independence accounts for the success and the failure of the treatment.³³⁻⁴⁶

One may question the advantage of using an *in vitro* experiment where the direct influence of LPT on osteoblasts and the MTA-scaffold could be analyzed. In the present study, we opted for using an *in vivo* model and not an *in vitro* one as the animal model allowed us a more detailed and "dose" to human tissue response analysis of the different treatments carried out as well as the host-responses to them. The host-response on *in vitro* model is very limited or not possible of simulation in many aspects. For instance, despite recent study⁵⁹ have found *in vivo* adhesion of osteoblasts to MTA, an *in vitro* report⁶⁰ using osteoblasts failed to get cell adhesion to MTA. In the present study, we often observed a close contact of the graft with the bone matrix and possibly inducing the formation of important components for bone neoformation as a result of the interaction of the MTA, the matrix, and the host.^{61,62} Then, biological responses may be similarly detected using different assessment methods.

CONCLUSION

The results showed different tissue response on all groups during the experimental time. Major changes were seen in irradiated subjects and included marked deposition of new bone seen in advanced maturation. It is concluded that NIR LPT improved the results of the use of the MTA on bone defects.

REFERENCES

- Pastori CM, Zorzatto DLG, Toledo Filho JL, Marola C. Implantes de bioapatita + osseobond® + membrana reabsorvível dentoflex + aglutinante dentoflex. [Implants of bioapatite + osseobond® + dentoflex reabsorbable membrane + dentoflex link agent: Surgical cases report]. Rev Bras Ciênc Estomatol 1996;151-63.
- Reddi AH. Initiation of fracture repair by bone morphogenetic proteins. Clin Orthop Relat 1998;355(Suppl):S66-S72.
- Park YJ. Enhanced guided bone regeneration by controlled tetracycline release from poly(L-lactide) barrier membranes. J Biomed Mater Res 2000;51:391-397.
- Segundo T. Avaliação dos Enxertos Ósseos e Homólogos Utilizados em Implantodontia. [Assessment of bone grafts and similar used in implantology]. RGO 2000;48:217-220.

5. Restrepo LL, Matzola C, Consolano A, Pereira AC, Toledo Filho JL, Andreato JC. Avaliação de implantes de osso bovino liofilizado "Osseobond"® e membrana reabsorvível de osso bovino liofilizado. [Assessment of lyophilized bovine bone "Osseobond"® and reabsorbable bovine bone membrane]. Available at <http://www.odontologia.com.br/artigos>. 02 March 2001.
6. Tago EM, Mulatinho J. Biomateriais para uso em Clínica Médico-Odontológica. [Biomaterials used on medical-dental clinics]. Available at <http://www.dentoflor.com.br>. 05 February 2001.
7. Nyman S, Lindhe J, Karring T, Rylander H. New attachment following surgical treatment of human periodontal disease. *J Clin Periodontol* 1982;9:290-296.
8. Pinheiro ALB, Gerbi MEMM. Photoengineering of bone repair processes. *Photomed Laser Surg* 2006;24:169-178.
9. Torabinejad M, Hong CU, Lee SJ, Monsef M, Pitt Ford TR. Investigation of mineral trioxide aggregate for root end filling in dogs. *J Endod* 1995;21:603-608.
10. Torabinejad M, Hong CU, Pitt Ford TR. Physical properties of a new root end filling material. *J Endod* 1995;21:349-353.
11. Torabinejad M, Hong CU, Pitt Ford TR, Kariyawasam SP. Tissue reaction to implanted super-EBA and mineral trioxide aggregate in the mandible of guinea pigs: A preliminary report. *J Endod* 1995;21:569-571.
12. Torabinejad M, Hong CU, Pitt Ford TR, Kettering JD. Cytotoxicity of four root end filling materials. *J Endod* 1995;21:489-492.
13. Torabinejad M, Pitt Ford TR, Abadi HR, Kariyawasam SP, Tang HM. Tissue reaction to implanted root-end filling materials in the tibia and mandible of guinea pigs. *J Endod* 1998;24:468-471.
14. Torabinejad M, Chivian N. Clinical applications of mineral trioxide aggregate. *J Endod* 1999;25:197-205.
15. Schwartz RS, Mauger M, Clement DJ, Walker WAM. Mineral trioxide aggregate: A new material for endodontics. *J Am Dent Assoc* 1999;130:967-975.
16. Zhu Q, Haglund R, Safavi KE, Spangberg LSW. Adhesion of human osteoblasts on root-end filling materials. *J Endod* 2000;26:404-406.
17. Regan JD, Gutmann JL, Witherspoon DE. Comparison of Diaket and MTA when used as root-end filling materials to support regeneration of the periodontal tissues. *Int Endod J* 2002;35:840-847.
18. Economides N, Pantelidou O, Kokkas A, Tziatas D. Short-term periodontal tissue response to mineral trioxide aggregate (MTA) as root-end filling material. *Int Endod J* 2003;30:44-48.
19. Al-Rabiah F, Parinpanayagam H, MacFarland D. Human alveolar bone cells interact with ProRoot and tooth-colored MTA. *J Endod* 2006;32:872-875.
20. Oviir T, Pagonis Ibarra G, Geurtsen W. Effects of gray and white mineral trioxide aggregate on the proliferation of oral keratinocytes and cementoblasts. *J Endod* 2006;32:210-213.
21. Holland R, de Souza V, Nery MJ, Otoboni Filho A, Barnabé PFE, Dзан E Jr. Reaction of dog's teeth to root canal filling with mineral trioxide aggregate or a glass ionomer sealer. *J Endod* 1999;25:728-730.
22. Moreton TR, Brown CE Jr, Legan JJ, Kafrawy AH. Tissue reactions after subcutaneous and intrasosseous implantation of mineral trioxide aggregate and ethoxybenzoic acid cement. *J Biomed Mater Res* 2000;52:528-533.
23. Bystrom A, Claesson R, Sundqvist G. The antibacterial effect of camphorated p-aminobenzoic acid, camphorated phenol and calcium hydroxide in the treatment of infected root canals. *Endod Dent Traumatol* 1995;1:170-175.
24. Mitchell PJ, Pitt Ford TR, Torabinejad M, McDonald F. Osteoblast biocompatibility of mineral trioxide aggregate. *Biomaterials* 1999;20:167-173.
25. Tronstad L, Andreasen JO, Hasselgren G, Kristerson L, Riis L. pH changes in dental tissues after root canal filling with calcium hydroxide. *J Endod* 1987;13:17-21.
26. De Moor RJ, DeWitte AM. Periapical lesions accidentally filled with calcium hydroxide. *Int Endod J* 2002;35:946-958.
27. De Rossi A, Silva LA, Leonardo MR, Rocha LB, Rossi MA. Effect of rotary or manual instrumentation, with or without a calcium hydroxide/1% chlorhexidine intracanal dressing, on the healing of experimentally induced chronic periapical lesions. *Oral Surg Oral Med Oral Pathol Oral Radiol Endod* 2005;99:628-636.
28. Tronstad L. Root resorption-etiology, terminology and clinical manifestations. *Endod Dent Traumatol* 1988;4:241-252.
29. Gottlow J, Nyman S, Karring T, Lindhe J. New attachment formation as the result of controlled tissue regeneration. *J Clin Periodontol* 1984;11:494-503.
30. Garrett S. Periodontal regeneration around natural teeth. *Ann Periodontol* 1996;1:621-666.
31. Stahl SS, Froum S, Tamow D. Human histologic responses to guided tissue regenerative techniques in intrabony lesions. Case reports on 9 sites. *J Clin Periodontol* 1990;17:191-198.
32. Cortellini P, Clauser C, Prato GP. Histologic assessment of new attachment following the treatment of a human buccal recession by means of a guided tissue regeneration procedure. *J Periodontol* 1993;64:387-391.
33. Pinheiro ALB, Gerbi MEMM, Lima FA Jr, Ponzi EAC, Marques AMC, Carvalho CM, Santos RC, Oliveira PC, Noll M, Ramalho LMP. Bone repair following bone grafting hydroxyapatite guided bone regeneration and infrared laser photobiomodulation: A histological study in a rodent model. *Lasers Med Sci* 2009;24:234-240.
34. Gerbi MEMM, Ponzi EAC, Ramalho LMP, Marques AMC, Carvalho CM, Oliveira RC, Oliveira PC, Noll M, Pinheiro ALB. Infrared laser light further improves bone healing when associated with bone morphogenetic proteins: An in vivo study in a rodent model. *Photomed Laser Surg* 2008;26:55-60.
35. Pinheiro ALB, Gerbi MEMM, Ponzi EAC, Ramalho LMP, Marques AMC, Carvalho CM, Oliveira RC, Oliveira PC, Noll M. Infrared laser light further improves bone healing when associated with bone morphogenetic proteins and guided bone regeneration: An in vivo study in a rodent model. *Photomed Laser Surg* 2008;26:167-174.
36. Torres CS, Santos JN, Monteiro JSC, Amorim PG, Pinheiro ALB. Does the use of laser photobiomodulation, bone morphogenetic proteins, and guided bone regeneration improve the outcome of autologous bone grafts? An in vivo study in a rodent model. *Photomed Laser Surg* 2008;26:371-377.
37. Gerbi MEMM, Pinheiro ALB, Ramalho LMP. Effect of IR laser photobiomodulation on the repair of bone defects grafted with organic bovine bone. *Lasers Med Sci* 2008;23:313-317.
38. Lopes CB, Pacheco MT, Silveira L Jr, Duarte J, Cangussu MC, Pinheiro ALB. The effect of the association of NIR laser therapy BMPs, and guided bone regeneration on tibial fractures treated with wire osteosynthesis: Raman spectroscopy study. *J Photochem Photobiol B* 2007;89:125-130.
39. Lopes CB, Pinheiro ALB, Sathiah S, Da Silva NS, Salgado MA. Infrared laser photobiomodulation (830 nm) on bone tissue around dental implants: A Raman spectroscopy and scanning electronic microscopy study in rabbits. *Photomed Laser Surg* 2007;25:96-101.
40. Weber JBB, Pinheiro ALB, Oliveira MG, Oliveira FAM, Ramalho LMP. Laser therapy improves healing of bone defects submitted to autogenous bone graft. *Photomed Laser Surg* 2006;24:38-44.
41. Lopes CB, Pinheiro ALB, Sathiah S, Duarte J, Martins MC. Infrared laser light reduces loading time of dental implants: A Raman spectroscopy study. *Photomed Laser Surg* 2005;23:27-31.
42. Gerbi MEMM, Pinheiro ALB, Matzola C, Lima Junior FA, Ramalho LMP, Ponzi EAC, Soares AO, Carvalho LC, Lima HV, Gonçalves TO. Assessment of bone repair associated with the use of organic bovine bone and membrane irradiated at 830 nm. *Photomed Laser Surg* 2005;23:382-388.
43. Pinheiro ALB, Lima Junior FA, Gerbi MEMM. Effect of low level laser therapy on the repair of bone defects grafted with inorganic bovine bone. *Braz Dent J* 2003;14:177-181.
44. Pinheiro ALB, Lima Junior FA, Gerbi MEMM, Ramalho LMP, Matzola C, Ponzi EAC, Carvalho LCB, Lima HCAV, Gonçalves TO, Soares AO. Effect of 830-nm laser light on the repair of bone defects grafted with inorganic bovine bone and decalcified cortical osseous membrane. *J Clin Laser Med Surg* 2003;21:383-388.
45. Pinheiro ALB, Oliveira MAM, Martins PPM. Biomodulação da cicatrização óssea pós-implantar com o uso da laserterapia não-cirúrgica: Estudo por microscopia eletrônica de varredura. [Biomodulation of Peri-implant bone repair with lasertherapy SEM study]. *Rev FOUFA* 2001;22:12-19.

46. Silva N Jr, Pinheiro ALB, Oliveira MGA, Weissmann R, Ramalho LMP, Nicolau RA. Computerized morphometric assessment of the effect of low-level laser therapy on bone repair: An experimental animal study. *J Clin Laser Med Surg* 2002;20:83-88.
47. Pinheiro ALB, Adole GTS, Cangussu MCT, Pacheco MTT, Silveira L Jr. Effects of laser phototherapy on bone defects grafted with mineral trioxide aggregate, bone morphogenetic proteins, and guided bone regeneration: A Raman spectroscopic study. *J Biomed Mater Res A* 2010;95:1041-1047.
48. Mooney MP, Siegel ML. Animal models for bone tissue engineering of critical-sized defects (CSDs), bone pathologies, and orthopedic disease states. In: Hollinger JO, Einhorn TA, Doll BA, Sfeir C, editors. *Bone Tissue Engineering*. Boca Raton, FL: CRC Press;2005. p217-244.
49. Oliveira EA, Oliveira VGM, Pires JA, Barreto ALS, Ribeiro MAG, Pinheiro ALP, Marques AMC, Melo CM, Albuquerque Júnior RLC. Effect of low-level laser therapy and mineral trioxide aggregate on alveolar bone repair. *Braz J Oral Sci* 2008;27:1657-1661.
50. Liebschner MA. Biomechanical considerations of animal models used in tissue engineering of bone. *Biomaterials* 2004;25:1697-1714.
51. Ebina H, Hatakeyama J, Onodera M, Honma T, Kamakura S, Shimauchi H, Sasano Y. Micro-CT analysis of alveolar bone healing using a rat experimental model of critical-size defects. *Oral Dis* 2009;15:273-280.
52. Young S, Kettow JD, Nguyen C, Bashous AG, Baggett LS, Jansen JA, Wong M, Mikos AG. Microcomputed tomography characterization of neovascularization in bone tissue engineering applications. *Tissue Eng Part B Rev* 2008;14:295-306.
53. Lee YL, Lee BS, Lin FH, Lin AY, Lin WH, Lin CP. Effects of physiological environments on the hydration behavior of mineral trioxide aggregate. *Biomaterials* 2004;25:787-793.
54. Romano PR, Caton JG, Puzas JE. The reversal line may be a key modulator of osteoblast function: Observations from an alveolar bone wound-healing model. *J Periodontol Res* 1997;32:143-147.
55. Palumbo C, Ferrati M, Ardizzone A. Osteocyte-osteoclast morphological relationships and the putative role of osteocytes in bone remodeling. *J Musculoskelet Neuronal Interact* 2001;1:327-332.
56. Domon T, Suzuki R, Takata K, Yamazaki Y, Takahashi S, Yamamoto, Wakita M. The nature and function of mononuclear cells on the resorbed surfaces of bone in the reversal phase during remodeling. *Ann Anat* 2001;83:103-110.
57. Matsuda C, Takagi M, Hattori T, Wakitani S, Yoshida T. Differentiation of human bone marrow mesenchymal stem cells to chondrocytes for construction of three-dimensional cartilage tissue. *Cytotechnology* 2005;47:11-17.
58. Coneglian PZA. Avaliação do processo evolutivo do reparo ósseo frente ao sulfato de cálcio e à hidroxiapatita. Estudo microscópico em alvéolos dentários de ratos. [Assessment of the bone repair following the use of calcium sulphate or hydroxyapatite. Light microscopic study on dental sockets of rats]. MSc Dissertation. Bauri (SP), School of Dentistry of Bauri, São Paulo University; 2007. 254 p.
59. Pefranayagam H. Cellular response to mineral trioxide aggregate root-end filling materials. *J Can Dent Assoc* 2009;75:369-372.
60. Perez AI, Spears R, Gutman JL, Opperman LA. Osteoblasts and MG-63 osteosarcoma cells behave differently when in contact with ProRoot MTA and White MTA. *Int Endod J* 2000;36:564-570.
61. Camilleri J, Pitt Ford TR. Mineral trioxide aggregate: A review of the constituents and biological properties of the material. *Int Endod J* 2006;39:747-754.
62. Saldon J, He J, Zhu Q, Safavi K, Spangberg LSW. Cell and tissue reactions to mineral trioxide aggregate and Portland cement. *Oral Surg Oral Med Oral Pathol Oral Radiol Endod* 2003;95:483-489.

AIP Conference Proceedings, Vol. 1364 Issue 1, p60

Bone Repair on Fractures Treated with Osteosynthesis, ir Laser, Bone Graft and Guided Bone Regeneration: Histomorfometric Study

Bone Repair on Fractures Treated with Osteosynthesis, ir Laser, Bone Graft and Guided Bone Regeneration: Histomorfometric Study

Jouber Mateus dos Santos Aciole^a, Gilberth Tadeu dos Santos Aciole^a, Luiz Guilherme Pinheiro Soares^a, Artur Felipe Santos Barbosa^a, Jean Nunes Santos^{a,c,d}, Antonio Luiz Barbosa Pinheiro^{a,b,c}.

^a Center of Biophotonics, School of Dentistry, Federal University of Bahia, 62 Araujo Pinho Ave, Canela, Salvador, BA, Brazil, 40110-150.

^b Biomedical Engineering Center - Unicastelo, Parque Tecnológico de São José dos Campos Rod. Pres. Dutra, km 138 - distrito de Eugênio de Melo São José dos Campos, SP, Brazil, 12247-004

^c National Institute of Science and Technology of Optics and Photonics, 400 Trabalhador São-Carlense Ave, Centro, São Carlos, SP, Brazil, 13560-970

^d Surgical Pathology Laboratory, Federal University of Bahia, 62 Araujo Pinho Ave, Canela, Salvador, BA, Brazil, 40110-150

Abstract. The aim of this study was to evaluate, through the analysis of histomorfometric, the repair of complete tibial fracture in rabbits fixed with osteosynthesis, treated or not with infrared laser light ($\lambda 780\text{nm}$, 50mW, CW) associated or not to the use of hydroxyapatite and guided bone regeneration (GBR). Surgical fractures were created, under general anesthesia (Ketamina 0,4ml/Kg IP and Xilazina 0,2ml/Kg IP), on the dorsum of 15 *Oryctolagus* rabbits that were divided into 5 groups and maintained on individual cages, at day/night cycle, fed with solid laboratory pelleted diet and had water ad libidum. On groups II, III, IV and V the fracture was fixed with wire osteosynthesis. Animals of groups III and V were grafted with hydroxyapatite and GBR technique used. Animals of groups IV and V were irradiated at every other day during two weeks ($16\text{J}/\text{cm}^2$, $4 \times 4\text{J}/\text{cm}^2$). Observation time was that of 30 days. After animal death (overdose of general anesthetics) the specimens were routinely processed to wax and underwent histological analysis by light microscopy. The histomorfometric analysis showed an increased bone neoformation, increased collagen deposition, less reabsorption and inflammation when laser was associated to the HATCP. It is concluded that IR laser light was able to accelerate fracture healing and the association with HATCP and GBR resulted on increased deposition of CHA.

Keywords: Bone Repair, Laser Photobiomodulation
PACS: 42.62B

INTRODUCTION

The reconstruction of bone defects, fractures, dental socket healing and periodontal bone loss, are some examples of processes involved in bone remodeling. Therefore, it was implied the need for dentists to know and change in a positive way, the physiology of bone tissue in order to correct the maxillo-mandibular defects [1].

In the treatment of bone fractures, we use the stalls with steel wires (semi importance for achieving the stabilization of the bone endings, and thus promote bone repair process -rigid), being of fundamental

In order to improve bone healing, implants are used as bone substitutes which hydroxyapatite (CHA). This biomaterial is produced in various compositions and shapes. Can be used alone or in the bone cavity associated with a biological membrane (GBR) serving as a scaffold for bone regeneration in the implanted area, and also to supplement autologous bone or bone marrow aspirate by combining during surgery [5].

Laser therapy with or without bone grafts and biomaterials is currently being used in order to improve the quality of bone repair. The use of laser phototherapy on bone healing by means of photochemical and photobiological properties have been increasingly used in numerous studies, both In Vivo and In Vitro, aiming to provide a better postoperative care through faster repair [6,7].

Advances in Laserology - Selected papers of Laser Florence 2010
AIP Conf. Proc. 1364, 60-65 (2011); doi: 10.1063/1.3626913
© 2011 American Institute of Physics 978-0-7354-0922-4/530.00

The optimization of the benefits of the use of biomaterials and associated GBR photobiomodulation laser has been observed by many previous studies [8,9,10,11,12,13].

The aim of this study was to evaluate the effect of histomorphometrically photobiomodulation laser in bone repair of surgical fractures fixed with wire osteosynthesis (WO), treated or not with Biphasic Ceramic Bone Graft (GenPhos® BAUMER HATCP) and Guided Bone Regeneration (GenDerm® BAUMER) in the tibia of rabbits.

MATERIALS E METHODS

All animal procedures were in accordance with principles of laboratory animal care (NIH publication 85-23, 1985) and were authorized by the Animal Ethics Committee of the School of Dentistry of the Federal University of Bahia, Brazil (Protocol 019/06). Fifteen rabbits *Oryctolagus Cuniculus* weighing an average of 2Kg were kept on 12:12 h light/ dark cycle and were fed with standard pelted diet and had water *ad libidum*. The animals were randomly divided into 5 groups with 3 animals in each: control group (GI), SRIF (GII), WO + Bone graft (GIII), WO + Laser (GIV) and WO + Bone graft + Laser (GV). Control had no experimental manipulation.

The animals were injected intraperitoneally with the general anesthetic ketamine (Ketalar®, 50mg/ml 0,4 ml / kg Parke Davis Lab Ltda, Sao Paulo, Brazil) and xylazine hydrochloride 2% (Rompum® 20mg/ml 2ml/kg, Bayer Health Care Lab SA, São Paulo, Brazil).

An incision in the lateral tibia was performed and tissue divulsed, thus having access to the tibia. After exposure of bone tissue, a surgical fracture was made complete with the aid of a diamond disc carborundum (Moyco Union Broach, York, PA, USA), using distilled water in a disposable syringe for irrigation. The bone stumps were immediately fixed with steel wire 0.30 mm (Morelli®, Sorocaba, SP, Brazil). Groups III and V received biphasic ceramic bone graft (BAUMER GenPhos HATCP), with a grain size of 0.5 mm and membrane of bovine bone (BAUMER, Genderm®) at the fracture site. Groups IV and V underwent photobiomodulation Laser (Twin Flex® MM OPITCS, São Carlos, Brazil, 780nm, 50mW power, continuous emission, the manner in focus, $\phi 0.5\text{cm}^2$, $16\text{J}/\text{cm}^2$ ($4 \times 4\text{J}/\text{cm}^2$) during 14 days. After the procedure, all animals received a single dose, as antibiotic therapy, intramuscular injection of pentabiotic® (penicillin, streptomycin 20.000 UI 0,2ml/Kg IM Lab. Forte Dogde Animal Health Ltda, Campinas, SP, Brazil) and Banamine® (flunixin Meglumine 10mg/ml 0,1ml/kg IM, Intervet Shering-Plough Animal Health, Cruzeiro, SP, Brazil), the latter being a potent analgesic and antiinflammatory.

At 30 days post-surgery was performed the sacrifice of animals by an overdose of general anesthetics. Then the specimens were removed approximately 1 cm from the edges of the fracture and surgical steel wires were carefully removed. The surgical specimens were fixed in 10% formalin and after decalcified in nitric acid solution 10%. They were then routinely processed and embedded in paraffin and stained with hematoxylin and eosin Harris alcoholic (H/E) and Picrosirius, the latter being specific for better visualization of collagen fibers for histomorphometric analysis.

Criteria were used for semi quantitative observation of bone resorption, bone formation, inflammatory response and collagen deposition described in table 1.

TABLE 1. Criteria used for semi-quantitative histomorphometric analysis

Criteria	Discreet	Moderate	Intense
Bone resorption	Presense <25% remaning bone resorption and/or surgical bed	25-50% of remaning bone resorption and/or surgical bed	>50% of remaning bone resorption and/or surgical bed
Bone formation	<25% of newly formed bone similar to adjacent untreated	25-50% of newly formed bone similar to adjacent untreated	>50% of newly formed bone similar to adjacent untreated
Inflammatory infiltrate	<25% of lymphocytes and/or macrophages	25-50% of lymphocytes and/or macrophages	>50% of lymphocytes and/or macrophages
Collagen deposition	<25% of collagen deposition	25-50% of collagen deposition	>50% of collagen deposition

All values obtained were analyzed with the aid of Minitab® 15 (Inc., San Diego, CA, USA) using the Fisher exact test, with significance level of 95% (p <0.05).

RESULTS

Histomorphometric analysis of the groups showed a greater intensity of bone formation in group WO + Graft + Laser, where the groups that showed a lower activity were healing were WO, WO + Graft and WO + laser (Fig.1). Comparing the groups, however, showed no significant difference between groups.

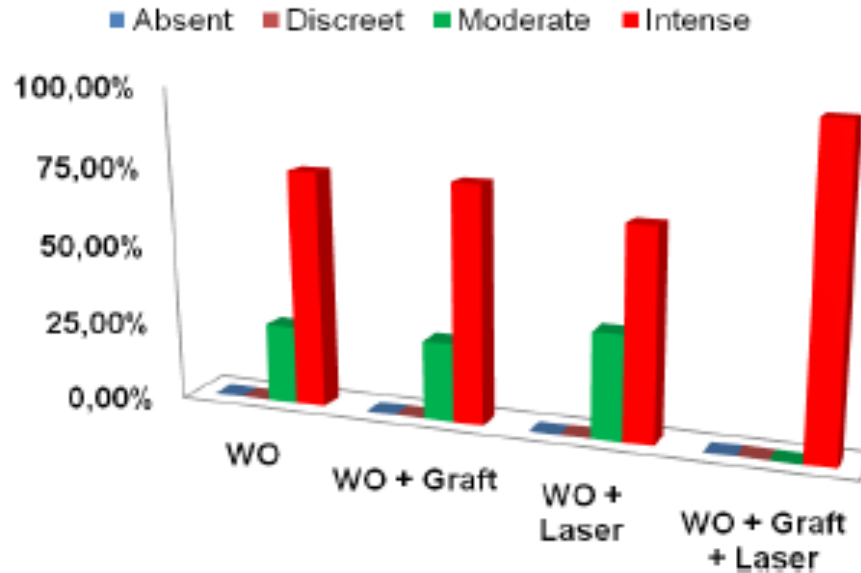


Figure 1. Results of histomorphometric examination showed the percentage of bone formation of experimental groups treated with WO.

Figure 2 show that the group WO + Graft + Laser showed a lower activity of bone resorption, unlike the group who obtained WO + Graft increased osteoclastic activity, but no significant difference between groups.

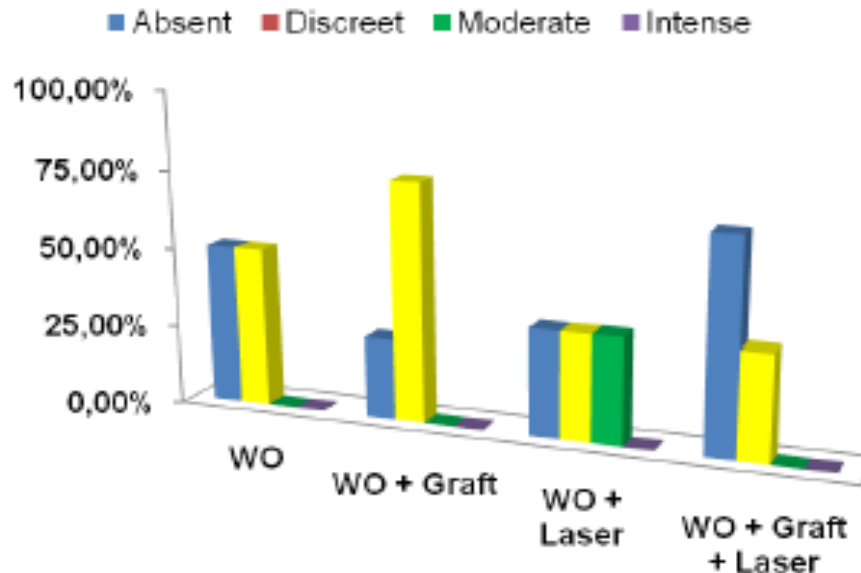


Figure 2. Results of histomorphometric examination showed the percentage of bone resorption in the groups treated with WO.

In relation to the inflammatory response, there was a greater intensity of chronic inflammatory infiltrate in group WO + Graft, unlike the groups WO + Graft + Laser and WO + Laser that had a less intense chronic inflammatory infiltrate, and in most cases absent (Fig. 3). The Fisher exact test showed significant difference between group WO + Graft + Laser and treated group WO + Graft ($p < 0.04$).

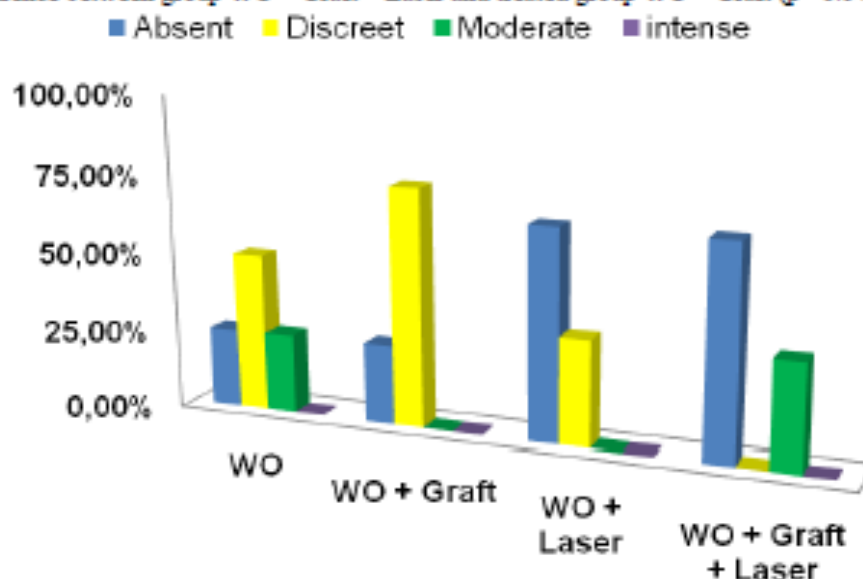


Figure 3. Results of histomorphometric examination showing the percentage of chronic inflammation in the groups treated with WO.

In relation to collagen deposition, there was a greater intensity in the group treated with WO + Graft + Laser and lower in the group WO (Fig.4). Statistical analysis (Fisher exact test) showed a significant difference in the group treated with WO + Graft + Laser and group treated WO ($p < 0.05$).

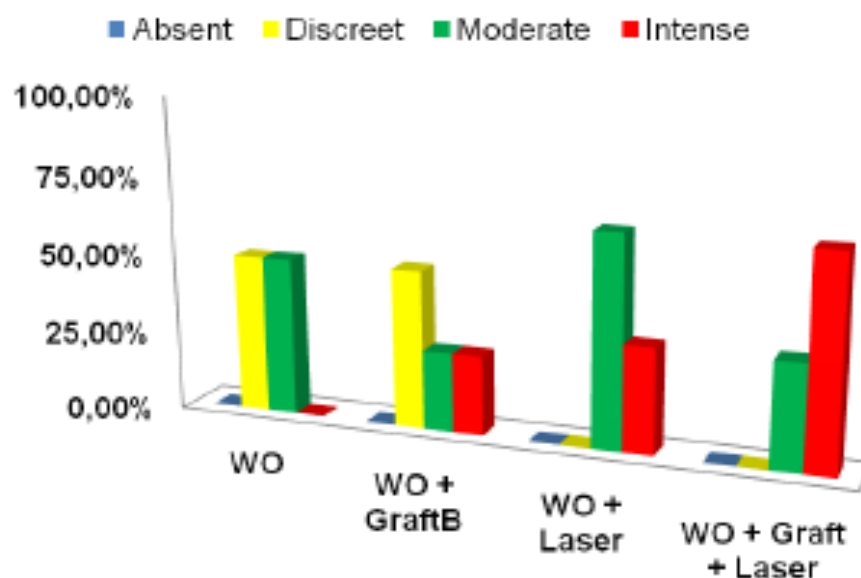


Figure 4. Results of histomorphometric examination showing the percentage of collagen deposition in the groups treated with WO.

DISCUSSION

The restorative treatment alternatives in the region maxillo-facial seek to address and better understand the mechanisms of wound healing and development of new techniques for reconstruction

using bone grafts. However, nowadays there is still a discussion about what kind of bone would be ideal for use as a graft and which type of technique best suited to get it [1].

For a better understanding of the results is required we may weave some comments: embryonic bone tissue is a highly mobile and fast formation, but relatively little is mineralized, with fibers oriented randomly and little resistance. It is then replaced by mature bone or lamellar, able to bear loads. Our results showed a significant increase in the deposition of collagen fibers, oriented in an orderly fashion when the bone is irradiated and therefore if the repair ends up with an arrangement of lamellar bone is more compact, with higher vascularization, achieving a standard of quality of bone tissue [14,15,16].

This study used osteosynthesis material: steel wire for fixation of bone fractures, for this fastening system is usually used in the treatment of bone fractures of the maxillofacial [17].

Numerous research have been conducted with the aim of finding means by which to achieve a faster bone repair. Several investigations have shown that the use of hydroxyapatite (CHA) serves as an osteoconductive agent in the repair of bone due to their osteogenic effect and its main function osteoconduction [9,10,11,13], corroborating with our results.

This study evaluated the effect of laser photobiomodulation using a laser GaAlAs (λ 780nm, 50mW, CW, $\Phi \sim 0.5$ cm, 4J/cm² by point 16J/cm² per session) in biomodulation bone after fracture of tibia rabbit, with or without the placement of implant and GBR HATCP by placing a biological membrane of demineralized bovine cortical. We used the laser diode infrared λ 780nm the property of greater tissue penetration in the subcutaneous tissues due to its low absorption in water or in the pigments of the skin (2-6 mm or more) [18,19].

Comparing the groups with respect to WO in histomorphometric analysis showed that the group treated with WO + Graft + Laser outperformed both the quality and the quantity of bone, as compared to other groups. These data corroborate the literature with regard to the quality of bone repair, because according to the authors photobiomodulation associated with the use of laser HATCP causes an increase in fibroblast proliferation and activity (collagen deposition) and osteoblasts, bone formation and decrease inflammation [11,15,16,20,21].

The results of this study suggest that laser photobiomodulation associated with the use of HATCP and membrane increased quantitatively and qualitatively the process of bone repair in the groups treated with WO.

CONCLUSION

The results of this study and based on the methodology used, we can conclude that photobiomodulation laser infrared associated with the use of HATCP and GBR was effective in improving and accelerating healing of bone fractures treated with WO, these results, obtained from the histomorphometric analysis showing an increased bone formation, reduced bone resorption, less inflammatory response and increased collagen deposition, in groups, which underwent laser photobiomodulation associated with the use of HATCP and GBR in those treated with WO.

REFERENCES

- 1- A. S. AJZEN, R. A. MOSCATIELLO, A. M. C. LIMA, et al, *Radiol. Braz.* **38**, (2005).
- 2- A. CHRITAH, S. K. LAZOW, J. R. BERGER, *Journal oral maxillofacial surg.* **63**, 1737-41 (2005).
- 3- C. ALFA, F. O'RYAN, S. ALESSANDRO, et al, *Journal of oral maxillofacial surgery*, **64**, 659-68, (2006).
- 4- Ö. ERDOĞAN, E. ESEN, Y. USTUN, et al, *American Association of Oral and Maxillofacial Surgeons*, **64**, 180-188, (2006).
- 5- L. LE GUEHENNEC, P. LAYROLLE, G. A. DACULSI, *European Cells And Materials*, **8**, 1-11, (2004).
- 6- A. L. B. PINHEIRO, F. A. LIMEIRA JUNIOR, M. E. M. M. GERBI, et al, *Journal of Clinical Laser Medicine and Surgery*, **21**, 383 - 388, (2003).
- 7- V. MORAES, et al, *Brazilian Dental Journal*, **15**, 87 (2004).
- 8- M. E. M. M. GERBI, A. L. B. PINHEIRO, C. MARZOLA, et al, *Photomedicine and Laser Surgery*, **23**, 382-388, (2005).
- 9- C. B. LOPES, A. L. B. PINHEIRO, S. SATHIAH, et. Al, *Photomedicine and Laser Surgery*, **23**, 27-31, (2005).
- 10- C. B. LOPES, M. T. PACHECO, L. SILVEIRA JUNIOR, et al. *J Photochem Photobiol B*, **89**, 125-130 (2007).

- 11- C. B. LOPES, A. L. B. PINHEIRO, S. SATHALAH, et al, *Photomedicine and Laser Surgery*, 25, 96-101, (2007).
- 12- M. E. M. M. GERBI, A. L. P. PINHEIRO, L. P. RAMALHO, *Lasers Medical Science*, 23, 313-317, (2008).
- 13- A. L. B. PINHEIRO, F. A. LIMEIRA JUNIOR, M. E. M. M. GERBI, et al, *Lasers in Medical Science*, 24, 234-240, (2009).
- 14- Y. A. OSAWA, N. A. SHIMIZU, G. A. KARYIA, et al, *Bone*, 22, 347-354, (1998).
- 15- F. A. LIMEIRA JUNIOR, A. L. B. PINHEIRO, M. E. M. M. GERBI, et al, *Brazilian Dental Journal*, 14, 177-181, (2003).
- 16- A. L. B. PINHEIRO, M. E. M. M. GERBI, *Photomedicine and Laser Surgery*, 24, 169-178, (2006).
- 17- L.F.H. LOPES, *Revista Odonto*, 16, 45-52, (2008).
- 18- J. R. BASFORD, *Lasers in Surg. and Med.*, 16, 331-342, (1995).
- 19- H. KOLÁROVÁ, D. DITRICHOVÁ, J. WAGNER, *Lasers Surg. Med.* 24, 231-235, (1999).
- 20- J. B. B. WEBER, A. L. B. PINHEIRO, M. G. OLIVEIRA, et al, *Photomedicine and Laser Surgery*, 24, 38-44, (2006).
- 21- C.S. TORRES, J. N. SANTOS, J. S. MONTEIRO, et al, *Photomedicine and Laser Surgery*. 6, 371-377, (2008).

Lasers Med Sci. 2012 Sep;27(5):903-16. doi: 10.1007/s10103-011-1010-2. Epub 2011 Oct 21.

Effects of LED phototherapy on bone defects grafted with MTA, bone morphogenetic proteins and guided bone regeneration: a Raman spectroscopic study

Effects of LED phototherapy on bone defects grafted with MTA, bone morphogenetic proteins and guided bone regeneration: a Raman spectroscopic study

Antonio L. B. Pinheiro · Luiz G. P. Soares · Maria Cristina T. Cangussú ·
Nicole R. S. Santos · Artur Felipe S. Barbosa · Landolfo Silveira Júnior

Received: 5 May 2011 / Accepted: 23 September 2011
© Springer-Verlag London Ltd 2011

Abstract We studied peaks of calcium hydroxyapatite (CHA) and protein and lipid CH groups in defects grafted with mineral trioxide aggregate (MTA) treated or not with LED irradiation, bone morphogenetic proteins and guided bone regeneration. A total of 90 rats were divided into ten groups each of which was subdivided into three subgroups (evaluated at 15, 21 and 30 days after surgery). Defects were irradiated with LED light (wavelength 850 ± 10 nm) at 48-h intervals for 15 days. Raman readings were taken at the surface of the defects. There were no statistically significant differences in the CHA peaks among the nonirradiated defects at any of the experimental time-points. On the other hand, there were significant differences between the defects filled with blood clot and the irradiated defects at all time-points ($p < 0.001$, $p = 0.02$, $p < 0.001$).

There were significant differences between the mean peak CHA in nonirradiated defects at all the experimental time-points ($p < 0.01$). The mean peak of the defects filled with blood clot was significantly different from that of the defects filled with MTA ($p < 0.001$). There were significant differences between the defects filled with blood clot and the irradiated defects ($p < 0.001$). The results of this study using Raman spectral analysis indicate that infrared LED light irradiation improves the deposition of CHA in healing bone grafted or not with MTA.

Keywords Biomaterial · Bone repair · Light emitting diode · MTA

A. L. B. Pinheiro (✉) · L. G. P. Soares · N. R. S. Santos ·
A. F. S. Barbosa
Center of Biophotonics, School of Dentistry,
Federal University of Bahia,
Av. Araújo Pinho, 62, Canela,
Salvador, BA CEP 40110-150, Brazil
e-mail: albp@ufba.br

A. L. B. Pinheiro · L. S. Júnior
Universidade Camilo Castelo Branco Núcleo do Parque
Tecnológico de São José dos Campos,
São José dos Campos, SP, Brazil

A. L. B. Pinheiro
Instituto Nacional de Ciência e Tecnologia de Óptica e Fotonica,
São Carlos, SP, Brazil

M. C. T. Cangussú
Oral Epidemiology and Public Health, School of Dentistry,
Federal University of Bahia,
Av. Araújo Pinho, 62, Canela,
Salvador, BA, Brazil

Introduction

It has been shown in various in vitro and in vivo models that near-infrared light irradiation stimulates the photo-acceptor cytochrome *c* oxidase, resulting in increased energy metabolism and production, stimulation of mitochondrial oxidative metabolism, and acceleration of tissue repair [1]. Bone is a complex, highly organized, very dynamic, specialized connective tissue, hard, rigid and strong. Microscopically it shows few metabolically active cells, hematopoietic elements of bone marrow and a large amount of intercellular substance formed from collagen fibers and stiffening substances [2]. It is composed of organic and inorganic elements [2, 3]. The latter consist primarily of calcium phosphate and calcium carbonate, with small quantities of magnesium, fluorine, and sodium. The mineral crystals form hydroxyapatite, which precipitates in an orderly arrangement around the collagen fibers of the osteoid. This latter is the nonmineralized organic matrix

secreted by osteoblasts and is composed of 90% type I collagen and 10% ground substance. The mineralization of osteoid by inorganic mineral salts gives bone its strength and rigidity. Its initial calcification normally occurs within a few days of its secretion but is completed over several months [3, 4].

The choice of bone graft is affected by anatomical, histological, and biochemical factors. In addition, several physiological properties of bone grafts, such as osteogenesis, osteoinduction and osteoconduction, directly affect the success or failure of graft incorporation [4]. Alloplasts are synthetic grafting materials used to help the repair of bone defects and to enhance bone ingrowth. Their chemical composition, physical form, and surface configuration, and differences in their porosity, geometry, solubility and density, determine their bioresorbability [5–7]. The treatment of bone defects using biomaterials has been extensively studied in the dental field [8]. Bone loss may be a result of several pathologies, trauma or surgical procedures. These aspects have led to extensive studies worldwide on the process of bone repair. Several techniques for the correction of bone defects have been proposed, including the use of several types of grafts, membranes and the combination of the two techniques [8].

Mineral trioxide aggregate (MTA) is a bacteriostatic powder aggregate containing 65% calcium oxide, 21% calcium silicate, 5% ferric oxide, 4% calcium aluminate, 2.5% calcium sulfates, 2% magnesium oxide, and 0.5% sodium and potassium oxide (pH 12.5). It is not cytotoxic and produces a good biological response. It stimulates tissue repair by increasing cellular adhesion, growth and proliferation at its surface. Unlike other cements, which demand a completely dry field, MTA is indicated when moisture control is inadequate. Under such conditions it shows no loss of its properties and it is not reabsorbed. Previous histological studies have indicated that new bone or cementum is formed adjacent to MTA when it is placed in contact with the periodontal tissue or in artificial bone defects [9–15].

Bone morphogenetic proteins (BMPs) also have osteoinductive characteristics, and inorganic materials such as bone substitutes cause no osteoinduction due to a lack of the proteins required for induction of stem cell differentiation. Calcium phosphates have a high affinity for proteins (such as BMPs) [5]. Guided bone regeneration (GBR) is a procedure based on the guided tissue regeneration technique which is a periodontal surgical procedure that has been in clinical use for more than a decade. Its principles are based on the selective permeability provided by the membranes for the isolation of tissues not essential for bone repair. The use GBR with biomaterials is considered to be beneficial for the healing of bone defects [6, 8, 15].

LEDs show a relatively narrow emission spectrum that may be optimally tuned to correspond to the requirements of a treatment eliminating unnecessary wavelengths from a particular therapy. Their light intensity can be adjusted and they produce high light levels with low radiant heat output and maintain useful output for long periods of time. LED-based devices may provide a homogeneous light dose at optimal intensity [1]. While lasers provide tissue stimulation, which increases cellular activity during wound healing, they have the limitation of a restricted wavelength. Lasers cannot easily produce wavelength combinations optimal for wound healing. The size of wounds that may be treated by the small beam width of laser is also limited. In contrast, the spectral composition of LEDs can be controlled and they may be arranged in flat arrays of all sizes for the treatment of both small and large areas. LEDs offer an effective alternative to the use of conventional light sources [1].

Despite the growing number of successful applications of LED phototherapy (LPT) in many fields, its use in bone repair has not yet been well studied. We were unable to find previous studies on the use of combinations of LED light and biomaterials. LEDs have been used both experimentally and clinically, and beneficial effects of their use have been reported elsewhere [16–21]. It is known that some wavelengths have the ability to stimulate cell proliferation including that of fibroblasts, and these cells have the capacity to secrete collagen, a main organic component observed during bone repair [8, 21–37]. Many techniques are used to improve the bone healing including light therapies. Several studies have demonstrated that irradiation with near-Infrared wavelengths can improve bone repair due to its high penetration into tissues compared to visible light [8, 21–37]. Although the use of LPT for bone healing has been growing steadily, and several studies have demonstrated positive results in the healing of bone tissue [8, 21–37], there are to date few reports of the use of combinations of LED light and MTA [37].

Raman spectroscopy is a relatively simple, reproducible and nondestructive vibrational spectroscopic technique that may be used to optically probe the molecular changes associated with diseased tissues. Only small amounts of material (micrograms to nanograms) with minimal sample preparation are required. In addition, the technique provides information at the molecular level, allowing investigation of functional groups, bonding types, and molecular conformations. Spectral bands in vibrational spectra are molecule-specific and provide direct information about the biochemical composition. These bands are relatively narrow, easy to resolve, and sensitive to molecular structure, conformation, and environment [38]. The Raman spectrum of bone shows prominent vibrational bands related to tissue composition. Some main Raman bands for tissues are at 862, 958, 1,070,

1,270, 1,326, 1,447 and 1,668 cm^{-1} . The band at 1,668 cm^{-1} and those at 1270 and 1326 cm^{-1} are attributed to amide I and amide III stretching modes, and those at 958 and 1070 cm^{-1} are attributed to phosphate and carbonate hydroxyapatite, respectively. The band at 862 cm^{-1} may be attributed to the vibration bands of C–C and C–C–H stretch of collagen and lipid. The band at 1,447 cm^{-1} is attributed to the bending and stretching modes of CH groups of lipids and proteins [27, 28, 30, 37].

Our team has used Raman spectroscopy to study the effects of both laser therapy and LPT on bone healing in animal models. Our previous results show that the use of near-infrared LPT is effective in improving bone repair. It seems that its higher penetration into bone is one of the factors involved. The use of LPT in studies involving bone healing is a striking topic these days, and many previous studies have demonstrated positive results, including when the light is combined with biomaterials and GBR [8, 21–37]. We have found strong evidence that the improvement in the maturation of irradiated bone is associated with an increased deposition of calcium hydroxyapatite (CHA) during the early stages of healing. This maturation may be a result of an increased secretion by osteoblasts in irradiated subjects. It is well accepted that deposition of CHA represents bone maturation, larger amounts of CHA on bone being indicative of a more resistant and calcified bone [8, 21–37].

Although several reports have suggested benefits of the individual and combined use of MTA, GBR and LEDs on wound healing, the combined use of all these techniques has not yet been studied by Raman spectroscopy.

Material and methods

The Animal Ethics Committee of Vale do Paraíba University (UNIVAP) approved this research. Ninety healthy adult male Wistar rats (about 2 months old, mean weight 295 ± 25 g) were kept under natural conditions of light, humidity and temperature in the animal house of the Research and Development Institute of UNIVAP during the experimental period. The animals were fed with standard laboratory pelleted diet and had access to water *ad libitum*. The animals were kept in groups of five in individual metal cages, and kept under a day/night light cycle and controlled temperature conditions during the experimental period. The animals were randomly distributed into ten groups each of which was then subdivided into three subgroups according to the experimental schedule. The treatment groups are shown in Table 1.

Prior to induction of general anesthesia, the animals received 0.04 ml/100 g of atropine subcutaneously. Anesthesia was induced by intramuscular injection of 10% ketamine (Syntec do Brasil, Cotia, SP, Brazil;

Table 1 Treatment groups

Group	Treatment
1	Blood clot
2	MTA
3	MTA+GBR
4	MTA+BMP
5	MTA+BMP+GBR
6	Blood clot + LED
7	MTA+LED
8	MTA+GBR+LED
9	MTA+BMP+LED
10	MTA+BMP+GBR+LED

0.1 ml/100 g)+2% xylazine (Syntec do Brasil; 0.1 ml/100 g). The right leg of the animals was shaved and a 3-cm incision was made over the right tibia with a no. 15 scalpel blade. Skin and subcutaneous tissues were dissected down to the periosteum, which was gently sectioned to expose the bone. A 2-mm partial thickness bone defect was surgically produced (low-speed drill, 1,200 rpm, under refrigeration) in each animal.

The bone defects in groups 1 and 6 were filled only with blood clot. Animals in group 6 were further irradiated with LED light. The bone defects in the animals in the remaining groups were filled with MTA (Angelus; Angelus Indústria de Produtos Odontológicos, Londrina, PR, Brazil) and collagen gel (Genco; Baumer, Mogi das Cruzes, São Paulo, Brazil). The animals in group 7 were further irradiated with LED light. In groups 3 and 8, the defects filled with the MTA were covered with a reabsorbable membrane (Gendern; Baumer). Animals in group 8 were further irradiated with LED light. In groups 4, 5, 9 and 10 a pool of BMPs (Genpro; Baumer) was added to the MTA. In group 5 the defects were covered with membrane. In group 9 the animals were further irradiated with LED light, and in group 10 the animals were further irradiated with LED light after the defects had been covered with membrane. All wounds were routinely sutured and the animals received a single dose of Pentabiotico (penicillin, streptomycin, 20,000 IU; Fort Dodge, Campinas, SP, Brazil; 0.02 ml/100 g) immediately after surgery. Animals were killed on days 15, 21 and 30 after surgery with an overdose of general anesthetics.

LPT was carried out using a FisiLED device (MMOptics, São Carlos, São Paulo, Brazil) with a wavelength of 850 ± 10 nm, a power of 150 mW, a spot size of about 0.5 cm^2 , and an energy density of 16 J/cm^2 . The LED was applied transcutaneously over the defect immediately after surgery and then at 48-h intervals over 15 days resulting in a total treatment dose of 112 J/cm^2 . The doses were based

upon previous studies carried out by our group using laser light [8, 21–37].

After the animals were killed, samples were longitudinally cut under refrigeration using a precision saw (IsoMet 1000; Buehler, Markham, Ontario, Canada) and stored in liquid nitrogen to minimize the growth of aerobic bacteria [27, 28, 30, 37] and because chemical fixation is not advisable due to fluorescence emissions from fixative substances [27, 28, 30, 37].

Prior to the Raman study, the samples were longitudinally cut and warmed gradually to room temperature, and 100 ml of saline was added to the surface during spectroscopic measurements. For Raman measurements, an Ti:sapphire laser with a wavelength of 830 nm pumped with an argon laser (model 3900S; Spectra Physics, Mountain View, CA) provided near-infrared excitation. A spectrograph (model 250 IS; Bruker Optics, Billerica, MA) with a spectral resolution of about 8 cm^{-1} dispersed the Raman-scattered light from the sample and a liquid nitrogen-cooled deep depletion charge-coupled device (model LN/CCD-1024-EHR1; Princeton Instruments, Tucson, AZ) was used to detect the Raman spectra. The system was controlled by a microcomputer, which stored and processed the data [27, 28, 30, 37]. The laser power used at the sample site was of 80 mW with a spectral acquisition time of 100 s. Two points were measured in transverse sections of healing bone resulting in two readings from each specimen and 180 total spectra. All spectra were acquired on the same day to avoid optical misalignments and changes in laser power. The mean values of the intensity of the peaks (about 958 cm^{-1} for phosphate ν_1 , and at about $1,447\text{ cm}^{-1}$ for CH groups of lipids and proteins ν_2) were determined as the average of the peaks in these regions. This intensities are related to the concentration of CHA and organic components of the bone. The data were analyzed using MatLab5.1 software (Newark, NJ) for calibration and background subtraction of the spectra.

For calibration, the Raman spectrum of the solvent indene with known peaks was used [27, 28, 30, 37] due to its intense bands ($800\text{--}1,800\text{ cm}^{-1}$) in the fingerprint region. The indene spectrum was also measured each time the sample was changed to be sure that the laser and collection optics were optimized. In order to remove the fluorescence background from the original spectrum, a 5th order polynomial fitting was found to give better results, facilitating the visualization of the peaks of CHA (about 958 cm^{-1}) and CH groups of lipids and proteins (about $1,447\text{ cm}^{-1}$) found in the bone (Fig. 1). This routine removed any continuous offset background noise due to CCD readout and refrigeration.

Statistical analysis was performed using Minitab 15.0 software (Minitab, Belo Horizonte, MG, Brazil). A baseline Raman spectrum of nontreated bone was also

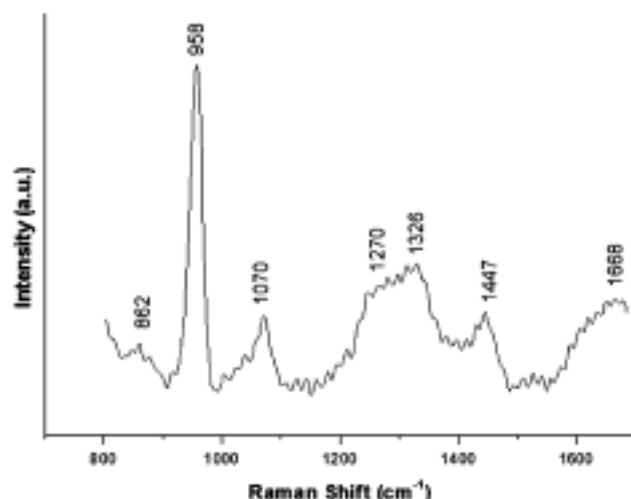


Fig. 1 Typical Raman spectrum of the components bone showing the two Raman shifts used as markers in this study (CHA at 958 cm^{-1} , CH vibration mode of lipids and proteins at $1,447\text{ cm}^{-1}$)

produced as a control. Raman analysis was carried out at the Biomolecular Spectroscopy Laboratory at the Research and Development Institute of UNIVAP.

Results

The Raman spectrum of bone shows prominent vibrational bands related to tissue composition (mineral and organic matrices). Figure 1 shows the main tissue Raman bands at 862 , 958 , $1,070$, $1,270$, $1,326$, $1,447$ and $1,668\text{ cm}^{-1}$. The band at $1,668\text{ cm}^{-1}$ and those at $1,270$ and $1,326\text{ cm}^{-1}$ are attributed to amide I and III stretching modes of lipids and proteins. The band at $1,447\text{ cm}^{-1}$ is attributed to the bending and stretching vibration modes of CH groups of lipids and proteins. The bands at 958 and $1,070\text{ cm}^{-1}$ are attributed to phosphate and carbonate hydroxyapatite from bone mineral, respectively, and that at 862 cm^{-1} may be attributed to the vibration bands of C–C stretch of collagen (tyrosine/proline ring).

Hydroxyapatite (CHA, 958 cm^{-1})

Figures 2, 3, 4, 5 and 6 show respectively the values of the mean intensity of each Raman shift of CHA (958 cm^{-1}) and the organic components of bone (CH vibration groups of lipids and proteins, $1,447\text{ cm}^{-1}$) obtained from treated and untreated animals on days 15, 21 and 30. The intensity of the Raman shift is directly related to the concentration/incorporation of CHA by the bone. So higher intensities represent higher concentrations of CHA. It should be noted that in some groups, irradiated or not, the initial value of the peak was higher than on day 21. This might have been

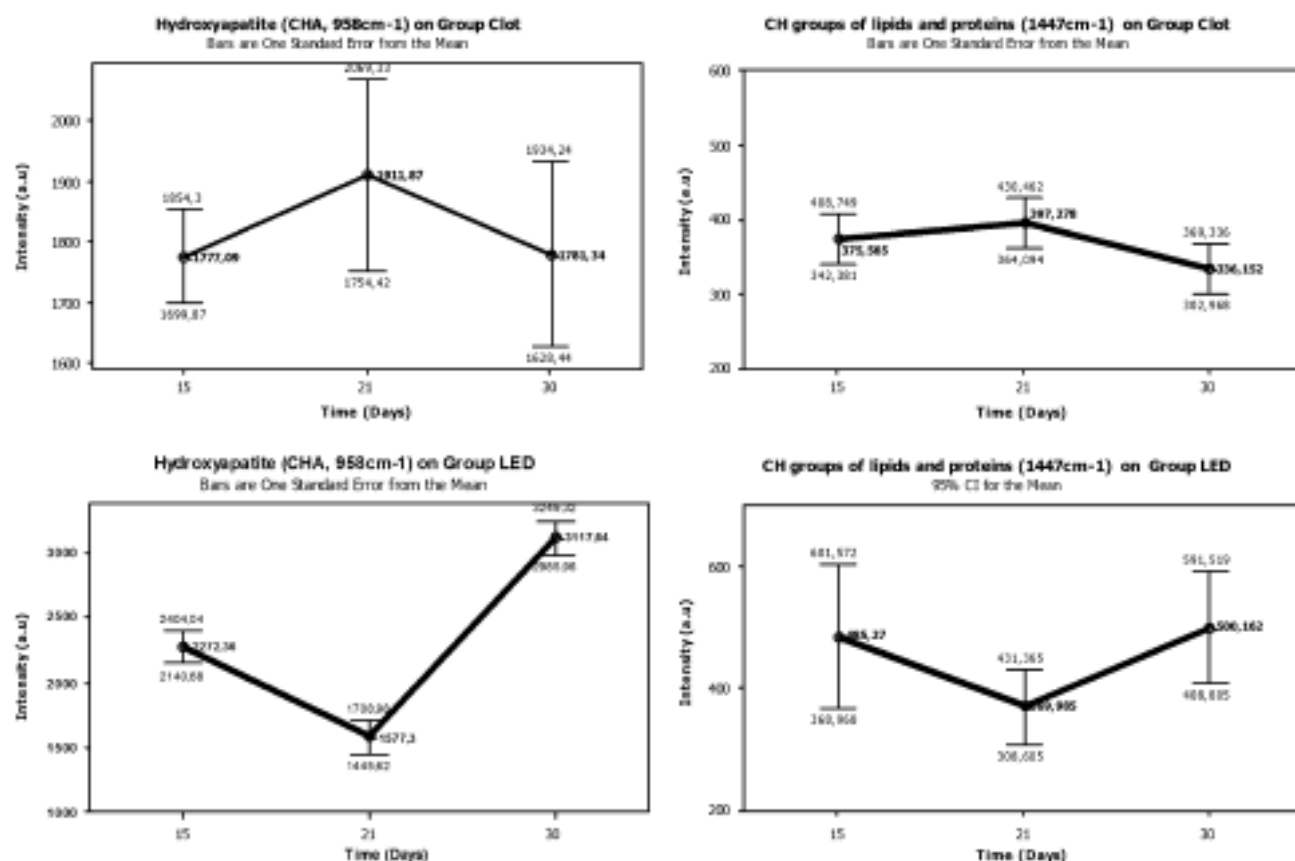


Fig. 2 Mean intensities of the Raman shifts of CHA (958 cm⁻¹) and CH vibration groups of lipids and protein (1,447 cm⁻¹) in group 1 (*Clot*) and group 6 (*LED*) on days 15, 21 and 30

caused by the characteristics of the MTA present at the site. Table 2 shows a summary of the statistical analysis at each time-point.

There were no statistically significant differences in the CHA peaks among the nonirradiated groups at all experimental time-points. On the other hand, there were statistically significant differences between group 1 and the irradiated groups at all time-points (ANOVA, $p < 0.001$, $p = 0.02$, $p < 0.001$). On day 15, group 9 showed a higher mean peak value ($3,042.9 \pm 209$) and group a lower value ($1,475.5 \pm 106$). On day 21 group 9 also showed a higher mean peak value ($2,371 \pm 778$) and group 10 a lower mean peak value ($1,404.2 \pm 71$). At the end of the experimental period, group 6 showed the highest mean peak value ($3,117.6 \pm 100$) and group 10 the lowest ($1,386 \pm 140$).

There was a statistically significant difference between the mean CHA peak in nonirradiated groups at all the experimental time-points (ANOVA, $p < 0.01$). The mean peak value in group 1 was significantly different from that in group 2 (Student's t -test, $p < 0.001$). A statistically significant difference was seen between group 1 and the irradiated groups (ANOVA, $p < 0.001$). Table 3 shows a summary of the statistical analysis for each treatment group.

CH vibration groups of lipids and proteins (1,447 cm⁻¹)

The results for the organic components of bone (CH vibration groups of lipids and proteins, 1,447 cm⁻¹) are shown in Table 4 and Figs. 2, 3, 4, 5 and 6. Higher peaks indicate a lower mineral content and higher readings denote higher levels of organic components.

The analysis of the CH peaks showed statistically significant differences among the nonirradiated groups on day 15 (ANOVA, $p = 0.007$). Group 1 showed the highest mean peak value (375.6 ± 35) and group 3 the lowest (270.28 ± 28). Despite no statistically significant difference being observed on day 21, at the end of the experimental period, a statistically significant difference was observed among the nonirradiated groups (ANOVA, $p = 0.003$) the highest mean peak value being seen in group 4 (434.9 ± 66) and the lowest in group 2 (304.1 ± 40).

Among the irradiated groups, statistically significant differences were also observed at similar time-points as seen in the nonirradiated groups. On day 15, group 6 showed the highest mean peak value (485.3 ± 111) and group 10 the lowest (314.7 ± 52) (ANOVA, $p = 0.003$). Despite no statistically significant difference being observed on day 21,

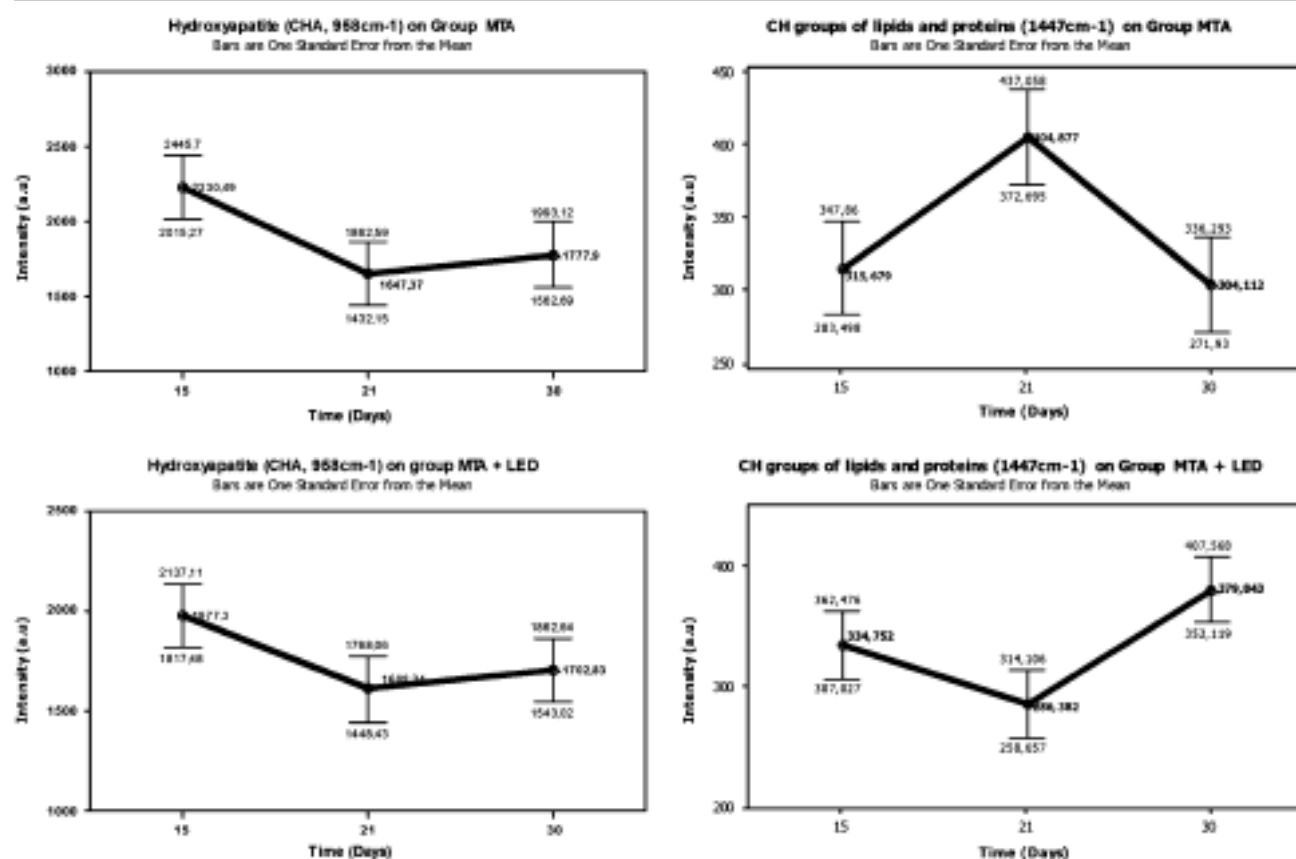


Fig. 3 Mean intensities of the Raman shifts of CHA (958 cm⁻¹) and CH vibration groups of lipids and protein (1,447 cm⁻¹) in groups 2 (MTA) and 7 (MTA+LED) on days 15, 21 and 30

there was a statistically significant difference at the end of the experimental period (ANOVA, $p=0.001$), the highest mean peak value being observed in group 6 (500.2 ± 87) and the lowest in group 8 (313.6 ± 44). Table 4 shows a summary of the statistical analysis at each time-point.

Statistically significant differences were seen among the nonirradiated groups at all experimental time-points (ANOVA, $p=0.05$), the highest mean peak value being seen in group 4 (374.51 ± 73.33) and the lowest in group 3 (307.8 ± 64). Among the irradiated groups, there was also statistically significant difference between group 1 and all the irradiated groups (ANOVA, $p<0.001$), the highest mean peak value being seen in group 6 (451.8 ± 102) and the lowest in group 10 (317 ± 75). Table 5 shows a summary of the statistical analysis for each treatment group.

Discussion

The Wistar rat model adopted in the present investigation shows a rapid healing period, is resistant to climatic changes and is routinely used to study bone healing. Despite LPT having been shown to improve bone healing

in several models [8, 21–37], there have been few studies of the use of LED light on bone and there are no studies until now of its combination with biomaterials. Studies of the effects of laser light on bone regeneration have indicated that its effect on bone healing depends not only on the total dose of irradiation, but also on the irradiation time and the irradiation mode [8, 21–37]. We were unable to find any previous reports in the literature concerning the use of the protocol used in the present investigation. This makes discussion of our results very difficult.

Previous studies have found that irradiated bone (mostly irradiated with IR wavelengths) shows increased osteoblastic proliferation, collagen deposition and bone neoformation when compared to nonirradiated bone. The protocol used in the present study using LED light is similar to those used by our team in previous studies using laser light [8, 21–36]. The results of the present study are promising and indicate that the combination of LED light and MTA, BMPs and GBR did improve the healing of bone.

Our team has been studying the effects of different light sources on bone healing using different assessment methods including histology, computerized morphometry, scanning electron microscopy and Raman spectroscopy [8,

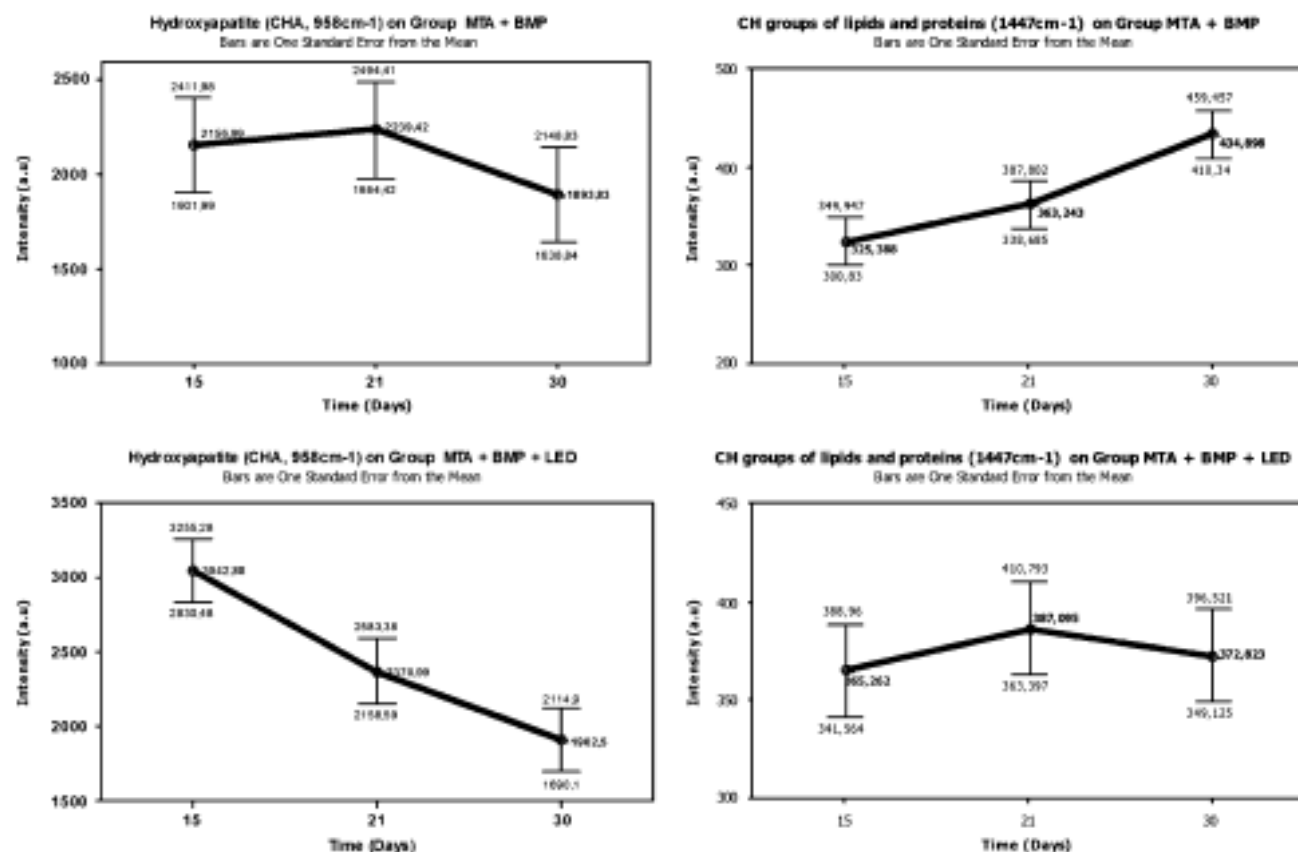


Fig. 4 Mean intensities of the Raman shifts of CHA (958 cm⁻¹) and CH vibration groups of lipids and protein (1447 cm⁻¹) in group 4 (MTA + BMP) and group 9 (MTA + BMP + LED) on days 15, 21 and 30

21–37]. Raman spectroscopy was used in the present study to analyze alterations in both mineral and organic components in healing bone as analysis of bone components is considered the gold standard in the study of bone healing [27, 28, 30, 37].

Raman spectra are a plot of the scattering intensity as a function of the energy difference between the incident and scattered photons and are obtained by pointing a monochromatic laser beam at a sample. The loss (or gain) in photon energy corresponds to the difference in the final and initial vibrational energy levels of the molecules participating in the interaction. The resultant spectra are characterized by shifts in wave numbers (inverse of wavelength in cm⁻¹) from the incident frequency. The frequency difference between incident and Raman-scattered light is termed the Raman shift, which is unique for individual molecules and is measured by the machines detector and is represented as 1/cm. Raman peaks are spectrally narrow, and in many cases can be associated with the vibration of a particular chemical bond (or a single functional group) in the molecule [38].

A number of researchers have reported on Raman spectroscopy of biological tissues, which include inves-

tigations on bone, cornea, cervical tissue, epithelial tissue, lung, breast, skin, gastrointestinal tissue, brain, oral tissue, liver, heme protein, atherosclerotic plaque, serum, human coronary arteries, lymphocytes, human red blood cells, mixed cancer cells, living human cells, microbial cells, individual cells, saliva, DNA, cancer genes, anticancer drugs, tissue processing, raft cultures, meningioma, cancerous cells, and mammalian cell cultures [38].

Our results indicate that infrared LED light causes a quicker repair process and improves the quality of the newly formed bone as marked by the CHA peaks. These findings are aligned with those of previous studies using laser light carried out by our team using several models [8, 21–37]. Our experience indicates that the advanced maturation seen in irradiated bone is due to an increased deposition of CHA. The enhancement in maturation represents the ability of irradiated osteoblasts to secrete more CHA. Increased amounts of CHA are indicative of bone maturation as well as of more resistant and calcified bone. We have also shown that infrared laser light is able to stimulate proliferation of fibroblasts which are major secretors of collagen and an important organic component on healing bone [8, 21–37]. The Raman spectroscopy results in the present investigation

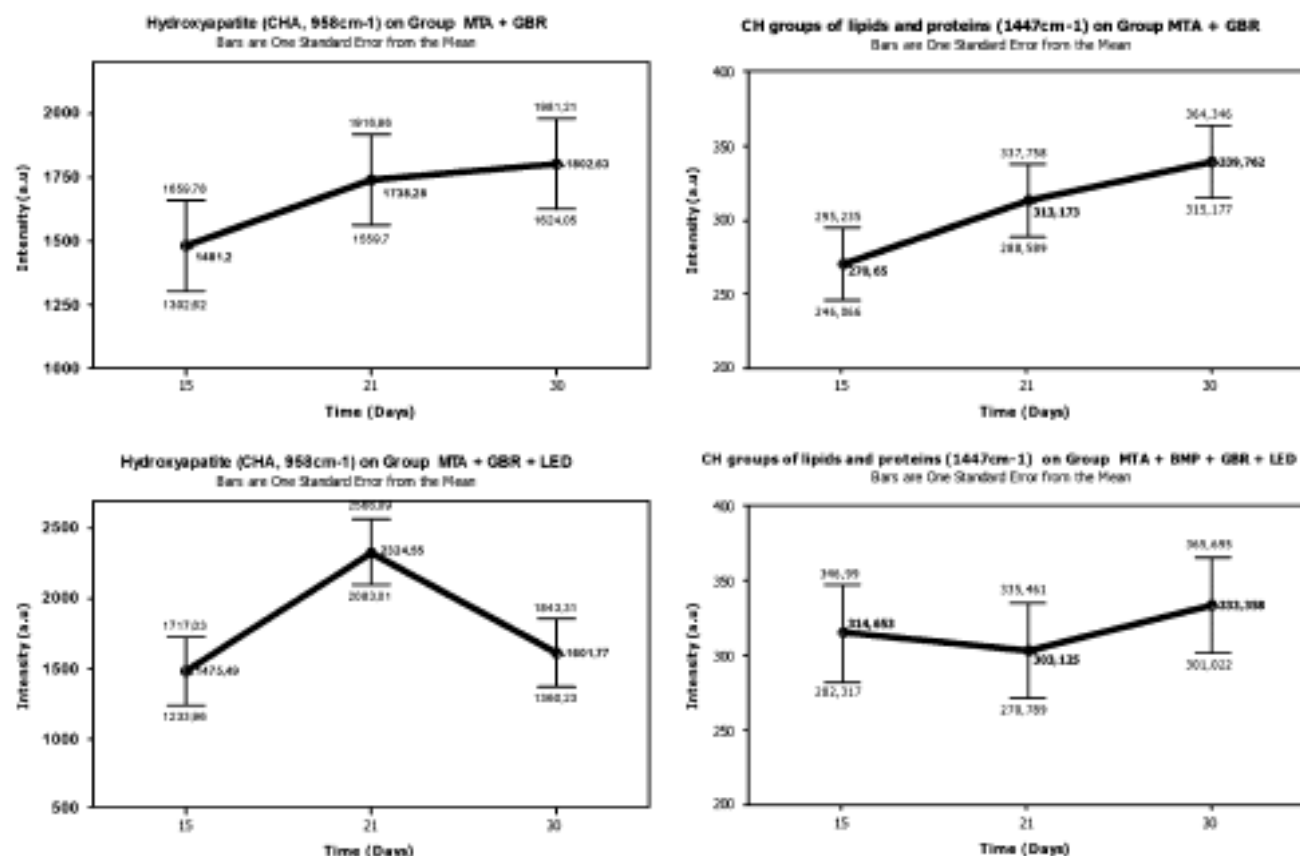


Fig. 5 Mean intensities of the Raman shifts of CHA (958 cm^{-1}) and CH vibration groups of lipids and protein (1447 cm^{-1}) in group 3 (MTA + GBR) and group 8 (MTA + GBR + LED) on days 15, 21 and 30

indicate the occurrence of such phenomena when LED light is used.

MTA appeared to be directly affected by the light. However, LPT positively affected bone healing as has been observed in other studies using other biomaterials and laser light [8, 21–36]. In the early stages of the bone repair, a higher mean CHA peak was seen in group 9 (MTA + BMP + LED) and at the end of the experimental period, and the highest mean peak was seen in group 6 (LED). We were not able to find in the literature any previous reports on the association between MTA and BMPs. However, the use of BMPs improves the outcome of bone healing when associated with LPT [23–25, 36, 37]. In the present study, this was the case up to day 21. Later, the use of LED light alone caused the greatest increase in the levels of CHA. However, analyzing all the changes throughout the experimental period, group 9 (MTA + BMP + LED) showed the higher mean CHA peak.

The behavior of the lipids and proteins varied greatly throughout the experimental period in most groups. This may indicate that other tissue components might have affected the readings. Although we were able to show differences in the peaks of lipids and proteins, LED-

irradiated bones showed a higher collagen content at early stages of repair, this possibly being associated with increased collagen deposition by fibroblasts that were stimulated by the LED light, similar to the observations when using laser light [27, 28, 30, 36, 37]. On the other hand, at the end of the experimental period, group 8 (MTA + GBR + LED) showed lower mean peaks. This may also represent the influence of the use of the GBR. The reason for this needs clarification. The overall content of lipids and proteins analyzed during the whole experimental period showed that the association of MTA + BMP + GBR + LED was associated with lower amounts of these components compared to all irradiated groups. However, the levels of lipids and proteins in this group was similar to the levels seen in group 2 (MTA), that showed the smallest peak. This was probably due to the properties of the MTA itself.

It has also been demonstrated by our group that the use of GBR is helpful in the healing of bone defects and that combining it with LPT improves the outcome of this therapeutic approach as demonstrated previously by our team using different models [8, 22–25, 27, 29, 31, 33]. However, its combination with MTA and/or LED light seemed not to have major influence. Probably, this was due

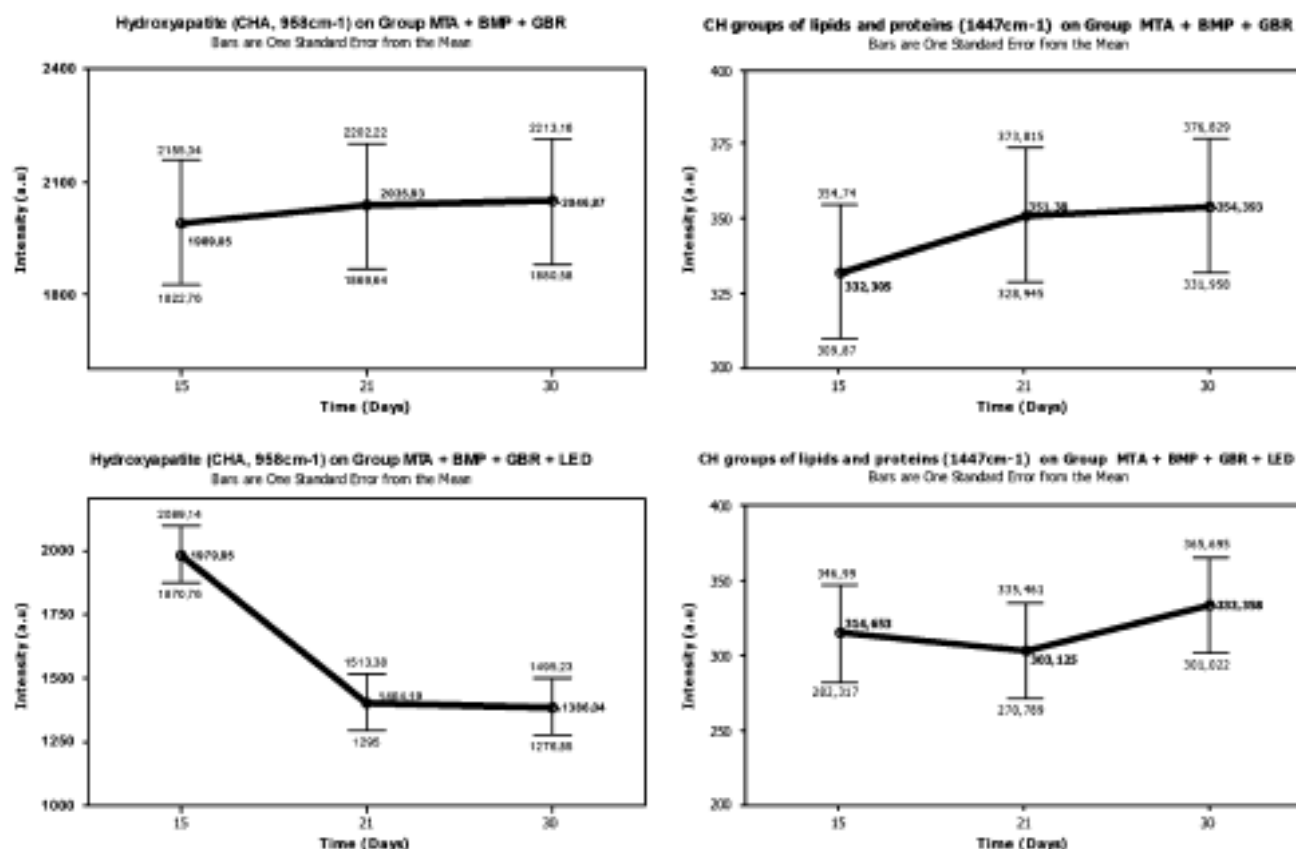


Fig. 6 Mean intensities of the Raman shifts of CHA (958 cm⁻¹) and CH vibration groups of lipids and protein (1447 cm⁻¹) in group 5 (MTA + BMP + GBR) and group 10 (MTA + BMP + GBR + LED) on days 15, 21 and 30

to the relative stiffness of the MTA graft that in some way may have acted as a barrier against invasion by the tissue. Another aspect that might have influenced the results observed in the LED-irradiated groups in which the GBR was used was the fact that the LED irradiation was carried out over the defect at a single point, differently from situations in which Laser light is used as many devices have a very small spot size. In the present study, the LED device

used had a relatively wide spot and probably the membrane acted as an attenuation barrier for light penetration.

One may question why the use of BMPs alone was not assessed on the present study. First, it is important to note that the use of BMPs alone is still complicated as their life-span in this situation is very short. So the use of some matrices, organic or inorganic, will delay the otherwise rapid dispersion of water-soluble, readily diffusible BMPs

Table 2 Values (means ± standard deviation) of the Raman peak for CHA (958 cm⁻¹) in all the treatment groups on days 15, 21 and 30

Group	Treatment	Group letter	Day 15	Day 21	Day 30
1	Blood clot	a	1,777.1±189.1 ^{fg,i}	1,912±157 ^{cd,j}	1,691±303 ^{cd,j}
2	MTA	b	2,230±677	1,647±508	1,778±343
3	MTA+GBR	c	1,481±420	1,738±490	1,803±396
4	MTA+BMP	d	2,157±715	2,239±639	1,894±501
5	MTA+BMP+GBR	e	1,989±368	2,035.9±227	2,047±557
6	LED	f	2,272±279 ^{ab,h}	1,577±474 ^a	3,117.6±100 ^{ab,h,i,j}
7	MTA+LED	g	1,977±646 ^{ab,i}	1,608.2±187	1,702.8±89 ^{cd}
8	MTA+GBR+LED	h	1,475.5±106 ^{cd,j}	2,325±996	1,601.8±214 ^f
9	MTA+BMP+LED	i	3,042.9±209 ^{ab,h,j}	2,371±778 ^a	1,903±403 ^{ab,i,j}
10	MTA+BMP+GBR+LED	j	1,980±436 ^{ab,i}	1,404.2±71 ^a	1,386±140 ^{ab,i,j}

Superscript letters indicate that the value is significantly different from the value of the group with the same letter

Table 3 Values (means \pm standard deviation) of the Raman peak for CHA (958 cm^{-1}) in all the treatment groups

Group	Treatment	Group letter	Mean \pm SD
1	Blood clot	a	$1,823.4 \pm 31.6^{b,j}$
2	MTA	b	$1,885 \pm 558^a$
3	MTA+GBR	c	$1,674 \pm 435^{d,e,j}$
4	MTA+BMP	d	$2,096 \pm 606^{c,i}$
5	MTA+BMP+GBR	e	$2,024 \pm 383^{c,j}$
6	LED	f	$2,322.4 \pm 71.5^{g,j}$
7	MTA+LED	g	$1,762.8 \pm 40.1^{f,i}$
8	MTA+GBR+LED	h	$1,800.6 \pm 67.6^i$
9	MTA+BMP+LED	i	$2,438.8 \pm 68.6^{a,d,g,h,j}$
10	MTA+BMP+GBR+LED	j	$1,590.1 \pm 37.9^{a,c,e,f,i}$

Superscript letters indicate that the value is significantly different from the value of the group with the same letter

from the implant site without which they, like other growth factors, would likely have a short serum half-life because of liver uptake and catabolism [39–42]. On the other hand, the use of some BMPs (2 and 7) is approved for clinical use for osseous repair and are well accepted as therapeutic modalities [43, 44].

Normal bone regeneration is a complex process that involves a large number of growth factors and cytokines in its regulation. No matter how influential one factor may appear in the process, its action in isolation may have little effect without interaction with endogenously produced growth factors and cytokines [45]. Among the many tissues in the body, bone has the highest potential for regeneration. Bone morphogenesis is a sequential multistep biological chain reaction and the key steps are chemotaxis of progenitors/stem cells, proliferation of cells and differentiation of true endochondral bone formation.

The role of growth factors in bone repair is widely recognized, particularly for BMPs, fibroblast growth factor (FGF), insulin-like growth factors (IGFs), platelet-derived growth factor (PDGF), transforming growth factor- β (TGF-

β) and vascular endothelial growth factor (VEGF). Growth factors are usually stored in the extracellular matrix (ECM), but after injury are actively released by the ECM, cells and platelets. The main growth factors acting on the skeleton are BMPs, TGF- β , FGF, PDGF, VEGF and IGFs. During bone repair, cells of the bone microenvironment, such as inflammatory cells, fibroblasts, endothelial cells, bone marrow stromal cells and osteoblasts produce growth factors. The migration of osteoprogenitors is enhanced by BMPs, PDGF, FGF and VEGF. The proliferation of periosteum-derived cells is stimulated by PDGF and FGF in the early stages of bone repair. Previous studies have found that light is capable of altering the release of several growth factors [46–50].

Artificial materials, such as the MTA, may influence the synthesis and release growth factors from cells. The final effect depends on both the biomaterial's physical and chemical properties and the cell involved. So, bone induction, and its subsequent regeneration, might not only be restricted to biological modulation but the environment might also be a crucial factor in the induction and subsequent regeneration of bone. There is evidence that the platelet release reaction is induced at a different level by some bone substitutes: collagen-grafted calcium metaphosphate induces a higher release reaction than nongrafted calcium metaphosphate or hydroxyapatite. These effects should be carefully considered and evaluated when a new material is proposed as a scaffold for bone engineering [51, 52]. We were unable to find a previous study assessing this aspects using MTA.

One drawback in using this material is that close proximity to the host bone was necessary to achieve osteoconduction. However, new bone growth is often strictly limited because these materials are not osteoinductive in nature. To overcome this limitation, a number of different bone-derived growth factors have been demonstrated to stimulate bone growth, collagen synthesis and fracture repair both in vitro and in vivo. MTA also suffers

Table 4 Values (means \pm standard deviation) of the Raman peaks for the CH groups of lipids and proteins ($1,447\text{ cm}^{-1}$) in all the treatment groups on days 15, 21 and 30

Group	Treatment	Group letter	Day 15	Day 21	Day 30
1	Blood clot	a	$375.6 \pm 35^{c,d,f,j}$	397.3 ± 12.7	$336.2 \pm 49^{d,f}$
2	MTA	b	315.7 ± 52	404.9 ± 120	$304.1 \pm 40^{c,d,e}$
3	MTA+GBR	c	$270.7 \pm 28^{a,d}$	313.2 ± 87	$339.8 \pm 50^{b,d,e}$
4	MTA+BMP	d	$325.4 \pm 38^{a,c}$	363.2 ± 71	$434.9 \pm 66^{a,b,c,e}$
5	MTA+BMP+GBR	e	332.3 ± 57	351.4 ± 53	$354.4 \pm 54^{b,c,d}$
6	LED	f	$485.3 \pm 111^{a,g,h,i,j}$	370 ± 58	$500.2 \pm 87^{a,g,h,i}$
7	MTA+LED	g	334.8 ± 78^f	286.4 ± 70	$379.8 \pm 54^{c,i,j}$
8	MTA+GBR+LED	h	343.9 ± 74^f	321.2 ± 104	$313.6 \pm 44^{c,i,j}$
9	MTA+BMP+LED	i	365.3 ± 35^f	387.1 ± 75	$372.8 \pm 57^{c,h}$
10	MTA+BMP+GBR+LED	j	$314.7 \pm 52^{a,f}$	303.1 ± 72	333.4 ± 105^g

Superscript letters indicate that the value is significantly different from the value of the group with the same letter

Table 5 Values (means \pm standard deviation) of the Raman peak for the CH groups of lipids and proteins ($1,447\text{ cm}^{-1}$) in all the treatment groups

Group	Treatment	Group letter	Mean \pm SD
1	Blood clot	a	369.6 \pm 81 ^{c,f}
2	MTA	b	341.5 \pm 87
3	MTA+GBR	c	307.8 \pm 64 ^{a,d,e}
4	MTA+BMP	d	374.5 \pm 73 ^c
5	MTA+BMP+GBR	e	346 \pm 52 ^c
6	LED	f	451.8 \pm 102 ^{a,b,h,i,j}
7	MTA+LED	g	333.6 \pm 75 ^d
8	MTA+GBR+LED	h	326.2 \pm 74 ^d
9	MTA+BMP+LED	i	375 \pm 55 ^{c,e,h,i}
10	MTA+BMP+GBR+LED	j	317 \pm 75 ^d

Superscript letters indicate that the value is significantly different from the value of the group with the same letter

from its inherent lack of microporosity for tissue invasion. Its pore size and inherent strength play major roles in its ultimate usefulness. Previously it was generally believed that calcium phosphate cements are reabsorbed with bone formed via osteoconduction. However, recent studies have indicated that calcium phosphate cements directly initiate osteogenesis. In addition, through a dissolution–precipitation process, the development of a bone-like mineral layer might initiate bone formation either by mimicry with the bone mineral structure or by the presence of osteogenic compounds (such as BMPs) [53, 54].

BMPs have been defined as a molecule (morphogen) that can initiate, promote and maintain metabolism and homeostasis [55]. However, the mere presence of BMPs is no guarantee of efficient bone healing. Although the presence of BMPs is essential for a number of processes during bone healing, BMP-mediated bone formation strongly depends on the local presence of various BMP activity regulating inhibitors and stimulators. The osteogenic potency of the BMPs requires a local and controlled delivery. Moreover, for clinical use of BMPs, their short half-life should be taken into account [56]. BMPs were initially discovered by the fact that demineralized bone matrix is capable of initiating bone formation when transplanted to ectopic sites in rodents [57]. These proteins were originally described to act as bone growth factors. The BMP family of cytokines comprises over 20 different ligands that belong to the TGF- β superfamily. Their importance in the development of multicellular organisms is obvious from their existence in all vertebrates as well as nonvertebrate animals [45]. Although BMPs are involved in numerous developmental and pathophysiological processes, their effects on bone formation have been studied most extensively. In bone, they are synthesized by skeletal cells such as osteoblasts and sequestered in the bone ECM [45].

It is known that when BMPs are implanted, their osteoinductive properties can initiate the complete cascade of bone formation, including the migration of mesenchymal stem cells and their differentiation into osteoblasts. This bone induction occurs through endochondral as well as intramembranous ossification and results in the formation of normal woven and/or lamellar bone [58]. Various proteins with an important role in this autoinductive process have been isolated and investigated for their therapeutic potential in bone regeneration, including BMPs [59], TGF- β , FGF, IGF, VEGF, PDGF, epidermal growth factor, parathyroid hormone/parathyroid hormone-related protein and interleukins [45].

The production of growth factors is a biological process that starts immediately after injury and stimulates the cells involved in the repair process to proliferate. TGF- β is a multifunctional cytokine secreted by platelets, T lymphocytes, macrophages, endothelial cells, fibroblasts and other tissues. It has a central action and has antiinflammatory and proliferative effects during tissue repair. Its effects include chemotaxis of leukocytes, fibroblasts and smooth muscle cells. It also influences both the formation and remodeling of the ECM, stimulates keratinocyte migration, and angiogenesis and fibroblastic differentiation, inhibits the proliferation of keratinocytes, regulates the expression of integrin and other cytokines, and also possesses an autoinduction property [46].

TGF- β is synthesized by many different cell types and is stored as an inactive complex with latency-associated peptide in the bone ECM. Another major source of this factor is platelets in the blood clot formed after a fracture or the creation of a bone defect. It is known that TGF- β stimulates migration of osteoprogenitor cells and is a potent regulator of cell proliferation, cell differentiation and ECM synthesis, and that it synergizes with BMPs. Early during repair, both growth factors may directly increase the number of osteoprogenitor cells by stimulating their migration. Circulation is one of the sources of osteoprogenitor cells during BMP-induced bone regeneration and cell recruitment may also be indirectly enhanced by their combined effect on angiogenesis. It has been suggested that TGF- β 1 and BMP-7 synergistically interact to enhance angiogenesis and vascular invasion since their coadministration increases vessel formation. The mitogenic effect of TGF- β may further increase the osteoprogenitor cell pool by stimulating cell proliferation [45]. As well as their combined effects on angiogenesis, cell recruitment and proliferation, TGF- β and BMPs also interact during osteoblast differentiation [60]. Light has also been shown to increase angiogenesis and to increase the number and activity of osteoblasts [8, 22–26, 29, 31–33, 35].

It has been suggested that TGF- β 1 may have stimulatory effects on osteoblast differentiation during early stages and an inhibitory effect on differentiation and mineralization

during later stages. Although TGF- β 1 seems to inhibit matrix mineralization during later stages, the in vivo consequences of these inhibitory effects might be limited since expression of TGF- β receptors is downregulated when cell differentiation progresses [45]. This aspect is important as it may be one explanation for our previous results indicating that infrared light fails to significantly enhance bone repair during the later stages [8, 22–37]. A pivotal role in the bone remodeling process has been assigned to TGF- β 1 because it has been proven to affect both bone resorption and formation. It is secreted in a latent form by bone cells and is stored in the ECM. Active resorbing osteoclasts are capable of activating TGF- β 1, which in turn attenuates further bone resorption by impairing osteoclastogenesis and promotes bone formation through chemotactic attraction and stimulation of proliferation and differentiation of osteoblast precursors [60]. There is also evidence in the literature suggesting that light positively affects the release of TGF- β [46].

It seems possible that LED light has beneficial effects similar to those of laser light, as there are several reports of the benefits of the use of LEDs operating at several wavelengths both in vitro and in vivo in both normal and pathological conditions [2, 61–64]. It is also possible that the mechanism involved are similar.

The rationale for combining MTA, BMPs and LED light in this work was based on the idea that BMPs combined with an osteoconductive substance, such as MTA, and LED light (with its well-recognized positive effects on cell proliferation and function as well as on secretion of many growth factors) would improve the repair of bone defects in a manner similar to that following autogenous bone grafting while avoiding the complications and limitations associated with autogenous bone grafting, that remains the gold standard for treating bone defects.

Despite the success we have observed using different light sources in bone repair using different models, our knowledge of the bone regeneration process and light interactions is still limited. Therefore, further molecular, cellular, and translational studies are required to obtain a better understanding of the actions and interactions of the different regulators of the regeneration process. Our results using Raman spectral analysis indicate that infrared LED light did improve the deposition of CHA in the healing bone grafted or not with MTA.

Acknowledgments We would like to thank the Conselho Nacional de Desenvolvimento Científico e Tecnológico (CNPq) for providing financial support for this project.

Conflicts of interest The authors received a grant from the Conselho Nacional de Desenvolvimento Científico e Tecnológico (CNPq), a government research agency, but have full control of all primary data and agree to allow the journal to review their data if requested.

References

- Bamlet D (2008) Light-emitting diodes (LEDs) in dermatology. *Semin Cutan Med Surg* 27:227–238
- Recker RR (1992) Embryology, anatomy, and microstructure of bone. In: Coe FL, Favus MJ (eds) *Disorders of bone and mineral metabolism*. Raven, New York, pp 219–240
- Muschler GF, Lane JM, Dawson EG (1990) The biology of spinal fusion. In: Cotler JM, Cotler HB (eds) *Spinal fusion: science and technique*. Springer, Berlin, pp 9–21
- Prolo DJ (1990) Biology of bone fusion. *Clin Neurosurg* 36:135–146
- Kalfas IH (2001) Principles of bone healing. *Neurosurg Focus* 10:E1
- Evans GH, Yukna RA, Cambre KM, Gardiner DL (1997) Clinical regeneration with guided tissue barriers: an analysis of the current literature. *Curr Opin Periodontol* 4:75–81
- Nascimento C, Issa JPM, Oliveira RR, Lyomasa MM, Siéssere S, Regalo SCH (2007) Biomateriais con aplicación en el proceso de reparación ósea. *Int J Morphol* 25:839–846
- Pinheiro AL, Gerbi ME (2006) Photoengineering of bone repair processes. *Photomed Laser Surg* 24:169–178
- Torbinejad M, Hong CU, Lee SJ, Monsef M, Pitt Ford TR (1995) Investigation of mineral trioxide aggregate for root end filling in dogs. *J Endod* 21:603–608
- Torbinejad M, Hong CU, Pitt Ford TR (1995) Physical properties of a new root end filling material. *J Endod* 21:349–353
- Torbinejad M, Chivian N (1999) Clinical applications of mineral trioxide aggregate. *J Endod* 25:197–205
- Schwartz RS, Mauger M, Clement DJ, Walker WA (1990) Mineral trioxide aggregate: a new material for endodontics. *J Am Dent Assoc* 130:967–975
- Bystrom A, Claesson R, Sundqvist G (1985) The antibacterial effect of camphorated paramonochlorophenol, camphorated phenol and calcium hydroxide in the treatment of infected root canals. *Endod Dent Traumatol* 1:170–175
- Mitchell PJ, Pitt Ford TR, Torbinejad M, McDonald F (1999) Osteoblast biocompatibility of mineral trioxide aggregate. *Biomaterials* 20:167–173
- Park YJ (2000) Enhanced guided bone regeneration by controlled tetracycline release from poly(L-lactide) barrier membranes. *J Biomed Mater Res* 51:391–397
- Whelan HT, Buchmann EV, Whelan NT et al (2001) NASA light emitting diode medical applications: from deep space to deep sea. *Space Technol Appl Int Forum* 552:35–45
- Whelan HT, Connolly MD, Hodgson BD et al (2002) NASA light emitting diodes for the prevention of oral mucositis in pediatric bone marrow transplant patients. *J Clin Laser Med Surg* 20:319–324
- Al-Warhan FA, Andres BL (2003) Polychromatic LED therapy in burn healing of non-diabetic and diabetic rats. *J Clin Laser Med Surg* 21:249–258
- Corazza AV, Jorge J, Kunchi C, Bagnato VS (2007) Photobiomodulation on the angiogenesis of skin wounds in rats using different light sources. *Photomed Laser Surg* 25:102–106
- Al-Warhan FA (1997) Laser acceleration of open skin wound closure in rats and its dosimetric dependence. *Lasers Life Sci* 7:237–247
- Smith KC (2005) Laser (and LED) therapy is phototherapy. *Photomed Laser Surg* 23:78–80
- Pinheiro AL, Gerbi ME, Lima Junior FA et al (2009) Bone repair following bone grafting hydroxyapatite guided bone regeneration and infrared laser photobiomodulation: a histological study in a rodent model. *Lasers Med Sci* 24:234–240
- Gerbi ME, Marques AM, Ramalho LM et al (2008) Infrared laser light further improves bone healing when associated with bone

- morphogenic proteins: an in vivo study in a rodent model. *Photomed Laser Surg* 26:55–60
24. Pinheiro AL, Gerbi ME, Ponzi EA et al (2008) Infrared laser light further improves bone healing when associated with bone morphogenetic proteins and guided bone regeneration: an in vivo study in a rodent model. *Photomed Laser Surg* 26:167–174
25. Torres CS, Santos JN, Monteiro JS, Amorim PG, Pinheiro AL (2008) Does the use of laser photobiomodulation, bone morphogenetic proteins, and guided bone regeneration improve the outcome of autologous bone grafts? An in vivo study in a rodent model. *Photomed Laser Surg* 26:371–377
26. Gerbi ME, Pinheiro AL, Ramalho LM (2008) Effect of IR laser photobiomodulation on the repair of bone defects grafted with organic bovine bone. *Lasers Med Sci* 23:313–317
27. Lopes CB, Pacheco MT, Silveira Junior L, Duarte J, Cangussu MC, Pinheiro AL (2007) The effect of the association of NIR laser therapy BMPs, and guided bone regeneration on tibial fractures treated with wire osteosynthesis: Raman spectroscopy study. *J Photochem Photobiol B* 89:125–130
28. Lopes CB, Pinheiro AL, Sathiaiah S, Da Silva NS, Salgado MA (2007) Infrared laser photobiomodulation (830 nm) on bone tissue around dental implants: a Raman spectroscopy and scanning electronic microscopy study in rabbits. *Photomed Laser Surg* 25:96–101
29. Weber JB, Pinheiro AL, Oliveira MG, Oliveira FA, Ramalho LM (2006) Laser therapy improves healing of bone defects submitted to autogenous bone graft. *Photomed Laser Surg* 24:38–44
30. Lopes CB, Pinheiro AL, Sathiaiah S, Ramalho LM (2005) Infrared laser light reduces loading time of dental implants: a Raman spectroscopy study. *Photomed Laser Surg* 23:27–31
31. Gerbi ME, Pinheiro AL, Ramalho LM et al (2005) Assessment of bone repair associated with the use of organic bovine bone and membrane irradiated at 830 nm. *Photomed Laser Surg* 23:382–388
32. Pinheiro AL, Lima Junior FA, Gerbi ME et al (2003) Effect of low level laser therapy on the repair of bone defects grafted with inorganic bovine bone. *Braz Dent J* 14:177–181
33. Pinheiro AL, Lima Junior FA, Gerbi ME et al (2003) Effect of 830-nm laser light on the repair of bone defects grafted with inorganic bovine bone and decalcified cortical osseous membrane. *J Clin Laser Med Surg* 21:383–388
34. Pinheiro AL, Oliveira MA, Martins PP (2001) Biomodulação da cicatrização óssea pós-implantar com o uso da laserterapia não-cirúrgica: estudo por microscopia eletrônica de varredura (Biomodulation of peri-implant bone repair with laser therapy: SEM study). *Rev FOUFBA* 22:12–19
35. Silva Junior N, Pinheiro AL, Oliveira MG, Weismann R, Ramalho LM, Nicolau RA (2002) Computerized morphometric assessment of the effect of low-level laser therapy on bone repair: an experimental animal study. *J Clin Laser Med Surg* 20:83–88
36. Lopes CB, Pacheco MT, Silveira L Jr, Cangussu MC, Pinheiro AL (2010) The effect of the association of near infrared laser therapy, bone morphogenetic proteins, and guided bone regeneration on tibial fractures treated with internal rigid fixation: a Raman spectroscopic study. *J Biomed Mater Res Part A* 94:1257–1263
37. Pinheiro AL, Aciole GT, Cangussu MC, Pacheco MT, Silveira L Jr (2010) Effects of laser phototherapy on bone defects grafted with mineral trioxide aggregate, bone morphogenetic proteins, and guided bone regeneration: a Raman spectroscopic study. *J Biomed Mater Res A* 95:1041–1047
38. Movasaghi Z, Rehman S, Ihtesham U, Rehman IU (2007) Raman spectroscopy of biological tissues. *Appl Spectrosc Rev* 42:493–541
39. Kirker-Head CA (2000) Potential applications and delivery strategies for bone morphogenetic proteins. *Adv Drug Deliv Rev* 43:65–92
40. Winn SR, Uludag H, Hollinger JO (1999) Carrier systems for bone morphogenetic proteins. *Clin Orthop Suppl* 367:S95–S106
41. Cook SD, Baffes GC, Wolfe MW, Sampath TK, Rueger DC (1994) Recombinant human bone morphogenetic protein-7 induces healing in a canine long-bone segmental defect model. *Clin Orthop* 301:302–312
42. Hunt TR, Hsu HH, Morris DC, Schwappach JR, Lark RG, Anderson HC (1993) Healing of a segmental defect in the rat femur using a bone inducing agent (BIA) derived from a cultured human osteosarcoma cell line (Saos-2). *Trans Orthop Res Soc* 18:489
43. Reddi AH (1998) Role of morphogenetic proteins in skeletal tissue engineering and regeneration. *Nat Biotechnol* 16:247–252
44. Nakashima M, Reddi AH (2003) The application of bone morphogenetic proteins to dental tissue engineering. *Nat Biotechnol* 21:1025–1032
45. Kempson DH, Creemers LB, Alblas J, Lu L, Verbout AJ, Yaszemski MJ, Dhert WJ (2010) Growth factor interactions in bone regeneration. *Tissue Eng Part B Rev* 16:551–566
46. de Sousa AP, de Aguiar Valença Neto AdA, Marchionni AM, de Araújo Ramos M, dos Reis Júnior JA, Pereira MC, Cangussu MC, de Almeida Reis SR, Pinheiro AL (2011) Effect of LED phototherapy ($\lambda 700 \pm 20$ nm) on TGF- β expression during wound healing: an immunohistochemical study in a rodent model. *Photomed Laser Surg* 29:605–611
47. Rocha Júnior AM, Vieira BJ, Andrade LCF, Aarestrup FM (2009) Low-level laser therapy increases transforming growth factor- $\beta 2$ expression and induces apoptosis of epithelial cells during the tissue repair process. *Photomed Laser Surg* 27:303–307
48. Saygun I, Karacay S, Sendar M, Ural AU, Sencimen M, Kurtis B (2008) Effects of laser irradiation on the release of basic fibroblastic growth factor (bFGF) insulin like growth factor 1 (IGF-1), and receptor of IGF-1 (IGFBP3) for gingival fibroblasts. *Lasers Med Sci* 23:211–215
49. Safavi SM, Kazemi B, Esmaeili M, Fallah A, Modarresi A, Mir M (2008) Effects of low-level He-Ne laser irradiation on the gene expression of IL-1 β , TNF- α , IFN- γ , TGF- β , bFGF, and PDGF in rat's gingiva. *Lasers Med Sci* 23:331–335
50. Ihsan FR (2005) Low-level laser therapy accelerates collateral circulation and enhances microcirculation. *Photomed Laser Surg* 23:289–294
51. Cho HS, Park SY, Kim S et al (2008) Effect of different bone substitutes on the concentration of growth factors in platelet-rich plasma. *J Biomater Appl* 22:545–557
52. Devescovi V, Leonardi E, Ciapetti G, Cenni E (2008) Growth factors in bone repair. *Chir Organi Mov* 92:161–168
53. Nandi SK, Roy S, Mukherjee P, Kundu B, De DK, Basu D (2010) Orthopaedic applications of bone graft and graft substitutes: a review. *Indian J Med Res* 132:15–30
54. Friedman CD, Costantino PD, Takagi S, Chow LC (1998) BoneSource hydroxyapatite cement: a novel biomaterial for craniofacial skeletal tissue engineering and reconstruction. *J Biomed Mater Res* 43:428–432
55. Reddi AH, Reddi A (2009) Bone morphogenetic proteins (BMPs): from morphogens to metabolites. *Cytokine Growth Factor Rev* 20:341–342
56. Lissensberg-Thunnissen SN, de Gorter DJ, Sier CF, Schipper IB (2011) Use and efficacy of bone morphogenetic proteins in fracture healing. *Int Orthop* 35:1271–1280
57. Urist MR, Dowell TA, Hay PH, Strates BS (1968) Inductive substitutes for bone formation. *Clin Orthop Relat Res* 59:59–96
58. Wozney JM (2002) Overview of bone morphogenetic proteins. *Spine* 27:S2

59. Wang EA, Rosen V, D'Alessandro JS, Bauduy M, Condes P, Hamada T, Israel DI, Hewick RM, Kerns KM, LaPan P et al (1990) Recombinant human bone morphogenetic protein induces bone formation. *Proc Natl Acad Sci U S A* 87:2220–2224
60. Janssens K, ten Dijke P, Janssens S, Van Hul W (2005) Transforming growth factor-beta1 to the bone. *Endocr Rev* 26:743–774
61. Desmet KD, Paz DA, Corry JJ et al (2006) clinical and experimental applications of NIR-LED photobiomodulation. *Photomed Laser Surg* 24:121–128
62. Lanzafame RJ, Stadler I, Whelan HT (2002) NASA LED photoradiation influences nitric oxide and collagen production in wounded rats. *Lasers Surg Med Suppl* 14:12
63. Tachibana R, Farinelli WA, Rox Anderson R (2002) Low intensity light-induced vasodilation in vivo. *Lasers Surg Med Suppl* 14:11
64. Vinck EM, Cagnie BJ, Cornelissen MJ, Declercq HA, Cambier DC (2003) Increased fibroblast proliferation induced by light emitting diode and low power laser irradiation. *Lasers Med Sci* 18:95–99

Lasers Med Sci. 2012 Sep;27(5):1013-24. doi: 10.1007/s10103-011-1033-8. Epub 2011 Dec 15.

Does LED phototherapy influence the repair of bone defects grafted with MTA, bone morphogenetic proteins, and guided bone regeneration? A description of the repair process on rodents

Does LED phototherapy influence the repair of bone defects grafted with MTA, bone morphogenetic proteins, and guided bone regeneration? A description of the repair process on rodents

Antonio L. B. Pinheiro · Luiz G. P. Soares ·
Artur F. S. Barbosa · Luciana M. P. Ramalho ·
Jean N. dos Santos

Received: 5 May 2011 / Accepted: 14 November 2011
© Springer-Verlag London Ltd 2011

Abstract This work carried out a histological analysis on bone defects grafted (MTA) treated or not with LED, BMPs, and membrane (GBR). Benefits of their isolated or combined usage on bone repair were reported, but not

No benefit of any kind will be received either directly or indirectly by the authors regarding this work.

A. L. B. Pinheiro (✉) · L. G. P. Soares · A. F. S. Barbosa ·
L. M. P. Ramalho
Center of Biophotonics, School of Dentistry,
Federal University of Bahia,
Av. Amálio Pinho, 62, Canela,
Salvador, BA CEP 40110-150, Brazil
e-mail: albp@ufba.br

L. G. P. Soares
e-mail: luizguilherme_@hotmail.com

A. F. S. Barbosa
e-mail: arturfelipes@gmail.com

L. M. P. Ramalho
e-mail: lucianaramalho@uol.com.br

A. L. B. Pinheiro
Camilo Castelo Branco University,
São José dos Campos, SP, Brazil 12245-230

A. L. B. Pinheiro · L. M. P. Ramalho · J. N. dos Santos
National Institute of Optics and Photonics,
São Carlos, SP, Brazil 13560-970

J. N. dos Santos
e-mail: jeanpatol@gmail.com

J. N. dos Santos
Laboratory of Surgical Pathology, School of Dentistry,
Federal University of Bahia,
Av. Amálio Pinho, 62, Canela,
Salvador, BA CEP 40110-150, Brazil

their association. Ninety rats were divided into ten groups and each subdivided into three. Defects on G II and I were filled with the blood clot. G II was further LED irradiated. G III and IV were filled with MTA; G IV was further LED irradiated. In G V and VI, the defects were filled with MTA and covered with a membrane (GBR). G VI was further LED irradiated. In G VII and VIII, BMPs were added to the MTA and group VIII was further LED irradiated. In G IX and X, the MTA+BMP graft was covered with a membrane (GBR). G X was further LED irradiated. LED was applied over the defect at 48-h intervals and repeated for 15 days. Specimens were processed, cut, and stained with H&E and Sirius red and underwent histological analysis. The use of LED light alone dramatically reduced inflammation. However, its use on MTA associated with BMP and/or GBR increased the severity of the inflammatory reaction. Regarding bone reabsorption, the poorest result was seen when the LED light was associated with the MTA+BMP graft. In the groups Clot and MTA+GBR, no bone reabsorption was detectable. Increased collagen deposition was observed when the LED light was associated with the use of the MTA associated with BMP and/or GBR. Increased new bone formation was observed when the LED light was used alone or associated with the use of MTA+GBR, MTA+BMP, on association of MTA+BMP+GBR and when BMP was added to the MTA. Our results indicate that the use of LED light alone or in association with MTA, MTA+BMP, MTA+GBR, and MTA+BMP+GBR caused less inflammation, and an increase of both collagen deposition and bone deposition as seen on both histological and morphometric analysis.

Keywords Biomaterial · Light emitting diode · Mineral trioxide aggregate

Introduction

Bone defects often demand the use of biomaterials as the body is often not able to repair itself alone. The heterotrophic formation of bone induced by devitalized demineralized bone matrix has been indicated as a very interesting way of treating bone defects, as it has osteoinductive properties due to the presence of soluble growth factors on its composition [1].

Bone loss occurs due to many pathologies, trauma, or as a consequence of surgical procedures. Several techniques for the treatment of bone defects have been proposed, including the use of several types of grafts, membranes, and the association of both techniques [1].

Mineral trioxide aggregate (MTA) is a powder aggregate containing mineral oxides that have no cytotoxicity and good biological response. It stimulates tissue repair by increasing cellular adhesion, growth, and proliferation at its surface. The use of MTA has been shown to cause an overgrowth of cementum and on facilitating the regeneration of the periodontal ligament as well as the deposition of new bone [2–10].

Previous histological reports have indicated that MTA stimulates the formation of bone or cementum on both periodontal or in artificial bone defects [2–10]. In addition, MTA has antibacterial properties [9], enhanced tissue dissolution, and also induces bone formation [10]. It has been suggested that a rise in pH induced by calcium hydroxide combined with the availability of Ca^{2+} and OH^- ions causes stimulation of the enzymatic pathways and, therefore, on bone mineralization [11].

Guided bone regeneration (GBR) is a technique based on the guided tissue regeneration (GTR) procedure that has been in use for more than a decade [12] and it is used to stimulate wound healing and to favor the regeneration of tooth-supporting structures [13]. The use of GBR associated with the use of biomaterials has been considered to be beneficial for the healing of bones [1].

We have shown that the use of near-infrared laser phototherapy (NIR-LPT) is effective in bone repair, including its association with biomaterials [1, 14–17]. We demonstrated that the improvement of bone neoformation and maturation on irradiated subjects is associated with the increased deposition of calcium hydroxyapatite (CHA) during the early stages of healing and that maturation represents increased secretion by osteoblasts on irradiated subjects. Large amounts of CHA on bone are indicative of a more resistant and calcified bone [1, 14–17].

It is known that laser phototherapy (LPT) has the ability to stimulate cell proliferation, including fibroblasts, which

have the capacity to secrete collagen, the main organic component observed during bone repair [1, 14–17].

Light emitting diodes (LEDs) are solid-state semiconductor devices that contain a single p–n junction, that is, the junction of a p-type layer where the carriers are positively charged holes and an n-type layer in which current is carried by mobile electrons. LEDs are complex and able to convert electrical current into incoherent narrow-spectrum light. Emitted light is now available at wavelengths ranging from ultraviolet (UV) to visible to near-infrared (NIR) bandwidth (247–1,300 nm). A significant difference between lasers and LEDs is the way the light energy is delivered. LEDs provide a much gentler delivery of the same wavelengths of light compared to lasers and at a substantially lower energy output. LEDs do not deliver enough power to damage tissues and do not have the same risk of accidental eye damage that lasers do [18].

Several studies, both *in vitro* and *in vivo*, have shown that LEDPT influences tissue repair. However, a full understanding of the mechanisms involved in this is not yet achieved. It seems possible that LEDPT presents beneficial effects similar to the ones observed when LPT is used, as several reports on the benefits of the use of LEDs operating at different wavelengths have been published elsewhere both *in vitro* and *in vivo* on both normal and pathologic conditions [19–27]. It is also possible that the mechanism involved may be similar.

Although several reports have suggested benefits of the isolated or combined use of MTA, BMPs, and GBR on the repair of bone defects, their use in association with LED phototherapy has not yet been studied. It might be possible that the observed benefits of the isolated use of each one could be improved with their association, as near-infrared LED light may be able to reproduce satisfactorily many of the effects of near-infrared laser light already reported elsewhere in the literature [1, 14–17].

The rationale for the association of MTA, BMPs, and LED light in this work was based on the idea that BMPs combined with an osteoconductive substance, such as the MTA, and LED light (with its well-recognized positive effects on cell proliferation and functioning as well as on the increase secretion of many growth factors) would improve the repair of bone defects in a manner similar to that observed when using an autogenous bone graft while avoiding the complications and limitations associated with autogenous bone grafting, which up to now remains as the gold standard for treating bone defects.

As suggested by previous reports in the current literature, LPT is capable of improving bone healing. In addition, it is possible that the use of LED light associated with the MTA may also improve the outcome of the treatment of bone defects. Thus, the aim of the present investigation was to study, histologically, the effect of NIR LEDPT on the healing

of bone defects grafted or not with MTA and associated or not with the use of BMPs and GBR on a rodent model.

Materials and methods

The Animal Ethics Committee of the Vale do Paraíba University¹ approved this work. Ninety healthy adult male Wistar rats (~2 months old, average weight 295 ± 25 g) were kept under natural conditions of light, humidity, and temperature at the Animal House of the Research and Development Institute of the Vale do Paraíba University during the experimental period. The animals were fed with standard laboratory pelleted diet and had water ad libitum. The animals were kept in groups of five on individual metallic cages; kept at day/night light cycle and controlled temperature during the experimental period. The animals were randomly distributed into ten groups and then subdivided into three subgroups according to the animal death timing. The distribution of the animals may be seen in Table 1.

Prior to intramuscular general anesthesia, the animals received 0.04 ml/100 g of atropine subcutaneously. The anesthesia was carried out with 10% ketamine (0.1 ml/100 g²)+2% xylazine (0.1 ml/100 g³). The animals had their right leg shaved and a 3-cm-long incision was performed at the right tibia with a no. 15 scalpel blade. Skin and subcutaneous tissues were dissected down to the periosteum, which was gently sectioned exposing the bone and a standard partial thickness 2-mm-round defect was surgically produced (low speed drill, 1,200 rpm, under refrigeration) in each animal.

The animals in groups II and I were filled only with the blood clot. Subjects in group II were further irradiated with LED light. The bone defects on the remaining groups were filled with MTA⁴+collagen gel.⁵ The animals of group IV were further irradiated with LED light. In groups V and VI, the bone defects, filled with the MTA, were covered with a reabsorbable membrane.⁶ The animals of group VI were further irradiated with LED light. In groups VII and VIII, a pool of BMPs⁷ was added to the biomaterial (MTA) and was further irradiated with LED light. In groups IX and X, the MTA+BMP graft was covered with the membrane. Subjects in group X were further irradiated with LED light. All wounds were routinely sutured and the animals received a single dose of Pentabiotico^{®8} (0.02 ml/100 g, penicillin,

streptomycin, 20,000 IU) immediately after surgery. Animal death occurred after 15, 21, and 30 days after the surgery with an overdose of general anesthetics.

LEDPT was carried out with the FioLED[®] device⁹ ($\lambda 850 \pm 10$ nm, 150 mW (0.15 W), area=0.5 cm², 54 s, 0.3 W/cm², 16 J/cm², 16 J), was transcutaneously applied over the defect at 48-h intervals (16 J/cm²) being the first session carried out immediately after surgery and repeated at every 48 h for 15 days (16 J/cm² per session) and a total treatment dose of 112 J/cm². Doses used here were based upon previous studies using laser light carried out by our group [1, 14–17].

Following animal death, the samples were longitudinally cut under refrigeration (Buehler[®], Isomet TM1000; Markham, Ontario, Canada) and the specimens kept on 10% formalin solution for 24 h. The specimens were routinely processed to wax, cut and stained with hematoxylin and eosin and Sirius red, and then underwent histological analysis at the Laboratory of Surgical Pathology of the School of Dentistry of the Federal University of Bahia by two experienced pathologists in a blind manner using a light microscope (AxioStar[®], Zeiss, Germany). The criteria used in the histological analysis are shown in Table 2 and were previously used by our team [1, 14–17]. Statistical analysis was carried out using Minitab 15 Software. Significance level was set at 5%.

Results

Clot

On day 15, the defect was partially filled with newly formed bone displaying non-aligned osteocytes with each other as well as thin and irregular trabeculi. Medullar tissue and moderate chronic inflammation were seen and scored as discrete. Osteoblastic activity could be seen and there were no signs of reabsorption (Fig. 1a). On day 21, the defect was mostly filled with new bone and it was more regular than at day 15, and with moderate chronic inflammation. Some specimens showed remnants of cartilaginous tissue and no signs of reabsorption were seen. At the end of the experimental period, the defect was completely filled by lamellar bone and few Haversian systems were seen. The trabeculi were more regularly disposed and showed some osteocytes and remnants of cartilage surrounded by bone. Neither reabsorption nor inflammation was observed.

MTA

At day 15, the defect was filled by neofomed bone characterized by interconnecting trabeculi showing osteocytes on its

¹ Approved, April 11, 2006, Law 6.638/1979

² Syntec do Brasil, Cotia, SP, Brazil

³ Syntec do Brasil, Cotia, SP, Brazil

⁴ Angelus[®], Angelus Indústria de Produtos Odontológicos S/A, Londrina, PR, Brazil

⁵ Gencol[®], Baumer S.A., Mogi das Cruzes, São Paulo, Brazil

⁶ Gendorm[®], Baumer S.A., Mogi das Cruzes, São Paulo, Brazil

⁷ Gemp[®], Baumer S.A., Mogi das Cruzes, São Paulo, Brazil

⁸ Fort Dodge Ltda, Campinas, SP, Brazil

⁹ MMÓptics, São Carlos, São Paulo, Brazil

Table 1 Distribution of the experimental groups

Group	Subgroup	n	Protocol
I	I15 / I21 / I30	9	Clot
II	II15 / II21 / II30	9	LED
III	III15 / III21 / III30	9	MTA
IV	IV15 / IV21 / IV30	9	MTA+LED
V	V15 / V21 / V30	9	MTA+guided bone regeneration
VI	VI15 / VI21 / VI30	9	MTA+Guided bone regeneration+LED
VII	VII15 / VII21 / VII30	9	MTA+bone morphogenetic proteins
VIII	VIII15 / VIII21 / VIII30	9	MTA+bone morphogenetic proteins+LED
IX	IX15 / IX21 / IX30	9	MTA+bone morphogenetic proteins+guided bone regeneration
X	X15 / X21 / X30	9	MTA+bone morphogenetic proteins+guided bone regeneration+LED

matrix and osteoblasts at the surface. Remnants of cartilage and moderate chronic inflammation were also seen dispersed within a fibro-vascular tissue. A few points of surface necrosis and remnants of the biomaterial could be seen. Discrete bone reabsorption was observed at this stage (Fig. 1b). At day 21, the defect was covered by a regular neoformed bone dispersed in few medullar spaces and discrete chronic inflammation was observed. On this, osteocytes were seen as well as basophilic reversal lines, and osteoblasts at the osseous surface. At the end of the experimental time, the defect was filled by bone showing discrete inflammation. Small bone trabeculi and medullar tissue, surface necrosis, discrete bone reabsorption and remnants of the biomaterial were also observed at this time.

MTA + GBR

At day 15, the defect was filled by interconnecting bone trabeculi showing non-aligned osteocytes with each other and active osteoblasts arranged as a lining at the periphery of bone trabeculi. In a few cases, delicate bone fragments many times immature were seen within highly vascularized medullar tissue. In some specimens, surface necrosis could be seen. In this group, beneath this necrosis, a band of

fibrous connective tissue was detected as well as moderate chronic inflammatory infiltrate and remnants of the biomaterial. At day 21, the defect was filled by a thick newly formed bone showing many times interconnecting bone trabeculi in addition to discrete chronic inflammation, non-aligned osteocytes, and basophilic reversal lines. Areas of superficial necrosis were also observed in some specimens as well as remnants of the biomaterial. At the end of the experimental time, the defect was filled by bone characterized by few medullar spaces, irregular small bone fragments, and discrete chronic inflammation. In a few specimens, remnants of cartilage could be seen as well as tissue necrosis extending down to the medulla. Remnants of the biomaterial were also seen at this stage (Fig. 1c).

MTA + BMP

At day 15, the defect was filled by interconnecting bone trabeculi, few medullar spaces, non-aligned osteocytes with each other and active osteoblasts arranged as a lining at the periphery of bone trabeculi. Evident bone reabsorption was seen. At the surface, a band of fibrous connective tissue and small areas of necrosis could be seen as well as remnants of the biomaterial (Fig. 1d). On the other hand, at day 21, the

Table 2 Semi-quantitative criteria used for the light microscopy analysis

Score criterion	Discrete	Moderate	Intense
Bone reabsorption	Presence of <25% of the reabsorption of the graft remnants and/or the surgical bed	Presence of 25–50% of the reabsorption of the graft remnants and/or the surgical bed	Presence of >50% of the reabsorption of the graft remnants and/or the surgical bed
Bone neoformation	Presence of <25% of newly formed bone similar to adjacent untreated bone tissue	Presence of 25–50% of newly formed bone similar to adjacent untreated bone tissue	Presence of >50% of newly formed bone similar to adjacent untreated bone tissue
Inflammatory infiltrate	Presence of <25% of neutrophils on the area	Presence of 25–50% of neutrophils on the area	Presence of >50% of neutrophils on the area
Collagen deposition	Presence of <25% of collagen deposition in the area.	Presence of 25–50% of collagen deposition in the area.	Presence of >50% of collagen deposition in the area.

newly formed bone was thick and irregular, showing irregular osteocytes and few medullar spaces. In a few cases, a band of fibrous connective tissue and remnants of the biomaterial covered the surface of the defect. These remnants were associated with foreign-body reaction, and there were signs of bone reabsorption. At the end of the experimental period, necrotic debris were seen at the surface as well as macrophages and bony fragments extending down to the center of the defect. The core of the defect showed irregular bone trabeculi and osteocytes. All periods of time studied showed discrete chronic inflammation.

MTA + BMP + GBR

At day 15, there was surface necrosis extending down to the core, irregular bone fragments, and few remnants of the biomaterial associated with macrophages. In many cases, area of necrosis was observed beneath a band of fibrous tissue. Large number of bony fragments associated with basophilic reversal lines and a large amount of remnants of cartilage were noticed in addition to evident bone reabsorption. Irregular osteoid tissue was also seen at this stage (Fig. 1e). At day 21, the defect was filled by newly formed tissue showing either regular or irregular deposition. Irregular osteocytes, basophilic reversal lines, and a few medullar spaces were also seen. At the surface, besides the presence of remnants of the biomaterial, a band of fibrotic tissue was also seen as well as evidence of bone reabsorption and moderate chronic inflammation. At the end of the experimental time, the defect was partially or completely filled by newly formed bone displaying non-aligned osteocytes and few medullar spaces. In some cases, at the surface, a band of fibrous tissue and remnants of the biomaterial were seen. No inflammation was found.

LED

At day 15, the defect was mostly filled by cancellous bone showing irregular trabeculi displaying irregular osteocytes within it. Osteoblasts were occasionally observed at the trabeculi surface (Fig. 1f). Evidence of bone reabsorption was seen at this time and rare cells inflammatory. At day 21, the aspect was similar to that observed at day 15. However, fewer medullar spaces were seen. No sign of reabsorption was seen at this stage. At the end of the experimental period, the defect was filled by newly formed bone showing a small number of medullar spaces. A focal area of reabsorption was seen in one case. Inflammation was only observed at the 15 day.

MTA + LED

At day 15, a band of fibrotic tissue covered the defect. The defect was partially filled by interconnecting irregular

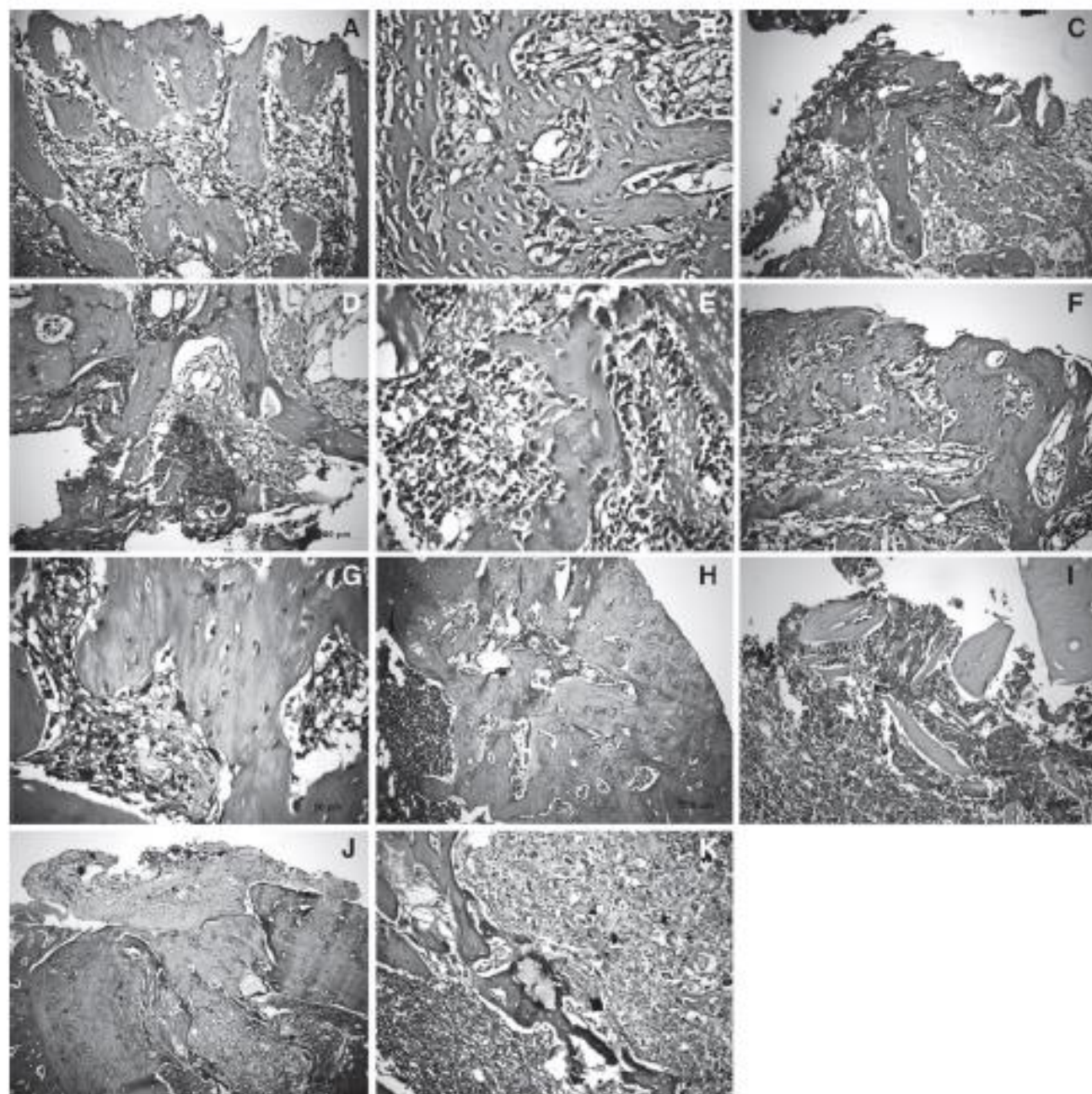
trabecular bone showing non-aligned osteocytes, basophilic reversal lines, and active osteoblasts that were arranged as a lining at the periphery of bone trabeculi. These findings were observed dispersed on a highly vascularized connective tissue that contained young fibroblasts as well as neutrophils or lymphocytes. Areas of focal bone reabsorption on the newly formed bone were also seen (Fig. 1g). At day 21, a large amount of delicate bone trabeculi containing osteocytes was seen exhibiting osteoblastic activity. No sign of reabsorption was seen. At the end of the experimental time, interconnecting bone trabeculi either delicate or thick showing osteocytes within them or few medullar spaces mostly filled the defect. Some level of osteoblastic activity was visible as well as areas of reabsorption. All periods of time studied showed discrete chronic inflammation.

MTA + GBR + LED

At day 15, the defect was partially filled by irregular trabecular bone showing also osteocytes. These trabeculi were mostly projected towards the medulla. Sometimes irregular bony fragments were seen partially filling the defect. In both cases, the bone was associated with medullar tissue and to a band of tissue fibrosis and rare neutrophils. Some remnants of cartilaginous tissue were also seen. No evidence of reabsorption was noticed. At day 21, the defect remained partially filled by an irregular and of variable thickness interconnected trabeculi containing osteocytes sometimes projecting themselves to the medulla. Some evidence of reabsorption and moderate chronic inflammatory infiltrate were seen at this stage. At the end of the experimental period, the defect was filled by either regular thick trabecular bone or by lamellar bone containing osteocytes and basophilic reversal lines, and these trabeculi were projecting themselves towards the borders of the cavity bridging the edges. Some specimens showed active giant cells (Fig. 1h) and moderate chronic inflammation.

MTA + BMP + LED

At day 15, an irregular trabecular bone of variable thickness containing non-aligned osteocytes filled the defect. Sometimes irregular bony fragments were observed partially filling the defect. On both cases, the bone was dispersed on medullar tissue with intense chronic inflammation. Some areas of reabsorption and remnants of the biomaterial were seen at this stage. At day 21, the defect was filled by trabecular bone of variable thickness and containing non-aligned osteocytes and basophilic reversal lines and osteoblastic activity and medullar tissue. Superficial necrosis was occasionally seen and beneath it granulation tissue rich in macrophages and lymphocytes were observed. Remnants of the biomaterial, macrophages, and Langerhans cells were



also seen (Fig. 11). At the end of the experimental time, the defect was covered by a regular and delicate bone trabeculi containing osteocytes; basophilic reversal lines and Haversian system were also observed at this stage. Beneath the defect, the replacement of the medullar tissue by a fibrosis and remnants of the biomaterial was observed. Discrete inflammatory reaction was seen at this stage.

MTA + BMP + GBR + LED

At day 15, the defect was partially filled by an interconnected trabecular bone, sometimes irregular;

exhibiting non-aligned osteocytes, basophilic reversal lines, and active osteoblasts arranged as a lining at the periphery of bone trabeculi. The bone tissue was dispersed on medullar tissue and a mononuclear inflammatory reaction could be seen at this stage. Remnants of the biomaterial and areas of focal necrosis were also observed. On day 21, trabecular bone and medullar tissue as well as remnants of the biomaterial and areas of focal necrosis filled the defect. At the end of the experimental period, the defect was filled by a mass of bone tissue exhibiting Haversian systems and osteocytes. Many times, the newly formed bone was bridging the edges. Medullar tissue and remnants of the biomaterial were also

Fig. 1 a Photomicrograph of a specimen from the clot group showing the bone defect filled by newly formed bone with non-aligned osteocytes, basophilic lines, and rimmed with osteoblasts, amidst fibrous tissue and mild chronic inflammation. b Photomicrograph of a specimen from the MTA group evidencing the bone defect filled by newly interconnecting and formed bone with and non-aligned osteocytes; in some areas, active multinucleated giant cells are observed. c Photomicrograph of a specimen from the MTA+GBR group showing the bone defect with areas of necrosis and biomaterial remnants at the surface, followed by newly formed bone displaying non-aligned osteocytes sometimes rimmed with osteoblasts. Cartilaginous tissue remnants are also observed. d Photomicrograph of a specimen from the MTA+BMP group evidencing the bone defect filled with newly formed bone displaying remnants of cartilage, amidst medullar tissue; in some areas, the latter is replaced by necrosis due to the biomaterial. e Photomicrograph of a specimen from the MTA+BMP+GBR group showing the defect with newly formed bone displaying osteoid rimmed with osteoblasts, and multinucleated giant cells on the surface. f Photomicrograph of a specimen from the LED group showing, on the right, the bone defect filled by a more mature bone tissue, displaying plump osteoblasts at the trabecular surface. g Photomicrograph of a specimen from the MTA+LED group evidencing the bone defect filled by newly formed bone with non-aligned osteocytes, basophilic lines, and few active giant cells. Also note the presence of chronic inflammatory cells. h Photomicrograph of specimen of a specimen from the MTA+GBR+LED group showing, on top left, newly formed bone represented by a extensive trabecular bone arising from bone defect and displaying basophilic reverse lines, non-aligned osteocytes, cartilage remnants, and medullar tissue. i Photomicrograph of a specimen from the MTA+BMP+LED group showing, at the defect surface, remnants of the biomaterial, areas with necrosis and bone spicules of variable thickness. Eventually, Langhans-like cells were also seen. j Photomicrograph of a specimen from the MTA+BMP+GBR+LED group showing the defect filled by newly formed bone arising from of the surgical margins, whose surface shows fibrous band with remnants of the biomaterial. k Extending down, there are macrophages, foreign-body reaction and the graft incorporated into bone, appearing as a crystalloid

seen. Close to the fragments, foreign-body reaction was seen as well as rare lymphocytes. In all cases, remnants of the biomaterial were still observed close to a fibrous band and area of surface necrosis. The graft was already incorporated to the bone and often showed a crystalline aspect (Fig. 1j, k).

Morphometric analysis

From the morphometric analysis, we may notice that the use of the MTA graft caused a reduction of the inflammatory reaction, increased collagen deposition, bone reabsorption, and new bone formation. On the other hand, when the GBR technique was used together with the MTA, this caused a similar response from the bone on regarding all parameters. When the BMP was associated with the MTA, there was reduction of the inflammation, and increase on both bone reabsorption and deposition. Associating both GBR and BMP to the MTA graft only increased bone reabsorption (Fig. 2a, b, c, d, e).

The morphometric analysis showed that when the defect was irradiated with the LED, no inflammatory reaction was

seen. When the LED was associated with the MTA+GBR, the inflammatory reaction was increased. Collagen deposition and bone deposition were increased and bone reabsorption was reduced. Using LED light on the MTA+BMP graft caused an increase in the inflammatory reaction, on collagen deposition as well as on both bone reabsorption and deposition. When the LED was used on the association of MTA+BMP+GBR, both collagen and bone deposition were increased (Fig. 2f, g, h, i, j).

Statistical analysis

Statistical analysis showed that defects irradiated with LED had significantly less inflammation than in all other groups irradiated or not ($p < 0.001$). On the other hand, inflammation was significantly less on the defects filed only with clot when compared to groups MTA, MAT + LED, MTA+GBR, MTA+BMP ($p = 0.05$). However, the opposite was observed when the clot group was compared to the MTA+BMP + LED group and was similar to all others groups. Collagen deposition was significantly increased on groups MTA + GBR, MTA + BMP + LED and MTA + BMP + GBR + LED when compared to all other ($p = 0.05$). Bone reabsorption was similar on groups clot, MTA + GBR, LED and MTA, and significant less than in all other groups ($p = 0.05$). On the other hand, the groups LED, MTA + GBR + LED, MTA + BMP + LED and MTA + BMP + GBR + LED showed significantly higher bone deposition when compared to all other groups ($p = 0.05$) (Fig. 3a, b, c, d).

Discussion

As far as we are concerned, this is probably the first histological report on the use of the association of LED light and MTA graft. The present investigation aimed to describe histologically the mechanisms of the repair bone defects treated or not with LED light, biomaterial, and GBR technique.

Despite the success we have observed using different light sources associated with bone repair using different models, our knowledge of the bone regeneration process and light interactions is still limited. Therefore, further molecular, cellular, and translational studies are required to obtain a better understanding of the actions and interactions of the different regulators of the regeneration process and the qualitative assessment of the tissue response is important as it provides a picture of the processes. This was the reason why we decided to carry out description of the repair histologically. This study was designed to carry out both quantitative and semi-quantitative assessment of the repair process and this work is one of the first reports of its kind. The description of the process considered an appropriated

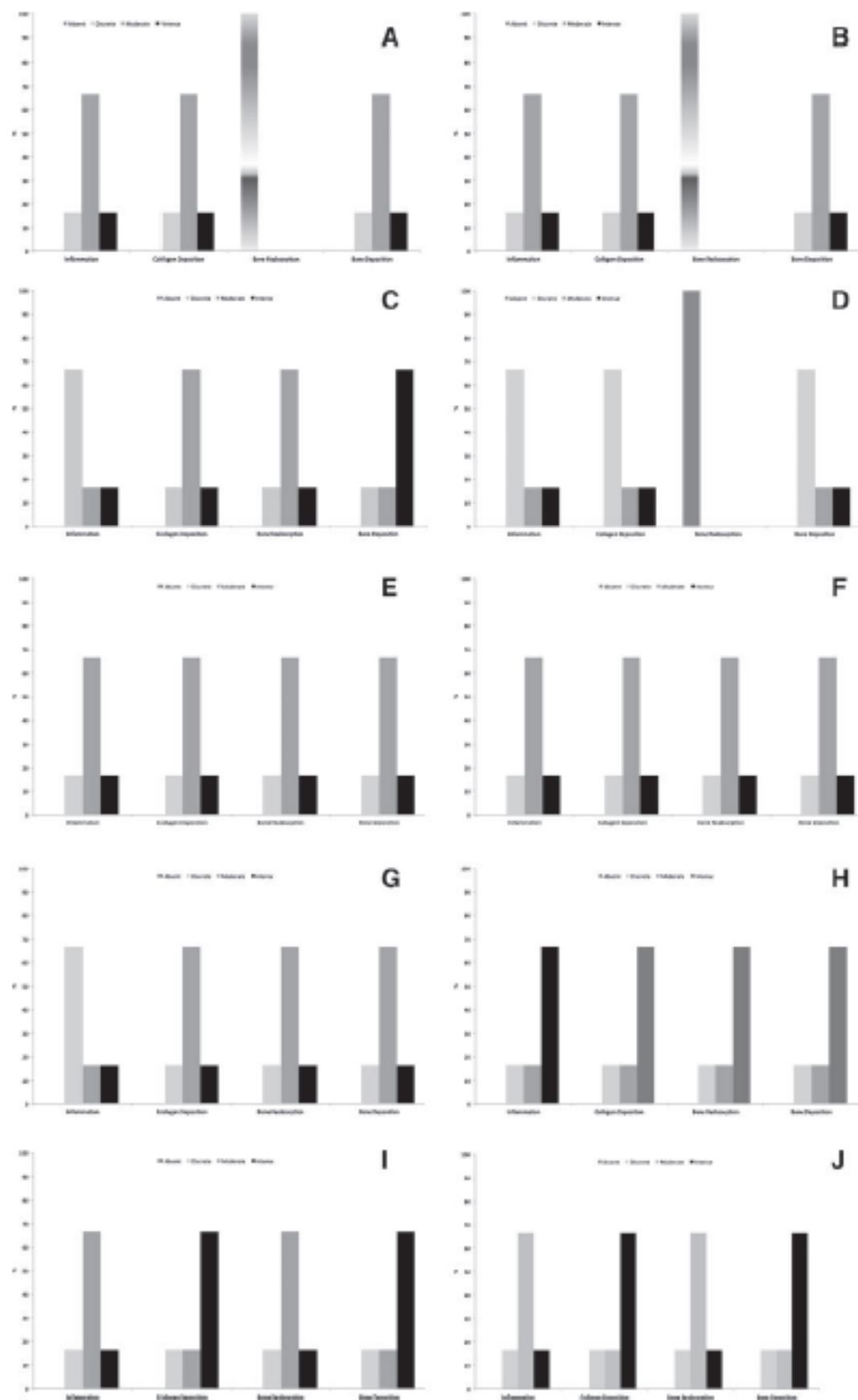


Fig. 2 Summary of the morphometric analysis of each individual group according with the parameters studied: a clot group, b MTA group, c MTA+BMP group, d MTA+GBR group, e MTA+BMP+GBR group, f LED group, g MTA+LED group, h MTA+BMP+LED group, i MTA+GBR+LED group, j MTA+BMP+GBR+LED group

method of assessing the effects of different techniques used both isolated or in combination, allowing us to have a qualitative “picture” of the process [1, 14–17].

We have recently described this process by using Raman spectroscopic analysis on a study using NIR laser showing that the observed results of the Raman study were very mostly aligned with the histological findings of the present study. On the Raman study, we found that laser-irradiated subjects showed significantly higher levels of CHA in the earlier period of healing. However, these levels were similar to the observed when the association of MTA + BMP + GBR + laser was used. The lowest levels of deposition were observed when MTA + laser and MTA + GBR were used. At the end of the experimental period, all defects were found to be similar. However, higher levels of CHA were seen on group MTA + GBR + laser and lower on group MTA + laser. As increased peaks of CHA are indicative of bone maturation, the association of MTA, GBR, and laser resulted

in a more advanced repair. So we decided to change the light source in order to verify if similar results could be achieved [28].

In the present study, we opted to use a larger bone defect instead of a critical size one intending to increase the severity of the damage to the bone. It is important to note that a similar model has been in use by our group for more than a decade and its effectiveness is well reported elsewhere in the literature [1, 14–17].

One may question if the follow-up period of 30 days used in the present study is enough to test bone healing as some previous studies (using the rat tibia as animal model) have used longer follow-up periods. However, our team has successfully reported this time line using different models of bone defects as well as different assessment models [1, 14–17, 28].

Visible/NIR-LED light therapy has been deemed as a non-significant risk by the FDA and has been approved for use in humans. Other advantages over lasers include the possibility of combining wavelengths with an array of various sizes. LED disperses over a greater surface area than lasers and may be used where large areas are targeted, resulting in faster treatment times [26].

LED PT is the newest category of non-thermal light therapies to find its way to the dental armamentarium and

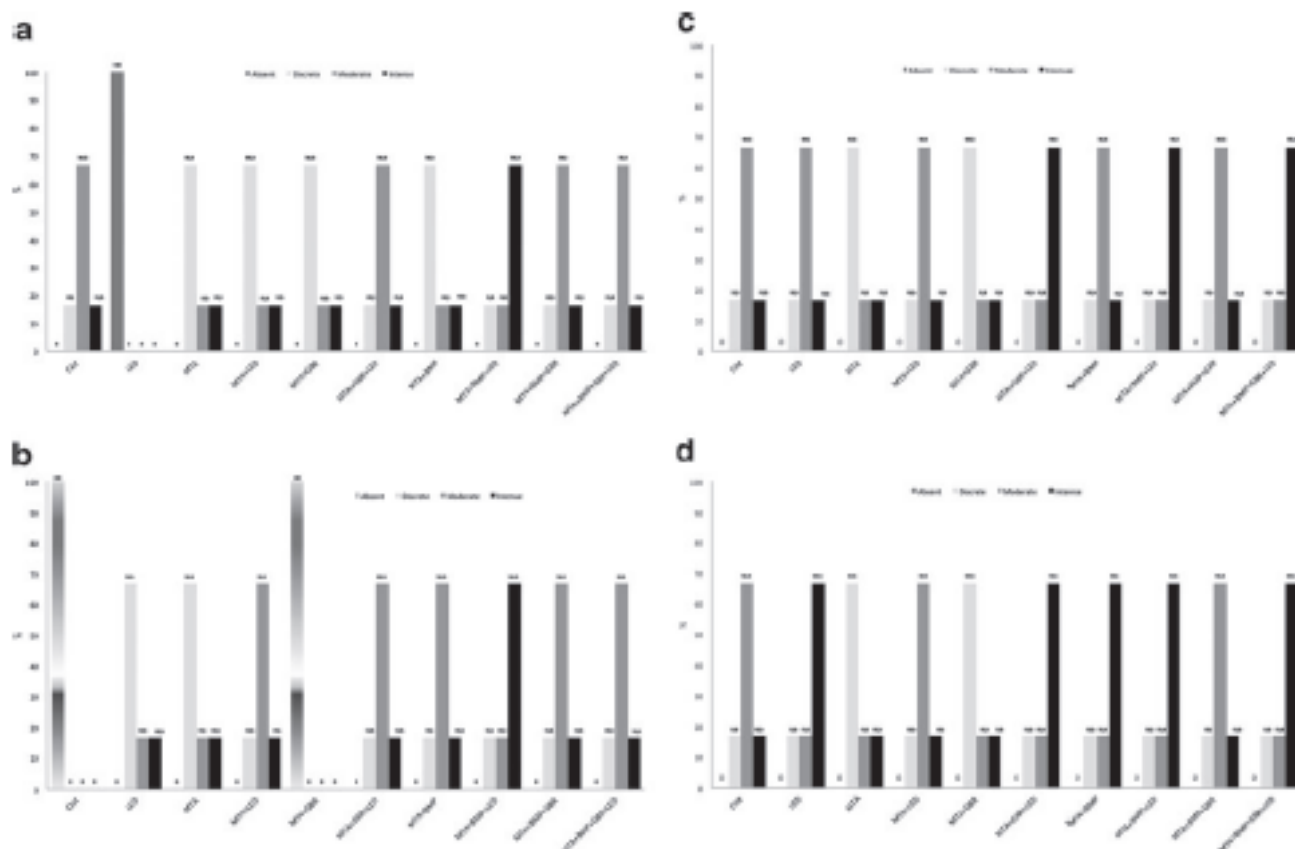


Fig. 3 Summary of morphometric analysis. a Inflammatory reaction, b bone resorption, c collagen deposition, and d bone resorption

was mainly developed by the National Aeronautics and Space Administration (NASA) that has investigated the use of LED therapy in wound healing and obtained positive results [26, 27]. Visible/NIR-LED light treatments at various wavelengths have been shown to significantly increase cell growth in a diversity of cell lines, including murine fibroblasts, rat osteoblasts, rat skeletal muscle cells, and normal human epithelial cells [27].

Over the past years, our group has been working extensively on the study of the effects of the use of phototherapy (NIR laser) on bone using different animal models. In these studies, we have also used many assessment methods to determine the effects of the phototherapy on bone including the use of histology, computerized morphometry, SEM, and Raman spectroscopy [1, 14–17, 28].

In all previously used protocols, models, and parameters, we were able to demonstrate that the use of laser light caused important tissue responses during healing and these were responsible for a quicker repair process as well as on the improved quality of the newly formed bone [1, 14–17, 28].

We found differences amongst all groups during all experimental timing. At an early stage, untreated subjects showed no signs of reabsorption, but the use of the MTA caused the appearance of areas bone reabsorption. This may have been caused by the MTA that probably acted as a local irritant even on being biocompatible. When the MTA was associated with GBR we observed crystalloid structures that may be attributable to the MTA as the anhydrous phases of the MTA involve the formation of crystals, an important physiologic event in the formation of the bone [29]. Again, these changes might be attributed to the presence of the biomaterial. The addition of BMPs to the MTA did not significantly improve the process. When the MTA + BMP graft was associated with GBR, the major observed change was the presence of a large number of bony fragments associated with basophilic reversal lines and a large amount of remnants of cartilage as well as a irregular osteoid tissue. This was a major difference that may be attributed to the GBR.

Later on, untreated controls and MTA-grafted subjects showed a similar healing pattern as seen at early stages, however, the newly formed bone was somewhat more regular. The MTA seemed to cause a small delay in the repair process. The use of the GBR caused the presence of a thick newly formed bone. The increased thickness might have been caused by the GBR technique. Adding BMPs to the biomaterial caused the appearance of thick and irregular newly formed bone and remnants of the graft and caused foreign-body reaction without reabsorption. The use of the BMPs might have caused more bone deposition during the repair. The use of the GBR to the association of MTA and BMPs caused no major improvement.

At the end of the experimental period, the controls showed the defect completely filled by lamellar bone. On MTA-grafted subjects, despite the defect being filled by bone, the trabeculi were small and thin. Adding GBR caused the presence of newly formed bone characterized by a few medullar spaces and the presence of irregular small bone fragments. The addition of BMPs caused the appearance necrotic debris that was seen at the surface as well as macrophages and bony fragments extending down to the center of the defect. The core of the defect showed irregular bone trabeculi. The use of MTA, BMPs, and GBR caused the presence of newly formed bone.

LED-irradiated subjects showed early formation of irregular trabecular cancellous bone and no signs of reabsorption up to the day 21. At the end of the experimental period, the defect was filled by newly formed bone. The association of MTA + LED resulted in an early deposition of interconnecting irregular trabecular bone. Later, the defect was filled by a delicate bone trabeculi. At the end of the experimental time, interconnecting bone trabeculi of irregular thickness and few medullar spaces filled the defect. When GBR was associated with the MTA + LED, at early stages, the defect was partially filled by irregular trabecular bone and a band of tissue fibrosis and remnants of cartilage were present. At the end of the experimental period, a regular thick trabecular bone projecting itself towards the borders of the cavity bridging the edges was seen. The use of the association of MTA + BMP + LED did not cause many changes other than those observed with the use of the MTA alone. The use of the MTA + BMP + GBR + LED caused a more advanced repair and at the end of the experimental period, the defect was filled by a mass of bone tissue exhibiting Haversian systems and osteocytes, characteristic of mature bone. The newly formed bone was bridging the edges, closing the defect. However, remnants of the MTA were still seen and these were associated with foreign-body reaction and were placed close to a fibrotic band and area of focal surface necrosis. The graft that was already incorporated to the bone and many times showed a crystalline aspect.

The comparison of our results with other previous reports is difficult. This is the first report of the use of this model in particular to the use of the MTA and LED. Our previous experience using other types of biomaterials and light source already reported in the literature is also suggestive that the association of NIR LPT with biomaterials causes improvement in the repair of bone defects. We found similar responses to the ones observed in previous studies using NIR LPT [1, 14–17].

MTA, due to its characteristics, seemed not to be directly affected by LED light. It is assumed that the MTA would act as a framework for the deposition of new bone as it is considered a osteoconductor material. However, the use of LEDPT positively affects bone healing around the graft

similarly to what was observed on different studies carried out by our team using other biomaterials and NIR-LPT. We were not able to find any previous reports on the association of the MTA with BMPs in the literature. Despite that we have shown that the use of BMPs improves the outcome of bone healing when associated with LPT, in the present study, it was not the case. This was probably due to the properties of the MTA.

It has also been demonstrated by our group that the use of GBR is helpful in the healing of bone defects and that the association with LPT improves the outcome of this therapeutic approach, as demonstrated previously by our team using different models [1, 14–17]. In the present study, despite some improvement in the overall healing process, no major effect was seen. This was probably due to the characteristics of the MTA.

Several reports indicated that laser and LEDs emitting between 630 and 1,000 nm presents stimulatory effects both in vitro and in vivo [30–32]. A study using polychromatic LEDs [30] suggested that this light source shows a similar pattern of stimulation/inhibition as observed when using lasers. A previous report showed that both laser and LED irradiation causes vasodilatation in vivo [31] and another study showed similar results in comparing laser and a LED regarding angiogenesis [32]. There is evidence that both LED and laser light at the same wavelength may result in similar biochemical effects [33, 34].

In the present study, we opted for using an in vivo model and not an in vitro one as the animal model allowed us a more detailed and “close” to human tissue response analysis of the different treatments carried out as well as the host-responses to them. The host response on the in vitro model is very limited or not possible of simulation in many aspects. For instance, despite a recent study [35] that has found in vivo adhesion of osteoblasts to MTA, an in vitro report [36] using osteoblasts failed to get cell adhesion to MTA. In the present study, we often observed a close contact of the graft with the bone matrix and possibly inducing the formation of important components for bone neoformation as a result of the interaction of the MTA, the matrix and the host [37–39]. Then, biological responses may be similarly detected using different assessment methods.

The use of LED light alone dramatically reduced inflammation. However, its use in MTA associated with BMP and/or GBR increased the severity of the inflammatory reaction. Regarding bone reabsorption, a less significant result was seen when the LED light was associated with the MTA + BMP graft. In the groups clot and MTA + GBR, no bone reabsorption was detectable. Increased collagen deposition was observed when the LED light was associated with the use of the MTA associated with BMP and/or GBR. Increased new bone formation was observed when the LED light was used alone or associated with the use of MTA +

GBR, MTA + BMP, on association of MTA + BMP + GBR and when BMP was added to the MTA.

The question these days is no longer whether LEDs have biological effects on bone tissue as well as on the outcome of the use of biomaterials, but rather what the optimal light parameters are for different uses as the biological effect depends on the parameters of the irradiation, similar to the use of lasers, such as wavelength, dose, intensity, irradiation time, and mode of emission. Furthermore, clinically, factors such as the frequency, intervals between treatments, and total number of treatments shall be considered.

Conclusions

Our results indicate that the use of LED light alone or in association with MTA, MTA + BMP, MTA + GBR and MTA + BMP + GBR caused less inflammation, increased both collagen deposition as seen on both histological and morphometric analysis.

Acknowledgements We would like to thank the Conselho Nacional de Desenvolvimento Científico e Tecnológico - CNPq for providing financial support for this project.

Author disclosure statement I certify that I have no affiliation with, or financial involvement in, any organization or entity with a direct financial interest in the subject matter or materials discussed in the manuscript.

References

1. Pinheiro ALB, Gerbi MEMM (2006) Photoengineering of bone repair processes. *Photomed Laser Surg* 24: 169–178
2. Torabinejad M, Hong CU, Lee SJ, Monsef M, Pitt Ford TR (1995) Investigation of mineral trioxide aggregate for root end filling in dogs. *J Endod* 21:603–608
3. Torabinejad M, Hong CU, Pitt Ford TR (1995) Physical properties of a new root end filling material. *J Endod* 21:349–353
4. Torabinejad M, Hong CU, Pitt Ford TR, Kaiyawasam SP (1995) Tissue reaction to implanted super-EBA and mineral trioxide aggregate in the mandible of guinea pigs: a preliminary report. *J Endod* 21:569–571
5. Torabinejad M, Chivian N (1999) Clinical applications of mineral trioxide aggregate. *J Endod* 25:197–205
6. Al-Rabieah E, Peninganayagam H, MacFarland D (2006) Human alveolar bone cells interact with ProRoot and tooth-colored MTA. *J Endod* 32:872–875
7. Regan JD, Gutmann JL, Witherspoon DE (2002) Comparison of Diaket and MTA when used as rootend filling materials to support regeneration of the periradicular tissues. *Int Endod J* 35:840–847
8. Moreton TR, Brown JR CE, Legan JJ, Kafrawy AH (2000) Tissue reactions after subcutaneous and intramuscular implantation of mineral trioxide aggregate and ethoxybenzoic acid cement. *J Biomed Mat Res* 52:528–533
9. Bystrom A, Claesson R, Sundqvist G (1995) The antibacterial effect of camphorated paramonochlorophenol, camphorated phenol

- and calcium hydroxide in the treatment of infected root canals. *Endod Dent Traumatol* 170–175
10. Mitchell PJ, Pitt Ford TR, Torabinejad M, McDonald F (1999) Osteoblast biocompatibility of mineral trioxide aggregate. *Biomater* 20:167–173
11. Tronstad L, Andreasen JO, Hasselgren G, Kristenson L, Riis I (1980) pH changes in dental tissues after root canal filling with calcium hydroxide. *J Endod* 7:17–21
12. Garrett S (1996) Periodontal regeneration around natural teeth. *Ann Periodontol* 621–666
13. Stahl SS, Froum S, Tarnow D (1990) Human histologic responses to guided tissue regenerative techniques in intrabony lesions. Case reports on 9 sites. *J Clin Periodontol* 17:191–198
14. Pinheiro ALB, Gerbi MEMM, Limeira Junior FA, Ponzi EAC, Marques AMC, Carvalho CM, Santos RC, Oliveira PC, Nôia M, Ramalho LMP (2009) Bone repair following bone grafting hydroxyapatite guided bone regeneration and infrared laser photobiomodulation: a histological study in a rodent model. *Lasers Med Sci* 24:234–240
15. Gerbi MEMM, Marques AMC, Ramalho LMP, Ponzi EAC, Carvalho CM, Santos RC, Oliveira PC, Nôia M, Pinheiro ALB (2008) Infrared laser light further improves bone healing when associated with bone morphogenetic proteins and guided bone regeneration: an in vivo study in a rodent model. *Photomed Laser Surg* 26:167–174
16. Torres CS, Santos JN, Monteiro JSC, Amorim PG, Pinheiro ALB (2008) Does the use of laser photobiomodulation, bone morphogenetic proteins, and guided bone regeneration improve the outcome of autologous bone grafts? An in vivo study in a rodent model. *Photomed Laser Surg* 26:371–377
17. Gerbi MEMM, Pinheiro ALB, Ramalho LMP (2008) Effect of IR laser photobiomodulation on the repair of bone defects grafted with organic bovine bone. *Lasers Med Sci* 23:313–317
18. Barolet D (2008) Light-emitting diodes (LEDs) in dermatology. *Semin Cutan Med Surg* 27:227–238
19. Al-Watban FA, Andres BL (2006) Polychromatic LED in oval full-thickness wound healing in non-diabetic and diabetic rats. *Photomed Laser Surg* 24:10–16
20. Weiss RA, McDaniel DH, Geronemus RG, Weiss MA, Beasley KL, Munavalli GM, Bellew SG (2005) Clinical experience with light emitting diode (LED) photomodulation. *Dermatol Surg* 31:1199–1205
21. Desmet KD, Paz DA, Cory JJ, Edls JT, Wong-Riley MT, Henry MM, Buchmann EV, Connelly MP, Dovi JV, Liang HL, Henshel DS, Yeager RL, Millsap DS, Lin J, Gould LJ, Das R, Jett M, Hodgson BD, Margolis D, Whelan HT (2006) Clinical and experimental applications of NIR-LED photobiomodulation. *Photomed Laser Surg* 24:121–128
22. Lazzafame RJ, Stadler I, Whelan HT (2002) NASA LED photoradiation influences nitric oxide and collagen production in wounded rats. *Lasers Surg Med Suppl* 14:12
23. Tachian R, Farinelli WA, Rox Anderson R (2002) Low intensity light-induced vasodilation in vivo. *Lasers Surg Med Suppl* 14:11
24. Vinck EM, Cagnie BJ, Cornelissen MJ, Declercq HA, Cambier DC (2005) Green light emitting diode irradiation enhances fibroblast growth impaired by high glucose level. *Photomed Laser Surg* 23:167–171
25. Higuchi A, Watanabe T, Noguchi Y, Chang Y, Chen W, Matsuoka Y (2007) Visible light regulates neurite outgrowth of nerve cells. *Cytotechnology* 54:181–188
26. Whelan HT, Smits JR RL, Buchmann EV, Whelan NT, Turner SG, Margolis DA, Cavenini V, Stinson H, Ignatius R, Martin T, Cwiklinski J, Philippi AF, Gmf WR, Hodgson B, Gould L, Kane M, Chen G, Caviness J (2001) Effect of NASA light emitting diode irradiation on wound healing. *J Clin Laser Med Surg* 19:305–314
27. Whelan HT, Buchmann EV, Whelan NT, Turner SG, Cavenini V, Stinson H, Ignatius R, Martin T, Cwiklinski J, Meyer GA, Hodgson B, Gould L, Kane M, Chen G, Caviness J (2001) NASA light emitting diode medical applications: from deep space to deep sea. *Space Technology and Applications International Forum*, pp 35–45
28. Pinheiro ALB, Aciole GTS, Cangussú MCT, Pacheco MTT, Silveira L Jr (2010) Effects of laser phototherapy on bone defects grafted with mineral trioxide aggregate, bone morphogenetic proteins, and guided bone regeneration: a Raman spectroscopic study. *J Biomed Mater Res A* 95(4):1041–1047
29. Lee YL, Lee BS, Lin FH, Lin AY, Lan WH, Lin CP (2004) Effects of physiological environments on the hydration behavior of mineral trioxide aggregate. *Biomater* 25:787–793
30. Al-Watban FA, Andres BL (2003) Polychromatic LED therapy in burn healing of non-diabetic and diabetic rats. *J Clin Laser Med Surg* 21:249–258
31. Tachiana R, Farinelli WA, Rox Anderson R (2002) Low intensity light-induced vasodilation in vivo. *Lasers Surg Med* 30:11
32. Corazza AV, Jorge J, Kurachi C, Bagnato VS (2007) Photobiomodulation on the angiogenesis of skin wounds in rats using different light sources. *Photomed Laser Surg* 25:102–106
33. Karu TI (2003) Low-power laser therapy. In: Frame JW (ed) *Biomedical photonics handbook*. CRC Press, Boca Raton, p 48
34. Sommer AP, Pinheiro AL, Mester AR, Franke RP, Whelan HT (2001) Biostimulatory windows in low-intensity laser activation: lasers, scanners, and NASA's light-emitting diode array system. *J Clin Laser Med Surg* 19:29–33
35. Perinpanayagam H (2009) Cellular response to mineral trioxide aggregate root-end filling materials. *J Can Dent Assoc* 75:369–372
36. Perez AL, Spears R, Gutman JL, Opperman A (2000) Osteoblasts and MG-63 osteosarcoma cells behave differently when in contact with ProRoot MTA and White MTA. *Int End J* 36:564–570
37. Camilleri J, Pitt Ford TR (2006) Mineral trioxide aggregate: a review of the constituents and biological properties of the material. *Int End J* 39:747–754
38. Morreton TR, Brown CE, Legan JJ, Kafrawy AH (2000) Tissue reactions after subcutaneous and intramuscular implantation of mineral trioxide aggregate and ethoxybenzoic acid cement. *J Biomed Mater Res* 52:528–533
39. Saidon J, He J, Zhu Q, Safavi K, Spangberg LSW (2003) Cell and tissue reactions to mineral trioxide aggregate and Portland cement. *Oral Surg Oral Med Oral Path Oral Rad End* 95:483–489

Lasers Med Sci. 2013 Feb;28(2):513-8. doi: 10.1007/s10103-012-1096-1. Epub 2012 Apr 24.

The efficacy of the use of IR laser phototherapy associated to biphasic ceramic graft and guided bone regeneration on surgical fractures treated with miniplates: a Raman spectral study on rabbits

The efficacy of the use of IR laser phototherapy associated to biphasic ceramic graft and guided bone regeneration on surgical fractures treated with miniplates: a Raman spectral study on rabbits

Antonio L. B. Pinheiro · Nicole Ribeiro Silva Santos ·
Priscila Chagas Oliveira ·
Gilberth Tadeu Santos Aciole · Thais Andrade Ramos ·
Tayná Assunção Gonzalez · Laís Nogueira da Silva ·
Artur Felipe Santos Barbosa · Landulfo Silveira Junior

Received: 4 October 2011 / Accepted: 9 April 2012
© Springer-Verlag London Ltd 2012

Abstracts The aim of the present study was to assess, by Raman spectroscopy, the repair of surgical fractures fixed with internal rigid fixation (IRF) treated or not with IR laser ($\lambda 780$ nm, 50 mW, 4×4 J/cm²–16 J/cm², $\phi=0.5$ cm², CW) associated or not to the use of hydroxyapatite and guided bone regeneration (GBR). Surgical tibial fractures were created under general anesthesia on 15 rabbits that were divided into five groups, maintained on individual cages, at day/night cycle, fed with solid laboratory pelleted diet and had water ad libitum. The fractures in groups II, III, IV and V were fixed with miniplates. Animals in groups III and V were grafted with hydroxyapatite and GBR technique used. Animals in groups IV and V were irradiated at every other

day during 2 weeks (4×4 J/cm², 16 J/cm²–112 J/cm²). Observation time was that of 30 days. After animal death, specimens were taken and kept in liquid nitrogen and used for Raman spectroscopy. Raman spectroscopy showed significant differences between groups ($p < 0.001$). Basal readings showed mean value of $1,234 \pm 220.1$. Group internal rigid fixation + biomaterial + laser showed higher readings ($3,521 \pm 2,670$) and group internal rigid fixation + biomaterial the lowest (212.2 ± 119.8). In conclusion, the results of the present investigation are important clinically as spectral analysis of bone component evidenced increased levels of CHA on fractured sites by using the association of laser light to a ceramic graft.

A. L. B. Pinheiro (✉) · N. R. S. Santos · P. C. Oliveira ·
G. T. S. Aciole · T. A. Ramos · T. A. Gonzalez · L. N. da Silva ·
A. F. S. Barbosa
Center of Biophotonics, School of Dentistry,
Federal University of Bahia,
Av. Araújo Pinho, 62, Camela,
Salvador, Bahia CEP: 40110-150, Brazil
e-mail: albp@ufba.br

N. R. S. Santos
e-mail: ribeironicole@hotmail.com

P. C. Oliveira
e-mail: pchagas2005@yahoo.com.br

G. T. S. Aciole
e-mail: gilberthaciole@hotmail.com

T. A. Ramos
e-mail: thais_andradeamos@hotmail.com

T. A. Gonzalez
e-mail: tayna_gonzalez@yahoo.com.br

L. N. da Silva
e-mail: lay_lica@hotmail.com

A. F. S. Barbosa
e-mail: arturfelipea@gmail.com

A. L. B. Pinheiro · L. S. Junior
Universidade Camilo Castelo Branco,
São José dos Campos, São Paulo 12245-230, Brazil
e-mail: land-jr@uol.com.br

A. L. B. Pinheiro
Instituto Nacional de Ciência e Tecnologia de Óptica e Fotônica,
São Carlos, São Paulo 13560-970, Brazil

L. S. Junior
Universidade Camilo Castelo Branco Núcleo do Parque
Tecnológico de São José dos Campos,
Rodovia Presidente Dutra, km. 138—Distrito de Eugênio de Melo,
São José dos Campos CEP 12247-004 São Paulo, Brazil

Keywords Biomaterials · Bonerepair · Internal rigid fixation · Phototherapy

Introduction

A fracture is a loss of the integrity of the bone and its structure fails and occurs when bone cannot withstand an intense force. The healing of a fracture is an extremely interesting process, and in optimal conditions, injured bone may be reconstituted without scarring [1–4].

The repair of fractures, bony defects, periodontal pockets and alveolar socket are typical examples of processes involving bone remodeling. Despite being extensively studied over the past years, many studies have tried to develop techniques to improve the treatment of bone defects. These techniques include the use of different types of grafts, the use of membranes and bone morphogenetic proteins (BMPs) or the combinations of them [1–18].

Fractures have been treated with immobilization, traction, amputation, and internal fixation throughout history. Immobilization by casting, bracing, or splinting a joint above and below the fracture was used for most long bone fractures. The treatment of fractures consists of the reduction and fixation of dislocated segments. Internal fixation is used in the treatment of fractures as it provides sufficient stability for fracture healing without excessive rigidity. The choice of the type of internal fixation depends on the type of fracture, the condition of the soft tissues and bone, the size and position of the bone fragments, and the size of the bony defect [1–4, 19–21].

Many types of biomaterials have been used instead of using autologous grafts to minimize the morbidity of the procedures avoiding two simultaneous surgical procedures. One of the most commonly used biomaterial is the hydroxyapatite (HA; calcium HA—CHA). This type of graft may be produced using different composition and shape. It may be used isolated, associated to the use of a membrane (guided bone regeneration—GBR), or mixed to an autologous bone graft [22]. Recently, the use of phototherapy has been proposed as a method to improve bone repair under different protocols, including the association to biomaterials and GBR [1–9, 14, 16].

Raman spectroscopy is a vibrational spectroscopic technique that may be used to optically probe the molecular changes associated with diseased tissues. This vibrational spectroscopic technique is relatively simple, reproducible, nondestructive to the tissue, and only small amounts of material (micrograms to nanograms) with a minimum sample preparation are required. In addition, these techniques provide molecular-level information, allowing investigation of functional groups, bonding types and molecular conformations. Spectral bands in vibrational spectra are molecule

specific and provide direct information about the biochemical composition. These bands are relatively narrow, easy to resolve and sensitive to molecular structure, conformation and environment [23].

Our group has strong evidences that the improvement of the maturation of irradiated bone is associated to an increased deposition of CHA during early stages of healing. This maturation may represent an increased secretion by osteoblasts on irradiated subjects. It is well accepted that deposition of CHA represents bone maturation being larger amounts of CHA on bone indicative of a more resistant and calcified bone [1–5, 11]. The aim of the present study was to assess, by Raman spectroscopy, the repair of fractures fixed with miniplates (internal rigid fixation—IRF) treated or not with a biphasic ceramic graft associated or not with GBR and irradiated or not with 1780 nm laser on an animal model.

Materials and methods

The Animal Ethics Committee of the School of Dentistry of the Federal University of Bahia has approved this research. Fifteen healthy adult male New Zealand rabbits (~8 months old, mean weight 2 kg) were kept under natural conditions of light, humidity, and temperature at the Laboratory of Animal Experimentation of the School of Dentistry of the Federal University of Bahia during the experimental period. The animals were fed with standard laboratory pelleted diet and had water *ad libitum*. The animals were kept in individual metallic cages, kept at day/night light cycle and controlled temperature during the experimental period. The animals were randomly distributed into five groups (Table 1).

Prior to intramuscular general anesthesia, the animals received acepromazine (2 mg/kg Acepran® 0.2 %; Univet S.A, Cambuci, SP, Brazil). The anesthesia was carried out 20 min later with ketamine (Ketalar®, 50 mg/ml 0.4 ml/kg; Lab. Parke Davis Ltda, São Paulo, São Paulo, Brazil) and 2 % xylazine (Rompum®, 20 mg/ml 0.2 ml/kg; Lab. Bayer Health Care S.A, São Paulo, São Paulo, Brazil). The animals had the right leg shaved, and a 3-cm-long incision was

Table 1 Description and distribution of the groups

Group	Procedure	Description
I	Basal bone	Control—no fracture
II	IRF	Fracture fixed with miniplate only
III	IRF + B	Fracture fixed with miniplate + Genphos® + Gen-dent®
IV	IRF + L	Fracture fixed with miniplate + laser
V	IRF + B + L	Fracture fixed with miniplate + Genphos® + Gen-dent® + laser

performed at the right tibia with a no. 15 scalpel blade. Skin and subcutaneous tissues were dissected down to the periosteum, which was gently sectioned exposing the bone. A complete surgical tibial fracture was created on animals in groups II, III, IV and V with a carborundum disk (Moyco Union Broach, York, PA, USA) under water refrigeration.

Animals in group II had the bone fragments fixed with miniplates only (Sistema 2.0 PROMM®; Comércio de Implantes Cirúrgicos Ltda, Porto Alegre, Rio Grande do Sul, Brazil). Animals in groups III and V were grafted with the 0.5-mm particle ceramic graft (GenPhos® HATCP, BAUMER®; Mogi Mirim, São Paulo, Brazil) and covered with a demineralized bovine bone membrane (Gen-derm®, BAUMER®; Mogi Mirim) prior similar fixation used on group I (Fig. 1). Animals in groups IV and V were further irradiated with laser light (λ780 nm, 50 mW, CW, spot area of 0.5 cm², TWIN FLEX®; MM Optics, São Carlos, São Paulo, Brazil).¹ The irradiation started immediately after treatment prior suturing (16 J/cm², 4×4 J/cm², 9 J) and was transcutaneously repeated at every other day during 2 weeks. After suturing (4-0 polyglactin, TRUSINTH®; Sutures India Pvt Ltd, Bangalore, Karnataka, India) and 4-0 nylon (TRUSINTH®, Sutures India Pvt Ltd.), the animals received intramuscular antibiotics (Pentabiotico®, penicillin, streptomycin, 20,000 UI 0.2 ml/kg IM; Lab. Forte Dogde Saúde Animal Ltda, Campinas, São Paulo, Brazil) and Banamine® (flunixin meglumine, 10 mg/ml, 0.1 ml/kg IM; Intervet Shering-Plough Animal Health, Cruzeiro, São Paulo, Brazil).

Following animal death 30 days after fracture, the samples were longitudinally cut under refrigeration (Bueler®, Isomet TM1000; Markham, ON, Canada) and stored in liquid nitrogen to minimize the growth of aerobics bacteria and because the chemical fixation is not advisable due to fluorescence emissions from the fixative substances [1–5, 11, 13].

Prior to Raman study, the samples were longitudinally cut and warmed gradually to room temperature and 100 ml of saline was added to the surface during spectroscopic measurements. For Raman measurements, a Raman system (P-1; Lambda Solutions, Inc., MA, USA) was used. Acquisition and storage of the Raman data were done in a PC (Dell Inspiron modelo 1501) and RamaSoft® software (Lambda Solutions, Inc.). The laser power used at the sample site was of 100 mW with spectral acquisition time 10 s. Three points were measured at the fractured site of each specimen. All spectra were collected at the same day to avoid optical misalignments and changes in laser power. The mean value of the intensity of the peak (~958 cm⁻¹, phosphate ν₁) was determined by the average of the peaks on this region. This intensity is related to the concentration of CHA of the bone. For calibration, the Raman spectrum of the solvent Indene with



Fig. 1 Experimental design. The fracture was fixed with miniplates. When necessary, the biomaterial and membrane were used

known peaks was used due to its intense bands (800–1,800 cm⁻¹) in the fingerprint region [1–5, 11, 13].

The indene spectrum was also measured each time the sample was changed to be sure that the laser and collection optics were optimized. In order to remove the “fluorescence background” from the original spectrum, a fifth-order polynomial fitting was found to give better results facilitating the visualization of the peaks of CHA (~958 cm⁻¹) found on the bone. A baseline Raman spectrum of nontreated bone (group I) was also produced and acted as control (Fig. 2). The data were analyzed by the MatLab5.1® software (Newark, New Jersey, USA) for calibration and background subtraction of the spectra. Statistical analysis was performed using Minitab 15.0® software (Minitab, Belo Horizonte, Minas Gerais, Brazil).

Results

The Raman spectrum of bone shows prominent vibrational bands related to tissue composition (mineral and organic

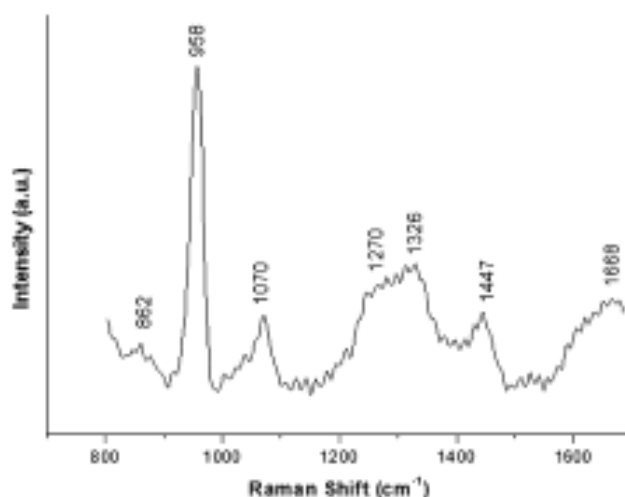


Fig. 2 Bone main Raman bands at 862, 958, 1,070, 1,270, and 1,326, 1,447 and 1,668 cm⁻¹

¹ The manufacturer calibrated the equipment before the experimentation.

matrices). Figure 2 shows the bone main Raman bands at 862, 958, 1,070, 1,270, and 1,326, 1,447 and 1,668 cm^{-1} . The band at 1,668 cm^{-1} and the ones at 1,270 and 1,326 cm^{-1} are attributed to amide I and III stretching modes of lipids and proteins; the band at 1,447 cm^{-1} is attributed to the bending and stretching vibration modes of CH groups of lipids and proteins. The ones at 958 and 1,070 cm^{-1} are attributed to phosphate and carbonate hydroxyapatite from bone mineral, respectively; the band at 862 cm^{-1} may be attributed to the vibration bands of C–C stretch of collagen (tyrosine/proline ring) [1–5, 11, 13].

Figure 3 shows the mean spectra (dislocated) of CHA ($\sim 958 \text{ cm}^{-1}$) on control and treated animals. The intensity of the Raman shift is directly related to the concentration/incorporation of CHA by the bone. So, higher intensity represents higher concentration of CHA. Basal readings showed a mean value of $1,234 \pm 220.1$. Groups IRF + biomaterial (B) + laser (L) showed higher readings ($3,521 \pm 2,670$) and group IRF + B the lowest (212.2 ± 119.8 , Fig. 4). Table 2 shows a summary of the statistical analysis.

Discussion

The animal model used on the present investigation is usual as the responses observed during bone repair in

rabbits are similar to the ones seen in humans [1–5, 11, 13]. Raman spectroscopy can be used to access the molecular constitution of a specific tissue and then classify it according to differences observed in the spectra [23–25]. Several studies found elsewhere on the literature has shown successful use of Raman spectroscopy as a diagnostic tool for healthy, diseased or healing bones [1–5, 11, 13, 23–26].

Of all of the biomaterials used to improve bone healing, HA is the most investigated one on both clinical and histological grounds. This biomaterial has been found to be effective in improving bone formation. Several techniques for the correction of bone defects have been proposed, amongst them the use of several types of grafts and membranes, and the combination of both techniques. It is accepted that although HA has osteoconductivity, the repair of the defect may be slow because of the need of the graft to be reabsorbed, slowing down the process. It is clear that the use of a graft prevents fibrosis of the lesion and also protects the cavity and acts as a framework for the deposition of newly formed bone [1, 6, 15, 16].

On the present study, the assessment of the CHA ($\sim 958 \text{ cm}^{-1}$) was chosen as it represents the peak of phosphated hydroxyapatite, which is one of the major components of mineralized bones [1–5]. Our previous results

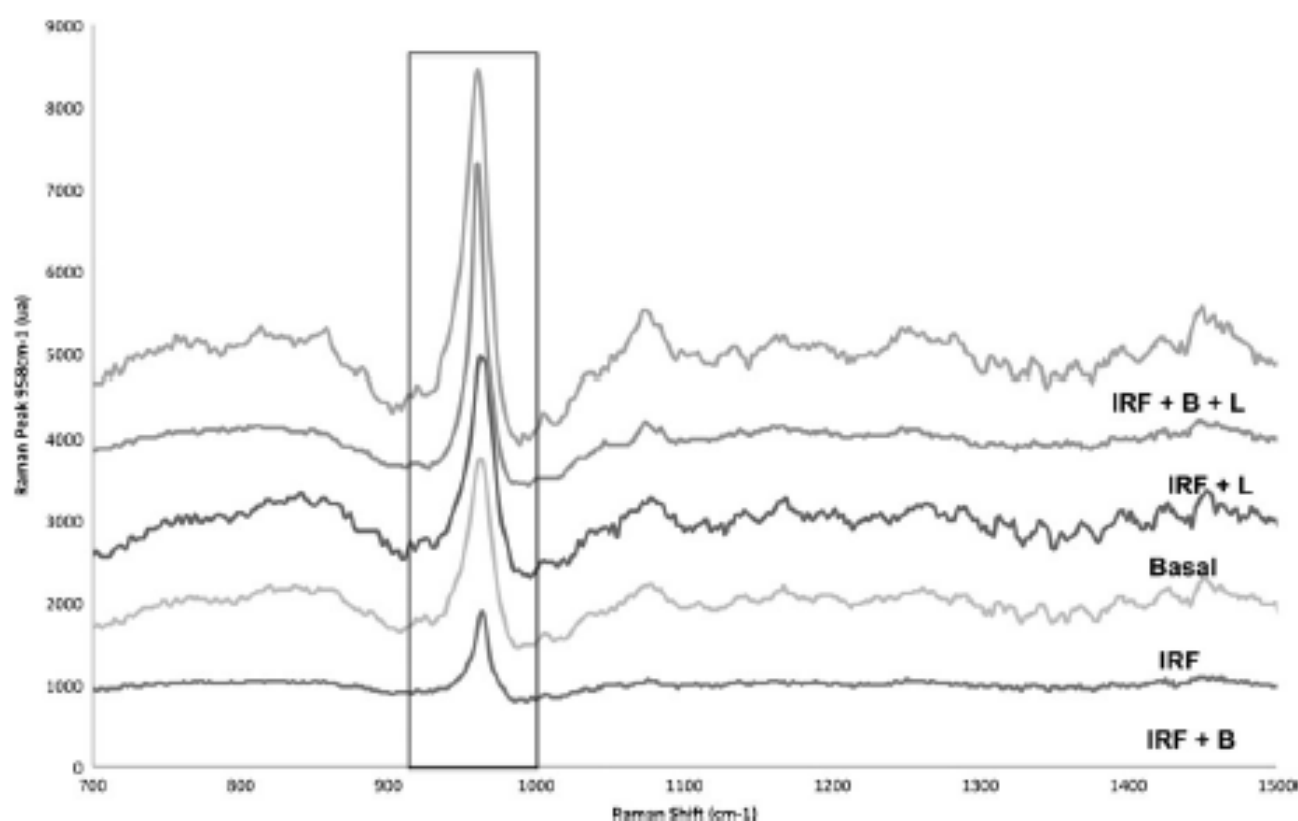
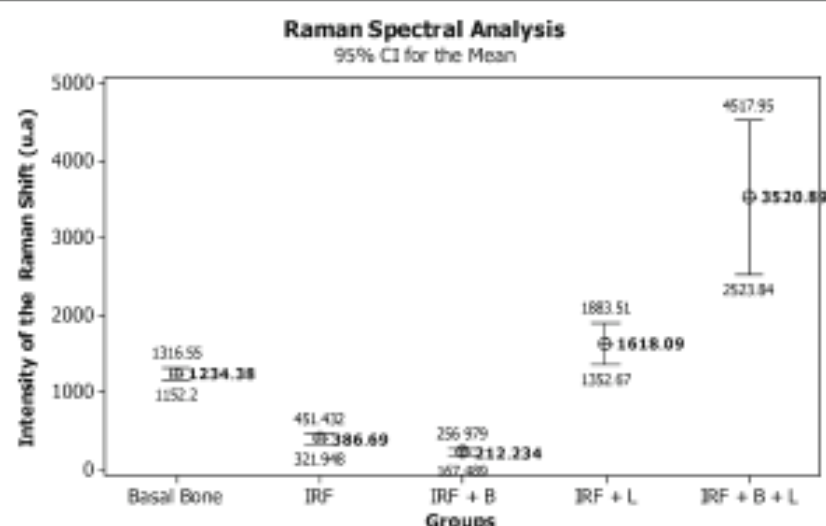


Fig. 3 Mean spectra of CHA ($\sim 958 \text{ cm}^{-1}$) on control and treated animals

Fig. 4 Graphical representation of the Raman data. Basal readings showed a mean value of $1,234 \pm 220.1$. Groups IRF + B + L showed higher readings ($3,521 \pm 2,670$) and group IRF + B the lowest (212.2 ± 119.8)



indicate that NIR LPT is effective to improve bone repair mainly due to its higher penetration into bone when compared to visible laser light [1–18].

On this study we used a similar model previously reported by our team in which a different biomaterial was used (2). On the previous study we assessed the level of CHA ($\sim 958 \text{ cm}^{-1}$) on complete fractures animals treated with IRF treated or not with low-level laser therapy (LLLT) and associated or not to BMPs and GBR using Raman spectroscopic analysis, and concluded that the use of near-infrared (NIR) LLLT associated to BMPs and GBR was effective in improving bone healing on fractured bones due to increased levels of CHA as determined by Raman data [2].

On the present investigation, higher Raman peaks on animals treated with IRF + B + L were observed. This might be attributable to increased levels of CHA on the site. This finding is aligned with previous reports in which other type of biomaterial containing CHA associated to laser light was used [1–5, 11, 13].

It is important to make clear that the use of this experimental protocol was due to the fact that it is known that the isolated use of HA, GBR, and laser brings benefits on many clinical situations. However, the association used on the present study remains poorly explored elsewhere in the literature. We decided to assess the combination of different protocols in order to verify if the positive effect already described on the literature could be improved or if disadvantages could be ameliorated.

The results of the present study indicated that the level of CHA on nontreated bone differed significantly from the observed on animals of all experimental groups. This result was expected as the pattern and stage of repair differed among the different treatments used. It would be desirable that the intensities were close to the one observed on normal

bone that would represent that the mineralization of the fractured bone. This was not observed when the IRF was used alone probably due to the fact that at the end of the experimental period, the gap of the fractured site was still on a more precocious stage of repair. The animals treated with IRF only showed significant lower intensity of CHA when compared to all experimental groups except the one seen on animals treated with the association to the biomaterial, when the intensity was lower. The use of the membrane also caused a decrease of the peak. This was probably due to an attenuation of the passage of light through the membrane reducing the amount of energy delivered to the tissue. The reason for this may be due to the fact that the insertion of the graft widened the gap and caused a delay of the mineralization as more time would be necessary to complete the repair of a larger area. However, when the biomaterial was associated to the laser, the intensity of the CHA peak increased in an impressive manner (Table 2).

The association of the IRF with the laser light caused a significant increase of the intensity of the peak of CHA when compared to all groups except when the laser was

Table 2 Mean and standard deviation of the peaks of the Raman peak of CHA ($\sim 958 \text{ cm}^{-1}$) on the groups

Group	Mean \pm SD
Basal	$1,234.4 \pm 220.1$ bcde*
(IRF)b	386.7 ± 73.4 acde*
(IRF + B)c	212.2 ± 119.8 abde*
(IRF + L)d	$1,618 \pm 711$ abce*
(IRF + B + L)e	$3,521 \pm 2,670$ abed*

Letters on right hand side column indicate the occurrence of significant differences between groups on the left hand side column

* $p \leq 0.05$

associated to the biomaterial and IRF that presented the highest intensity being also this difference significant. This finding is fully aligned with previous reports from our group that showed that irradiated bone, mostly with IR wavelengths, shows increased osteoblastic proliferation, collagen deposition, increased deposition of CHA and bone neoformation when compared to non-irradiated bone. The protocol used on the present study is similar to those used on previous reports from our team using different models [1–18]. In conclusion, the results of the present investigation are important clinically as spectral analysis of bone component evidenced increased levels of CHA on fractured sites by using the association of laser light to a ceramic graft.

References

- Carvalho FB, Aciole GTS, Aciole JMS, Silveira-Junior L, Santos JN, Pinheiro ALB (2011) Assessment of bone healing on tibial fractures treated with wire osteosynthesis associated or not with infrared laser light and biphasic ceramic bone graft (HATCP) and guided bone regeneration (GBR): Raman spectroscopy study. *Proceedings—SPIE 7887: 7887OT-1–7887OT-6*
- Lopes CB, Pacheco MTT, Silveira-Junior L, Cangussu MC, Pinheiro ALB (2010) The effect of the association of near infrared laser therapy, bone morphogenetic proteins, and guided bone regeneration on tibial fractures treated with internal rigid fixation: a Raman spectroscopic study. *J Biomed Mater Res Part A* 94:1257–1263
- Pinheiro ALB, Lopes CB, Pacheco MTT, Bragnera A, Zanin FAA, Cangussu MCT, Silveira-Junior L (2010) Raman spectroscopy validation of DIAGNOdent-assisted fluorescence readings on tibial fractures treated with laser phototherapy, BMPs, guided bone regeneration, and miniplates. *Photomed Laser Surg* 28:89–97
- Lopes CB, Pacheco MT, Silveira-Junior L, Duarte J, Cangussu MCT, Pinheiro ALB (2007) The effect of the association of NIR laser therapy BMPs, and guided bone regeneration on tibial fractures treated with wire osteosynthesis: Raman spectroscopy study. *J Photochem Photobiol B* 89:125–130
- Pinheiro ALB, Aciole GTS, Cangussu MCT, Pacheco MTT, Silveira-Junior L (2010) Effects of Laser phototherapy on bone defects grafted with mineral trioxide aggregate, bone morphogenetic proteins, and guided bone regeneration: a Raman spectroscopic study. *J Biomed Mater Res A* 95:1041–1047
- Pinheiro ALB, Gerbi MEMM, Limeira Junior FA et al (2009) Bone repair following bone grafting hydroxyapatite guided bone regeneration and infrared laser photobiomodulation: a histological study in a rodent model. *Lasers Med Sci* 24:234–240
- Gerbi MEMM, Marques AMC, Ramalho LMP et al (2008) Infrared laser light further improves bone healing when associated with bone morphogenetic proteins: an in vivo study in a rodent model. *Photomed Laser Surg* 26:55–60
- Pinheiro ALB, Gerbi MEMM, Ponzi EAC et al (2008) Infrared laser light further improves bone healing when associated with bone morphogenetic proteins and guided bone regeneration: an in vivo study in a rodent model. *Photomed Laser Surg* 26:167–174
- Tomes CS, Santos JN, Monteiro JC, Amorim PG, Pinheiro ALB (2008) Does the use of laser photobiomodulation, bone morphogenetic proteins, and guided bone regeneration improve the outcome of autologous bone grafts? An in vivo study in a rodent model. *Photomed Laser Surg* 26:371–377
- Gerbi MEMM, Pinheiro ALB, Ramalho LMP (2008) Effect of IR laser photobiomodulation on the repair of bone defects grafted with organic bovine bone. *Lasers Med Sci* 23:313–317
- Lopes CB, Pinheiro ALB, Sathiah S, Da Silva NS, Salgado MA (2007) Infrared laser photobiomodulation (830 nm) on bone tissue around dental implants: a Raman spectroscopy and scanning electronic microscopy study in rabbits. *Photomed Laser Surg* 25:96–101
- Weber JBB, Pinheiro ALB, Oliveira MG, Oliveira FAM, Ramalho LMP (2006) Laser therapy improves healing of bone defects submitted to autogenous bone graft. *Photomed Laser Surg* 24:38–44
- Lopes CB, Pinheiro ALB, Sathiah S, Ramalho LMP (2005) Infrared laser light reduces loading time of dental implants: a Raman spectroscopy study. *Photomed Laser Surg* 23:27–31
- Gerbi MEMM, Pinheiro ALB, Ramalho LMP et al (2005) Assessment of bone repair associated with the use of organic bovine bone and membrane irradiated at 830 nm. *Photomed Laser Surg* 23:382–388
- Pinheiro ALB, Limeira Junior FA, Gerbi MEMM (2003) Effect of low level laser therapy on the repair of bone defects grafted with inorganic bovine bone. *Braz Dent J* 14:177–181
- Pinheiro ALB, Limeira Junior FA, Gerbi MEMM et al (2003) Effect of 830-nm laser light on the repair of bone defects grafted with inorganic bovine bone and decalcified cortical osseous membrane. *J Clin Laser Med Surg* 21:383–388
- Pinheiro ALB, Oliveira MAM, Martins PPM (2001) Biomodulação da cicatrização óssea pós-implantar com o uso da laserterapia não-cirúrgica: estudo por microscopia eletrônica de varredura (Biomodulation of peri-implant bone repair with lasertherapy: SEM study). *Rev FOUFBA* 22:12–19
- Silva Junior N, Pinheiro ALB, Oliveira MGA, Weismann R, Ramalho LMP, Nicolau RA (2002) Computerized morphometric assessment of the effect of low-level laser therapy on bone repair: an experimental animal study. *J Clin Laser Med Surg* 20:83–88
- Alpha C, O'Ryan F, Alessandro S et al (2006) The incidence of postoperative wound healing problems following sagittal ramus osteotomies stabilized with miniplates and monocortical screws. *J Oral Maxillofac Surg* 64:659–668
- Erdogan O, Esen E, Ustun Y et al (2006) Effects of low-intensity pulsed ultrasound on healing of mandibular fractures: an experimental study in rabbits. *J Oral Maxillofac Surg* 64:180–188
- Chritah A, Lazow SK, Berger JR (2005) Transoral 2.0 mm locking miniplate fixation of mandibular fractures plus 1 week of maxillo-mandibular fixation: a prospective study. *J Oral Maxillofac Surg* 63:1737–1741
- Le Guhenec L, Layrolle P, Duculsi G (2007) A review of bio-ceramics and fibrin sealant. *Eur Cell Mater* 8:1–11
- Movasaghi Z, Rehman S, Ihtesham U, Rehman IU (2007) Raman spectroscopy of biological tissues. *Appl Spectrosc Rev* 42:498–541
- Nogueira GV, Silveira Junior L, Martin AA A, Zangaro RA, Pacheco MTT, Chavantes MC, Pasqualucci CA (2005) Raman spectroscopy study of atherosclerosis in human carotid artery. *J Biomed Opt* 10:031117–1–031117-7
- Penel G, Delfosse C, Descomps M, Lemy G (2005) Composition of bone and apatitic biomaterials as revealed by intravital Raman microspectroscopy. *Bone* 36:893–901
- Carden A, Morris MD (2000) Application of vibrational spectroscopy to the study of mineralized tissues (review). *J Biomed Opt* 5:259–268

Lasers Med Sci. 2013 May;28(3):815-22. doi: 10.1007/s10103-012-1166-4. Epub 2012 Jul 26.

The efficacy of the use of IR laser phototherapy associated to biphasic ceramic graft and guided bone regeneration on surgical fractures treated with wire osteosynthesis: a comparative laser fluorescence and Raman spectral study on rabbits

The efficacy of the use of IR laser phototherapy associated to biphasic ceramic graft and guided bone regeneration on surgical fractures treated with wire osteosynthesis: a comparative laser fluorescence and Raman spectral study on rabbits

Antônio Luiz Barbosa Pinheiro · Nicole Ribeiro Silva Santos ·
Priscila Chagas Oliveira · Gilberth Tadeu Santos Aciole ·
Thais Andrade Ramos · Tainá Assunção Gonzalez ·
Laís Nogueira da Silva · Artur Felipe Santos Barbosa ·
Landulfo Silveira Jr

Received: 4 October 2011 / Accepted: 12 July 2012
© Springer-Verlag London Ltd 2012

Abstract The aim of the present study was to assess, by Raman spectroscopy and laser fluorescence, the repair of surgical fractures fixed with wire osteosynthesis treated or not with infrared laser ($\lambda 780$ nm, 50 mW, 4×4 J/cm²–16 J/cm², $\phi=0.5$ cm², CW) associated or not to the use of hydroxyapatite and guided bone regeneration. Surgical tibial fractures were created under general anesthesia on 15 rabbits that were divided into five groups, maintained on individual cages, at day/night cycle, fed with solid laboratory pelted diet, and had water ad libitum. The fractures in groups II, III, IV, and V were fixed with wires. Animals in groups III and V were grafted with hydroxyapatite (HA) and guided bone regeneration (GBR) technique used.

Animals in groups IV and V were irradiated at every other day during 2 weeks (4×4 J/cm², 16 J/cm²–112 J/cm²). Observation time was that of 30 days. After animal death, specimens were taken and kept in liquid nitrogen and used for Raman spectroscopy. The Raman results showed basal readings of $1,234.38 \pm 220$. Groups WO+B+L showed higher readings ($1,680.22 \pm 822$) and group WO+B the lowest (501.425 ± 328). Fluorescence data showed basal readings of 5.83333 ± 0.7 . Groups WO showed higher readings (6.91667 ± 0.9) and group WO+B+L the lowest (1.66667 ± 0.5). There were significant differences between groups on both cases ($p < 0.05$). Pearson correlation was negative and significant ($R^2 = -0.60$; $p < 0.001$), and it was indicative that, when the Raman peaks

A. L. B. Pinheiro (✉) · N. R. S. Santos · P. C. Oliveira ·
G. T. S. Aciole · T. A. Ramos · T. A. Gonzalez · L. N. da Silva ·
A. F. S. Barbosa
Center of Biophotonics, School of Dentistry,
Federal University of Bahia,
Av. Araújo Pinho, 62, Canela,
Salvador, BA 40110-150, Brazil
e-mail: albp@ufba.br

N. R. S. Santos
e-mail: ribeironicole@hotmail.com

P. C. Oliveira
e-mail: pchagas2005@yahoo.com.br

G. T. S. Aciole
e-mail: gilberthaciole@hotmail.com

T. A. Ramos
e-mail: thais_andraderamos@hotmail.com

T. A. Gonzalez
e-mail: taina_gonzalez@yahoo.com.br

L. N. da Silva
e-mail: lay_lica@hotmail.com

A. F. S. Barbosa
e-mail: arturfelipes@gmail.com

A. L. B. Pinheiro · L. Silveira Jr
Universidade Camilo Castelo Branco Núcleo do Parque
Tecnológico de São José dos Campos,
Rodovia Presidente Dutra, km. 138 - Distrito de Eugênio de Melo,
São José dos Campos, 12247-004, SP, Brazil

L. Silveira Jr
e-mail: land-jr@uol.com.br

A. L. B. Pinheiro
Instituto Nacional de Ciência e Tecnologia de Óptica e Fotônica,
São Carlos, SP, Brazil 13560-970

of calcium hydroxyapatite (CHA) are increased, the level of fluorescence is reduced. It is concluded that the use of near-infrared lasertherapy associated to HA graft and GBR was effective in improving bone healing on fractured bones as a result of the increasing deposition of CHA measured by Raman spectroscopy and decrease of the organic components as shown by the fluorescence readings.

Keywords Biomaterials · Bone repair · Internal rigid fixation · Phototherapy

Introduction

The discovery of anesthesia allowed a significant advance on the treatment of fractures, such as the use of direct intraosseous wires. The treatment of fractures consists of the reduction and fixation of dislocated segments [1]. Internal fracture fixation provides mechanical stability to a fractured bone, allowing weight bearing, early use of the affected bone, and rapid bone healing. It is indicated when anatomical reduction is essential, as with articular or growth plate fractures. The selection of internal fixation is based on multiple mechanical, biologic, and clinical parameters associated with each patient and fracture, not just the fracture pattern itself [2]. The choice of internal fixation depends on the type of fracture, the condition of the soft tissues and bone, the size and position of the bone fragments, and the size of the bony defect. Numerous devices are available for internal fixation. These devices can be roughly divided into a few major categories: wires; pins and screws; plates; and intramedullary nails or rods. Staples and clamps are also used occasionally for osteotomy or fracture fixation [3, 4].

Stainless steel wire is the traditional material used for fracture fixation because it is a biologically inert material; rigid; provides precise repositioning of the bone fragments; easy to use; and has a reasonable cost [5]. Although internal fixation provides superb mechanical support, it is usually disruptive to the biologic environment. Internal fixation requires a surgical approach; thus, it disrupts the soft tissues and vascularity surrounding the fracture. Attempts are always made to provide the most rigid mechanical fixation while minimizing the surgical trauma [6]. Inter-fragmentary micro-motion causes high levels of strain on the fracture ends, leading to bone resorption, followed by callus formation and transformation of fibrocartilage to bone. This is common when pins and wires are the only fixations utilized [7].

Despite that small rodents possess only a primitive bone structure without a Haversian system, their fracture repair processes are similar to larger mammals [8]. Therefore, this model may be used to investigate bone repair [9]. Several murine models using long bone fractures are commonly described analyzing therapeutic options of different

stabilization techniques or the systemic influence of an additional impact in trauma models. Due to the small size, only large long bones, especially tibia and femur, have been studied [10]. Similar to murine models, rats are used investigating fracture healing. However, due to the missing Haversian system, intra-cortical remodeling cannot be detected in rats representing an essential difference to humans [11]. Similar to murine models, the fracture may be technically simulated by an osteotomy or fractured manually after weakening the bone [12, 13]. To stabilize the fracture, an intramedullary pin or wire may be used [14].

There are fractures in which handling is further complicated due to the loss of bone. These losses may be related to several etiologies and require further efforts from the body to fully recover. Although grafts have been used to minimize the problems associated to bone losses, considerable limitations associated with autografts and allografts have prompted increased interest in alternative bone graft substitutes. The main types of commercially available bone graft substitutes are demineralized allograft bone matrix; ceramics and ceramic composites; composite graft of collagen and mineral; coralline hydroxyapatite; calcium phosphate cement; bioactive glass; and calcium sulfate [15–17].

The healing of various types of bone defect with complete bone fill has been reported following the use of the guided bone regeneration (GBR) technique [18]. GBR is a technique used to prevent the migration of soft tissues, which has more pronounced proliferative activity, into the bone defect. GBR promotes bone formation by the use of a mechanical barrier such as membranes, and these may be resorbable or non-resorbable and may also be associated or not to bone substitutes. The GBR is widely used for treating periodontal defects and other bone defects [19].

Raman scattering is a powerful light scattering technique used to diagnose the internal structure of molecules and crystals. Raman spectroscopy is the measurement of the wavelength and intensity of inelastically scattered light from molecules. The Raman scattered light occurs at wavelengths that are shifted from the incident light by the energies of molecular vibrations. The mechanism of Raman scattering is different from that of infrared absorption, and Raman and infrared (IR) spectra provide complementary information. Typical applications are in structure determination, multi-component qualitative analysis, and quantitative analysis [3, 4]. Its use allows less invasive and nondestructive analysis of biological samples, allowing one to get precise information on biochemical composition. It has been considered effective to assess tissues at the molecular level and has been used on several noninvasive diagnostic applications of biological samples such as cancer; human coronary arteries; blood analysis; implants; cell culture; bone disease; and bone healing and to evaluate the microstructure of human cortical bone (osteon) and biomaterials.

We have used Raman spectroscopy as a method of assessment of the effects of laser phototherapy (LPT) on bone healing under different models [20–24], including fractures [3, 4]. Our previous results indicate that near-infrared (NIR) LPT is effective to improve bone repair mainly due to its higher penetration into bone when compared with visible laser light [15–17, 19, 25, 26]. The use of LPT on studies involving bone healing is a hot topic lately, and many have demonstrated positive stimulatory effects even when associated to biomaterials [3, 4, 15, 17, 19–24, 26–29].

By using infrared excitation ($\lambda 785$ or $\lambda 830$ nm), one can minimize the interference of the autofluorescence on the Raman spectra from biological specimens [3, 4]. On the other hand, there are molecules capable of interacting with light in a different way. The absorption of the light occurs on the chromophores that are molecules capable of absorbing and emitting light by fluorescence. The absorbing sites are known as fluorophores. These molecules will absorb energy of a specific wavelength and re-emit energy at a different (but equally specific) wavelength. The amount and wavelength of the emitted energy will depend on both the fluorophore and on its chemical environment. On this group, we may include flavins, proteins, collagen, elastin, NADH, and porphyrins. This is the case of a commercial device called DIAGNOdent®.

Many molecules are able to interact with light by its absorption by chromophores that, on molecules also capable of emitting light (fluorescence), are known as fluorophores. These structures will absorb energy of a specific wavelength and re-emit it at a different, but equally specific, wavelength. Flavins, proteins, collagen, elastin, NADH, and porphyrins are fluorophores. The intensity of the fluorescence is directly related to the amount of fluorophores at the site. Fluorescence on living organisms is mainly related to organic components; apatite also plays a small role in that [30–32].

The DIAGNOdent® ($\lambda 655$ nm, modulated, 1 mW peak power diode laser combined with a long pass filter transmission $>\lambda 680$ nm as the detector) was used initially for the diagnosis of dental caries, but we have used it previously as an optical biopsy method to assess bone healing on tibial fractures [29]. We found that Pearson correlation showed that fluorescence readings correlated negatively with the Raman data and concluded that the use of both methods indicates that the use of the biomaterials associated with infrared LPT resulted in a more advanced and higher quality of bone repair in fractures treated with miniplates and that the device may be used to perform optical biopsy on bone [29].

In summary, fractures are common and disabling lesions. It may be treated by means of several techniques and devices. The choice of the treatment depends on the type, site, and etiology of the trauma. Usually, internal fixation of the

fragments either by plating or wiring is the method of choice as they reduce dislocation of the fragments preventing fibrosis and reducing the gap between fragments. Plating is most often the recommended choice; however, it is costly. Wire osteosynthesis is the second option as it is semi-rigid. In cases of large bone losses, the use of bone grafts and membrane is recommended. The use of light to improve bone repair has been widely reported in the literature. These aspects prompted us to study if improvement of the repair of fractures treated by wiring, biomaterial, membrane, and laser would result in a repair similar to the one observed when plating is used, as a way of possibly reducing the cost of the treatment.

The aim of this study was to evaluate, by laser fluorescence and Raman spectroscopy, the repair of complete tibial fracture in rabbits treated by wire osteosynthesis associated or not to the use of a biphasic ceramic graft associated or not to the use of GBR and irradiated or not with $\lambda 780$ nm laser in rabbits.

Materials and methods

The Animal Ethics Committee of the School of Dentistry of the Federal University of Bahia has approved this research. Fifteen healthy adult male New Zealand rabbits (~8 months old; mean weight, 2 kg) were kept under natural conditions of light, humidity, and temperature at the Laboratory of Animal Experimentation of the School of Dentistry of the Federal University of Bahia during the experimental period. The animals were fed with standard laboratory pelleted diet and had water *ad libitum*. The animals were kept in individual metallic cages; kept at day/night light cycle; and controlled temperature during the experimental period. The animals were randomly distributed into five groups (Table 1).

Prior intramuscular general anesthesia, the animals received acepromazine (2 mg/kg Aceprom®; 0.2 % Univet S.A, Cambuci, SP, Brazil). The anesthesia was carried out 20 min later with ketamine (Ketalar®, 50 mg/ml 0.4 ml/kg, Lab. Parke Davis Ltd, São Paulo, SP, Brazil) and 2 % xylazine (Rompum®, 20 mg/ml 0.2 ml/kg, Lab. Bayer Health Care S.A., São Paulo, SP, Brazil). The animals had the right leg shaved, and a 3-cm-long incision was performed at the right tibia with a no. 15 scalpel blade. Skin and subcutaneous tissues were dissected down to the periosteum, which was gently sectioned, exposing the bone. A complete surgical tibial fracture was created on animals in groups II, III, IV, and V with a carbonundum disk (Moyco Union Broach, York, PA, USA) under water refrigeration.

Animals in group II had the bone fragments fixed with wire osteosynthesis (0.3 mm, Morelli®, Sorocaba, SP, Brazil). Animals in groups III and V were grafted with the 0.5-

Table 1 Description and distribution of the groups on the study

Group	Procedure	Description
I	Basal bone	Control—no fracture
II	Wire osteosynthesis (WO)	Fracture fixed with wire only
III	Wire osteosynthesis+biomaterial (WO+B)	Fracture fixed with wire+Genphos®+Genderm®
IV	Wire osteosynthesis+laser (WO+L)	Fracture fixed with wire+laser
V	Wire osteosynthesis+biomaterial+laser (WO+B+L)	Fracture fixed with wire+Genphos®+Genderm®+laser

mm particle ceramic graft (GenPhos® HATCP, BAUMER®, Mogi Mirim, SP, Brazil) and covered with a demineralized bovine bone membrane (Gen-derm®, BAUMER®, Mogi Mirim, SP, Brazil) prior similar fixation used on group I (Fig. 1). Animals in groups IV and V were further irradiated with laser light ($\lambda 780$ nm, 50 mW, CW, spot area of 0.5 cm^2 ,¹ TWIN FLEX®, MM Optics, São Carlos, SP, Brazil). The irradiation started immediately after treatment prior suturing (16 J/cm^2 , $4 \times 4\text{ J/cm}^2$, 9 J per point) and was transcutaneously repeated at every other day during 2 weeks. After suturing (4-0 polyglactin, TRUSINTH®, Sutures India Pvt Ltd. Bangalore, Karnataka, India) and (4-0 nylon, TRUSINTH®, Sutures India Pvt Ltd. Bangalore, Karnataka, India), the animals received intramuscular antibiotics (Pentabiotico®, penicillin, streptomycin, 20.000 UI 0.2 ml/Kg IM, Lab. Forte Dodge Saúde Animal Ltda, Campinas, SP, Brazil) and (Banamine®, flunixinmeglumine, 10 mg/ml, 0.1 ml/kg IM, Intervet Schering-Plough Animal Health, Cruzeiro, SP, Brazil).

Fluorescence readings

A commercial device (DIAGNOdent 2095®) was used to collect the fluorescence readings ($\lambda 665$ nm) according to the instructions of the manufacturer (Kavo, Germany). Prior to the analysis of the specimens, a pilot study determined the mean values of the readings at the surface (baseline) of non-treated subjects. The data were statistically analyzed, and no significant differences were found between the readings of the tested samples ($p > 0.001$). On the experimental specimens, the data were collected twice: prior to the experiment (baseline, four points at the surface) and at the end of the experimental time before the removal of the specimen (four points at the fracture surface). The results were analyzed using Minitab 15.0® software (Minitab, Belo Horizonte, MG, Brazil). Data normality was assessed by the Kolmogorov-Smirnov test. ANOVA and Student's *t* tests were used to identify differences between groups.

Raman spectroscopy

Following animal death 30 days after fracture, the samples were longitudinally cut under refrigeration (Bueler®, Isomet TM1000; Markham, Ontario, Canada) and stored in liquid nitrogen to minimize the growth of aerobic bacteria and because the chemical fixation is not advisable due to fluorescence emissions from the fixative substances [3, 4, 29, 33].

Prior to Raman study, the samples were longitudinally cut and warmed gradually to room temperature, and 100 mL of saline was added to the surface during spectroscopic measurements. For Raman measurements, a Raman system (P-1, Lambda Solutions, Inc., MA, USA) was used. Acquisition and storage of the Raman data were done with a PC (Dell Inspiron mod. 1501) and RamaSoft® software (Lambda Solutions, Inc., MA, USA). The laser power used at the sample site was of 100 mW with spectral acquisition time 10 s. Three points were measured at the fractured site of each specimen. All spectra were collected on the same day to avoid optical misalignments and changes in laser power. The mean value of the intensity of the peak ($\sim 958\text{ cm}^{-1}$, phosphate ν_1) was determined by the average of the peaks on this region. This intensity is related to the concentration of calcium hydroxyapatite (CHA) of the bone. For calibration, the Raman spectrum of the solvent indene with known peaks was used due to its intense bands ($800\text{--}1,800\text{ cm}^{-1}$) in the fingerprint region [3, 4, 29, 33].

The indene spectrum was also measured each time the sample was changed to be sure that the laser and collection optics were optimized. In order to remove the “fluorescence background” from the original spectrum, a fifth-order polynomial fitting was found to give better results facilitating the



Fig. 1 Final setup of the surgical site. Note the presence of the wire and membrane covering the particles of the biomaterial

¹ Beam area was measured with a calibrated digital caliper.

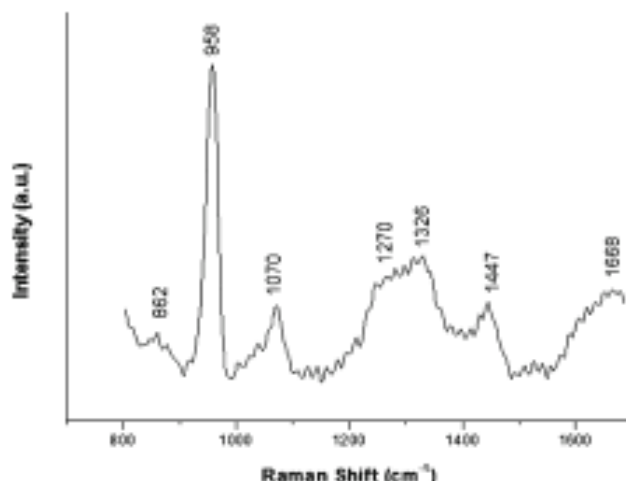


Fig. 2 Diagram showing the main Raman peaks observed on bone tissue

visualization of the peaks of CHA ($\sim 958 \text{ cm}^{-1}$) found on the bone. A baseline Raman spectrum of non-treated bone (group I) was also produced and acted as control (Fig. 2). The data were analyzed by the MatLab 5.1® software (Newark, NJ, USA) for calibration and background subtraction of the spectra. Statistical analysis was performed using Minitab 15.0® software (Minitab, Belo Horizonte, MG, Brazil). Correlation between Raman and fluorescence data was carried out with Pearson correlation. Significance level in all cases was set at 5 %.

Results

The Raman spectrum of bone shows prominent vibrational bands related to tissue composition (mineral and organic matrices). Figure 2 shows the bone main Raman bands at 862,

Fig. 3 Spectra of basal and experimental groups. Each individual spectrum is dislocated to reflect the mean value of the peak of CHA ($\sim 958 \text{ cm}^{-1}$)

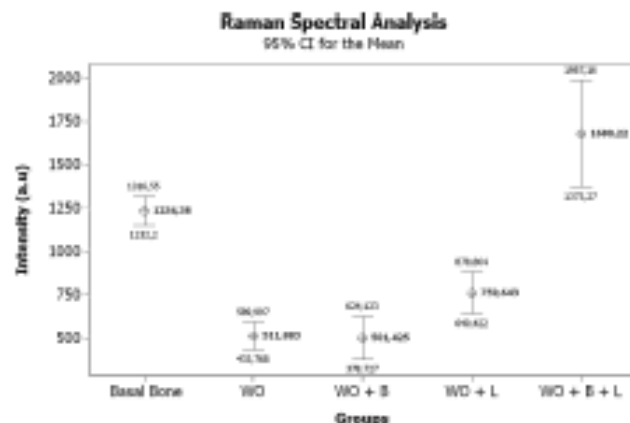
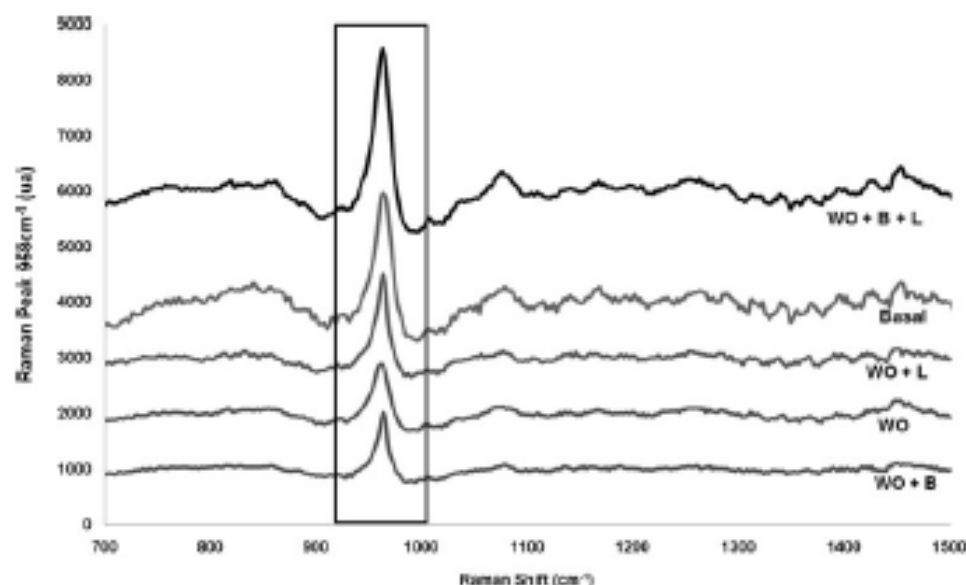


Fig. 4 Mean intensity of the peak of CHA ($\sim 958 \text{ cm}^{-1}$) on control and treated animals

958, 1,070, 1,270 and 1,326, 1,447, and 1,668 cm^{-1} . The band at 1,668 cm^{-1} and the ones at 1,270 and 1,326 cm^{-1} are attributed to amide I and III stretching modes of lipids and proteins; the band at 1,447 cm^{-1} is attributed to the bending and stretching vibration modes of CH groups of lipids and proteins. The ones at 958 and 1,070 cm^{-1} are attributed to phosphate and carbonate hydroxyapatite (HA) from bone mineral, respectively; the band at 862 cm^{-1} may be attributed to the vibration bands of C-C stretch of collagen (tyrosine/proline ring).

Figure 3 shows the mean spectra (dislocated) of CHA ($\sim 958 \text{ cm}^{-1}$) on control and treated animals. The intensity of the Raman shift is directly related to the concentration/incorporation of CHA by the bone. So, higher intensity represents higher concentration of CHA. Basal readings showed a mean value of $1,234.38 \pm 220$. Groups WO+B+L showed higher readings ($1,680.22 \pm 822$) and group WO+B the lowest (501.425 ± 328) (Fig. 4). Table 2 shows a summary of the statistical analysis.

Table 2 Mean and standard deviation of the peaks of the Raman shift of CHA (-958 cm^{-1}) on the groups

Group	Média \pm DP
Basal Bone a	1,234.38 \pm 220 b,c,d,e
WO b	511.883 \pm 209 a,d
WO+B c	501.425 \pm 328 a,d,e
WO+L d	759.643 \pm 319 a,b,c,e
WO+B+L e	1,680.22 \pm 822 a,b,c,d

Letters on right-hand side column indicate the occurrence of significant differences between groups on the left-hand side column

$p\leq 0.05$

Fluorescence basal readings showed a mean value of 5.8333 ± 0.7 ; group WO showed higher readings (6.91667 ± 0.9) and group WO+B+L the lowest (1.66667 ± 0.5) (Fig. 5). A summary of the fluorescence readings and statistical analysis may be seen on Table 3.

Pearson correlation was negative and significant ($R^2=-0.60$; $p<0.001$), and it was indicative that, when the Raman peaks of CHA are increased, the level of fluorescence is reduced (Fig. 6).

Discussion

Raman spectroscopy may be used to access the molecular constitution of a specific tissue and then classify it according to differences observed in the spectra [34, 35]. Several studies found elsewhere on the literature has shown successful use of near-infrared spectroscopy (NIRS) as a diagnostic tool for healthy, diseased, or healing bones [3, 4, 27, 29, 33–35]. We have successfully used Raman spectroscopy to determine both mineral and organic component changes on the healing bone. This method of assessment is considered by our team and others as a gold standard to study bone components [3, 4, 27, 29, 33–35].

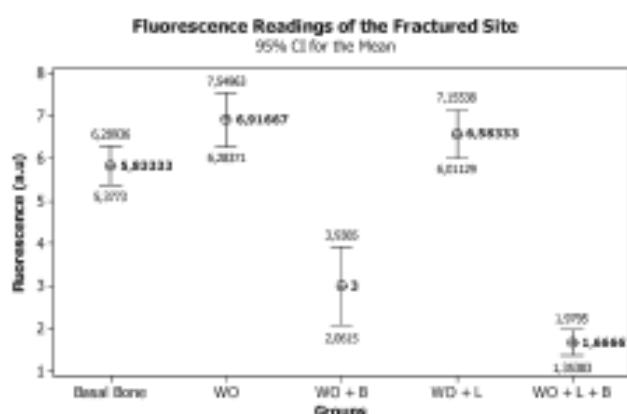


Fig. 5 Mean fluorescence readings on control and treated animals

Table 3 Mean and standard deviation of the fluorescence (a.u) readings on the groups

Group	Mean \pm SD
Basal bone a	5.8333 \pm 0.7 b,c,d,e
WO b	6.91667 \pm 0.9 a,c,e
WO+B c	3 \pm 1.4 a,b,d,e
WO+L d	6.58333 \pm 0.9 a,c,e
WO+B+L e	1.66667 \pm 0.5 a,c,d

Letters on right-hand side column indicate the occurrence of significant differences between groups on the left-hand side column

$p\leq 0.05$

The DIAGNOdent® is a device originally designed to diagnose caries. The literature reported the detection of tricalciumphosphate, dicalciumphosphate-dihydrate, and calcium carbonate measured by fluorescence of pure pellets with excitation at $\lambda 655\text{ nm}$. It is important to mention that it has been shown that this device presents good reproducibility both in vivo and in vitro. We found only one report on the literature on the use of this device as an optical biopsy method, and similar to that report, we decided to use Raman spectroscopy as gold standard [29].

One of the models we have used for assessing the effects of laser light on bone is the complete tibial fracture one. This model is very complex and allows several treatment approaches. These include the use WO and miniplates. Associated to these treatment methods, we have also associated them to biomaterials and guided bone regeneration [3, 4, 29].

The use of phototherapies has been successfully reported for the improvement of bone repair under different conditions [3, 4, 15, 20–24, 29, 30, 33]. The effects of the use of light sources on bone are still controversial, as previous reports show different or conflicting results. It is possible

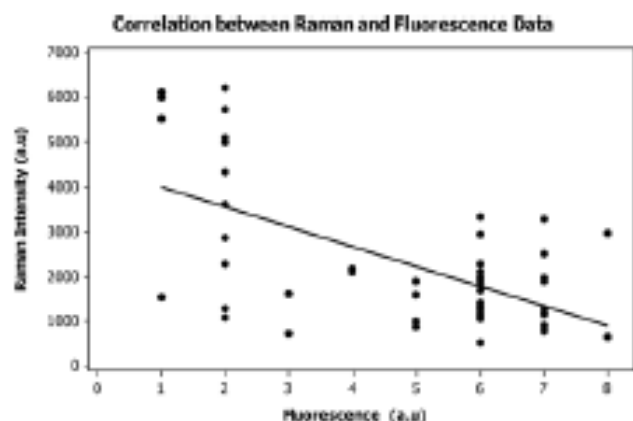


Fig. 6 Graphical illustration of the Pearson correlation. It is shown as a negative and significant correlation being indicative that, when the Raman peaks of CHA are increased, the level of fluorescence was reduced

that the effect of different light sources on bone regeneration depends not only on the total dose of irradiation but also on the irradiation time and the irradiation mode [3, 4, 15, 20–24, 29, 30, 33].

Many studies indicated that irradiated bone, mostly with IR wavelengths, shows increased osteoblastic proliferation, collagen deposition, and bone neo-formation when compared with non-irradiated bone [3, 4, 15, 20–24, 29, 30, 33]. The irradiation protocol used in this study is similar to those used on previous reports [3, 4, 15, 20–24, 29, 30, 33]. Our group has shown, using different models, that association of bone grafts, BMPs, and guided tissue regeneration does improve the healing of bone tissue [3, 4, 15, 20–24, 29, 30, 33].

In all protocols, models, and parameters we used previously, we were able to demonstrate that NIR LPT caused important tissue responses during healing, and these were responsible for a quicker repair process as well as on the improved quality of the newly formed bone [3, 4, 15, 20–24, 29, 30, 33].

We only found a previous report using a similar model to the one used in the present study, and the complete understanding of our results remains difficult [3]. There are several aspects to consider with regard to the technique used. Initially, it is important to consider that the repair of fractured bones is lengthy, when compared with other types of bony defects, and demands stability of the fragments in order not to develop nonunion. In our study, no such case was found. The present investigation was analyzed by NIRS, the intensity of the shift of the CHA (-958 cm^{-1}) [3], and fluorescence [29] of sites of complete tibial fractures in rabbits. The fractures were routinely treated by open reduction and internal fixation using wire osteosynthesis [3].

The irradiation protocol used on the present study was based upon previous reports [3, 4, 15, 20–24, 29, 30, 33]. We have previously found that the levels of CHA on deep areas of healing bone of irradiated and non-irradiated subjects differ significantly from day 30 after treatment [3, 4, 15, 20–24, 29, 30, 33]. In this study, we were able to detect differences on the CHA levels of fractured sites when internal fixation was associated to the use of biomaterial and lasertherapy. On the present study, the intensity of the Raman shift was found being directly related to the concentration/incorporation of CHA by the bone. So, higher intensity represented higher concentration of CHA. The Raman results showed basal readings of $1,234.38 \pm 220$, and group WO+B+L was the one with higher readings ($1,680.22 \pm 822$), and group WO+B showed the lowest (501.425 ± 328). The fluorescence data are coherent with the Raman data as these showed basal readings of 5.83333 ± 0.7 , and groups WO presented higher readings (6.91667 ± 0.9) and group WO+B+L the lowest (1.66667 ± 0.5). It is important to notice that the Pearson correlation was negative and significant ($R^2 = -0.60$; $p < 0.001$), and it was indicative that, when the Raman peaks of CHA were increased, the level of

fluorescence was reduced (Fig. 6). This was expected, as the Raman data were associated to the levels of mineralization and the fluorescence data to the level of demineralization. This is in complete agreement with our previous report [29]. The use of both methods indicates that the use of the biomaterial associated to NIR LPT resulted on a more advanced quality bone repair on fractures treated with WO and that the DIAGNOdent® may be used to perform optical biopsy on bone.

It is concluded that the use of NIR laser phototherapy associated to HA graft and GBR was effective in improving bone healing on fractured bones as a result of the increasing deposition of CHA measured by Raman spectroscopy and decrease of the organic components as shown by the fluorescence readings.

References

1. Erdogan O, Esen E, Ustun Y, Kurkcu M, Akova T, Gonulsen G, Uysal H, Cevlik F (2006) Effects of low-intensity pulsed ultrasound on healing of mandibular fractures: an experimental study in rabbits. *J Oral Maxillofac Surg* 64:180–188
2. Axon DN, Palmer RH, Johnson AL (1995) Biologic strategies and a balanced concept for repair of highly comminuted long bone fractures. *Compend Contin Educ Pract Vet* 17:35–49
3. Lopes CB, Pacheco MTT, Silveira Junior L, Duarte J, Cangussu MCT, Pinheiro ALB (2007) The effect of the association of NIR laser therapy BMPs, and guided bone regeneration on tibial fractures treated with wire osteosynthesis: Raman spectroscopy study. *J Photochem Photobiol B Biol* 89:125–130
4. Lopes CB, Pacheco MTT, Silveira-Junior L, Cangussu MC, Pinheiro ALB (2010) The effect of the association of near infrared laser therapy, bone morphogenetic proteins, and guided bone regeneration on tibial fractures treated with internal rigid fixation: a Raman spectroscopic study. *J Biomed Mater Res A* 94:1257–1263
5. Broadbent WC, Holloway KL, Winters CJ, Bullock MR, Graham RS, Mathem BE, Ward JD, Young HF (2002) Titanium miniplates or stainless steel wire for cranial fixation: a prospective randomized comparison. *J Neurosurg* 96:244–247
6. Hulth E, Hyman B (2003) Fracture biology and biomechanics. In: Slatter D (ed) *Textbook of small animal surgery*, 3rd edn. Saunders, Philadelphia, pp 1785–1792
7. Stiffler KS (2004) Internal fracture fixation. *Clin Tech Small Anim Pract* 19:105–113
8. Nunamaker DM (1998) Experimental models of fracture repair. *Clin Orthop Relat Res* 355:S56–S65
9. Holstein JH, Garcia P, Histing T et al (2009) Advances in the establishment of defined mouse models for the study of fracture healing and bone regeneration. *J Orthop Trauma* 23:S31–S38
10. Maturano JE, Cleveland BC, Byrne MA, O'Connell SL, Wixted JJ, Billiar KL (2008) An improved murine femur fracture device for bone healing studies. *J Biomech* 41:1222–1228
11. Manabe T, Mori S, Mashiba T et al (2007) Human parathyroid hormone (1–34) accelerates natural fracture healing process in the femoral osteotomy model of cynomolgus monkeys. *Bone* 40:1475–1482
12. Utvag SE, Korsnes L, Rindal DB, Reikeras O (2001) Influence of flexible nailing in the later phase of fracture healing: strength and mineralization in rat femora. *J Orthop Sci* 6:576–584

13. Schoen M, Rotter R, Schattner S et al (2008) Introduction of a new interlocked intramedullary nailing device for stabilization of critically sized femoral defects in the rat: a combined biomechanical and animal experimental study. *J Orthop Res* 26(1):84–189
14. Frink M, Andruszkow H, Zedek C, Krettek C, Hildebrand F (2011) Experimental trauma models: an update. *J Biomed Biotechnol*. doi:10.1155/2011/797383
15. Pinheiro ALB, Gerbi MEMM (2006) Photoengineering of bone repair processes. *Photomed Laser Surg* 24:169–178
16. Weber JB, Pinheiro ALB, Oliveira MG, Oliveira MGO, Ramalho LMP (2006) Laser therapy improves healing of bone defects submitted to autologous bone graft. *Photomed Laser Surg* 24:38–44
17. Pinheiro ALB, Limeira Junior FA, Gerbi MEMM, Ramalho LMP, Marzola C, Ponzi EAC (2003) Effect of low level laser therapy on the repair of bone defects grafted with inorganic bovine bone. *Braz Dent J* 14:177–181
18. Denos N, Kostopoulos L, Karring T (2002) Augmentation of the mandible with GTR and onlay cortical bone grafting. An experimental study in the rat. *Clin Oral Implants Res* 13:175–184
19. Gerbi MEMM, Pinheiro ALB, Marzola C, Limeira Junior F, Ramalho LMP, Ponzi EAC, Soares AO, Carvalho LCB, Lima HCAV, Gonçalves TO (2005) Assessment of bone repair associated with the use of organic bovine bone and membrane irradiated at 830-nm. *Photomed Laser Surg* 23:382–388
20. Pinheiro ALB, Gerbi MEMM, Limeira Junior FA et al (2009) Bone repair following bone grafting hydroxyapatite guided bone regeneration and infra-red laser photobiomodulation: a histological study in a rodent model. *Lasers Med Sci* 24:234–240
21. Gerbi MEMM, Marques AMC, Ramalho LMP et al (2008) Infrared Laser light further improves bone healing when associated with bone morphogenetic proteins: an in vivo study in a rodent model. *Photomed Laser Surg* 26:55–60
22. Pinheiro ALB, Gerbi MEMM, Ponzi EAC et al (2008) Infrared laser light further improves bone healing when associated with bone morphogenetic proteins and guided bone regeneration: an in vivo study in a rodent model. *Photomed Laser Surg* 26:167–174
23. Torres CS, Santos JN, Monteiro JSC, Gomes PTCC, Pinheiro ALB (2008) Does the use of laser photobiomodulation, bone morphogenetic proteins, and guided bone regeneration improve the outcome of autologous bone grafts? An in vivo study in a rodent model. *Photomed Laser Surg* 26:371–377
24. Gerbi MEMM, Pinheiro ALB, Ramalho LMP (2008) Effect of IR laser photobiomodulation on the repair of bone defects grafted with organic bovine bone. *Lasers Med Sci* 23:313–317
25. Pinheiro ALB, Limeira Junior FA, Gerbi MEMM et al (2003) Effect of 830-nm laser light on the repair of bone defects grafted with inorganic bovine bone and decalcified cortical osseous membrane. *J Clin Laser Med Surg* 21:383–388
26. Pinheiro ALB, Oliveira MAM, Martins PPM (2001) Biomodulação da cicatrização óssea pós-implantar com o uso da laserterapia foto-cirúrgica: estudo por microscopia eletrônica de varredura. *Rev FOUFBA* 22:12–19
27. Lopes CB, Pinheiro ALB, Sathiaiah S, Duarte J, Martins MC (2005) Infrared laser light reduces loading time of dental implants: a Raman spectroscopy study. *Photomed Laser Surg* 23:27–31
28. Silva Junior AN, Pinheiro ALB, Oliveira MG, Weissmann R, Ramalho LMP, Nicolau RA (2002) Computerized morphometric assessment of the effect of low-level laser therapy on bone repair: an experimental animal study. *J Clin Laser Med Surg* 20:83–88
29. Pinheiro ALB, Lopes CB, Pacheco MTT, Brugnem A, Zanin FAA, Cangussú MCT, Silveira-Junior L (2010) Raman spectroscopy validation of DIAGNOdent-assisted fluorescence readings on tibial fractures treated with laser phototherapy, BMPs, guided bone regeneration, and miniplates. *Photomed Laser Surg* 28:89–97
30. Pinheiro ALB, Aciole GTS, Cangussú MCT, Pacheco MTT, Silveira-Junior L (2010) Effects of laser phototherapy on bone defects grafted with mineral trioxide aggregate, bone morphogenetic proteins, and guided bone regeneration: a Raman spectroscopic study. *J Biomed Mater Res A* 95:1041–1047
31. Shi Q, Tranaeus S, Angmar-Mansson B (2001) Validation of DIAGNOdent for quantification of smooth-surface caries: an in vitro study. *Acta Odontol Scand* 59:74–78
32. Hilbot R, Paulus R, Lussi A (2001) Detection of occlusal caries by laser fluorescence. Basic and clinical investigations. *Med Laser Appl* 16:205–213
33. Lopes CB, Pinheiro ALB, Sathiaiah S, Silva NS, Salgado MC (2007) Infrared laser photobiomodulation (830 nm) on bone tissue around dental implants: a Raman spectroscopy and scanning electron microscopy study in rabbits. *Photomed Laser Surg* 25:96–101
34. Penel G, Delfosse C, Descomps M, Leroy G (2005) Composition of bone and apatitic biomaterials as revealed by intravital Raman microspectroscopy. *Bone* 36:893–901
35. Carden A, Morris MD (2000) Application of vibrational spectroscopy to the study of mineralized tissues (review). *J Biomed Opt* 5:259–268

Lasers Med Sci. 2013 Feb 21. [Epub ahead of print]

Effect of the laser and light-emitting diode (LED) phototherapy on midpalatal suture bone formation after rapid maxilla expansion: a Raman spectroscopy analysis

Effect of the laser and light-emitting diode (LED) phototherapy on midpalatal suture bone formation after rapid maxilla expansion: a Raman spectroscopy analysis

Cristiane Becher Rosa · Fernando Antonio Lima Habib ·
Telma Martins de Araújo · Juliana Silveira Aragão ·
Rafael Soares Gomes · Artur Felipe Santos Barbosa ·
Landulfo Silveira Jr · Antonio L. B. Pinheiro

Received: 4 October 2012 / Accepted: 7 February 2013
© Springer-Verlag London 2013

Abstract The aim of this study was to analyze the effect of laser or light-emitting diode (LED) phototherapy on the bone formation at the midpalatal suture after rapid maxilla expansion. Twenty young adult male rats were divided into four groups with 8 days of experimental time: group 1, no treatment; group 2, expansion; group 3, expansion and laser irradiation; and group 4, expansion and LED irradiation. In groups 3 and 4, light irradiation was in the first, third, and fifth experimental days. In all groups, the expansion was accomplished with a helicoid 0.020" stainless steel orthodontic spring. A diode laser ($\lambda 780$ nm, 70 mW, spot of 0.04 cm^2 , $t=257$ s, spatial average energy fluence (SAEF) of 18 J/cm^2) or a LED ($\lambda 850$ nm, $150\text{ mW} \pm 10\text{ mW}$, spot of 0.5 cm^2 , $t=120$ s, SAEF of 18 J/cm^2) were used. The samples were analyzed by Raman spectroscopy carried out at midpalatal suture and at the cortical area close to the

suture. Two Raman shifts were analyzed: ~ 960 (phosphate hydroxyapatite) and $\sim 1,450\text{ cm}^{-1}$ (lipids and protein). Data was submitted to statistical analysis. Significant statistical difference ($p \leq 0.05$) was found in the hydroxyapatite (CHA) peaks among the expansion group and the expansion and laser or LED groups. The LED group presented higher mean peak values of CHA. No statistical differences were found between the treated groups as for collagen deposition, although LED also presented higher mean peak values. The results of this study using Raman spectral analysis indicate that laser and LED light irradiation improves deposition of CHA in the midpalatal suture after orthopedic expansion.

Keywords Laser therapy · Palatal expansion technique · Orthodontics · Bone regeneration · Raman spectroscopy

C. B. Rosa · F. A. L. Habib · J. S. Aragão · R. S. Gomes ·
A. F. S. Barbosa · A. L. B. Pinheiro (✉)
Center of Biophotonics, School of Dentistry,
Federal University of Bahia, Av. Araújo Pinho, 62, Canela,
Salvador, BA 40110-150, Brazil
e-mail: albp@ufba.br

C. B. Rosa
e-mail: becherrosa@gmail.com

F. A. L. Habib
e-mail: fhabib@terra.com.br

J. S. Aragão
e-mail: angao.juliana@yahoo.com.br

R. S. Gomes
e-mail: rafasoa@yahoo.com.br

A. F. S. Barbosa
e-mail: arturfelipes@gmail.com

T. M. de Araújo
Orthodontic, School of Dentistry, Federal University
of Bahia, Av. Araújo Pinho, 62, Canela,
Salvador, BA 40110-150, Brazil
e-mail: tmatelma@iglobo.com

L. Silveira Jr · A. L. B. Pinheiro
Camilo Castelo Branco University,
Núcleo do Parque Tecnológico de São
José dos Campos: Rod. Presidente Dutra Km 139,
Eugênio de Melo, São José dos Campos,
SP 12247-004, Brazil

A. L. B. Pinheiro
National Institute of Optics and Photonics,
University of São Paulo, Physics Institute of São Carlos,
São Carlos, SP, Brazil 13560-970

Introduction

Posterior cross bite is one of the most frequent malocclusions observed in the different phases of the dentition. Several reports indicate that this alteration is not self-corrected and recommend that treatment shall be carried out at the initial stage of the permanent dentition [1].

Rapid maxilla expansion is one of the most common treatments for maxillary atresia [2–4] that is one of the main causes of posterior cross bite and has been used for more than 30 years [5]. The changes caused by the treatment are primarily located in the basal bone, increasing the upper arch dimensions through the midpalatal suture (orthopedic effect), with posterior teeth movement through the alveolar processes in different intensities depending on the patient's age and maturity (orthodontic effect) [1, 6].

The clinical procedure for maxilla expansion includes an active phase that releases lateral forces and a passive phase, which includes the use of a retainer. The active phase lasts 1–2 weeks, depending on the magnitude of the maxillary atresia [7]. Expanded arches can relapse rapidly if a retainer is not used for a long period [4]. After the expansion, maintaining the expansion appliance in place for a minimum period ranging from 3 [7] up to 5 or more months [6, 8] is recommended to allow reorganization of the maxillary suture and dissipation of accumulated forces [6, 7]. When the expansion device is removed, the patient has yet to use a retainer for minimum of 6 months [6, 7], for chances of relapse are diminished if the retainer use is extended [9, 10].

One of the main causes of relapse is insufficient bone regeneration in the midpalatal suture. It would be beneficial to accelerate bone formation in the region to avoid relapse and decrease the period of use of the retainer [4].

Low-intensity light therapy, commonly referred to as “photobiomodulation,” when used on bone tissue, uses mainly wavelengths in the far-red to near-infrared (NIR) region of the spectrum, capable of modulating numerous cellular functions [11]. Bone formation acceleration is one of the various biostimulating effects of phototherapies [4]. Laser efficiency in bone healing has been shown in various previous reports [12–14] and there has also been reference to accelerating orthodontic tooth movement by stimulating cellular events [15–18], as well as accelerating bone neoformation in midpalatal expansion cases [4, 19, 20]. Laser irradiation could potentially stimulate the recruitment of osteoblasts and/or their maturation throughout the bone edges of the midpalatal suture in expansion [4]. Odontoblasts would then anticipate and increase the deposit of calcium hydroxyapatite resulting in bone maturation and resistance [13]. Therefore, the laser action could increase bone repair and quality of bone resistance [20], leading to a lower period of retainer use and a more stable occlusion. However, most studies in regard to laser therapy with suture expansion have different protocols as to total dosage, time, mode and

frequency of irradiations, factors that influence final results and prevent precise comparisons between studies.

An effective alternative to lasers are light-emitting diodes (LEDs). LED arrays produce light in the far-red to NIR at optimal wavelengths and energy densities and do not emit any heat, which eliminates the danger of additional tissue damage. Further, NIR-LED light therapy has been deemed a nonsignificant risk by the FDA and has been approved for use in humans [11]. Recent studies by our team have proved that infrared LED light irradiation improves deposition of hydroxyapatite (CHA) in healing bone wounds. Results indicate that LED light causes quicker repair process and improves the quality of newly formed bone [21, 22]. There are no studies however of the effect of LED light associated to midpalatal suture expansion.

Even though light microscopy and imaging are the usual methods used to obtain information on bone formation, they are unable to provide data in a molecular level [23]. Raman spectroscopy is a vibrational spectroscopy technique used to assess scattered light from biologic molecules and ions. Raman spectroscopy occurs when molecules within a specimen are excited by incident laser light. Vibrational motions within the molecules lead to small fraction of the light losing energy and being scattered at longer wavelengths [24]. The wavelength difference between scattered and incident light corresponds to molecular-specific vibrations called the Raman shift and leads to spectral bands that provide direct information about the biochemical composition. Raman peaks are spectrally narrow, and in many cases can be associated with the vibration of a particular chemical bond (or a single functional group) in the molecule [21]. The Raman spectrum of bone shows prominent vibrational bands related to tissue composition [21, 24]. Raman spectroscopy has recently been used in several studies related to bone formation [21–26].

There are no reports of the use of LED phototherapy in the midpalatal suture after expansion and only a few with laser phototherapy. The results of these procedures have not yet been analyzed by Raman spectroscopy also. Therefore, the objective of this study is to evaluate the effect of LED and laser phototherapy in bone formation in the midpalatal suture after rapid maxillary expansion using Raman spectroscopy.

Materials and methods

This research has been developed according to legal and ethical specifications for animal experiments and approved by the Animal Experimentation Ethics Committee of the School of Dentistry of the Federal University of Bahia, Brazil (Protocol no 03/10).

In this study, a total of 20 male Wistar rats¹ were used and maintained in the Laboratory of animal experiment of

¹ Six weeks old; mean weight, 170 ± 20 g.

the School of Dentistry of the Federal University of Bahia (FOUFBA). The animals were kept in cages containing five animals each, in room temperature of 22–26 °C with day/night light cycle. Before the expansion procedures, the animals were put under anesthesia with 12 ml/100 g of xetamine (Vetaset®, São Paulo, SP, Brazil) and 6 ml/100 g of xylazine (Coopazine®, Coopers, São Paulo, SP, Brazil). The expansion device consisted of a triple helicoid spring made of 0.020" stainless steel orthodontic wire (Morelli®, Sorocaba, SP, Brazil). The triple helicoid spring occupied a 1.5 mm space between the incisors when installed and had lateral hooks that served as a support for resin bonding of the device to the teeth (Fig. 1). All devices were manufactured in the same size and the triple helicoid measured with a digital caliper.

The rat's superior incisors were separated with a resin spatula and the expansion spring installed in the midline. Enamel conditioning of the incisors with 37 % phosphoric acid gel (Alpha Acid®, DFL, Rio de Janeiro, RJ, Brazil) for 60 s was performed, followed by rinsing and drying of the teeth's surface for 20 s. The bonding was accomplished with an adhesive system (Magic Bond®, Vigodente, Rio de Janeiro, RJ, Brazil) and compound resin (Fill Magic®, Vigodente, Rio de Janeiro, RJ, Brazil), simultaneously light cured for 40 s (ULTRALED XP®, Dabi Atlante, Ribeirão Preto, SP, Brazil).

The rats were divided into four groups with 8 days of experimental time: group 1 basal, no treatment; group 2, expansion; group 3, expansion and laser application; group 4, expansion and LED application (Table 1). In group 3, there was laser application in the first, third, and fifth experimental days (48 h intervals). The parameters chosen in this research are similar to the ones used by our team in previous studies involving bone formation in wound healing with positive results [12, 21, 22]. A Diode laser (Twin



Fig. 1 The triple helicoid spring used on the study. The spring occupied a 1.5 mm space between the incisors and had lateral hooks that served as a support for resin bonding of the device to the teeth

Table 1 Protocol of expansion, laser, and LED irradiations

Group	Treatment	Laser or LED
1	Basal (no treatment)	No
2	Expansion	No
3	Expansion+laser	48-h interval
4	Expansion+LED	48-h interval

Flex®, MMOptics, São Carlos, SP, Brazil) or a LED (FisioLED®, MMOptics, São Carlos, SP, Brazil) was used and irradiation carried out perpendicularly in a single point at the midpalatal suture just behind the superior incisors. In order to deliver to the tissue the equivalent energy (J) of 18 J for both laser and LED equipments, considering that the light sources presented spots and output values very discrepant from each other, spatial average energy fluence (SAEF) was calculated (18 J/cm^2) and used as our administered dosage. The area used for the calculus of SAEF was of 1 cm^2 , instead of the spot area, regarding the scattering in the tissue and the Gaussian distribution. Furthermore, it was requested to the manufacturer that the laser and LED equipment used in this research be calibrated considering this area of 1 cm^2 in the calculus for its supply of the energy dosage, therefore providing a more fair comparison between the equipments. The total dose used for groups 3 and 4 was 54 J/cm^2 (Table 2).

At every irradiation session, the animals were under anesthesia with the same substance used while the expansion device was installed, but with only one third of the dose, since laser irradiation demanded less time than when installing the device. A mouth opener was used during the procedures of laser irradiation. The animals were killed at the end of each experimental period (8 days) with general anesthesia overdose.

The rat's maxilla of all groups was dissected and stored in liquid nitrogen to be evaluated by Raman spectroscopy. Liquid nitrogen is used to minimize bacterial growth and also because chemical fixation is not advisable due to fluorescence emissions from fixative substances. The area evaluated corresponded to the same point in the midpalatal suture where LED and laser light were applied. A baseline Raman spectrum of nontreated bone (cortical bone) was also generated and acted as a control.

Raman spectroscopy

Raman measurements were performed at the Laboratory of Raman spectroscopy of the Center for Biophotonics, School of Dentistry—Federal University of Bahia. A dispersive near-infrared Raman spectrometer (Andor Technology, model Shamrock SR-303i®, Belfast, Northern Ireland) was used.

Table 2 Laser and LED parameters

Parameters	Laser	LED
Wavelength (nm)	780	850
SAEF (J/cm^2)	18	18
Energy (J)	18	18
Output (mW)	70	150±10
Output (W)	0.07	0.15±0.010
Illuminated area in the tissue (cm^2)	1	1
Mode	CW	CW
Application	Contact	Contact
Spot (cm^2)	0.04	0.5
Energy density (J/cm^2)	450	36
Power density (W/cm^2)	1.75	0.3
Exposure time per session (s)	257	120

The equipment uses a wavelength-stabilized diode laser tuned at 785 nm (B&W TEK, model BRM-785-0.30-100-0.22.s, Newark, DE, USA) with 500 mW of nominal power coupled to a fiber-optic based "Raman probe" (B&W TEK, model BAC-100-785, Newark, DE, USA) in order to provide excitation of the sample and collection of the Raman spectra in repeatable excitation collection geometry. The Raman probe has an excitation fiber of 105 μm and a collecting fiber of 200 μm . The collection fiber is coupled to a dispersive spectrometer, composed of an imaging spectrograph and a "back thinned, deep depletion" CCD camera (Andor Technology, model IDUs[®] DU401A-BR-DD, Belfast, Northern Ireland; 1,024×128 pixels, Peltier cooled, -70 °C), which disperses and detects the Raman scattered light. The Solis software (Andor Technology, Solis (i) software, Belfast, Northern Ireland) controls both CCD camera and spectrograph in terms of grating position, slit aperture, number of accumulations and time exposure, as well as spectral calibration of the Raman shift. The slit and grating configurations provided a spectral resolution of about 4 cm^{-1} in the spectral range of 400–1,800 cm^{-1} . The laser power measured at the end of the Raman probe excitation tip was 300 mW.

The Raman system was controlled by a Windows-based microcomputer, which stored and preprocessed the spectral data. The spectral acquisition time for each collection spot was that of 20 s. Five points were measured at the surface of the cortical area of the defect, resulting in total of 200 spectra. All spectra were acquired on the same day and room conditions to avoid optical misalignments and changes in laser power.

For spectrograph calibration², used respectively, a spectral irradiance lamp (Oriel Instruments, model 63358, Stratford, CT, USA) with known spectral curve, which has been

² Intensity correction and wavenumber calibration

measured with long exposure time (~10 min) and used to correct the differences in the intensity response of all optical components along the spectral range, and seven major bands of the naphthalene, where pixel position and known Raman shift were fitted with a third-order polynomial, because this compound has spaced bands in the spectral region 700–1,700 cm^{-1} , which is the region of interest to the Raman spectroscopy when used for biological materials analysis. The calibration of the spectral data was performed using a routine developed under Matlab 5.1 software (The Mathworks, Newark, NJ, USA). Baseline spectra of nontreated bone used on the present study were produced and peaks of interest specified. Spectrum of each animal were taken as previously described. Following acquisition, background fluorescence was filtered using a fifth-order polynomial function applied to the gross spectrum in the 400–1,800 cm^{-1} region using a routine developed under Matlab. Then Raman spectra of each animal were averaged (Fig. 2).

The Raman spectrum of bone presents prominent vibrational bands related to tissue composition (mineral and organic components). The intensity of phosphate (~960 cm^{-1}) is related to the concentration of CHA (hydroxyapatite) and CH groups of lipids and proteins (~1,450 cm^{-1}) levels correspond to organic components (collagen) of the bone. All data collected was submitted to statistical analysis using ANOVA and Student's *t* tests.

Results

Midpalatal suture

The intensity of the Raman shift at ~1,450 cm^{-1} (relative to matrix collagen) represents presence of collagen. There was significant statistical difference in the collagen peaks when comparing all groups 1, 2, 3, and 4 (ANOVA, $p<0.001$). Comparison of group 1 to all other groups (2, 3, and 4) showed significant statistical difference in all cases (Student's *t* test, $p<0.001$). When only treated groups (2, 3, and 4) were analyzed no statistical difference was observed (ANOVA, $p=0.383$). The paired Student's *t* test also showed no statistical difference, even though group 4 presented the highest mean peak value (8.410±1.777; Table 3).

The intensity of the Raman shift at ~960 cm^{-1} (relative to mineral phosphate) is directly related to the concentration/incorporation of CHA by the bone. Higher intensities represent higher concentrations of CHA. There was a statistically significant difference in the CHA peaks among all groups 1, 2, 3, and 4 (ANOVA, $p<0.001$) in the midpalatal suture, with group 4 presenting the highest mean peak value (46.144±17.704). Significant statistical difference was also observed when comparing only the treated groups 2, 3, and 4 (ANOVA, $p=0.019$) with group 4 also having the highest

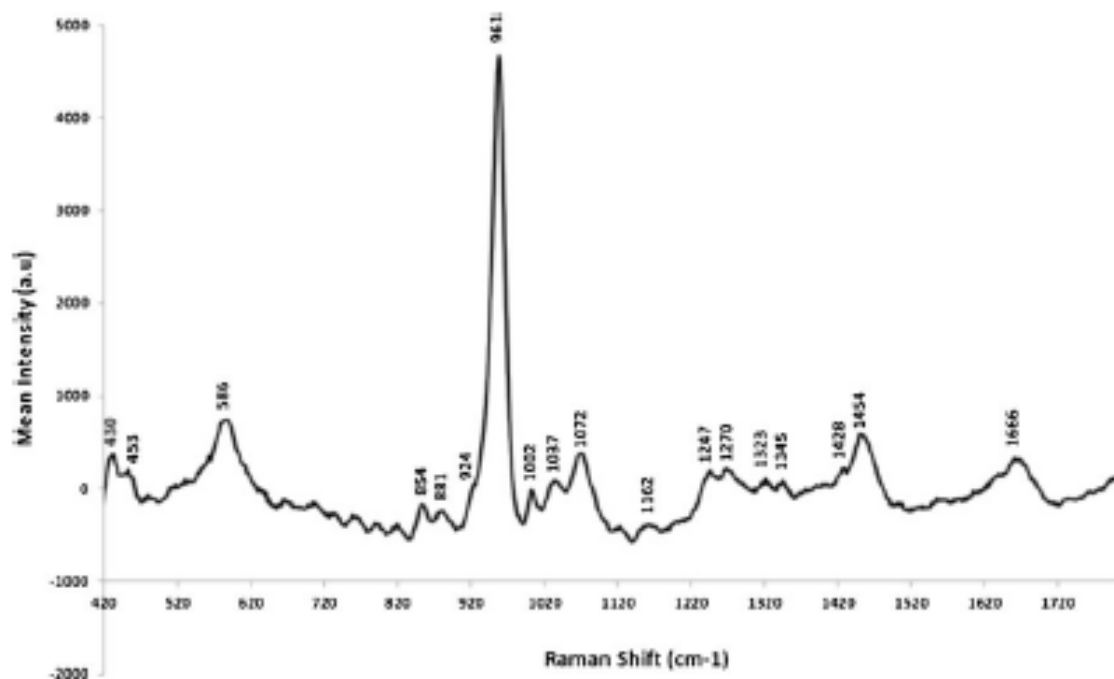


Fig. 2 Raman spectrum of nontreated cortical bone, with labeled peaks

mean peak value. When comparing group 1 to each of the treatment groups 2, 3, or 4 individually, significant statistical difference was found for all comparisons (Student's *t* test, $p=0.012$, $p=0.002$, $p<0.001$). Group 1 had the lowest mean peak value (16.037 ± 2.613). Group 2 compared individually to the irradiated groups 3 and 4 also presented significant statistical difference (Student's *t* test, $p=0.04$, $p=0.009$; Table 4).

Cortical bone

There was significant statistical difference when comparing the collagen peaks among all groups 1, 2, 3, and 4 in the cortical bone (ANOVA, $p=0.001$), and group 1 had the lowest mean peak value (3.513 ± 997). When only treated groups were compared no statistical difference was found (ANOVA, $p=0.313$). Group 4, however, presented the lowest mean peak value (5.520 ± 168 ; Table 5).

Table 3 Mean values \pm SD of the Raman peaks for collagen ($\sim 1,450\text{ cm}^{-1}$) in the midpalatal suture of all groups ($n=5$)

Group	Treatment	Group letter	Means \pm SD
1	Basal	a	$3.310\pm727^{b,c,d}$
2	Expansion	b	7.784 ± 2.004
3	Expansion+laser	c	7.291 ± 2.686
4	Expansion+LED	d	8.410 ± 1.777

Superscript letters indicate that the value is significantly different from the value of the group with the same letter

Significant statistical difference was found when comparing the CHA peaks in the cortical bone among all groups 1, 2, 3, and 4 (ANOVA, $p=0.010$), and group 1 presenting the lowest mean peak (19.920 ± 6.196). No statistical difference was found when comparing only treated groups 2, 3, and 4 (ANOVA, $p=0.189$), although group 4 presented the highest mean peak value (30.731 ± 2.613 ; Table 6).

Discussion

In this study, the presence of collagen was evaluated in the midpalatal suture and statistical difference was only observed when comparison was made between the basal group (group 1) and all treated groups (2, 3, and 4). The basal group had the lowest mean peak value. It was not submitted to any treatment, therefore had no external stimulus to accelerate collagen deposition and latter mineralization

Table 4 Mean values \pm SD of the Raman peaks for collagen ($\sim 960\text{ cm}^{-1}$) in the midpalatal suture of all groups ($n=5$)

Group	Treatment	Group letter	Means \pm SD
1	Basal	a	$16.037\pm2.613^{b,c,d}$
2	Expansion	b	$27.048\pm15.834^{c,d}$
3	Expansion + laser	c	34.479 ± 19.701
4	Expansion + LED	d	46.144 ± 17.704

Superscript letters indicate that the value is significantly different from the value of the group with the same letter

Table 5 Mean values \pm SD of the Raman peaks for collagen ($\sim 1,450\text{ cm}^{-1}$) in cortical bone of all groups ($n=5$)

Group	Treatment	Group letter	Means \pm SD
1	Basal	a	3.513 \pm 997 ^{a,c,d}
2	Expansion	b	6.503 \pm 2.559
3	Expansion+laser	c	7.030 \pm 3.573
4	Expansion+LED	d	5.520 \pm 1.680

Superscript letters indicate that the value is significantly different from the value of the group with the same letter

rather than the normal suture's closure process. Among the treated groups (2, 3, and 4), no statistical difference was found related to collagen deposition, however, the LED group presented the highest mean value.

Other studies have related that in control animals, not submitted to any treatment, such as in our basal group, only minor suture changes related to normal growth occur and the width of the suture remains the same [27].

Expansion alone is already a stimulus to collagen deposition in the midpalatal suture, for bone neoformation begins with an organic nonmineral matrix. Fibroblasts proliferate and repair sutural connective tissues before osteogenesis and remodeling of the suture takes place [8, 28]. In a suture under tension, as in expansion procedures, more extracellular matrix is added at the edges of the suture, for it responds by producing more collagen type III [28]. The use of laser or LED is known to stimulate proliferation of fibroblasts, which are major secretors of collagen, and intensify collagen deposition [21]. Although no statistical difference was found between laser and LED regarding collagen formation in our study, LED irradiation resulted in higher mean peak values. According to previous studies, LED irradiated bones show a high quantity of collagen possibly associated with increased collagen deposition by fibroblasts stimulated by LED light, similar to when using laser light [21, 29].

When comparing the mean peak values for CHA in the midpalatal suture, significant statistical difference was found between the basal group (group 1, no treatment) and all treatment groups. The basal group had the lowest mean peak value. Comparison between only treated groups, submitted to expansion associated or not to laser or LED

(groups 2, 3, and 4), also demonstrated statistical difference as to the presence of CHA. The use of laser (group 3) or LED (group 4) after expansion resulted in higher mineralization of the midpalatal suture as compared when only the expansion procedure was executed (group 2). Even though no difference was found between laser and LED groups, the use of LED resulted in higher mean peak value of CHA, therefore indicating a greater mineralization of the area.

Previous studies have observed that maxillary rapid expansion increases suture width compared with corresponding non-treated groups and also increases significantly new formed bone in the area. This suggests that bone-formative potentials in response to mechanical stimuli exist when suture is expanded [30]. After expansion, the suture starts a remodeling process which can include reabsorption and new bone formation with a rearrangement of the collagen fibers. Simultaneously, the number of osteoprogenital cells increases for bone neoformation until the suture region reaches a structural equilibrium with an aspect similar to the one previous to the expansion [10, 27]. After expansion, suture is filled with new bone and maxillary stabilization than occurs [8].

Osteoprogenital cells are numerous on all bone surfaces, possess receptors for growth factors, and originate osteoblasts. These cells accumulate on the bone surface and synthesize, transport, and release proteins of the matrix initiating mineralization [13]. Mineralization starts when high local concentrations of Ca^{+2} and PO_4^{3-} are reached in order to induce their precipitation into amorphous calcium phosphate, leading to hydroxyapatite crystal formation [23]. Osteocytes are cells resulting from the imprisonment of the osteoblast by mineralized matrix. These cells are intimately linked to the bone matrix and interfere on the metabolism of both Ca^{+2} and P^{+2} [13]. In the matrix, hydroxyapatite crystals grow in clusters, which later coalesce to completely calcify the matrix, filling the spaces between and within the collagen fibers [23]. Growth factor TGF- β 1 is known to stimulate migration of osteoprogenitor cells and is a potent regulator of cell proliferation, cell differentiation, and extracellular matrix synthesis [21, 28]. High levels of the active form of TGF- β 1 are present in osteoblasts, fibroblasts, and endothelial cells during the early stages of midpalatal suture expansion [31]. Findings in previous studies suggest that in an active site, where the tensile forces exerted due to expansion and endogenous TGF- β 1 expression was high, TGF- β 1 had a marked stimulatory effect on bone formation. TGF- β 1, which has been first purified from human platelets, is particularly abundant in bone and platelets in its latent form. After activation, it binds to surface receptors of many cell types, including osteogenic cells and is suggested to be one of the local regulators of bone formation and reabsorption [31]. Its presence may be a synergetic effect on bone formation in response to mechanical and biological stimuli [28].

Table 6 Mean values \pm SD of the Raman peaks for collagen ($\sim 960\text{ cm}^{-1}$) in the cortical bone of all groups ($n=5$)

Group	Treatment	Group letter	Means \pm SD
1	Basal	a	19.920 \pm 6.196
2	Expansion	b	24.101 \pm 11.325
3	Expansion+laser	c	28.682 \pm 12.822
4	Expansion+LED	d	30.731 \pm 2.613

Light irradiation increases the number and activity of osteoblasts [13]. The increase in proliferation and differentiation of osteoblasts, when compared to non-irradiated cells, leads to a higher calcium accumulation rate and bone repair [32]. There is also evidence in the literature suggesting that laser and LED light positively affect the release of TGF- β 1 and several other mediators [21]. Laser therapy on hypoxic-cultured osteoblast stimulates osteoblast differentiation and proliferation through increased expression of BMP-2, osteocalcin, and TGF- β 1 [33]. Previous studies using Raman spectral analysis have also demonstrated higher deposition of CHA in laser- or LED-irradiated bone wounds and may indicate presence of more mature osteoblasts with improved ability of secreting CHA, whereas in other non-irradiated groups, cell proliferation was still occurring [29]. Increased amounts of CHA may be positively correlated to bone mineral density, for higher calcium intakes result in an increase in bone mineral density [23]. Deposition of CHA represents bone maturation [29].

Researchers have observed that laser therapy associated to midpalatal suture expansion is effective for bone regeneration, accelerating mineral apposition velocity, and producing a faster repair process in the area [4, 14, 19, 20]. Reports have demonstrated that a single laser application after rapid expansion induces changes in the osteoblastic activity that persists for an extensive period of time [34]. Other studies have observed a higher mineralized area and higher mineral deposition rate in groups irradiated with laser at early stages throughout 7 days [4], in accordance to our results in this study. Laser irradiation could potentially recruit osteoblasts and/or their maturation throughout the bone borders of the midpalatal suture [4]. Since we were unable to find any previous reports in the literature concerning the use of LED associated to expansion of the midpalatal suture, it makes our discussion of our results very difficult in this aspect. The protocol used in the present study using LED light is similar to the laser protocol used by our team in previous studies and also in this research. Recent researches have indicated that LED, operating in several wavelengths, has beneficial effects and similar mechanisms as the ones observed when laser is used [25], *in vitro* and *in vivo*, in both normal and pathologic conditions [11, 35]. Experimentation using LED light treatments at various wavelengths have shown to significantly increase cell growth in a variety of cell lines, including fibroblasts and osteoblasts [11]. LED irradiated bone (mostly irradiated with IR wavelengths) seem to increased osteoblastic proliferation, collagen deposition, and bone neoformation [13], and also improve in the quality of the newly formed bone due to increased deposition of CHA as seen in other Raman studies when compared to non-irradiated bone [21]. This also corroborates with our findings.

Since in the midpalatal suture the bone evaluated was a newly formed one due to direct active orthopedic treatment

effects of suture expansion, the maxillary cortical bone, a mature bone, was used as a control for comparison. The collagen presence in the maxillary cortical bone presented similar results as to the ones found in the midpalatal suture. Statistical difference was found when comparing the basal group to all treated groups, but no difference occurred when comparing treated groups among themselves. Since the cortical bone is a more mature bone, there is a correspondence to the lower intensities of collagen [24].

Also in accordance to the results in the midpalatal suture, significant statistical difference of CHA deposition was found between the cortical of the basal group and of the treatment groups. The basal group presented the lowest mean peak values for CHA. However, no difference was obtained between values for CHA for the cortical bones among expansion groups with or without laser or LED irradiation. The maxillary cortical bone was not a direct site of orthopedic effect, for the expansion appliance used was not even anchored in the palatal structure. Recruitment of osteoblastic cells to the expansion area could have had an effect in the cortical bone increasing the mineral deposition on the cortical bone. Laser and LED irradiation could also have implied in some effect in the cortical bone area, for the spot area of both light appliances were larger than the midpalatal suture area. Higher mean peak values for CHA in the cortical bone when using LED are in accordance to the higher mean peak values found for LED in the midpalatal suture.

Raman spectroscopy used to analyze alterations in both mineral and organic bone components, is considered a gold standard analysis [21]. No other previous study has evaluated through Raman the CHA and collagen concentrations after laser or LED irradiation in the midpalatal suture after expansion. Furthermore, although LED phototherapy has been shown to improve bone healing, there was no report in literature until now of the influence of LED light in bone neoformation after midpalatal suture expansion.

In this study, Raman spectral analysis indicates that both laser and LED phototherapy improved CHA deposition in the midpalatal suture after expansion which could point to an acceleration of bone maturation in the area that is favorable for reducing the retention period and consequently reducing orthodontic treatment time. Therefore, during expansion, a few visits to the dental office for phototherapy could lead to a faster response and be beneficial for the patient.

According to our results, LED irradiation associated to rapid maxillary expansion could be an alternative to the use of laser in accelerating bone formation in the midpalatal suture. LED radiation has the advantage of a lower cost compared to the laser and it can safely be applied to body surfaces [36, 37]. Another advantage of using LED is the

reduced exposure time of the irradiation, which is less than half of the lasers' exposure time with the same dosage applied, saving more treatment time. Even though we observed favorable results when using different light sources, our knowledge of bone neof ormation and light interactions are still limited. More studies, specially using LED light, are required.

Acknowledgments We would like to thank the Conselho Nacional de Desenvolvimento Científico e Tecnológico (CNPq) for providing financial support for this project.

Conflicts of interest The authors received a grant from Conselho Nacional de Desenvolvimento Científico e Tecnológico (CNPq), a government research agency, but have full control of all primary data and agree to allow the journal to review their data if requested.

References

- Sari Z, Uysal T, Usamez S, Basciftci F (2003) Rapid Maxillary Expansion. Is it better in the mixed or in the permanent dentition? *Angle Orthod* 73:654–661
- Ant ZM, Gökalp H, Atasver T et al (2003) 99mTechnetium-labeled methylene diphosphonate uptake in maxillary bone during and after rapid maxillary expansion. *Angle Orthod* 73:545–549
- Braun S, Bottrel JA, Lee K et al (2000) The biomechanics of rapid maxillary suture expansion. *Am J Orthod Dentofac Orthop* 118:257–261
- Saito S, Shimizu N (1997) Stimulatory effects of low-power laser irradiation on bone regeneration in midpalatal suture during expansion in the rat. *Am J Orthod Dentofac Orthop* 111:525–532
- Monamara JA, Bradon WL (2002) Orthodontics and Dentofacial Orthopedics. Needham Press, Ann Arbor
- Monamara JA (2002) Treatment of children in mixed dentition phase. In: Gruber TM, Vanandall RL (eds) Current principals and techniques, 3rd edn. Guanabara Koogan, Rio de Janeiro, pp 467–496
- Capezolla Filho L, Silva Filho OG (1997) Rapid Maxillary Expansion: a general approach and clinical applications. Part I. *Rev Dent Press Ortod Ortop Maxilofac* 2:88–102
- Zahrowski JJ, Turley PK (1992) Force magnitude effects upon osteoprogenitor cells during premaxillary expansion in rats. *Angle Orthod* 62:197–202
- Marini I, Bonetti GA, Achilli V, Salemi G (2007) A photogrammetric technique for the analysis of palatal three-dimensional changes during rapid maxillary expansion. *Eur J Orthod* 29:26–30
- Lee K, Sugiyama H, Imoto S, Tanne K (2001) Effects of Bisphosphonate on the remodeling of rat sagittal suture after rapid expansion. *Angle Orthod* 71:265–273
- Desmet KD, Paz DA, Correy JJ et al (2006) Clinical and Experimental Applications of NIR-LED Photobiomodulation. *Photomed Laser Surg* 24:121–128
- Pinheiro ALB, Santos NRS, Oliveira PC et al (2012) The efficacy of the use of IR laser phototherapy associated to biphasic ceramic graft and guided bone regeneration on surgical fractures treated with miniplates: a Raman spectral study on rabbits. *Lasers Med Sci*. doi:10.1007/s10103-012-1166-4 [Epub ahead of print]
- Pinheiro ALB, Gebi MEMM (2006) Photoengineering of bone repair processes. *Photomed Laser Surg* 24:169–178
- Merli LAS, Santos MTBR, Genovese WJ, Faloppa F (2005) Effect of low-intensity laser irradiation on the process of bone repair. *Photomed Laser Surg* 23:212–215
- Habib FAL, Gama SKC, Ramalho LMP et al (2012) Effect of laser phototherapy on the hyalinization following orthodontic tooth movement in rats. *Photomed Laser Surg* 30:179–185
- Habib FAL, Gama SKC, Ramalho LMP et al (2010) Laser-Induced alveolar bone changes during orthodontic movement: a histological study on rodents. *Photomed Laser Surg* 28:823–830
- Youssef M, Ashkar S, Hamade E et al (2008) The effect of low level laser therapy during orthodontic movement: a preliminary study. *Lasers Med Sci* 23:27–33
- Kawasaki K, Shimizu N (2000) Effects of low-energy laser irradiation on bone remodeling during experimental tooth movement in rats. *Lasers Surg Med* 26:282–291
- Cepera F, Torres FC, Scanavini MA et al (2012) Effect of a low-level laser on bone regeneration after rapid maxillary expansion. *Am J Orthod Dentofac Orthop* 141:444–450
- Angeletti P, Pereira MD, Gomes HC et al (2010) Effect of low-level laser therapy (GaAlAs) on bone regeneration in midpalatal anterior suture after surgically assisted rapid maxillary expansion. *Oral Surg Oral Med Oral Pathol Oral Radiol Endod* 109:38–46
- Pinheiro ALB, Soares LGP, Cangussu MCT et al (2012) Effects of LED phototherapy on bone defects grafted with MTA, bone morphogenetic proteins and guided bone regeneration: a Raman spectroscopic study. *Lasers Med Sci* 5:903–916
- Pinheiro ALB, Soares LGP, Barbosa APS et al (2012) Does LED phototherapy influence the repair of bone defects grafted with MTA, bone morphogenetic proteins, and guided bone regeneration? A description of the repair process on rodents. *Lasers Med Sci* 27:1013–1024
- Lopes CB, Pinheiro ALB, Sathiah S et al (2005) Infrared laser light reduces loading time of dental implants: a Raman spectroscopic study. *Photomed Laser Surg* 23:27–31
- Morris MD, Mandair GS (2011) Raman assessment of bone quality. *Clin Orthop Relat Res* 469:2160–2169
- Paschalis EP, Mendelsohn R, Boskey AL (2011) Infrared assessment of bone quality. *Clin Orthop Relat Res* 469:2170–2178
- Lopes CB, Pinheiro ALB, Sathiah S et al (2007) Infrared laser photobiomodulation (830 nm) on bone tissue around dental implants: a Raman spectroscopy and scanning electronic microscopy study in rabbits. *Photomed Laser Surg* 25:96–101
- Hou B, Fukui N, Olsen BR (2007) Mechanical force-induced midpalatal suture remodeling in mice. *Bone* 40:1483–1493
- Alaqel SM, Hinton RJ, Opperman LA (2006) Cellular response to force application at craniofacial sutures. *Orthod Craniofac Res* 9:111–122
- Lopes CB, Pacheco MTT, Silveira Junior L et al (2010) The effect of the association of near infrared laser therapy, bone morphogenetic proteins, and guided bone regeneration on tibial fractures treated with internal rigid fixation: a Raman spectroscopic study. *J Biomed Mater Res A* 94:1257–1263
- Kanekawa M, Shimizu N (1998) Age-related changes on bone regeneration in midpalatal suture during maxillary expansion in the rat. *Am J Orthod Dentofac Orthop* 114:646–653
- Sawada M, Shimizu S (1996) Stimulation of bone formation in the expanding mid-palatal suture by transforming growth factor-beta 1 in the rat. *Eur J Orthod* 18:169–179
- Stein A, Benayahu D, Maltz I, Oron U (2005) Low-level laser irradiation promotes proliferation and differentiation of human osteoblasts in vitro. *Photomed Laser Surg* 23:161–166
- Pyo SJ, Song WW, Kim IR et al (2012) Low-level laser therapy induces the expressions of BMP-2, osteocalcin, and TGF- β 1 in

- hypoxic-cultured human osteoblasts. *Lasers Med Sci*. doi:10.1007/s10103-012-1109-0 [Epub ahead print]
34. Silva APRB, Petri AD, Crippa GE et al (2012) Effect of low-level laser therapy after rapid maxillary expansion on proliferation and differentiation of osteoblastic cells. *Lasers Med Sci* 27:777–783
35. Souza APC, Neto AABAV, Marchionni AMF et al (2011) Effect of LED phototherapy (170020 nm) on TGF- β expression during wound healing: an immunohistochemical study in a rodent model. *Photomed Laser Surg* 29:605–6011
36. Uysal T, Ekizer A, Akoay H et al (2012) Resonance frequency analysis of orthodontic miniscrews subjected to light-emitting diode photobiomodulation therapy. *Eur J Orthod* 34:44–51
37. Smith KC (2006) Laser (and LED) therapy is phototherapy. *Photomed Laser Surg* 24:78–80

Proc. SPIE 8569, Mechanisms for Low-Light Therapy VIII, 85690L;
doi:10.1117/12.2002584

Raman Study of the Effect of LED Light on Grafted Bone Defects

Raman Study of the Effect of LED Light on Grafted Bone Defects

Luiz G. P. Soares^{a,b}, Joubert M. S. Aciole^a, Gilberth T. S. Aciole^a, Artur F. S. Barbosa^a, Landulfo Silveira-Júnior^b, Antonio L. B. Pinheiro^{a,b,c}

^aCenter of Biophotonics, School of Dentistry, Federal University of Bahia, Salvador, BA, Brazil, 40110-150; ^bNacional Institute of Optics and Photonics, São Carlos, SP, Brazil, 13560-970, ^cCamilo Castelo Branco University, São José dos Campos, SP, Brazil, 12245-230

ABSTRACT

Benefits of the isolated or combined use light and biomaterials on bone healing have been suggested. Our group has used several models to assess the effects of laser on bone. A Raman spectral analysis on surgical bone defects grafted or not with Hydroxyapatite (HA), treated or not with LED was carried out. 40 rats were divided into 4 groups. On Group I the defect was filled with the clot. On Group II, the defect was filled with the HA. On groups III the defect was filled with Clot and further irradiated with LED and on group IV the defects was filled with the HA and further irradiated with LED. LED ($\lambda 850 \pm 10\text{nm}$, 150mW, $A = 0.5\text{cm}^2$, 68s, 20 J/cm² per session, 140 J/cm² per treatment) was applied at 48 h intervals during 15 days. Specimens were taken after 15 and 30 days after surgery and kept on liquid nitrogen, and underwent Raman analysis. For this, the peak of hydroxyapatite ($\sim 960\text{ cm}^{-1}$) was used as marker of bone mineralization. Significant difference was observed at both times ($p < 0.05$). When the biomaterial was used higher peaks were observed. Association with LED further improved the intensity. Conclusion: It is concluded that LED light improved the effect of the HA.

Key Words: Biomaterial, Bone, Phototherapy, Raman Spectroscopy.

1. INTRODUCTION

Surgeons are challenged daily by the need to recover bone losses due to several etiologic factors¹. The loss of bone fragments or the removal of necrotic or pathologic bone, or even some surgical procedures may create bone defects and often demands the use of biomaterials as the body is not able to repair itself. Many types of biomaterials have been used instead of using autologous grafts to minimize the morbidity of the procedures avoiding two simultaneous surgical procedures. One of the most commonly used biomaterial is the HA. This type of graft may be produced using different composition and shape. It may be used isolated, associated to the use of a membrane (Guided Bone Regeneration - GBR), or mixed to an autologous bone graft².

Many techniques are used to improve the bone healing, including light therapies. Several studies have demonstrated that irradiation with near-Infrared wavelengths can improve bone repair due to its high penetration into tissues compared to visible light³⁻¹⁶. Although the use of LPT for bone healing has been growing steadily, and several studies have demonstrated positive results in the healing of bone tissue³⁻¹⁶, there are to date few reports of the use of combinations of LED light and HA.

LEDs show a relatively narrow emission spectrum that may be optimally tuned to correspond to the requirements of a treatment eliminating unnecessary wavelengths from a particular therapy. Their light intensity can be adjusted and they produce high light levels with low radiant heat output and maintain useful output for long periods of time. LED-based devices may provide a homogeneous light dose at optimal intensity¹⁷⁻¹⁹.

*albp@ufba.br; phone 55 71 3283-9010; fax 55 71 3283-9010; www.laser.odontologia.ufba.br

Mechanisms for Low-Light Therapy VIII, edited by Michael R. Hamblin, Praveen R. Arany, James D. Carroll,
Proc. of SPIE Vol. 8569, 85690L · © 2013 SPIE · CCC code: 1605-7422/13/\$18 · doi: 10.1117/12.2002584

Proc. of SPIE Vol. 8569 85690L-1

Vibrational techniques such as Raman spectroscopy have been employed in order to provide information on the metabolic status of graft, such as the mineral content and matrix composition of the tissue that may provide early indications of graft success or failure^{4,5}. Raman spectra brings information regarding the chemical bonds through the inelastic scattering of light during the polarization of the electronic cloud, so the unique molecular information of the biochemical composition of a sample can be assessed in vivo, rapid and nondestructively²⁰, and may probe, through remote optical cables, the molecular changes of bio-tissues²¹.

The aim of this study was to evaluate the level of bone mineralization, through the analysis of the intensities of Raman spectra of HA ($\sim 960\text{ cm}^{-1}$) on the repair of bone defects grafted or not with biphasic synthetic micro-granular HA + β - calcium triphosphate associated or not with LED phototherapy $\lambda 850\text{ nm}$ (LEDPT).

2. MATERIAL AND METHODS

2.1 Ethics, animal model, housing, and sampling

The Animal Ethics Committee of the Federal University of Bahia approved this work. Forty healthy adult male Wistar rats (~ 2 months old, average weight $295 \pm 25\text{ g}$) were kept under natural conditions of light, humidity, and temperature at the Laboratory of Animal Experimentation of the School of Dentistry of the Federal University of Bahia during the experimental period. The animals were fed with standard laboratory diet (Labina[®], Purina, São Paulo – Brazil) and had water ad libitum. The animals were kept in individual micro-isolators and accommodated in ventilated shelves (INSIGHT Equipamentos Ltda - Monte Alegre, Ribeirão Preto - São Paulo, Brazil). This system provides a controlled environment with decreased risk of infection and good sanitary condition. Controlled day/night light cycle and temperature was performed during the experimental period. The animals were randomly distributed into 4 groups and then subdivided into 2 subgroups according to the animal death timing. The distribution of the animals may be seen in Table 1.

Table 1: Distribution of the animals according the treatment protocol.

Groups	Animal Death (days)	Phototherapy	Biomaterial	n
Group I	15 or 30	No	No	10
Group II	15 or 30	No	X	10
Group III	15 or 30	LED	No	10
Group IV	15 or 30	LED	X	10

2.2 Surgical procedure

Prior to intramuscular general anesthesia, the animals were sedated (0.04 ml/100g of atropine subcutaneously) and 20 minutes later general anesthesia was carried out (10% ketamine (0.1 mL/100g - Cetamin[®], Syntec, São Paulo - Brazil) + 2% xylazine (0.1 mL/100g; Xilazin[®], Syntec, São Paulo – Brazil). The animals had their right leg shaved and a 3-cm-long incision was performed at the right tibia with a no. 15 scalpel blade. Skin and subcutaneous tissues were dissected down to the periosteum, which was gently sectioned exposing the bone and a standard partial thickness 2-mm-round defect was surgically produced using trephine drill (SIN, São Paulo – Brazil) mounted on a 16:1 reduction contra angle handpiece (NSK, Tochigi – Japan), maximum resistance of 35N with low speed drill, 1.200 rpm, under refrigeration (Driller 600[®], SIN, São Paulo – SP – Brazil) in each animal.

Defects on animals in groups Clot and LED were filled only with the blood clot. Defects in groups Biomaterial and LED + Biomaterial were filled with biomaterial. The animals on groups LED and LED + Biomaterial were further irradiated with LED light (FisioLED[®], MMOptics, São Carlos, São Paulo, Brazil). All wounds were routinely sutured and the animals received a single dose of antibiotics (Pentabiotico[®], 0.2ml; Fort Dodge Animal Health, Overland Park, Kansas – USA). For the present study a biphasic synthetic micro-granular HA + β - calcium triphosphate (70%/30% respectively) completely filled the bone defects when indicated, as recommended by the manufacturer.

2.3 Phototherapy protocol

LEDPT was carried out with the FizioLED[®] device (MMOptics, São Carlos, São Paulo, Brazil, $\lambda 850 \pm 10\text{nm}$, 150mW, $\phi \sim 0.5\text{cm}^2$, 20 J/cm² per session, 140 J/cm² per treatment), and light was transcutaneously applied over the defect at 48-h intervals, being the first session carried out immediately after surgery. Energy densities used were based upon previous studies carried out by our group³⁻¹⁵. LED output power was confirmed by using a calibrated power meter (Power Meter Thorlabs PM30-121, Thorlabs GmbH, Munich, Germany).

2.4 Animal death and sample manipulation

Animal death occurred after 15 and 30 days after the surgery in a CO₂ chamber (Insight Equipamentos, model EB 248, Ribeirão Preto, SP, Brasil). Following animal death, the samples were longitudinally cut under refrigeration (Driller 600[®], SIN, São Paulo – SP – Brazil), snap-frozen in liquid nitrogen and kept deep-refrigerated (-80°C) until spectral analysis in order to minimize the growth of aerobic bacteria and because chemical fixation is not advisable due to fluorescence emission and scattering from fixative substances and tissue biochemical changes due to protein denaturation^{5,6,22,23}.

2.5 Raman spectroscopy

Raman measurements were performed at the Laboratory of Raman Spectroscopy of the Center for Biophotonics, School of Dentistry - Federal University of Bahia. A dispersive near-infrared Raman spectrometer (Andor Technology, model Shamrock SR-303i[®], Belfast, Northern Ireland) was used.

The equipment uses a wavelength-stabilized diode Laser tuned at 785 nm (B&W TEK, model BRM-785-0.30-100-0.22.s, Newark, DE, USA) with 500 mW of nominal power coupled to a fiber-optic based "Raman Probe" (B&W TEK, model BAC-100-785, Newark, DE, USA) in order to provide excitation of the sample and collection of the Raman spectra in repeatable excitation-collection geometry. The Raman probe has an excitation fiber of 105 μm and a collecting fiber of 200 μm . The collection fiber is coupled to a dispersive spectrometer, composed of an imaging spectrograph and a "back thinned, deep depletion" CCD camera (Andor Technology, model IDUs[®] DU401A-BR-DD, Belfast, Northern Ireland, 1024 x 128 pixels, Peltier-cooled down to -70 °C), which disperses and detects the Raman scattered light. The Solis software (Andor Technology, Solis (i) software, Belfast, Northern Ireland) controls both CCD camera and spectrograph in terms of grating position, slit aperture, number of accumulations and time exposure, as well as spectral calibration of the Raman shift. The slit and grating configurations provided a spectral resolution of about 4 cm⁻¹ in the spectral range of 400 to 1800 cm⁻¹. The laser power measured at the end of the Raman probe excitation tip was 300 mW.

The Raman system was controlled by a Windows-based microcomputer, which stored and pre-processed the spectral data^{5,6,22,23}. The spectral acquisition time for each collection spot was that of 20 s. Five points were measured at the surface of the cortical area of the defect in each one of the 40 samples, resulting in total of 200 spectra. All spectra were acquired on the same day and room conditions to avoid optical misalignments and changes in laser power.

For spectrograph calibration it was used, respectively, a spectral irradiance lamp (Oriel Instruments, model 63358, Stratford, CT, USA) with known spectral curve, which has been measured with long exposure time (~10 min) and used to correct the differences in the intensity response of all optical components along the spectral range, and seven major bands of the naphthalene, where pixel position and known Raman shift were fitted with a 3rd order polynomial, because this compound has spaced bands in the spectral region 700 - 1700 cm⁻¹, which is the region of interest to the Raman spectroscopy when used for biological materials analysis^{5,6,22,23}. The calibration of the spectral data was performed using a routine developed under Matlab 5.1 software (The Mathworks, Newark, NJ, USA).

2.6 Spectra processing and peak detection

Baseline spectra of non-treated bone and of the biomaterial used on the present study were produced, and peaks of interest specified (Fig. 1). Spectrum of each animal were taken as previously described.

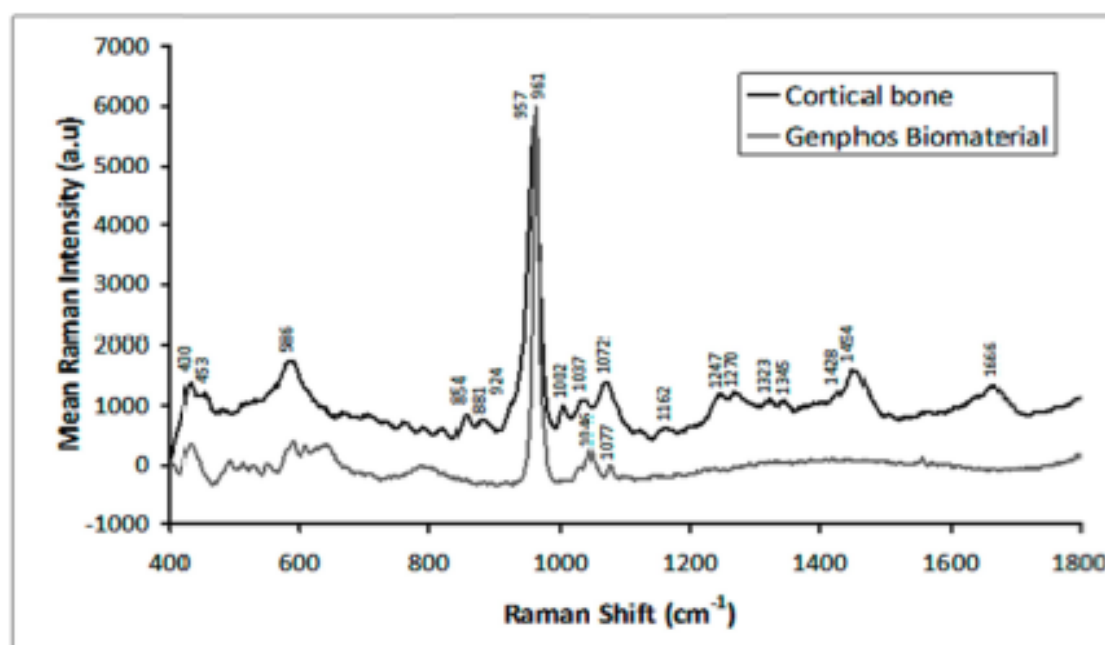


Figure 1. Dislocated peaks of cortical bone and GenPHOS biomaterial.

Following acquisition, background fluorescence was filtered using a 5th order polynomial function applied to the gross spectrum in the 400 - 1800 cm^{-1} region using a routine developed under Matlab. Then Raman spectra of each animal were averaged and smoothed by "moving average" technique, which consisted of calculating the mean of five adjacent points.

Absolute intensities as well as their standard deviations were calculated and plotted using Microsoft Excel or Minitab software and the statistical analysis (t-test and ANOVA, $p < 0.05$) in the peak intensities was performed using Minitab 15.0[®] (Minitab, Belo Horizonte, MG, Brazil) software.

2. RESULTS

Measurements of the intensities of peaks related to the inorganic contents (HA), at the day 15th, showed, for $\sim 960 \text{ cm}^{-1}$, highest mean on group Biomaterial (9392 ± 4287) and lowest on group Clot (4196 ± 1047). At the 30th day, measurements of the inorganic content of all groups showed that, for $\sim 960 \text{ cm}^{-1}$, highest mean on group Biomaterial (7128 ± 2117) and lowest on group Clot (3949 ± 1522). The summary of the intensities of all groups could be seen on Figure 2.

Table 4: Summary of the statistical analysis (t-test) of the Raman peaks between groups at the 30th day.

Group Raman Shift (cm ⁻¹)	Clot ^a	Biomaterial ^b	LED ^c	LED + Biomaterial ^d
~960	3949 ± 1522 ^{b,c,d}	7128 ± 2117 ^{a,c,d}	5270 ± 1159 ^{a,b}	5084 ± 2373 ^{a,b}

Letters indicates significant differences (p < 0.05)

4. DISCUSSION

The Wistar rat model adopted on the present investigation allows a rapid healing period, is resistant to climatic changes and is routinely used to study bone healing.

Despite LPT being shown effective on improving bone healing on several models⁵⁻²², the use of LED light on bone is still poorly studied and its association to biomaterials was up to now inexistent. Studies involving the use of laser light on bone regeneration suggested that its effect on bone healing depends not only on the total dose of irradiation, but also on the irradiation time and the irradiation mode³⁻¹⁴.

Many previous reports are suggestive that irradiated bone, mostly with IR wavelengths, shows increased osteoblastic proliferation, collagen deposition, and bone neoformation when compared to non-irradiated bone³⁻¹⁶.

Raman spectroscopy has been employed to access the molecular constitution of a specific tissue and then classify it according to differences observed in the spectra^{21,24,25}. Several studies found elsewhere on the literature has shown successful use of NIR Raman spectroscopy as a diagnostic tool for healthy, diseased or healing bones^{5,6,26-28}. Our group has successfully used this technique to determine both mineral and organic components changes on the healing bone. Our team and others consider this method of assessment as a gold standard to study bone components and constitution^{5,6,8,16,24-28} and to reveal biochemical changes associated to the healing process.

Our group previously found that the levels of HA on deep areas of healing bone of irradiated and non-irradiated subjects differ significantly from day 30th after treatment^{3-6,8,16}. On this study, we were not able to detect differences on the healing of bone defects associated to the combined use of biomaterial and LED light. This was probably due to the presence of the Biomaterial that is mainly composed of HA and was well preserved at the site at the end of the experiment. However, the use of de LED was capable of increasing mineralization when compared to the Clot only group.

Deposition of HA represents bone maturation and increased amount of HA in bone is indicative of a more resistant bone. The observed differences in the rate of deposition of HA between irradiated and non-irradiated subjects is probably due to the ability of the LED light to induce changes at cellular levels, such as improved ATP synthesis, early osteoblastic differentiation and the release of growth factors¹.

5. CONCLUSION

It is concluded that the use of the LED light on HA grafted bone did not improved the outcome of the treatment as the persistence of the HA on the defect may had interfered with the Raman reading.

REFERENCES

- [1] Pinheiro, A.L.B., Gerbi, M. E. M. M., "Photoengineering of Bone Repair Processes," *Photomed Laser Surg* 24(2), 169-178 (2006).
- [2] Torres, C.S., Santos, J.N., Monteiro, J.S.C., Gomes, P.T.C.C., Pinheiro, A.L.B., "Does the Use of Laser Photobiomodulation, Bone Morphogenetic Proteins, and Guided Bone Regeneration Improve the Outcome of Autologous Bone Grafts? An in Vivo Study in a Rodent Model," *Photomed Laser Surg* 26, 371-377 (2008).
- [3] Pinheiro, A.L.B., Soares, L.G.P., Barbosa, A.F.S., Ramalho, L.M.P., Santos, J.N., "Does LED phototherapy influence the repair of bone defects grafted with MTA, bone morphogenetic proteins, and guided bone regeneration? A description of the repair process on rodents," *Lasers Med Sci* 27(5), 1013-24 (2011).

- [4] Lopes, C. B., Pinheiro, A.L.B., Sathiaiah S. S. N. S., Salgado, M.C., "Infrared laser photobiomodulation (830nm) on bone tissue around dental implants: A Raman spectroscopy and Scanning Electronic Microscopy study in rabbits," *Photomed Laser Surg* 25, 96-101 (2007).
- [5] Pinheiro, A.L.B., Aciole, G.T.S., Cangussu, M.C.T., Pacheco, M.T.T., Silveira Jr, L., "Effects of laser phototherapy on bone defects grafted with mineral trioxide aggregate, bone morphogenetic proteins, and guided bone regeneration: A Raman spectroscopic study" *J Biomed Mater Res A* 95(4), 1041-1047 (2010).
- [6] Lopes, C.B., Pacheco, M.T.T., Silveira Jr, L., Cangussu, M.C.T., Pinheiro, A.L.B., "The effect of the association of near infrared laser therapy, bone morphogenetic proteins, and guided bone regeneration on tibial fractures treated with internal rigid fixation: A Raman spectroscopic study," *J Biomed Mater Res A* 4(4), 1257-63 (2010).
- [7] Torres, C.S., Santos, J.N., Monteiro, J.S.C., Gomes, P.T.C.C., Pinheiro, A.L.B., "Does the Use of Laser Photobiomodulation, Bone Morphogenetic Proteins, and Guided Bone Regeneration Improve the Outcome of Autologous Bone Grafts? An in Vivo Study in a Rodent Model," *Photomed Laser Surg* 26, 371-377 (2008).
- [8] Pinheiro, A.L.B., Oliveira, M.G., Martins, P.P.M., Ramalho, L.M.P., Oliveira, M.A.M., Novaes Jr, A., Nicolau, R. A., "Biomodulatory effects of LLLT on bone regeneration," *Laser Ther* 13, 73-79 (2001).
- [9] Weber, J.B.B., Pinheiro, A.L.B., Oliveira, M.G., Oliveira, F.A.M., Ramalho, L. M. P., "Laser therapy improves healing of bone defects submitted to autogenous bone graft," *Photomed Laser Surg* 24, 38-44 (2006).
- [10] Pinheiro, A.L.B., Gerbi, M.E.M.M., Limeira Junior, F.A., Ponzi, E.A.C., Marques, A.M.C., Carvalho, C.M., Santos, R.C., Oliveira, P.C., Nôia, M., Ramalho, L.M.P., "Bone repair following bone grafting hydroxyapatite guided bone regeneration and infrared laser photobiomodulation: a histological study in a rodent model," *Lasers Med Sci* 24, 234-240 (2009).
- [11] Gerbi, M.E.M.M., Marques, A.M.C., Ramalho, L.M.P., Ponzi, E.A., Carvalho, C.M., Santos, R.C., Oliveira, P.C., Nôia, M., Pinheiro, A.L.B., "Infrared Laser Light Further Improves Bone Healing When Associated with Bone Morphogenetic Proteins: An in Vivo Study in a Rodent Model," *Photomed Laser Surg* 26, 55-60 (2008).
- [12] Pinheiro, A.L.B., Gerbi, M.E.M., Ponzi, E.A.C., Ramalho, L.M.P., Marques, A.M.C., Carvalho, C.M., Santos, R.C., Oliveira, P.C., Nôia, M., "Infrared Laser Light Further Improves Bone Healing When Associated with Bone Morphogenetic Proteins and Guided Bone Regeneration: An in Vivo Study in a Rodent Model," *Photomed Laser Surg* 26, 167-174 (2008).
- [13] Gerbi, M.E.M.M., Pinheiro, A.L.B., Ramalho, L.M.P., "Effect of IR laser photobiomodulation on the repair of bone defects grafted with organic bovine bone," *Lasers Med Sci* 23, 313-317 (2008).
- [14] Gerbi, M.E., Pinheiro, A.L.B., Marzola, C., Limeira Junior, F.A., Ramalho, L.M.P., Ponzi, E.A.C., Soares, A.O., Carvalho, L.C., Lima, H.V., Gonçalves, T.O., "Assessment of Bone Repair Associated with the Use of Organic Bovine Bone and Membrane Irradiated at 830 nm," *Photomed Laser Surg* 23, 382-388 (2005).
- [15] Lopes, C.B., Pacheco, M.T., Silveira Junior, L., Duarte, J., Cangussu, M.C., Pinheiro, A.L., "The effect of the association of NIR laser therapy BMPs, and guided bone regeneration on tibial fractures treated with wire osteosynthesis: Raman spectroscopy study" *J Photochem Photobiol B* 89(2-3), 125-30 (2007).
- [16] Karu, T.I., Pyatibrat, L.V., Afanasyeva, N.I., "A Novel Mitochondrial Signalling Pathway Activated by Visible-to-near Infrared Radiation," *Photochem and Photobiol* 80, 366-72 (2004).
- [17] Whelan, H.T., Smits, J.R.R.L., Buchman, E.V., Whelan, N.T., Turner, S.G., Margolis, D.A., Cavenini, V., Stinson, H., Ignatius, R., Martin, T., Cwiklinski, J., Philippi, A.F., Graf, W.R., Hodgson, B., Gould, L., Kane, M., Chen, G., Caviness, J., "Effect of NASA light emitting diode irradiation on wound healing," *J Clin Laser Med Surg* 19, 305-314 (2001).
- [18] Whelan, H.T., Buchmann, E.V., Whelan, N.T., Turner, S.G., Cavenini, V., Stinson, H., Ignatius, R., Martin, T., Cwiklinski, J., Meyer, G. A., Hodgson, B., Gould, L., Kane, M., Chen, G., Caviness, J., "NASA light emitting diode medical applications: from deep space to deep sea," *Space Technology and Applications International Forum*, 35-45 (2001).
- [19] Barolet, D., "Light-emitting diodes (LEDs) in dermatology," *Semin Cutan Med Surg* 27, 227-238 (2008).
- [20] Hanlon, E.B., Manoharan, R., Koo, T.W., Shafer, K.E., Motz, J.T., Fitzmaurice, M., Kramer, J.R., Itzkan, I., Dasari, R.R., Feld, M.S., "Prospects for in vivo Raman spectroscopy," *Phys Med Biol* 45, R1-R59 (2000).
- [21] Kavukcuoglu, N.B., Patterson-Buckendahl, P., Mann, A., "Effect of osteocalcin deficiency on the nanomechanics and chemistry of mouse bones," *J Mech Behav Biomed* 2, 254-348 (2009).
- [22] Timlin, J.A., Carden, A., Morris, M.D., "Chemical Microstructure of Cortical Bone Probed by Raman Transverse," *Appl Spectrosc* 53(11), 1429-1435 (1999).
- [23] Pinheiro, A.L.B., Lopes, C.B., Pacheco, M.T.T., Brugnara, A., Zanin, F.A.A., Cangussu, M.C.T., Silveira-Junior,

- L., "Raman spectroscopy validation of DIAGNOdent-assisted fluorescence readings on tibial fractures treated with laser phototherapy, BMPs, guided bone regeneration and miniplates," *Photomed Laser Surg* 28, 89-97 (2010).
- [24] Penel, G., Delfosse, C., Descamps, M., Leroy, G., "Composition of bone and apatitic biomaterials as revealed by intravital Raman microspectroscopy," *Bone* 36, 893-901 (2005).
- [25] Carden, A., Morris, M.D., "Application of vibrational spectroscopy to the study of mineralized tissues (review)," *J Biomed Opt* 5, 259-268 (2000).
- [26] Pinheiro, A. L. B., Santos, N. R. S., Oliveira, P. C., Aciole, G. T. S., Ramos, T. A., Gonzalez, T. A., Silva, L. N., Barbosa, A. F. S., Silveira-Junior, L., "The efficacy of the use of IR laser phototherapy associated to biphasic ceramic graft and guided bone regeneration on surgical fractures treated with miniplates: a Raman spectral study on rabbits," *Lasers Med Sci* DOI 10.1007/s10103-012-1096-1(2012)
- [27] Carvalho, F. B., Aciole, G. T. S., Aciole, J. M. S., Silveira-Junior, L., Santos, J. N., Pinheiro, A. L. B., "Assessment of bone healing on tibial fractures treated with wire osteosynthesis associated or not with infrared laser light and biphasic ceramic bone graft (HATCP) and guided bone regeneration (GBR): Raman spectroscopy study," *Proc. SPIE* 7887, 1-6 (2011).
- [28] Pinheiro, A. L. B., Lopes, C. B., Pacheco, M. T. T., Brugnera, A., Zanin, F. A. A., Cangussú, M. C. T., Silveira-Junior, L., "Raman spectroscopy validation of DIAGNOdent-assisted fluorescence readings on tibial fractures treated with laser phototherapy, BMPs, guided bone regeneration and miniplates," *Photomed Laser Surg* 28, 89-97 (2010).

Lasers Med Sci. 2013 Mar 24. [Epub ahead of print]

Raman study of the repair of surgical bone defects grafted with biphasic synthetic microgranular HA+ β -calcium triphosphate and irradiated or not with λ 780 nm laser

Raman study of the repair of surgical bone defects grafted with biphasic synthetic microgranular HA + β -calcium triphosphate and irradiated or not with λ 780 nm laser

LuizGuilherme P. Soares · Aparecida Maria C. Marques ·
Artur Felipe S. Barbosa · Nicole R. Santos ·
Jouber Mateus S. Aciolo · Caroline Mathias C. Souza ·
Antonio Luiz B. Pinheiro · Landulfo Silveira Jr.

Received: 16 October 2012 / Accepted: 28 February 2013
© Springer-Verlag London 2013

Abstract Thetreatment of bone loss due to different etiologic factors is difficult, and many techniques aim to improve repair, including a wide range of biomaterials and, recently, photobioengineering. This work aimed to assess, through

Raman spectroscopy, the level of bone mineralization using the intensities of the Raman peaks of both inorganic (~ 960 , $\sim 1,070$, and $\sim 1,077$ cm^{-1}) and organic ($\sim 1,454$ and $\sim 1,666$ cm^{-1}) contents of bone tissue. Forty rats were divided into four groups each subdivided into two subgroups according to the time of killing (15 and 30 days). Surgical bone defects were made on femur of each animal with a trephine drill. On animals of group Clot, the defect was filled only by blood clot; on group Laser, the defect filled with the clot was further irradiated. On animals of groups Biomaterial and Laser+Biomaterial, the defect was filled by biomaterial and the last one was further irradiated ($\lambda 780$ nm, 70 mW, $\Phi \sim 0.4$ cm^2 , 20 J/ cm^2 session, 140 J/ cm^2 treatment) in four points around the defect at 48-h intervals and repeated for 2 weeks. At both 15th and 30th day following killing, samples were taken and analyzed by Raman spectroscopy. At the end of the experimental time, the intensities of both inorganic and organic contents were higher on group Laser+Biomaterial. It is concluded that the use of laser phototherapy associated to biomaterial was effective in improving bone healing on bone defects as a result of the increasing deposition of calcium hydroxyapatite measured by Raman spectroscopy.

L. G. P. Soares · A. M. C. Marques · A. F. S. Barbosa · N. R. Santos ·
J. M. S. Aciolo · C. M. C. Souza · A. L. B. Pinheiro (✉)
Center of Biophotonics, School of Dentistry, Federal University of
Bahia, Av. Amâjo Pinho, 62, Canela, Salvador,
BA 40110-150, Brazil
e-mail: albp@ufba.br

L. G. P. Soares
e-mail: luizguilherme_@hotmail.com

A. M. C. Marques
e-mail: cidamanques77@hotmail.com

A. F. S. Barbosa
e-mail: arturfelipes@gmail.com

N. R. Santos
e-mail: ribeirnicole@hotmail.com

J. M. S. Aciolo
e-mail: jouber.aciolo@hotmail.com

C. M. C. Souza
e-mail: Caroline.mathias@hotmail.com

A. M. C. Marques · A. L. B. Pinheiro
National Institute of Optics and Photonics, Physics Institute of São
Carlos, University of São Paulo, São Carlos, SP, Brazil 13560-970

A. L. B. Pinheiro · L. Silveira Jr.
Camilo Castelo Branco University, Núcleo do Parque Tecnológico
de São José dos Campos: Rod. Presidente Dutra Km 139, São José
dos Campos, Eugênio de Melo, SP 12247-004, Brazil

L. Silveira Jr.
e-mail: landulfo.silveira@gmail.com

Keywords Biomaterial · Bone repair · Hydroxyapatite ·
Laserphototherapy

Introduction

Bone is a dynamic, highly organized, and specialized biological tissue composed of metabolically active cells that are

integrated into a rigid framework (organic and inorganic components). Microscopically, it shows few metabolically active cells, hematopoietic elements of bone marrow, and a large amount of intercellular substance formed from collagen fibers and stiffening substances [1–4].

The inorganic content of bone consists primarily of calcium phosphate and calcium carbonate, with small quantities of Mg, F, and Na. The mineral crystals form hydroxyapatite (HA), which precipitates in an orderly arrangement around the collagen fibers of the osteoid. The mineralization of osteoid by inorganic mineral salts gives bone its strength and rigidity. The initial calcification of osteoid typically occurs within a few days of secretion but is completed over the course of several months [1–4]. The healing potential of bone is influenced by a variety of biochemical, biomechanical, cellular, hormonal, and pathological mechanisms. A continuously occurring state of bone deposition, reabsorption, and remodeling facilitates the repair process [1, 5].

Surgeons are challenged daily by the need to recover bone losses due to several etiologic factors [4]. The loss of bone fragments or the removal of necrotic or pathologic bone or even some surgical procedures may create bone defects. These defects may be too large for spontaneous and physiologic repair. Bone is the most common type of graft used in oral

implantology, in prosthetic surgery, in the treatment of congenital defects, and in reconstructive procedures of the jaws. Often autologous bone grafts are used, and they may be taken from several parts of the skeleton. Biocompatibility and osteointegration, as well as substantial osteogenic potential [6, 7], characterize autologous bone grafts.

Many types of biomaterials have been used instead of using autologous grafts to minimize the morbidity of the procedures avoiding two simultaneous surgical procedures. One of the most commonly used biomaterial is the HA. This type of graft may be produced using different composition and shape. It may be used isolated, associated to the use of a membrane (guided bone regeneration), or mixed to an autologous bone graft [7]. Both autologous and xenografts have been used to provide a framework or stimulate new bone formation, and many times, these grafts respond positively to the use of selected wavelengths of light [4].

As a means of improving the recovery of large bone defects, the use of several techniques, including grafts and photobiomodulation, has been extensively studied [4–7]. Many techniques are used to improve the bone repair; recently, laser light has been used for improving bone repair in several conditions such as in dental implants [8, 9] and autologous bone graft [7, 10] and several types of bone defects [4, 11–17].

Table 1 Tentative attribution and peak positions of the main Raman bands from baseline cortical bone and biomaterial Genphos® used in the study

Raman peak	Attribution	Importance in bone healing and tissue remodeling	Present in		References
			Bone	Biomaterial	
958–961	ν_1 symmetric stretching of phosphate apatite (PO_4^{3-})	Band position and bandwidth highly sensible to carbonate substitution in the phosphate apatite. Band position at 956 cm^{-1} indicates an amorphous, highly carbonated bone; at 962 cm^{-1} indicates a high crystalline phosphate apatite. Smaller bandwidth indicates lower substitution of phosphate by carbonate in the apatite lattice (higher crystallinity). Higher bandwidth indicates smaller and unordered crystallites by carbonate substitution of phosphate. As bone matures, the size of the individual mineral crystal was found to increase.	X	X	[20–23]
1,070	ν_1 symmetric stretching B-type carbonate (CO_3^{2-})	Substitution of the carbonate ion in the phosphate position in the hydroxyapatite lattice structure. Peak intensity increases with carbonate substitution	X		[20, 21, 23, 24]
1,077	ν_3 asymmetric stretching of phosphate apatite (PO_4^{3-})	In carbonated apatite the band broadens and the peak shifts to lower wavenumbers. The overlap with the carbonate band at $1,072\text{ cm}^{-1}$ may reduce the measurement precision even with lower carbonated apatite		X	[20, 22, 23, 25]
1,454	CH_2/CH_3 bending/wagging of methylene side chain—collagen matrix	Collagen I is the most abundant in mature bone while collagen II occurs in the initial phase of cartilage callus. Its wavenumber is at around $1,443\text{ cm}^{-1}$ for collagen I and changes to $1,454\text{ cm}^{-1}$ for collagen II	X		[23, 26–29]
1,666	Amide I (C=O stretching, out-of-plane C-N stretching, CCN deformation, NH in-plane bending)—collagen matrix	Its wavenumber is at around $1,660\text{ cm}^{-1}$ for collagen I and changes to $1,668\text{ cm}^{-1}$ for collagen II. This peak is sensitive to breakdown or rupture of collagen cross-link as bone matures	X		[23, 26–29]

Several studies have demonstrated that near-infrared laser phototherapy (NIR LPT) is the most suitable for bone repair due to its higher penetration depth in the bone tissue when compared to visible laser light [6]. Although the use of Laser phototherapy (LPT) on the bone healing has been growing steadily and several studies have demonstrated positive results on the healing of bone tissue, there are few reports on the association of LPT and biomaterials [4–17].

It has been shown in various *in vitro* and *in vivo* models that LPT at the cellular level stimulates the photoacceptor cytochrome c oxidase, resulting in increased energy metabolism and production and stimulation of mitochondrial oxidative metabolism. It can modulate fibroblast proliferation, attachment, and synthesis of collagen and procollagen; promote angiogenesis; and stimulate macrophages and lymphocytes, thus accelerating bone repair process [4, 21]. Our group has found, in *in vivo* studies, an increased collagen synthesis at early stages of the repair on irradiated subjects using histological analysis [12–16], Raman spectroscopy [5, 6, 8, 14, 15, 17], and electron microscopy [8].

Vibrational techniques such as Raman spectroscopy have been employed in order to provide information on the metabolic status of graft, such as the mineral content and matrix composition of the tissue that may provide early indications of graft success or failure [5]. Raman spectra brings information regarding the chemical bonds through the inelastic scattering of light during the polarization of the electronic cloud, so the unique molecular information of the biochemical composition of a sample can be assessed *in vivo*, rapid, and nondestructively [18], and may probe, through remote optical cables, the molecular changes of bio-tissues [19].

The Raman spectrum of bone shows prominent vibrational bands related to tissue composition. The main Raman bands of bone tissues are located at ~ 960 , $\sim 1,070$, $\sim 1,072$, $\sim 1,454$, and $\sim 1,666$ cm^{-1} . The band at ~ 960 cm^{-1} is attributed to phosphate HA component, and the one at $\sim 1,070$ cm^{-1} is attributed to carbonate HA. The bands at 1,454 and 1,666 cm^{-1} are attributed to the collagen matrix components (Table 1).

In summary, despite bone repair occurs spontaneously most of the time, there are situations in which it takes longer time or does not occur. It is important to realize that the bone repair process aims to restore both anatomy and function. On these cases, the use of grafts is indicated. Due to the morbidity associated to autologous grafting, the use of biomaterials is widely accepted as a way to minimize and speed up the repair process. One of the most used biomaterial is the hydroxyapatite, which has been proven to be a very effective osteoconductor of bone formation. Bone repair comprises a series of cellular and biochemical events that lead to the formation of new bone. Initially, the newly formed bone is highly cellular; the collagen fibers are randomly orientated, relatively less mineralized, and less

Table 2 Distribution of the animals according the treatment protocol

Groups	Animal death (days)	Phototherapy	Biomaterial	n
Group I	15 or 30	No	No	10
Group II	15 or 30	No	X	10
Group III	15 or 30	Laser	No	10
Group IV	15 or 30	Laser	X	10

resistant than the mature one (a cartilaginous tissue which is rich of collagen II). Later, it is replaced, through mineralization, to a mature or lamellar bone and a more resistant and mature collagen I matrix [4, 6, 11].

The use of light as therapeutic agents has been reported as effective on improving bone repair under different conditions. The effects of the use of light sources on bone have been shown very effective. Many studies indicated that irradiated bone, mostly with NIR wavelengths, shows increased osteoblastic proliferation, collagen deposition, and bone neoformation when compared to nonirradiated bone. The irradiation protocol used in this study is similar to those used on previous reports. Our group has shown, using different models, that association of bone grafts and biomaterials does improve the healing of bone tissue [4–6, 8, 11–17].

The aim of this study was to evaluate the level of bone mineralization through the analysis of the intensities of Raman spectra of both inorganic (~ 960 , $\sim 1,070$, and $\sim 1,072$ cm^{-1}) and organic ($\sim 1,454$ and $\sim 1,666$ cm^{-1}) on the repair of bone defects grafted or not with biphasic synthetic microgranular HA + β -calcium triphosphate associated or not with laser phototherapy (780 nm).

Materials and methods

Ethics, animal model, housing, and sampling

The Animal Ethics Committee of the Federal University of Bahia approved this work.¹ Forty healthy adult male Wistar rats² were kept under natural conditions of light, humidity, and temperature at the Laboratory of Animal Experimentation of the School of Dentistry of the Federal University of Bahia during the experimental period. The animals were fed with standard laboratory diet³ and had water *ad libitum*. The animals were kept in individual microisolators and accommodated in ventilated shelves.⁴ This system provides a controlled

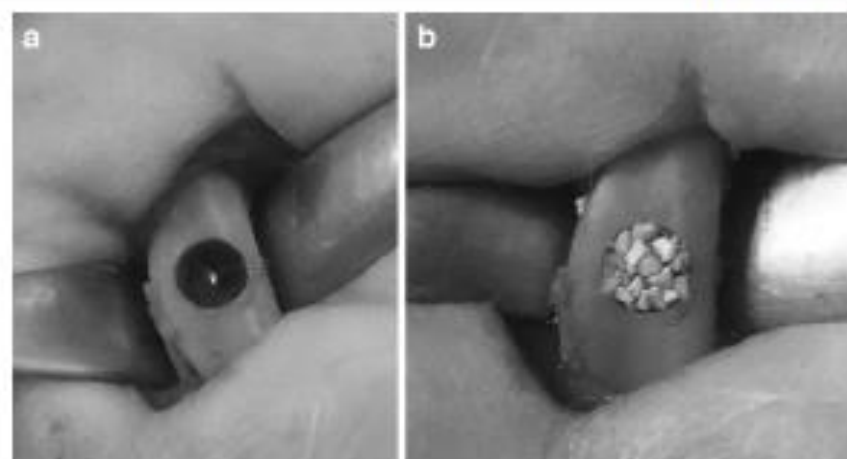
¹ Protocol 08.2010.

² About 2 months old, average weight 295 ± 25 g.

³ Labina®, Purina, São Paulo, Brazil.

⁴ INSIGHT Equipamentos Ltda—Monte Alegre, Ribeirão Preto, São Paulo, Brazil.

Fig. 1 **a** Clinical aspect of the surgical bone defect created on the right tibia of each animal. **b** Clinical aspect of the surgical bone defect created on the right tibia of each animal filled with the biomaterial



environment with decreased risk of infection and good sanitary condition. Controlled day/night light cycle and temperature was performed during the experimental period. The animals were randomly distributed into four groups and then subdivided into two subgroups according to the killing timing. The distribution of the animals may be seen in Table 2.

Surgical procedure

Prior to intramuscular general anesthesia, the animals were sedated,⁵ and 20 min later, general anesthesia⁶ was carried out. The animals had their right leg shaved, and a 3-cm-long incision was performed at the right tibia with a number 15 scalpel blade. Skin and subcutaneous tissues were dissected down to the periosteum, which was gently sectioned exposing the bone, and a standard partial thickness 2-mm-round defect was surgically produced using trephine drill⁷ mounted on a 16:1 reduction contra angle handpiece,⁸ maximum resistance of 35 N with low speed drill, 1,200 rpm, under refrigeration⁹ in each animal (Fig. 1a). Defects on animals in groups Clot and Laser were filled only with the blood clot. Defects in groups Biomaterial and Laser+Biomaterial were filled with biomaterial¹⁰. The animals on groups Laser and Laser+Biomaterial were further irradiated with laser light. All wounds were routinely sutured, and the animals received a single dose of antibiotics.¹⁰ For the present study, a biphasic synthetic microgranular HA+ β -calcium triphosphate (70 %/30 %, respectively) completely filled the bone defects when indicated, as recommended by the manufacturer (Fig. 1b).

Phototherapy protocol

Laser phototherapy was carried out using a diode laser¹¹ and transcutaneously applied at 4 points around the defect ($4 \times 5 \text{ J/cm}^2$) at 48-h intervals, being the first session carried out immediately after surgery. Total energy delivered was that of 20 J/cm^2 per session and 140 J/cm^2 per treatment. Energy densities used were based upon previous studies carried out by our group [4–7, 10–15, 30–33]. Laser output power was confirmed using a calibrated power meter.¹²

Animal death and sample manipulation

Following the killing (15 and 30 days after the surgery) in a CO_2 chamber,¹³ the samples were longitudinally cut under refrigeration,¹⁴ snap-frozen in liquid nitrogen, and kept deep-refrigerated (-80°C) until spectral analysis in order to minimize the growth of aerobic bacteria and because chemical fixation is not advisable due to fluorescence emission and scattering from fixative substances and tissue biochemical changes due to protein denaturation [5, 6, 21, 30–32].

Raman spectroscopy

For Raman measurements, a dispersive near-infrared Raman spectrometer,¹⁵ as diagramed in Fig. 2a, was used. The equipment uses a wavelength-stabilized diode laser tuned at 785 nm ¹⁶ coupled to a fiber-optic “Raman probe”¹⁷ in

⁵ 0.04 ml/100 g of atropine subcutaneously.

⁶ 10 % ketamine (0.1 mL/100 g—Cetamin®, Syntec, São Paulo, Brazil)+2 % xylazine (0.1 mL/100 g; Xilazin®, Syntec, São Paulo, Brazil).

⁷ SIN, São Paulo, Brazil.

⁸ NSK, Tochigi, Japan.

⁹ Driller 600®, SIN, São Paulo, SP, Brazil.

¹⁰ Pentabiotico®, 0.2 ml; Fort Dodge Animal Health, Overland Park, KS, USA.

¹¹ TwinFlex Evolution®, MMOptics, São Carlos, São Paulo, Brazil; $\lambda 780 \text{ nm}$, 70 mW, $\Phi \sim 0.4 \text{ cm}^2$, 20 J/cm^2 .

¹² Power Meter Thorlabs PM30-121, Thorlabs GmbH, Munich, Germany.

¹³ Insight Equipamentos, model EB 248, Ribeirão Preto, SP, Brazil.

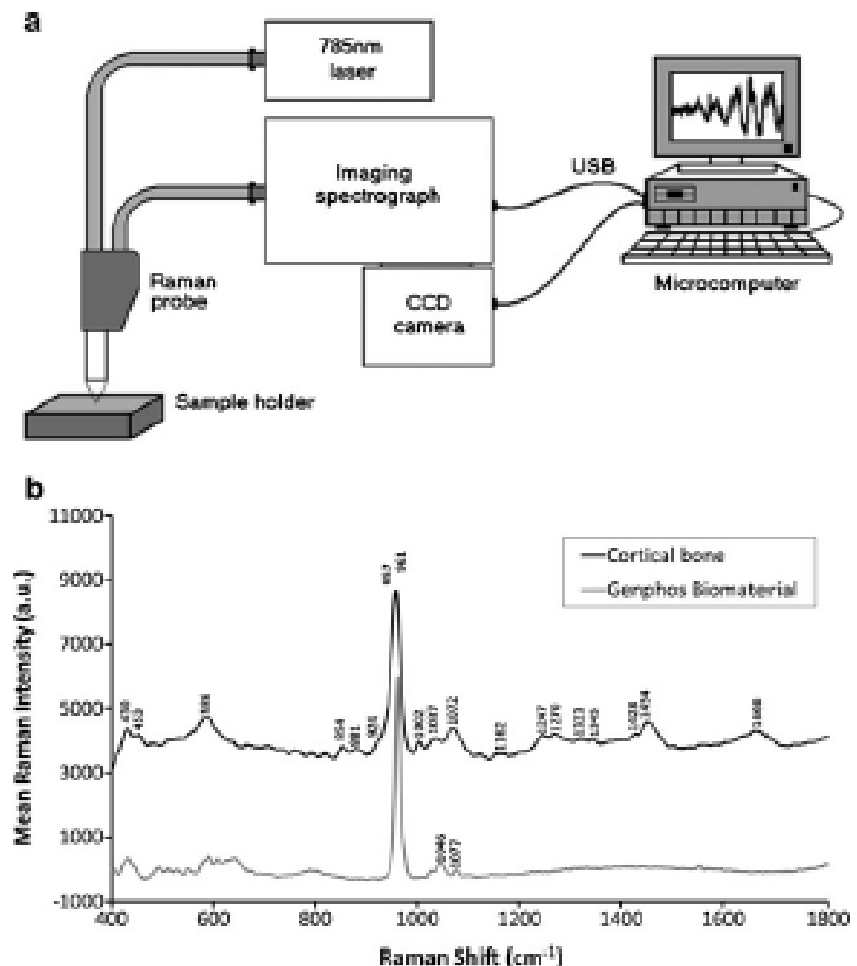
¹⁴ SIN-DRILLER 600 BML, São Paulo, SP, Brazil.

¹⁵ Andor Technology, model Shamrock SR-303i®, Belfast, Northern Ireland.

¹⁶ B&W TEK, model BRM-785-0.30-100-0.22 s, Newark, DE, USA.

¹⁷ B&W TEK, model BAC-100-785, Newark, DE, USA.

Fig. 2 **a** Schematic diagram of the dispersive Raman spectrometer used on the present study. Wavelength, 785 nm; laser power at probe tip, 300 mW; spectral resolution, 4 cm^{-1} . **b** Raman spectrum of nontreated cortical bone and phosphate biomaterial Genphos[®], with labeled peaks attributed in Table 1



order to provide excitation of the sample and collection of the Raman spectra in repeatable excitation–collection geometry, using an excitation fiber of 105 μm and a collecting fiber of 200 μm . The collection fiber is coupled to a dispersive spectrometer, composed of an imaging spectrograph and a back thinned, deep depletion charge-coupled device (CCD) camera¹⁸ (1,024 \times 128 pixels, Peltier-cooled down to -70°C), which disperses and detects the Raman scattered light.

The Raman system was controlled by the Solis software¹⁹ installed in a Windows-based microcomputer, which controls both CCD camera and spectrograph in terms of grating position, slit aperture, number of accumulations, and time exposure, as well as performs the spectral calibration of the Raman shift and stores and preprocesses the spectral data [5, 6, 21, 30–32]. The slit and grating configurations provided a spectral resolution of about 4 cm^{-1} in the spectral range of 400 to 1,800 cm^{-1} . The laser power

measured at the excitation tip of the Raman probe was 300 mW and the spectral acquisition time for each collection spot was 20 s. Five points were measured at the surface of the cortical area of the defect in each one of the 40 samples, resulting in total of 200 spectra. All spectra were acquired on the same day and room conditions.

For spectrograph calibration,²⁰ a spectral irradiance lamp²¹ with known spectral curve was used, which has been measured with long exposure time (~ 10 min) and used to correct the differences in the intensity response of all optical components along the spectral range, and seven major bands of the naphthalene in the spectral region 700–1,700 cm^{-1} , where measured pixel position and known Raman shift were fitted with a third order polynomial and used as abscissa (x -axis) [5, 6, 21, 30–32]. The calibration of the spectral data was performed using a routine developed under Matlab 5.1 software.²²

¹⁸ Andor Technology, model IDUs[®] DU401A-BR-DD, Belfast, Northern Ireland.

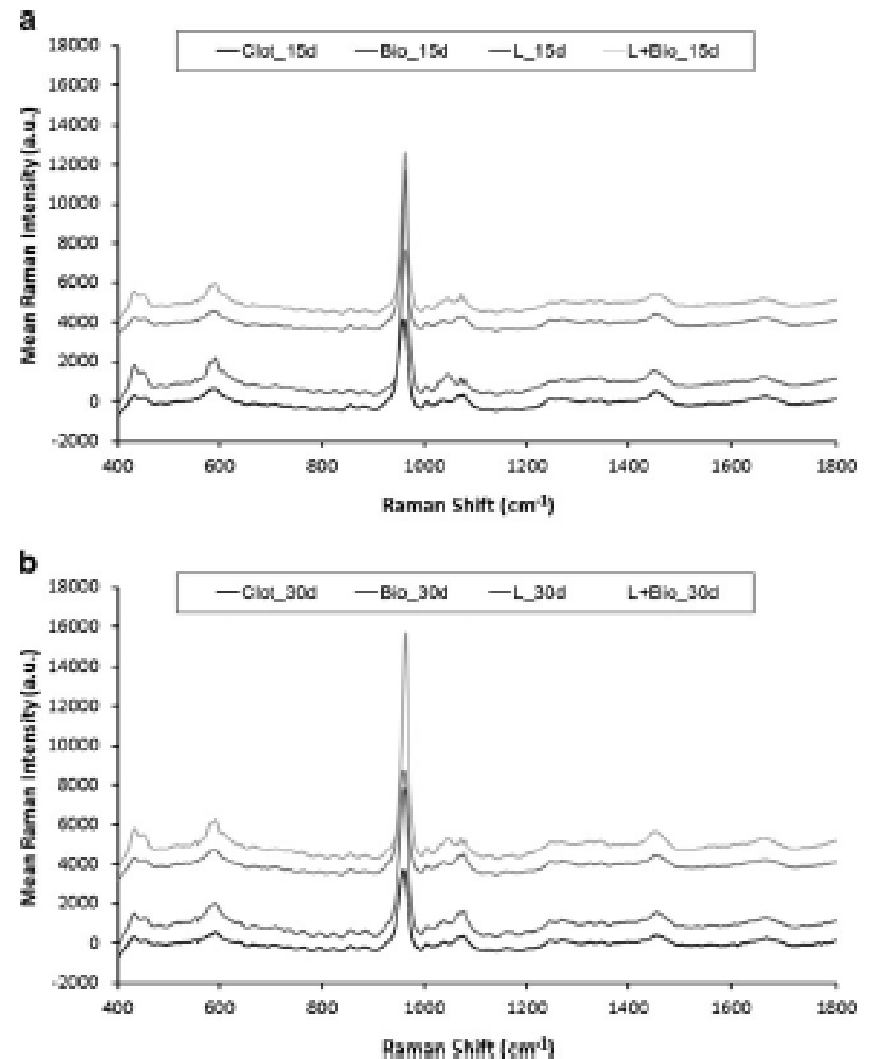
¹⁹ Andor Technology, Solis (i) software, Belfast, Northern Ireland.

²⁰ Intensity correction and wavenumber calibration.

²¹ Oriel Instruments, model 63358, Stamford, CT, USA.

²² The Mathworks, Newark, NJ, USA.

Fig. 3 Dislocated spectra of all groups at the 15th day (a) and 30th day (b)



Spectra processing and peak detection

Baseline spectra of nontreated bone and of the biomaterial used in the present study were produced, and peaks of interest such as inorganics (mainly hydroxyapatite) and organics (mainly collagen) were identified, as specified in Fig. 2b and Table 1. Spectrum of each animal was taken as previously described. Following acquisition, background fluorescence was filtered using a fifth order polynomial function applied to the gross spectrum in the 400–1,800 cm^{-1} region using a routine developed under Matlab. Then, Raman spectra of each animal were smoothed by “moving average” technique, which consisted of calculating the mean of five adjacent points.

In order to verify the influence of the use of the light and biomaterial on the bone repair, the spectra were segmented in four spectral regions (900–1,000, 1,000–1,100, 1,400–1,500,

and 1,600–1,700 cm^{-1}), and the absolute intensity and standard deviation of Raman bands related to HA and proteins (with tentative attributions according to Table 1) were determined for each sample. These data were used for plotting the peak's absolute intensity of each group, mainly the peaks at ~960, ~1,070, ~1,077, ~1,454, and ~1,666 cm^{-1} . Absolute intensities as well as standard deviations were calculated and plotted using Microsoft Excel or Minitab software, and the statistical analysis (*t* test and ANOVA, $p < 0.05$) in the peak intensities was performed using Minitab 15.0²³ software.

Results

Raman intensities

The mean dislocated spectra of each group at each experimental time (15 and 30 days) may be seen in Fig. 3a and b.

²³ Minitab, Belo Horizonte, MG, Brazil.

Measurements of the intensities of peaks related to the inorganic contents (HA), at day 15, showed the highest mean on group Biomaterial and lowest on group Laser (Fig. 4a) for $\sim 960\text{ cm}^{-1}$. For $\sim 1,070\text{ cm}^{-1}$, highest mean values were seen on group Biomaterial and lowest on group Laser (Fig. 4b), and for $\sim 1,077\text{ cm}^{-1}$, highest mean values were seen on group Clot and lowest on group Laser (Fig. 4c). At the 30th day, measurements of the inorganic content of all groups showed that, for $\sim 960\text{ cm}^{-1}$, highest mean on group Laser+Biomaterial and lowest on group Clot (Fig. 4a). For $\sim 1,070\text{ cm}^{-1}$, highest mean values were seen on group Laser+Biomaterial and lowest on group Clot (Fig. 4b); for $\sim 1,077\text{ cm}^{-1}$, highest mean values were seen on group Laser+Biomaterial and lowest on group Clot (Fig. 4c).

With regard to the organic contents in bone tissue, for $\sim 1,454\text{ cm}^{-1}$, highest mean was seen on group Biomaterial and lowest on group Laser (330.6 ± 491) (Fig. 5a), and for $\sim 1,666\text{ cm}^{-1}$, highest mean was seen on group Biomaterial and lowest on group Laser+Biomaterial (Fig. 5b). At the 30th day, the highest value for the $\sim 1,454\text{ cm}^{-1}$ peak was seen on group Laser+Biomaterial and lowest on group Clot (Fig. 5a), and for

the $\sim 1,666\text{ cm}^{-1}$, highest mean was seen on group Laser+Biomaterial and lowest on group Laser (Fig. 5b).

The data were initially analyzed to verify their normality. In the second stage, analysis of the difference between groups at each time point was carried out by ANOVA (Table 3). Due to the number of peaks assessed on the present study, they were divided into two main groups. In the first group were the peaks related to the inorganic components (phosphate and carbonated HA) represented by the peaks of ~ 960 , $\sim 1,070$, and $\sim 1,077\text{ cm}^{-1}$. In the second group, peaks related to the organic content (proteins) of the matrix were included and corresponded to $\sim 1,454$ and $\sim 1,666\text{ cm}^{-1}$. A summary of the results can be seen in Tables 4, 5, and 6.

Discussion

In all protocols, models, and parameters that our group has previously used, we were able to demonstrate that NIR LPT caused important tissue responses during healing, and these were responsible for a quicker repair process as well as on the improved quality of the newly formed bone [4–6, 8,

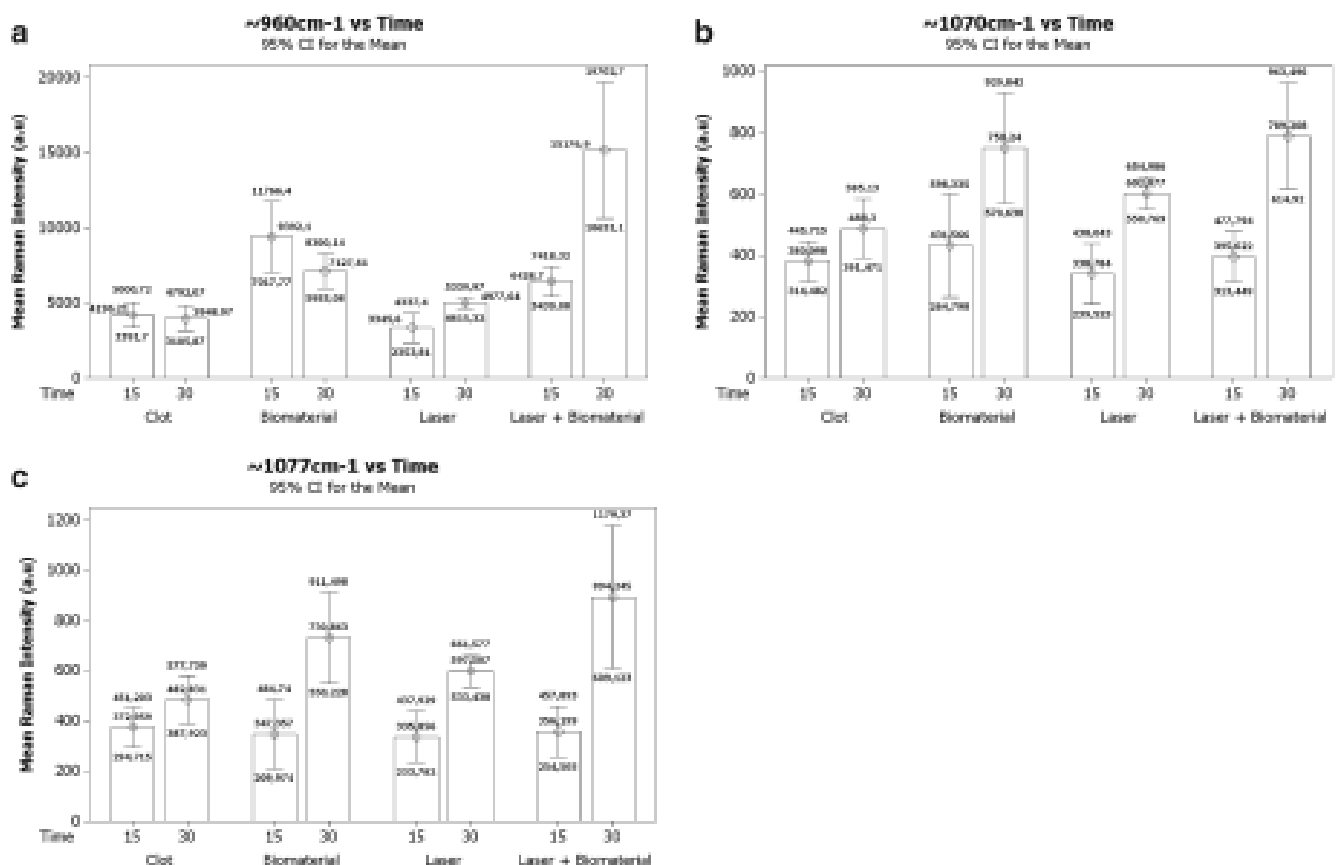
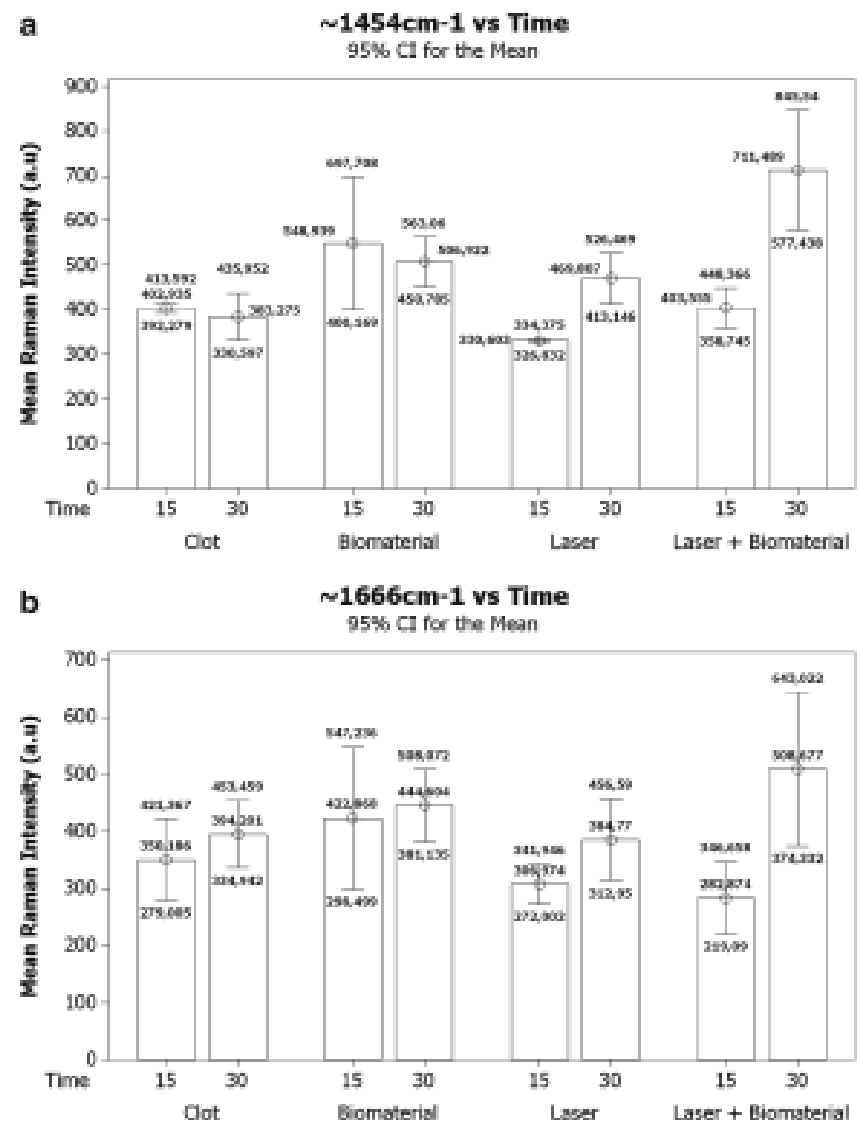


Fig. 4 Mean intensity and standard deviation of the peaks at ~ 960 (a), $\sim 1,070$ (b), and $\sim 1,077\text{ cm}^{-1}$ (c) at both experimental times

Fig. 5 Mean intensity and standard deviation of the peak $\sim 1,454$ (a) and $\sim 1,666$ cm^{-1} (b) at both experimental times



11–17, 30–34]. Our group previously found that the levels of HA on deep areas of healing bone of irradiated and nonirradiated subjects differ significantly from day 30 after treatment [4–6, 8, 11–17, 30–32]. In this study, we were able to detect differences on the healing of bone defects associated to the combined use of biomaterial and laser light.

Table 3 ANOVA results for each peak on both periods 15 and 30 days

Raman shift (cm^{-1})	15 days	30 days
~ 960	$p < 0.001$	$p < 0.001$
$\sim 1,070$	NS	$p = 0.005$
$\sim 1,077$	NS	$p = 0.006$
$\sim 1,454$	$p = 0.01$	$p < 0.001$
$\sim 1,666$	NS	NS

NS not significant

Raman spectroscopy has been employed to access the molecular constitution of a specific tissue and then classify it according to differences observed in the spectra [18, 35, 36]. Several studies found elsewhere on the literature have shown successful use of NIR Raman spectroscopy as a diagnostic tool for healthy, diseased, or healing bones [5, 6, 30–32]. Our group has successfully used this technique to determine both mineral and organic component changes on the healing bone. This method of assessment is considered by our team and others as a gold standard to study bone components and constitution [5, 6, 8, 17, 30–32, 34–36] and to reveal biochemical changes associated to the healing process (Table 1).

The results of the present study evidenced that despite the fact that both the laser light and the biomaterial present different mechanism of action during bone repair, their use aims the same, i.e., the improvement

Table 4 Summary of the statistical analysis (*t* test) of the Raman peaks within each group in relation to time

Group	Raman shift (cm ⁻¹)	Time (days)	Clot	Biomaterial	Laser	Laser+Biomaterial
	~960	15 ^a	4,196±1,047	9,392±4,287	3,345.6±1,290.3 ^b	6,429±1,558 ^b
		30 ^b	3,949±1,522	7,128±2,117	4,977.6±654.3 ^a	1,5177±8,193 ^a
	~1,070	15 ^a	380.1±85.4	431.6±301.1 ^b	338.8±124.1 ^b	395.6±129.3 ^b
		30 ^b	488.3±174.9	750.2±324.3 ^a	602.9±94.1 ^a	602.9±94.1 ^a
	~1,077	15 ^a	373±101.8	347.4±248.7 ^b	335.9±132.8 ^b	356.2±186.1 ^b
		30 ^b	482.8±171.4	730.9±326.2 ^a	597.5±115.7 ^a	894.2±514.9 ^a
	~1,454	15 ^a	402.9±13.8	548.9±268.6	330.6±491 ^b	403.6±70.5 ^b
		30 ^b	383.2±95.1	506.9±101.4	469.81±102.3 ^a	711.1±247.1 ^a
	~1,666	15 ^a	350.6±92.6	422.9±224.6	307±45.5	282.9±100.4 ^b
		30 ^b	394.2±107	444.6±114.6	384.8±129.7	508.7±242.6 ^a

Superscripted letters indicate significant differences ($p < 0.05$)

of the repair. This improvement is mainly related, in both therapies, to chemotaxis, proliferation of undifferentiated cells, increased proliferation and secretion of osteoblasts and chondroblasts, improvement of collagen deposition, increased deposition of osteoid, and mineralization [4, 6, 11, 17, 30–32]. This study showed, by Raman analysis of the intensity of most important peaks associated to bone tissue constitution, that the association of the techniques resulted in increased bone deposition and mineralization of the bone as previously reported by our team [4, 6, 11, 17, 30–32].

The results of the present investigation showed that the use of laser light associated to biomaterial achieved best results with regard to mineralization (Fig. 4a–c). This aspect has been described in previous studies in which the use of laser light associated to hydroxyapatite caused increased proliferation of fibroblasts and their secretion of collagen, precursor of the bone matrix. The increased formation of new bone is closely related to both increased number of osteoblasts and of their secretion [4].

The results of the present study are well aligned with previous reports from our group [4–6, 8, 11–17, 30–34] and indicate that the association of laser light with HA graft improves the repair of bone defects [4, 6, 11, 17,

30–32]. The overall analysis of the results of the present investigation indicates that statistically significant differences between most of the peaks studied were mostly detectable at the end of the experimental period (HA peaks at ~960, ~1,070, and ~1,077 cm⁻¹ and the collagen peak at 1,454 and ~1,066 cm⁻¹).

During early stages of healing, the osteoblastic activity is chiefly proliferative, and deposition starts later; this results in the formation of immature bone, still poor in HA. This later maturation represents the improved ability of more mature osteoblasts to secrete HA in irradiated subjects.

The reason why the effect of laser irradiation is not much detectable until 30 days after treatment is due to the fact that, during early stages of bone healing, the cellular component (chiefly fibroblasts and osteoblasts) is more prominent and more prone to be affected by the light. With the progression of the repair process, the bone matrix becomes the main component of the repairing tissue [4]. This is the reason why the frequency of application of LPT is effective when carried out during the cellular phase, when the number of osteoblasts is increasing. Later, the higher number of cells results in a larger deposition of bone matrix, which later incorporates HA, characterizing maturation of the bone.

Table 5 Summary of the statistical analysis (*t* test) of the Raman peaks between groups at the 15th day

Group	Raman shift (cm ⁻¹)	Clot ^a	Biomaterial ^b	Laser ^c	Laser+Biomaterial ^d
	~960	4,196±1,047 ^{b,d}	9,392±4,287 ^{a,c,d}	3,345.6±1,290.3 ^{b,d}	6,429±1,558 ^{a,b,c}
	~1070	380.1±85.4	431.6±301.1	338.8±124.1	395.6±129.3
	~1077	373±101.8	347.4±248.7	335.9±132.8	356.2±186.1
	~1454	402.94±13.86 ^{b,c}	548.9±268.6 ^{a,c}	330.6±491 ^{a,b,d}	403.6±70.5 ^c
	~1666	350.6±92.6	422.9±224.6	307±45.5	282.9±100.4

Superscripted letters indicate significant differences ($p < 0.05$)

Table 6 Summary of the statistical analysis (*t* test) of the Raman peaks between groups at the 30th day

Group Raman shift (cm^{-1})	Clot ^a	Biomaterial ^b	Laser ^c	Laser+Biomaterial ^d
~ 960	$3,949 \pm 1,522^{bc,d}$	$7,128 \pm 2,117^{a,c,d}$	$4,977.6 \pm 654.3^{a,b,d}$	$15,177 \pm 8,193^{a,b,c}$
$\sim 1,070$	$488.3 \pm 174.9^{bc,d}$	750.2 ± 324.3^a	602.9 ± 94.1^a	789.2 ± 314.7^a
$\sim 1,077$	$373 \pm 101.8^{bc,d}$	347.4 ± 248.7^a	335.9 ± 132.8^a	356.2 ± 186.1^a
$\sim 1,454$	$383.27 \pm 95.1^{bc,d}$	$506.9 \pm 101.4^{a,d}$	$469.81 \pm 102.32^{a,d}$	$711.15 \pm 247.1^{a,b,c}$
$\sim 1,666$	394.2 ± 107	444.67 ± 114.6	384.8 ± 129.7	508.7 ± 242.6

Superscripted letters indicate significant differences ($p < 0.05$)

The present work found that, at the end of the experimental time, the measurements of the inorganic content of all groups (remarkably, the peaks related to mineralization ~ 960 , $\sim 1,070$, and $\sim 1,077 \text{ cm}^{-1}$) were higher on group Laser+Biomaterial. From our results, it is possible to note that the intensity of these peaks increased in all groups and that this would be indicative of the increased deposition of HA along the repair time and of the increased mineralization of the newly formed bone. The time significantly influenced these three peaks when the biomaterial, the laser, or the association of both was used [4, 6, 11, 17, 30–32].

Deposition of HA represents bone maturation and increased amount of HA in bone is indicative of a more resistant bone. The observed differences in the rate of deposition of HA between irradiated and nonirradiated subjects are probably due to the ability of the laser light to induce changes at cellular levels, such as improved ATP synthesis, early osteoblastic differentiation, and the release of growth factors [4].

With regard to the organic content, as marked by Raman peaks in the $\sim 1,400$ to $\sim 1,700 \text{ cm}^{-1}$ region, the differences in the intensity depending upon the time of maturation for the $\sim 1,454 \text{ cm}^{-1}$ peak on groups Laser and Laser+Biomaterial and for the $\sim 1,666 \text{ cm}^{-1}$ peak only for the group Laser+Biomaterial, this difference seemed to be related to changes in the organic content. It is important to note that the peak $\sim 1,454 \text{ cm}^{-1}$ was reduced along the repair time in nonirradiated groups and increased in groups Laser and Laser+Biomaterial, the difference being significant. This peak appears to be related to the amount of collagen II deposited along the bone repair, and which intensity is increased in more mature bone and indicates a more organized and mature bone matrix where HA can be incorporated. Thus, this may be indicative of the presence of a more advanced and mature bone tissue on irradiated subjects. However, when comparing the two irradiated groups, it is clear that this phenomenon was more intense in group Laser+Biomaterial, i.e., more cicatricial collagen. Interestingly, similar pattern was not observed when analyzing the $\sim 1,666 \text{ cm}^{-1}$ peak, where its intensity can be more dependent on collagen cross-

linking rather than concentration or collagen type as bone matures. Unlike what happened with the $\sim 1,454 \text{ cm}^{-1}$ peak, the $\sim 1,666 \text{ cm}^{-1}$ one presented a nonsignificant difference of the intensity for all groups, despite its increase along the time. This may indicate that this peak might not be sensitive enough to detect changes in the organic matrix as the $\sim 1,454 \text{ cm}^{-1}$ one.

Comparing the different groups, at the end of the experimental time, the Laser+Biomaterial group showed higher intensity for both organic matrix peaks. Significant differences in the $\sim 1,454 \text{ cm}^{-1}$ peak were seen between the Laser+Biomaterial group and all others. The same was also observed in relation to the group Clot that showed significantly smaller peak when compared to all other groups. Despite the intensity for the $\sim 1,666 \text{ cm}^{-1}$ peak of the two peaks being higher on the Laser+Biomaterial group at the end of the experimental time, this was not significant. As previously discussed, this peak might not be ideal to efficiently detect changes in the organic matrix.

Finally, it is important to consider that the findings of improved bone healing in an animal model, with adjunctive LPT associated or not to the use of different types of biomaterials, observed on this study are consistent with other previously reported effects of the isolated or associated use of them [4–6, 8, 11–17, 30–34], specifically in relation to the use of LPT, effects on the cellular reactions such as ATP synthesis promotion, electron transport chain stimulation, and cellular pH reduction [37, 38], and these biochemical and cell membrane changes may increase activities of macrophage, fibroblast, lymphocyte, and the other healing cells [39, 40], increase in collagen and DNA synthesis, increase in Ca deposition [41–43], increase in periosteum cells function [44], increase in osteoblast and osteocyte function [20, 23], and improved neovascularization [42, 43], which are some of the positive effects of LPT on bone repair that have been reported and may explain the results of this study.

It is concluded that the use of laser phototherapy associated to biphasic synthetic microgranular HA+ β -calcium triphosphate graft was effective in improving bone healing on bone defects as a result of the increasing deposition of HA measured by Raman spectroscopy.

References

- Prolo DJ (1990) Biology of bone fusion. *Clin Neurosurg* 36:135–146
- Recker RR (1992) Embryology, anatomy, and microstructure of bone. In: Coe FL, Favus MJ (eds) *Disorders of bone and mineral metabolism*. Raven, New York, pp 219–240
- Kalfas IH (2001) Principles of bone healing. *Neurosurg Focus* 10(4):7–10
- Pinheiro ALB, Gerbi MEMM (2006) Photoengineering of bone repair processes. *Photomed Laser Surg* 24(2):169–178
- Pinheiro ALB, Aciole GTS, Cangussú MCT, Pacheco MTT, Silveira L Jr (2010) Effects of laser phototherapy on bone defects grafted with mineral trioxide aggregate, bone morphogenetic proteins, and guided bone regeneration: a Raman spectroscopic study. *J Biomed Mater Res A* 95(4):1041–1047
- Lopes CB, Pacheco MTT, Silveira L Jr, Cangussú MCT, Pinheiro ALB (2010) The effect of the association of near infrared laser therapy, bone morphogenetic proteins, and guided bone regeneration on tibial fractures treated with internal rigid fixation: A Raman spectroscopic study. *J Biomed Mater Res A* 4(4):1257–63
- Torres CS, Santos JN, Monteiro JSC, Gomes PTCC, Pinheiro ALB (2008) Does the use of laser photobiomodulation, bone morphogenetic proteins, and guided bone regeneration improve the outcome of autologous bone grafts? An in vivo study in a rodent model. *Photomed Laser Surg* 26:371–377
- Lopes CB, Pinheiro ALB, Sathiaiah S, Silva NS, Salgado MC (2007) Infrared laser photobiomodulation (830 nm) on bone tissue around dental implants: a Raman spectroscopy and scanning electronic microscopy study in rabbits. *Photomed Laser Surg* 23:96–101
- Pinheiro ALB, Oliveira MG, Martins PPM, Ramalho LMP, Oliveira MAM, Novais A Jr, Nicolau RA (2008) Biomodulatory effects of LILT on bone regeneration. *Laser Ther* 13:73–79
- Weber JBB, Pinheiro ALB, Oliveira MG, Oliveira FAM, Ramalho LMP (2006) Laser therapy improves healing of bone defects submitted to autogenous bone graft. *Photomed Laser Surg* 24:38–44
- Pinheiro ALB, Gerbi MEMM, Lima Junior FA, Ponzi EAC, Marques AMC, Carvalho CM, Santos RC, Oliveira PC, Nôia M, Ramalho LMP (2009) Bone repair following bone grafting hydroxyapatite guided bone regeneration and infrared laser photobiomodulation: a histological study in a rodent model. *Lasers Med Sci* 24:234–240
- Gerbi MEMM, Marques AMC, Ramalho LMP, Ponzi EA, Carvalho CM, Santos RC, Oliveira PC, Nôia M, Pinheiro AL (2008) Infrared laser light further improves bone healing when associated with bone morphogenetic proteins: an in vivo study in a rodent model. *Photomed Laser Surg* 26:55–60
- Pinheiro ALB, Gerbi MEM, Ponzi EAC, Ramalho LMP, Marques AMC, Carvalho CM, Santos RC, Oliveira PC, Nôia M (2008) Infrared laser light further improves bone healing when associated with bone morphogenetic proteins and guided bone regeneration: an in vivo study in a rodent model. *Photomed Laser Surg* 26:167–174
- Gerbi MEMM, Pinheiro ALB, Ramalho LMP (2008) Effect of IR laser photobiomodulation on the repair of bone defects grafted with organic bovine bone. *Lasers Med Sci* 23:313–317
- Gerbi ME, Pinheiro ALB, Matzola C, Lima Junior FA, Ramalho LMP, Ponzi EAC, Soares AO, Carvalho LC, Lima HV, Gonçalves TO (2005) Assessment of bone repair associated with the use of organic bovine bone and membrane irradiated at 830 nm. *Photomed Laser Surg* 23:382–388
- Lopes CB, Pacheco MT, Silveira Junior L, Duarte J, Cangussú MC, Pinheiro AL (2007) The effect of the association of NIR laser therapy BMPs, and guided bone regeneration on tibial fractures treated with wire osteosynthesis: Raman spectroscopy study. *J Photochem Photobiol B* 89(2–3):125–30
- Karu TI, Pyatibrat LV, Afanasyeva NI (2004) A novel mitochondrial signalling pathway activated by visible-to-near infrared radiation. *Photochem Photobiol* 80:366–72
- Hanlon EB, Manoharan R, Koo TW, Shafer KE, Motz JT, Fitzmaurice M, Kramer JR, Itkan I, Dasari RR, Feld MS (2000) Prospects for in vivo Raman spectroscopy. *Phys Med Biol* 45:R1–R59
- Kavukcuoglu NB, Patterson-Buckendahl P, Mann A (2009) Effect of osteocalcin deficiency on the nanomechanics and chemistry of mouse bones. *J Mech Behav Biomed* 2:334–348
- Penel G, Leroy G, Rey C, Bess E (1998) MicroRaman spectral study of the PO_4 and CO_3 vibrational modes in synthetic and biological apatites. *Calcif Tissue Int* 63(6):475–481
- Timlin JA, Cadden A, Morris MD (1999) Chemical microstructure of cortical bone probed by Raman transects. *Appl Spectrosc* 53(11):1429–1435
- Penel G, Cui E, Delfosse C, Rey C, Hardouin JJ, Delecourt C, Lemaire J, Leroy G (2003) Raman microspectrometry studies of calcified tissues and related biomaterials. *Raman studies of calcium phosphate biomaterials*. *Dent Med Probl* 40(1):37–43
- Morris MD, Mandair GS (2011) Raman assessment of bone quality. *Clin Orthop Relat Res* 469:2160–2169
- Okagbare PI, Begun D, Tecklenburg M, Anonusi A, Goldstein SA, Morris MD (2012) Noninvasive Raman spectroscopy of rat tibiae: approach to in vivo assessment of bone quality. *J Biomed Opt* 17(9):1–3, 090502
- Anonusi A, Morris MD, Tecklenburg MM (2007) Carbonate assignment and calibration in the Raman spectrum of apatite. *Calcif Tissue Int* 81:46–52
- Movasaghi Z, Rehman S, Rehman IU (2007) Raman spectroscopy of biological tissues. *Appl Spectrosc Rev* 43(5):493–541
- Lin SY, Li MJ, Cheng WT (2007) FT-IR and Raman vibrational microspectroscopies used for spectral diagnosis of human tissues. *Spectrosc* 21:1–30
- Silveira L Jr, Silveira FL, Bodanese B, Zingaro RA, Pacheco MTT (2012) Discriminating model for diagnosis of basal cell carcinoma and melanoma in vitro based on the Raman spectra of selected biochemicals. *J Biomed Opt* 17(7):077003
- Barth A, Zscherp C (2002) What vibrations tell us about proteins. *Q Rev Biophys* 35(4):369–430
- Pinheiro ALB, Santos NRS, Oliveira PC, Aciole GTS, Ramos TA, Gonzalez TA, Silva LN, Barbosa AFS, Silveira-Junior L (2012) The efficacy of the use of IR laser phototherapy associated to biphasic ceramic graft and guided bone regeneration on surgical fractures treated with miniplates: a Raman spectral study on rabbits. *Lasers Med Sci*. doi:10.1007/s10103-012-1096-1
- Carvalho FB, Aciole GTS, Aciole JMS, Silveira-Junior L, Santos JN, Pinheiro ALB (2011) Assessment of bone healing on tibial fractures treated with wire osteosynthesis associated or not with infrared laser light and biphasic ceramic bone graft (HATCP) and guided bone regeneration (GBR): Raman spectroscopic study. *Proceedings – SPIE* 7887:7887OT-1–7887OT-6
- Pinheiro ALB, Lopes CB, Pacheco MTT, Brugnem A, Zanin FAA, Cangussú MCT, Silveira-Junior L (2010) Raman spectroscopy validation of DIAGNOdent-assisted fluorescence readings on tibial fractures treated with laser phototherapy, BMPs, guided bone regeneration and miniplates. *Photomed Laser Surg* 28:89–97
- Pinheiro ALB, Soares LGR, Aciole GTS, Correia NA, Barbosa AFS, Ramalho LMP, Santos JN (2011) Light microscopic description of the effects of Laser phototherapy on bone defects grafted with mineral trioxide aggregate, bone morphogenetic proteins, and guided bone regeneration in a rodent model. *J Biomed Mater Res A* 98(2):212–21
- Lopes CB, Pinheiro ALB, Sathiaiah S, Martins MC (2005) Infrared laser light reduces loading time of dental implants: a Raman Spectroscopic study. *Photomed Laser Surg* 23:27–31

35. Penel G, Delfosse C, Descamps M, Leroy G (2005) Composition of bone and apatitic biomaterials as revealed by intravital Raman microspectroscopy. *Bone* 36:893–901
36. Cauden A, Morris MD (2000) Application of vibrational spectroscopy to the study of mineralized tissues (review). *J Biomed Opt* 5:259–268
37. Cameron MH, Perez D, Otano Lata S (1999) Electromagnetic radiation in physical agents. In: Cameron MH (ed) *Rehabilitation, from research to practice*. WB Saunders, Philadelphia, pp 303–344
38. Kara TI (1989) Molecular mechanisms of the therapeutic effects low intensity Laser radiation. *Lasers Life Sci* 2:53–74
39. Young S, Bolton P, Dyson M, Harvey W, Diamantopoulos C (1989) Macrophage responsiveness to light therapy. *Lasers Surg Med* 9:497–505
40. Passarella S, Casamassima E, Quagliariello E, Caretto G, Jirillo E (1985) Quantitative analysis of lymphocyte-*Salmonella* interaction and effects of lymphocyte irradiation by He-Ne Laser. *Biochem Biophys Res Commun* 130:546–552
41. Yamada K (1991) Biological effects of low power laser irradiation on clonal osteoblastic cells (MC3T3-E1). *J Jpn Orthop Assoc* 65:101–114
42. Tang XM, Chai BP (1986) Effect of CO₂ laser irradiation on experimental fracture healing: a transmission electron microscopic study. *Lasers Surg Med* 6(3):346–352
43. Motomura K (1984) Effects of various laser irradiation on callus formation after osteotomy. *Nippon Reza Igakkai Shi (J Japan Soc for Laser Med)* 4(1):195–196
44. Treilles MA, Mayayo E (1987) Bone fracture consolidate faster with low power Laser. *Lasers Surg Med* 7:36–45

Braz Dent J. 2013;24(1):59-63.

Use of Laser Fluorescence in Dental Caries Diagnosis: a Fluorescence x Biomolecular Vibrational Spectroscopic Comparative Study

Use of Laser Fluorescence in Dental Caries Diagnosis: a Fluorescence x Biomolecular Vibrational Spectroscopic Comparative Study

Fabiola Bastos de Carvalho¹, Artur Felipe Santos Barbosa^{1,2}, Fátima Antonia Aparecida Zanin³, Aldo Brugnera Júnior^{3,4}, Landolfo Silveira Júnior⁴, Antonio Luiz Barbosa Pinheiro^{1,4,5}

¹Biophotonics Center, Dental School, UFBA - Federal University of Bahia, Salvador, BA, Brazil
²São Camilo School, Salvador, BA, Brazil
³Brugnera & Zanin Institute, São Paulo, SP, Brazil
⁴São José dos Campos Technological Park, Camilo Castelo Branco University, São José dos Campos, SP, Brazil
⁵National Institute of Optics and Photonics, USP - University of São Paulo, São Carlos, SP, Brazil

Correspondence: Prof. Dr. Antônio Luiz Barbosa Pinheiro, Avenida Araújo Pinho, 62, Canela, 40110-150 Salvador, BA, Brazil. Tel: +55-71-3283-9010. e-mail: albp@ufba.br

The aim of this work was to verify the existence of correlation between Raman spectroscopy readings of phosphate apatite ($\sim 960\text{ cm}^{-1}$), fluoridated apatite ($\sim 575\text{ cm}^{-1}$) and organic matrix ($\sim 1450\text{ cm}^{-1}$) levels and Diagnodent® readings at different stages of dental caries in extracted human teeth. The mean peak value of fluorescence in the carious area was recorded and teeth were divided in enamel caries, dentin caries and sound dental structure. After fluorescence readings, Raman spectroscopy was carried out on the same sites. The results showed significant difference (ANOVA, $p < 0.05$) between the fluorescence readings for enamel (16.4 ± 2.3) and dentin (57.6 ± 23.7) on carious teeth. Raman peaks of enamel and dentin revealed that ~ 575 and $\sim 960\text{ cm}^{-1}$ peaks were more intense in enamel caries. There was significant negative correlation ($p < 0.05$) between the ~ 575 and $\sim 960\text{ cm}^{-1}$ peaks and dentin caries. It may be concluded that the higher the fluorescence detected by Diagnodent the lower the peaks of phosphate apatite and fluoridated apatite. As the early diagnosis of caries is directly related to the identification of changes in the inorganic tooth components, Raman spectroscopy was more sensitive to variations of these components than Diagnodent.

Key Words: vibrational spectroscopy, hydroxyapatite, dental caries, tooth demineralization.

Introduction

Caries is a chronic infectious multifactorial disease and the most prevalent disease in the oral cavity. It occurs due to the demineralization of tooth surfaces by organic acids (originated from the fermentation of carbohydrates by bacteria) and by organic matrix degradation (1). This process is dynamic and may be reversed at its early stages (2).

The formation of a carious lesion and its progress occurs when periods of demineralization are more frequent than those of remineralization. Thus the disease is characterized by an imbalance between the demineralization and remineralization occurring in enamel. Despite the small mineral loss of enamel is not clinically visible at very early stages, the injury exists. As demineralization progresses, a whitish area appears when the enamel continues losing mineral (3). The mineral loss due to disease progression, causes visual changes on the tooth surface, starting in a subclinical stage (white spot) and followed by cavitation (4).

The enamel is composed of 96% inorganic material (calcium phosphate in the form of hydroxyapatite) and the remaining 4% is water and organic material. The dentin presents in its composition approximately 70% inorganic material, 18% organic material and 12% water. It is mainly composed of hydroxyapatite and its organic content is formed by approximately 90% of type I collagen. The remaining tissue is a mixture of citrate, lipids and non-

collagenous proteins, including phosphor-proteins and proteoglycans (5).

Continuous laboratory studies on caries disease together with clinical research increase the knowledge on this topic resulting in changes of routines and procedures. This includes improvement of the diagnostic ability, allowing the diagnosis of subtle and early stage lesions. To be considered an ideal diagnostic method it has to be reliable, detect lesions in early stages, be able of differentiating reversible and irreversible lesions, enable its documentation, have affordable cost, be comfortable to the patient, be both fast and easy to implement, and applicable to all sites of the tooth with the same efficiency (6).

In the 1990's, good perspectives on the use of laser fluorescence for the diagnosis of caries were presented and this technology was proven able of detecting early demineralization, especially when a fluorescent dye is added to the mineralized surface (7).

The inexistence of a method able of diagnosing disease (sensitivity) and soundness (specificity) led to the development diagnostic tools, e.g. laser fluorescence (Diagnodent®; KaVo, Biberach, Germany), which has been considered a promising method (8). The principle of using a laser beam for diagnosis relies on the fact that an altered mineralized surface irradiated by a longitudinal light wave emits fluorescent radiation. Diagnodent is a diagnostic

device that has a probe that emits light directed on the mineralized surface to be examined. If this surface has some form of structural change, it will emit a fluorescent light that is captured back by the probe and the device will display values ranging from 0 to 99 (9).

Diagnodent has been tested extensively, including for detection of occlusal and smooth surface caries, comparing its results with visual inspection, histology, radiography and quantitative light-induced fluorescence (7,9).

Raman spectroscopy is a powerful technique for measuring light dispersion, which is used to analyze the internal structure of molecules. Raman spectroscopy is based on measurement of the wavelength and intensity of inelastically dispersed light. Raman scattering occurs at wavelengths that are displaced from the incident light by the energy of molecular vibrations. Although the mechanism of Raman scattering is different from that of infrared absorption, it provides additional information and its applications include structural and multicomponent qualitative and quantitative analyses. This technique has been used in different areas as a noninvasive diagnostic resource of biological samples, such as periimplant and bone healing, and combination with biomaterials (10-12).

The Raman spectrum of tooth shows prominent vibrational bands related its composition. Some of the main Raman bands on tissues are at ~575, ~960, ~1450 cm^{-1} . The ~1450 band is attributed to amide I and amide III stretching modes as well as to the bending and stretching modes of CH groups of lipids and proteins; the ones at ~960 and ~575 cm^{-1} are attributed to phosphate and fluoridated apatite, respectively (11,12).

The aim of this study was to correlate the results of fluorescence readings and Raman spectroscopy regarding the levels of phosphate apatite (~960 cm^{-1}), fluoridated apatite (~575 cm^{-1}) and organic matrix (~1450 cm^{-1}) at different stages of dental caries in extracted human teeth.

Material and Methods

The Ethics Committee of the Dental School of the Federal University of Bahia, Brazil (Protocol #17/11) approved the present study. Twenty extracted human teeth were used. Five sound teeth (extracted due to periodontal or orthodontic reasons) and 15 teeth with carious lesions on one smooth surface (mesial, distal buccal or lingual) were collected and stored in 10% formalin. At the moment of the readings, the teeth were washed in running tap water and cleaned for removal of all traces of formalin, stains or calculi and were then stored in saline.

Fluorescence readings were taken with Diagnodent ($\lambda=655 \text{ nm}$). The device was calibrated according the manufacturer's instructions and readings were made with the flat tip (point B) positioned perpendicular to the

analyzed surface (6). For reading on sound dentin, a sound tooth was sectioned longitudinally with water-cooled carborundum disk to expose a smooth dentin surface.

The mean peak value of the maximum fluorescence reading was recorded and the teeth were grouped ($n=5$) as follows: sound enamel (0 to 10), sound dentin (0 to 10), enamel caries (11 to 20), and dentin caries (21 to 99). Reference values used were those suggested by the manufacturer (6). For all groups, five readings were taken from each sample in order to calculate the mean and standard deviation.

After the readings of laser fluorescence, the samples were analyzed using a dispersive Raman spectrometer (Andor Shamrock SR303i; Andor Technology, Belfast, Northern Ireland) and a stabilized diode laser ($\lambda=785 \text{ nm}$, 500 mW; B & W TEK, Newark, DE, USA). The excitation of the sample and collection of Raman spectra was performed by a fiber optic cable (Raman Probe) positioned in contact with the samples. The band used for analysis ranged from 200 to 1800 cm^{-1} .

Detection of scattered light signal of the sample was done by a back-illuminated thinned, deep depletion (1024x128 pixels) iDUS CCD camera (Andor Technology) cooled by cooler thermocouple, reaching a working temperature of -70°C in 5 min after the start of spectrometer operation. Acquisition and storage of the spectra were performed by a microcomputer using the Andor Solis software via USB connection, controlling the exposure time of the detector, number of acquisitions per sample and provides storage of the spectra for further analysis and interpretation.

The exposure time to obtain the spectra was 20 s, accumulated at a single time, with power of 500 mW. This acquisition time and power does not damage the sample. The spectrometer wavelength was calibrated by the manufacturer before data collection. Verification was done by collecting the spectrum of naphthalene and comparing the position (Raman shift) of the main bands of the compound obtained in the literature, in the spectral region 500 to 1800 cm^{-1} . This is the region of interest to the Raman spectroscopy when used for biological materials analysis ("fingerprint" region). After calibration of Raman shift and the acquisition of the spectra *in vitro* they were pre-processed and stored for subsequent statistical evaluation.

The preprocessing consisted of removing the background fluorescence, which calculates a 5th order polynomial, adjusted to the low-frequency spectral components (fluorescence) and its subsequent subtraction from the original data, revealing the high frequency spectral components (Raman). The spectra had their original intensities maintained. This pre-processing was carried out using an operational default protocol in the Matlab 4.0

(The Mathworks, Natick, MA, USA) software (11).

Five readings were taken from each sample at the same point where the fluorescence readings were taken in order to calculate the mean and standard deviation. The data were analyzed using the Minitab 15 software (Minitab, Belo Horizonte, MG, Brazil) and significance level was set at 5%.

Results

The results of fluorescence readings are summarized in Table 1. Fluorescence readings of carious enamel and dentin showed significant differences (ANOVA, $p < 0.05$) with mean values of 57.6 ± 23.7 for dentin and 16.4 ± 2.3 for enamel (Fig. 1). The readings for sound enamel and dentin were 3.6 ± 0.5 and 5.4 ± 0.5 , respectively.

In the Raman spectroscopic study the $\sim 960 \text{ cm}^{-1}$ (phosphate apatite), $\sim 575 \text{ cm}^{-1}$ (fluoridated apatite) and $\sim 1450 \text{ cm}^{-1}$ (organic matrix) peaks were analyzed. There was significant difference ($p < 0.05$) between sound enamel and dentin for all evaluated peaks (Fig. 2). The higher intensity of the peaks is related to the inorganic components ($\sim 575 \text{ cm}^{-1}$ and $\sim 960 \text{ cm}^{-1}$) in enamel.

Analysis of Raman caries peaks in enamel and dentin showed a statistically significant difference ($p < 0.05$) for all peaks (Fig. 3). Raman peaks showed significant positive

correlation (Pearson correlation $p < 0.05$) to both enamel and dentin (Table 2).

Analyzing carious and non-carious teeth in enamel and dentin, a lower intensity of the peaks was observed on the carious ones (Fig. 4) this difference being statistically significant ($p < 0.05$) only for the $\sim 575 \text{ cm}^{-1}$ peak in dentin.

The correlation between Diagnodent readings and Raman peaks showed a negative and significant correlation (Pearson, $p < 0.05$) only between the $\sim 575 \text{ cm}^{-1}$ and $\sim 960 \text{ cm}^{-1}$ peaks in dentin caries. The $\sim 1450 \text{ cm}^{-1}$ Raman peak and Diagnodent readings in dentin caries showed no significant correlation. In enamel, no significant correlation was found between Diagnodent readings and Raman peaks (Table 3).

Discussion

Diagnodent emits a diode laser at 655 nm wavelength, which is absorbed by the dental tissues. Part of this light is re-emitted as fluorescence. Fluorescence increases

Table 1. Summary of the results of Diagnodent fluorescence readings

Tooth	Diagnodent readings	Diagnosis
a	47/ 46/ 46/ 48/ 48	Dentin caries
b	46/ 55/ 46/ 45/ 50	Dentin caries
c	61/ 65/ 75/ 68/ 64	Dentin caries
d	99/ 99/ 99/ 98/ 99	Dentin caries
e	29/ 32/ 33/ 33/ 31	Dentin caries
f	19/ 19/ 18/ 18/ 16	Enamel caries
g	18/ 17/ 14/ 12/ 19	Enamel caries
h	13/ 16/ 19/ 15/ 18	Enamel caries
i	13/ 18/ 13/ 10/ 19	Enamel caries
j	12/ 14/ 13/ 16/ 14	Enamel caries
Dentin	5/ 5/ 6/ 5/ 6	Sound dentin
Enamel	4/ 4/ 3/ 4/ 3	Sound enamel

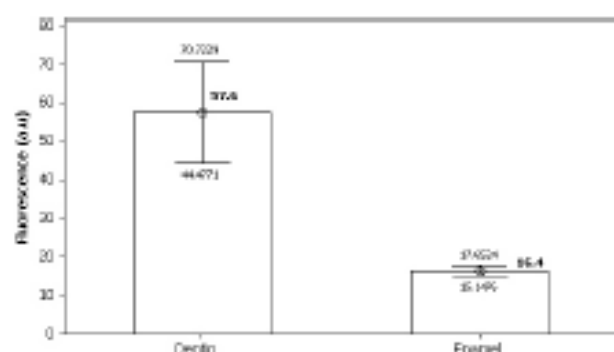


Figure 1. Mean values of Diagnodent readings in enamel and dentin.

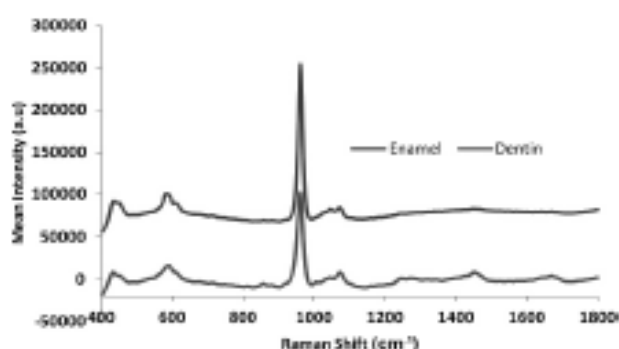


Figure 2. Raman spectra of sound enamel and dentin components.

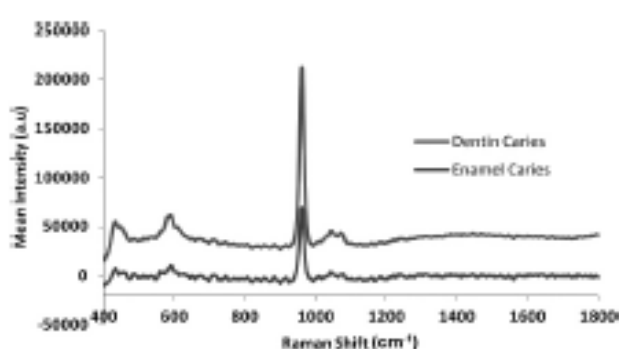


Figure 3. Raman spectra of caries in enamel and dentin.

with the progression of caries (7,13). In the present study, significant differences were observed between the Diagnodent readings for caries in enamel and dentin, with higher values of fluorescence related to dentin. This shows that more advanced processes of caries as in dentin have higher fluorescence.

Caries begins on tooth enamel, which has hydroxyapatite (HA) as its main component. When a solution containing fluoride comes in contact with HA, OH⁻ ions may be replaced by F⁻ ions resulting in the formation of fluoridated apatite. This compound is found both in enamel and dentin (14,15).

Raman spectroscopy shows the chemical structure of the tissues. In this study were observed enamel and dentin peaks related to the inorganic components ~960 cm⁻¹ (phosphate apatite) and ~575 cm⁻¹ (16) (attributed to fluoridated apatite), both with greater intensity in enamel, confirming its higher mineral content. The ~1450 cm⁻¹ peak related to the organic content was observed in higher intensity in dentin.

Raman spectroscopy of carious and non-carious teeth revealed reduction of the intensity of peaks from inorganic components, but were not statistically significant. Unlike

a previous study (17) that reported changes in the Raman peak of phosphate between sound and carious enamel, in this study was observed a significant reduction only for the ~575 cm⁻¹ peak in dentin caries.

In the correlation of Diagnodent readings with Raman peaks was observed a negative and significant correlation only between the ~575 cm⁻¹ and ~960 cm⁻¹ peaks and dentin caries. The lower the intensity of these inorganic components the higher the value obtained in Diagnodent readings in dentin. This finding reinforces the observation of another study (18), which concluded that the depth of dental caries has greater influence than the mineral loss in Diagnodent readings. The increased values in the Diagnodent readings were probably due to a higher fluorescence, which might be attributed to bacterial metabolic activity (9) and also to the amount of organic matrix (13,18) rather than from disintegration of crystals.

There was no significant correlation between Diagnodent readings in enamel and Raman peaks, proving that Diagnodent does not measure accurately small changes in mineral content. These findings corroborate a previous study (19) in which Diagnodent showed the lowest

Table 2. Correlation between Raman peaks obtained in enamel and dentin

Correlated Peaks	r ²	p value
Enamel ~575 X ~960	0.934	>0.001
Enamel ~575 X ~1450	0.746	0.001
Enamel ~960 X ~1450	0.671	0.006
Dentin ~960 X ~1450	0.785	0.001
Dentin ~960 X ~575	0.863	>0.001
Dentin ~575 X ~1450	0.663	0.007

*Pearson's correlation.

Table 3. Correlation between Raman peaks and Diagnodent® readings in carious teeth

Correlated peaks	r ²	p value
Dentin ~575; Diagnodent Dentin	- 0.645	0.009*
Dentin ~960; Diagnodent Dentin	-0.807	>0.001**
Dentin ~1450; Diagnodent Dentin	-0.370	0.175
Enamel ~575; Diagnodent Enamel	0.232	0.389
Enamel ~960; Diagnodent Enamel	0.234	0.402
Enamel ~1450; Diagnodent Enamel	0.140	0.620

*Pearson's correlation; **Statistically significant.

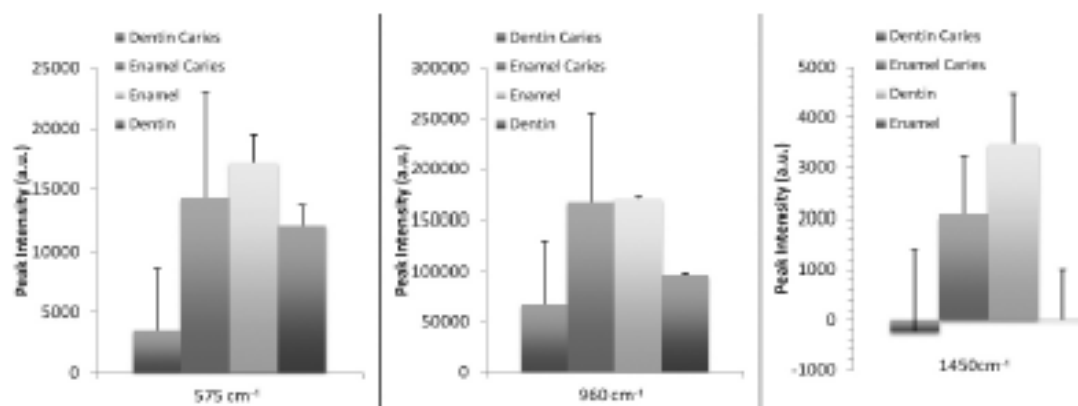


Figure 4. Mean values of Raman readings in sound and carious enamel and dentin.

sensitivity (0.66-0.75) when compared with all other studied detection methods. According to the authors (19), less sensitivity could be explained by the Diagnodent pen device, since the study refers mainly to enamel lesions and not to dentinal ones. In general, all studies agree that Diagnodent performs well when used for dentinal lesions (9).

Within the limitations of this *in vitro* study, these results suggest that Diagnodent readings reflect changes in organic matter instead of inorganic contents. In a previous report (18) the correlation between mineral loss in enamel, measured by microradiography, and Diagnodent readings was only 0.65.

Another study (20) revealed differences between sound enamel and initial caries at the peak of HA, disagreeing with the findings of this study in that the $\sim 960\text{ cm}^{-1}$ peak in enamel caries and sound enamel had no significant difference.

Since the early diagnosis of caries is directly related to the identification of changes in inorganic components of the tooth, Raman spectroscopy was more sensitive to variations of these components when compared with Diagnodent.

Resumo

O objetivo desse estudo foi verificar por meio da espectroscopia Raman, a existência de correlação entre os níveis de apatita fosfatada ($\sim 960\text{ cm}^{-1}$), apatita fluoretada ($\sim 575\text{ cm}^{-1}$) e matriz orgânica ($\sim 1450\text{ cm}^{-1}$) e as leituras do Diagnodent® em diferentes estágios de cárie dental em dentes humanos extraídos. O valor médio do pico de fluorescência na área da cárie foi anotado e os dentes divididos em cárie de esmalte, dentina e dente higido. Após as leituras de fluorescência, foi realizada a espectroscopia Raman nos mesmos sítios. Os resultados mostraram diferença significativa (ANOVA $p < 0,05$) entre as leituras de fluorescência para esmalte ($16,4 \pm 2,3$) e dentina ($57,6 \pm 23,7$) nos dentes cariados. Os picos Raman para esmalte e dentina evidenciaram que os picos ~ 575 e $\sim 960\text{ cm}^{-1}$ foram mais intensos em cárie de esmalte. Houve correlação negativa e significativa ($p < 0,05$) entre os picos ~ 575 e $\sim 960\text{ cm}^{-1}$ e cárie de dentina. Pode-se concluir que quanto maior a fluorescência detectada pelo Diagnodent menor o pico da apatita fosfatada e fluoretada. O diagnóstico precoce da cárie está diretamente relacionado com a identificação de mudanças nos componentes inorgânicos do dente, assim a espectroscopia Raman foi mais sensível para variações desses componentes quando comparada ao Diagnodent.

References

- Nakornchai S, Atsawasuwan P, Kitamura E, Surarit R, Yamauchi M. Partial biochemical characterisation of collagen in carious dentin of human primary teeth. Arch Oral Biol 2004;49:267-273.
- Núñez DP, Bacallao LG. Bioquímica de la caries dental. Rev Haban Cienc Méd 2012;9:156-166.

- Cury JA, Tenuta LMA. Enamel remineralization: controlling the caries disease or treating early caries lesions? Braz Oral Res 2009;23:23-30.
- Rodrigues JA, Diniz MB, Josgrilberg EB, Condeiro RL. In vitro comparison of laser fluorescence performance with visual examination for detection of occlusal caries in permanent and primary molars. Lasers Med Sci 2009;24:501-506.
- Frank RM. Structural events in the caries process in enamel, cementum, and dentin. J Dent Res 1990;69:559-566.
- Lussi A, Hellwig E. Performance of a new laser fluorescence device for the detection of occlusal caries in vitro. J Dent 2006;34:467-471.
- Lussi A, Hülst R, Paulus R. Diagnodent: an optical method for caries detection. J Dent Res 2004;83:C80-C83.
- Iwami Y, Yamamoto H, Hayashi M, Ebisu S. Relationship between laser fluorescence and bacterial invasion in arrested dentinal carious lesions. Lasers Med Sci 2011;26:439-444.
- Megert B, Longbottom C, Reich E, Francescut P. Clinical performance of a laser fluorescence device for detection of occlusal caries lesions. Eur J Oral Sci 2001;109:14-19.
- Pinheiro ALB, Santos NRS, Oliveira PC, Acirole GTS, Ramos TA, Gonzalez TA, et al. The efficacy of the use of IR laser phototherapy associated to biphasic ceramic graft and guided bone regeneration on surgical fractures treated with miniplates: a Raman spectral study on rabbits. Lasers Med Sci 2013;28:513-518.
- Pinheiro ALB, Lopes CB, Pacheco MT, Brugnera Junior A, Zanin FAA, Cangussu MCT, et al. Raman spectroscopy validation of Diagnodent-assisted fluorescence readings on tibial fractures treated with laser phototherapy, bmps, guided bone regeneration and miniplates. Photomed Laser Surg 2010;28:S89-S97.
- Lopes CB, Pacheco MT, Silveira L Jr, Duarte J, Pinheiro ALB. The effect of the association of NIR laser therapy BMPs and guided bone regeneration on tibial fractures treated with wire osteosynthesis: Raman spectroscopy study. J Photochem Photobiol B 2007;89:125-130.
- Mendes FM, Pinheiro SL, Bengtson AL. Effect of alteration in organic material of the occlusal caries on Diagnodent readings. Braz Oral Res 2004;18:141-144.
- Wei M, Evans JH, Bostrom T, Grondahl L. Synthesis and characterization of hydroxyapatite, fluoride-substituted hydroxyapatite and fluorapatite. J Mater Sci Mater Med 2003;14:311-320.
- Campillo M, Lacharme PD, Reparaz JS, Goni AR, Valiente M. On the assessment of hydroxyapatite fluoridation by means of Raman scattering. J Chem Phys 2010;132:2445011-2445015.
- Evans JA, Alvarez R. Characterization of the calcium biomineral in the radular teeth of *Chiton pelliserpentis*. JBIC 1999;4:166-170.
- Yokoyama E, Kakino S, Matsuura Y. Raman imaging of carious lesions using a hollow optical fiber probe. App Opt 2008;47:4227-4230.
- Shi XK, Tranau S, Angmar-Mansson B. Validation of Diagnodent for quantification of smooth-surface caries: an in vitro study. Acta Odontol Scand 2001;59:74-78.
- Archilellou EE, Rahiotis C, Kakaboura A, Vougiouklakis. Evaluation of a new fluorescence-based device in the detection of incipient occlusal caries lesions. Lasers Med Sci 2013;28:193-201.
- Ko ACT, Hewko M, Sowa MG, Dong CCS, Cleghorn B, Choo-Smith LP. Early dental caries detection using a fibre-optic coupled polarization-resolved Raman spectroscopic system. Opt Express 2008;16:6274-6284.

Received October 4, 2012
Accepted December 4, 2012

9. PREMIAÇÕES

International Academy Laser Medicine and Surgery

This is to certify that

Dr. Arthur Barbosa

Received the AWARD for Best Poster

**Evaluation of Photodynamic Antimicrobial Therapy
(PACT) against Trypomastigotes of *Trypanosoma
cruzi*: In Vitro Study**

presented on Laser Florence 2010

*Leonardo Longo, MD
IALMS President*

Leonardo Longo

Firenze, November 7th, 2010

Founded in Florence, Italy, October 2000

Borgo Pinti, 57, 50121 Firenze
www.ialms.com



Phone/Fax 0039 0552342330
ialms@laserflorence.org



CENTRO DE BIOFOTÔNICA - FOUFBA

Menção Honrosa



Ao trabalho intitulado "Evaluation of Photodynamic Antimicrobial Chemotherapy (PACT) against trypomastigotes of *Trypanosoma cruzi*: *in vitro* study", tendo como autores: Barbosa AFS, Galdino SL, Pitta IR, Pinheiro ALB pela relevância da pesquisa e excelência da apresentação no II CONGRESSO INTERNACIONAL DE LASER DA BAHIA e III JORNADA INTERNACIONAL DE LASER DA BAHIA, realizada no período de 8 a 10 de dezembro de 2011 no Centro de Convenções do Sol Barra Hotel – Salvador/Bahia

Prof. Antônio Luiz Barbosa Pinheiro, PhD
Coordenador Geral

Salvador, 08 de dezembro de 2011

Prof.^a Dr.^a Aparecida Maria Cordeiro Marques
Secretária Geral

Prof. Dr. Jean Nunes dos Santos
Coordenador Científico